



## Durham E-Theses

---

### *Vibrational spectroscopic studies of hydrogen bonding interactions*

Ackroyd, Robert

#### How to cite:

---

Ackroyd, Robert (1978) *Vibrational spectroscopic studies of hydrogen bonding interactions*, Durham theses, Durham University. Available at Durham E-Theses Online: <http://etheses.dur.ac.uk/8326/>

#### Use policy

---

The full-text may be used and/or reproduced, and given to third parties in any format or medium, without prior permission or charge, for personal research or study, educational, or not-for-profit purposes provided that:

- a full bibliographic reference is made to the original source
- a [link](#) is made to the metadata record in Durham E-Theses
- the full-text is not changed in any way

The full-text must not be sold in any format or medium without the formal permission of the copyright holders.

Please consult the [full Durham E-Theses policy](#) for further details.

VIBRATIONAL SPECTROSCOPIC STUDIES  
OF HYDROGEN BONDING INTERACTIONS

The copyright of this thesis rests with the author  
No quotation from it should be published without  
his prior written consent and information derived  
from it should be acknowledged



A thesis submitted to  
The University of Durham

by

Robert Ackroyd, B.Sc.

(Van Mildert College)

for the degree of  
Doctor of Philosophy

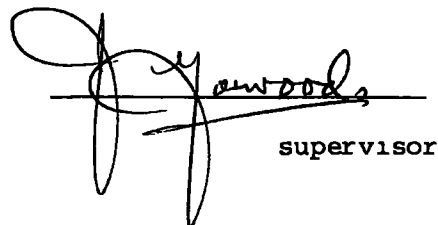
December 1978

To my  
Mother and Father

DECLARATION

The work described in this thesis was carried out by me in the Chemistry Department of the University of Durham and the Institut für Physikalische Chemie der Technischen Universität, Braunschweig between September 1975 and October 1978. I declare that this work has not been accepted in substance for any degree, and is not being concurrently submitted in candidature for any other degree. The work is my original work except where indicated by reference to other work.

signed:

A handwritten signature in cursive script, appearing to read "R. Ackroyd", written over a horizontal line.A handwritten signature in cursive script, appearing to read "J. Jewood", written over a horizontal line.  
supervisor

date: 8th December 1978

ABSTRACT

A study of hydrogen bonding interactions in the liquid phase.

Infrared absorbance data were obtained in digital form for the  $\nu_s$  (OH) band of phenol when complexed by hydrogen bond formation to each of the bases acetonitrile and 1,4-dioxan, along with the  $\nu_s$  (OD) bands of their deuterated analogues, each in carbon tetrachloride solution. Similar data were obtained for the complex formed between phenol and acetonitrile when in chloroform-d solution. The vibrational phase relaxation of the  $\nu_s$  vibrational modes as related to the model, published by Robertson and Yarwood, which characterises the relaxation.

Similar data for the hydrogen-bonded complex formed between phenol and pyridine in carbon tetrachloride solution and for the decoupled  $\nu_s$  (OH) and  $\nu_s$  (OD) vibrational modes of water in isotopically-dilute solutions were also obtained.

Far-infrared spectral data for the complex formed between phenol and each of the bases 1,4-dioxan and pyridine were obtained and related to the mid-infrared data.

Raman spectral data for the  $\nu_1$  vibrational mode of acetonitrile when in solution in the presence of methanol-d<sub>4</sub> were also obtained and interpreted in terms of the theories of vibrational phase relaxation.

ACKNOWLEDGEMENTS

I am indebted to many people for help and advice during the period of research leading to this thesis.

Above all, I must express my appreciation for the unfailing interest, enthusiasm and inexhaustible supply of ideas of my supervisor, Dr J. Yarwood. The Science Research Council must be thanked for financial support in the form of a Research Studentship.

I would further like to acknowledge the help with theoretical aspects given by Dr G. N. Robertson of the University of Cape Town and also the development and supply of computer programmes.

Financial assistance from N.A.T.O. to facilitate travel to Braunschweig in West Germany to obtain Raman spectral data at the Institut für Physikalische Chemie der Technischen Universität was very much appreciated, as was the help and hospitality provided there by Professor G. Döge, Dr R. Arndt, Dr A. Khuen and their families and friends.

Thanks are due to many people in the Chemistry Department at the University of Durham for technical advice and useful discussions.

Finally, I would like to record my appreciation of the efforts of Mrs R. L. Reed in converting my manuscript into typed form.





	page number
4.10 Conclusions Drawn from the Application of the Robertson-Yarwood Model to the Complexes of Phenol with Acetonitrile and with 1,4-Dioxan ...	111
4.11 The $\nu_s$ (OH) Absorption Band of the Phenol-Pyridine Complex in Carbon Tetrachloride ... ..	114
4.12 The $\nu_s$ (OH) and $\nu_s$ (OD) Absorption Bands of Isotopically Dilute Water <sup>s</sup> Solutions ... ..	118
 <u>Chapter Five. Results in the Far-Infrared Region and their Interpretation</u>	
5.1 Introduction ... ..	128
5.2 Far-Infrared Studies of the Complexes of Phenol with Acetonitrile and with 1,4-Dioxan ... ..	128
5.3 Far-Infrared Studies of the Complex of Phenol with Pyridine ... ..	133
 <u>Chapter Six. A Raman Spectral Study of Vibrational Relaxation in a Hydrogen Bonded Complex</u>	
6.1 Introduction ... ..	145
6.2 Instrumentation, Experimental Method and Computation	146
6.3 Theory of Vibrational Relaxation Processes ... ..	149
6.4 Experimental Results and their Interpretation ...	154
6.5 Summary and Conclusions ... ..	168
<u>References</u> ... ..	170
 <u>Appendices</u>	
1. Vibrational Relaxation of Hydrogen Bonded Species in Solution. II. Analysis of $\nu_s$ (OH) Absorption Bands. (J. Yarwood, R. Ackroyd and G.N. Robertson, Chemical Physics, <u>32</u> , 283 (1978))	
2.1 Research Colloquia, Research Seminars and Lectures by External Speakers Arranged by the Department of Chemistry of the University of Durham between 1 October 1976 and 30 September 1978	
2.2 Research Conferences Attended by the Author during the period 1 October 1975 to 30 September 1978	

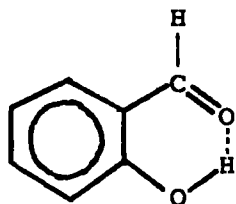
**CHAPTER ONE**

**INTRODUCTION**

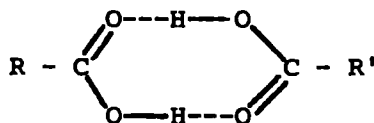
## 1.1 General Introduction

In the most general sense a hydrogen bond is said to exist when a hydrogen atom can be considered to be bonded to more than one other atom. The idea was first put forward early in this century to explain the behaviour of amines and ammonium salts (1,2). The system will be designated X-H---Y where X and Y are two other atoms which may be alike or different. Hydrogen bonds can be symmetric when the distances XH and HY are equal, as in the ion  $[\text{F}-\text{H}-\text{F}]^-$  (3,4) or, more commonly, asymmetric when these distances are unequal. Typical X---Y distances lie between 240 pm and 340 pm. The proton donor group X-H consists of hydrogen covalently bonded to an electro-negative atom which is commonly oxygen, nitrogen, sulphur or a halogen, but can also be carbon, silicon or phosphorus. The proton acceptor Y is usually an atom with high electron density due to the presence of lone-pair electrons but can also be a molecule with electron density in a  $\pi$ -electron orbital. Typical proton acceptors are therefore oxygen, nitrogen and halogen atoms and the  $\pi$ -electron systems in benzenes, alkynes, nitriles etc.

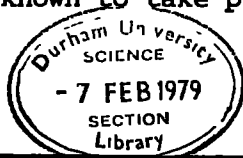
Hydrogen bonds may be intramolecular where X and Y are in the same molecule as in salicylaldehyde,



or intermolecular where X and Y are in different molecules. Examples of this type can be self-associated as in carboxylic acid dimers



and also water and alcohols, or involve mixed association. Hydrogen bonding interactions are known to take place in the gas, liquid and solid



phases, but in this thesis mixed association in the liquid phase will form most of the subject matter. Enthalpies of formation can lie between  $6.86 \text{ kJ mol}^{-1}$  (for aniline-benzene (N-H- $\pi$ )) (5) and  $155 \text{ kJ mol}^{-1}$  in the ion  $[\text{HF}_2]^-$  (6) although values in the range  $24\text{-}40 \text{ kJ mol}^{-1}$  are more typical.

The following operational definition of a hydrogen bond was given by Pimentel and McClellan in 1960 (7). "A hydrogen bond is said to exist when: (i) there is evidence of a bond, and (ii) there is evidence that this bond specifically involves a hydrogen atom already bonded to another atom." In view of the enormous number of types of hydrogen bonds and the present lack of exact information about the forces involved in their formation this definition is the one which must be still used today. Certain instances of hydrogen being bonded to two atoms are usually considered aside from hydrogen bonding, one example being diborane and similar compounds where the hydrogen atoms bonded to two boron atoms carry a formal negative charge.

Because of the involvement of hydrogen bonding in so many important problems in chemistry, physics and the biological sciences, the subject has attracted an enormous amount to research attention. To give a few examples, the involvement of hydrogen bonding in the structure of D.N.A. (8) and other biologically important compounds is well-known, the structure and properties of water depend on the presence of hydrogen bonds (9,10) and despite a high research effort in many different fields the system is far from being fully understood, the exhibition of ferroelectric phenomena (11) by crystals such as potassium dihydrogen phosphate depends upon the presence of hydrogen bonds in the crystal structure and the action of some anaesthetics is thought to involve the breaking of hydrogen bonds *in vivo* (12,13).

From these few examples it should be clear that hydrogen bonding is of great importance in many scientific disciplines and no attempt can

be made here to provide even a comprehensive introduction. Many books on the topic exist and those of Pimentel and McClellan (7), Vinogradov and Linnel (14), Joesten and Schaad (15) and Schuster, Zundel and Sandorfy (16) can be mentioned in particular.

## 1.2 Previous vibrational spectroscopic studies of hydrogen bonded complexes

When a non-linear molecule of  $n$  atoms ("A") (having  $3n - 6$  vibrational degrees of freedom) forms a molecular complex with another non-linear molecule of  $m$  atoms ("B") the resulting complex has  $3(n+m) - 6$  vibrational degrees of freedom. Thus three vibrational and three rotational degrees of freedom are lost and six new vibrational degrees of freedom of the complex arise. Of these six modes, one is a stretching mode, four are bending modes, and one is a torsional mode. Using the nomenclature of Wood (17), these modes are designated as follows:

$\nu_{\sigma}$  is the intermolecular stretching mode

$\nu_{\beta}$  and  $\nu_{\gamma}$  are out-of-plane bending modes

$\nu_{\delta}$  and  $\nu_{\epsilon}$  are in-plane bending modes

and  $\nu_{\alpha}$  is a torsional mode described by oscillation of one molecule relative to the other about the axis of the hydrogen bond.

If either A or B, or both, are linear, or if a linear complex is formed, there are fewer intermolecular modes. Some complexes of this type have been investigated by Thomas (18). Of these six modes,  $\nu_{\sigma}$  is expected to be the highest in frequency and it is the only one to have been studied in detail. Apart from these modes, certain 'internal' vibrational modes of the molecules A and B show marked changes when the molecules are involved in hydrogen bonding and so have also been studied more or less extensively. If the complex formed is now designated X-H---Y, the modes of particular

interest are:

- $\nu_s$  corresponding to X - H stretching
- $\nu_d$  the in-plane X - H bending mode
- and  $\nu_g$  the out-of-plane X - H bending mode.

Indeed, it is one of these modes,  $\nu_g$ , which has been the subject of most vibrational spectroscopic investigations into hydrogen bonded complexes, and it is with this mode that this work is principally concerned. Certain vibrational modes of the molecule B also undergo changes on complex formation, but these have been investigated rather less. By far the greater amount of work has used infrared spectroscopy; Raman studies have been hindered in the past by the lack of instrumentation, and although this has now largely been overcome, the inherent low Raman scattering cross-sections of many groups involved in hydrogen bonding is a serious drawback in such studies. For these reasons this chapter will concentrate on infrared studies; all Raman investigations will be reserved for Chapter 6.

When the complex between molecules A and B containing the grouping of atoms X - H---Y is formed, the infrared spectrum of the complex commonly shows the following changes when compared with the sum of the spectra of the individual components.

(i) The band corresponding to  $\nu_s$  is shifted to lower frequency. This may be ascribed to a reduction in the force constant for X - H stretching due to weakening of the X-H bond. (Here care must be taken since there must also be a change in the normal coordinate in which the vibration takes place.)

(ii) The  $\nu_s$  (XH) band also broadens considerably, showing that a change in the vibrational relaxation of the mode has probably taken place, although other processes may also influence the bandwidth (see Chapter 4).

(iii) The band shows a large increase in integrated intensity indicating that the dipole moment derivative  $\left(\frac{\partial \mu}{\partial Q}\right)$  has increased on hydrogen bond formation.

(iv) The bands corresponding to X-H bending modes ( $\nu_d, \nu_g$ ) shift upwards in frequency and do not change markedly in intensity. This suggests that the redistribution of electron density on formation of the complex takes place predominantly along the axis of the X-H bond.

(v) New intermolecular modes of vibration give rise to new absorption bands in the far-infrared region (see above).

(vi) Changes in bandshape, position and intensity take place in the spectrum of the proton-accepting molecule but these are typically much smaller than those in the spectrum of the donor (see Chapter 6).

It is because of the nature of the changes that take place and because the band occurs commonly in a spectral region free from other absorptions that the  $\nu_s$  (XH) vibrational mode has been studied so extensively. The more pertinent aspects of these studies will now be outlined, bearing in mind that the field has been extensively reviewed recently (19), and many other chapters and review articles on the subject exist (17, 20-23).

A great deal of effort has been put into the correlation of thermodynamic properties (enthalpies and entropies of formation) of these complexes with the infrared shift in  $\nu_s$  ( $\Delta\nu$ ) or the relative shift  $\Delta\nu/\nu$ . This follows from the well-known Badger-Bauer linear relationship between frequency shift and interaction energy (24). However, the more recent and detailed studies have shown that these relationships only hold, if at all, within limited groups of very similar compounds (23,25) and in some cases the infrared shift becomes greater as the hydrogen bond strength decreases (26,27). The main objection to these correlations is that the infrared shift involves only the  $\nu_s$  (XH) band whereas the heat of complex formation includes effects attributable to both the formation of the H---Y bond and the weakening of the X - H bond.

7

A few full normal coordinate analyses have been carried out on less complicated examples but have met with limited success partly because they have not taken full account of the anharmonicity of the  $\nu_s$  hydrogen bond; a factor which is thought to be very important in explaining the broadening of the  $\nu_s$  (XH) band. Systems treated in this way include the dimers of formic acid and acetic acid (28,29), a hydrogen dicarboxylate ion (31), complexes of chloroacetic acids with dimethyl sulphoxide (30), and some complexes of phenol with various pyridines and amines (32,33).

### 1.3 Theories of broadening of the $\nu_s$ infrared absorption band

Attention will now be turned to theories of broadening of  $\nu_s$  absorption bands in the infrared. Hadzi and Bratos have classified the theories of broadening into four groups (see ref. 19), and these are:

- (1) the fluctuation theory (Landsberg and Baryshanskaya) (34)
- (1.1) Stepanov's theory and predissociation theory (35)
- (1.1.1) the double-minimum theories
- and (1v) the anharmonicity and anharmonic coupling theories (36).

The possible effects of Fermi resonance interaction contributing to the bandshape and the structure will be discussed later.

#### (1) The fluctuation theory

This theory proposes simply that due to the weakness of the hydrogen bond compared with conventional chemical bonds the intermolecular forces (in a liquid) can bring about considerable fluctuations in the geometry of the hydrogen bond, and these fluctuations are reflected in the force constant of the X - H bond and thus the molecule absorbs over a range of frequencies. It is not clear, however, why in the gas phase  $\nu_s$  (XH) bands of considerable breadth can be observed when intermolecular forces would be much reduced.



(ii) Stepanov's theory (and predissociation theory)

Stepanov's theory is known as the predissociation theory but, as pointed out by Wood (ref. (17), p. 332), this term tends to suggest the theory which is better known as "relaxation line broadening" (see below). Stepanov's theory will be considered as the one which gives rise to sum and difference bands  $\nu_s \pm n\nu_\sigma$ . In this theory he envisages interaction between the  $\nu_s$  and the  $\nu_\sigma$  modes with the result that sub-levels representing the  $\nu_\sigma$  energy levels are superimposed upon the  $\nu_s$  energy levels.

The breadth of the absorption band is due to transitions taking place to and from different sub-levels in the  $v = 0$  and  $v = 1$  vibrational states, and the effect of intermolecular interactions causes these sum and difference bands to merge and form the complete absorption band. This is illustrated in Figure 1.1 and the mechanism is discussed in detail by Wood (see ref. (17)). This method is appropriate because the frequencies of the  $\nu_s$  (XH) and  $\nu_\sigma$  (XH---Y) modes are very different, and so by a Born-Oppenheimer type approximation the two modes are taken to be adiabatically separable. For the same reason, what might be called a vibration-vibration analogue of the Franck-Condon principle may be used to predict the intensities of the various transitions; because the frequencies are so different it may be said that the X---Y distance does not change whilst absorption of energy takes place, that is, the transitions are "vertical". A final point worthy of note made by Wood (17) is that the spacing of the sub-maxima in the predicted  $\nu_s$  (XH) band is equal to the  $\nu_\sigma$  (XH---Y) vibrational frequency in the upper vibrational state (see Figure 1.1) which is not necessarily the same as the frequency in the lower state which would be the frequency measured in the far-infrared spectrum.

Stepanov also observed that in many cases the  $\nu_s$  (XH) vibrational quantum is greater than the hydrogen bond dissociation energy and that if this energy were all transferred to the low-frequency mode, dissociation would occur. If coupling between the modes

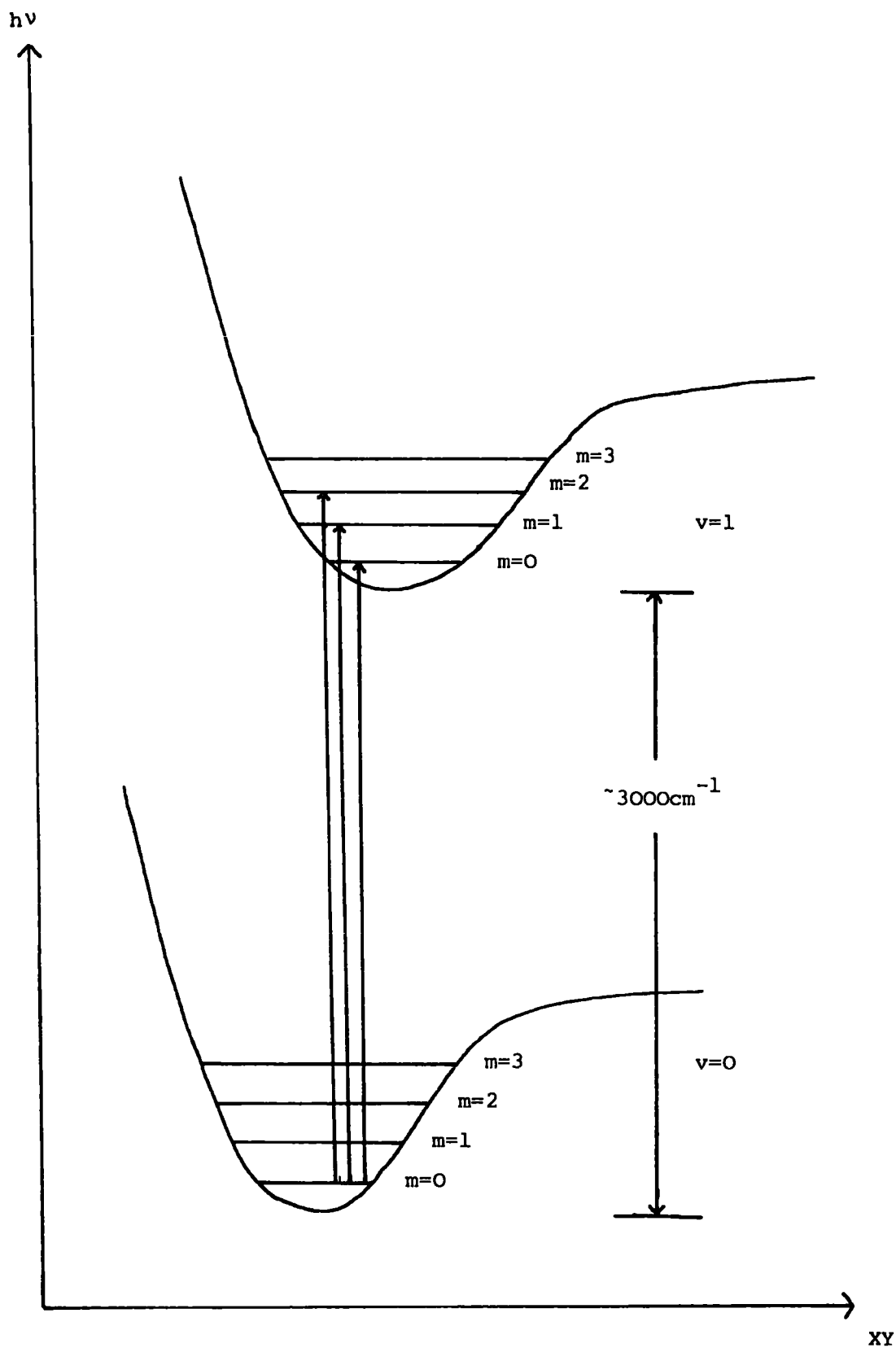


Figure 1.1 The Stepanov mechanism. The diagram shows potential energy curves as a function of the X---Y distance for the  $v=0$  and  $v=1$  energy levels of the  $\nu_s$  vibrational mode. The sub-levels are the vibrational energy levels of the  $\nu_o$  mode. A series of transitions from the  $v=0, m=0$  level is shown.

is strong (as appears to be the case), then this transfer is to some extent probable and the lifetime of the upper vibrational level of  $\nu_s$  is finite. By using the uncertainty principle that  $\Delta\omega\Delta\tau \approx 1$  ( $\omega$  = frequency,  $\tau$  = time), it can be seen that the upper level must have a certain uncertainty in its width and this width causes broadening of the spectral lines. This is known as predissociation, but as pointed out previously the term "relaxation line broadening" is to be preferred. This mechanism has however been shown to be of no great importance in the explanation of the breadth and structure of the  $\nu_s$  (ClH) band of the hydrogen chloride-dimethyl ether gas-phase complex by Coulson and Robertson (37).

(iii) The double-minimum theories

The theories which propose a double minimum to the potential well in which the X - H stretching motion takes place have been reviewed by Wood (ref. (17) pp. 335-345). In them it is proposed that the proton has two positions of stability (i.e. minimum energy) and the consequent increase in the number of energy levels of the system results in the broad absorption band which is observed. These theories have met with success mostly when applied to systems involving very strong and symmetric or near-symmetric hydrogen bonds such as the ion  $[\text{F-H-F}]^-$  (38). One problem encountered is that of distinguishing, from the  $\nu_s$  band profile, between a one-minimum and a two-minimum potential once thermal motions have been taken into account (see also ref. (3)).

(iv) The anharmonicity and anharmonic coupling theories

The more modern broadening theories will now be described. These are essentially the theory of Witkowski and Maréchal which describes an isolated gas-phase complex, and the theories of Rösch and Ratner and of Bratos which describe a complex in solution. These theories also include

the idea of interaction between the  $\nu_g(\text{XH})$  and  $\nu_g(\text{XH}---\text{Y})$  modes as proposed by Stepanov (see (ii) above). This section will provide a background to the theory of Robertson which is discussed in Chapter 4.

Since all these theories invoke the idea of anharmonicity of the  $\nu_g(\text{XH})$  vibration, the distinction between the terms "mechanical" and "electrical" anharmonicity is important. (i) Mechanical anharmonicity arises simply from the failure of the vibration to obey Hooke's law, that is, the restoring force when the bond is stretched is not proportional to the displacement from the equilibrium position. (ii) Electrical anharmonicity is the appearance of quadratic and higher terms in the expansion of the dipole moment by a Taylor series:

$$\mu = \mu_e + \left(\frac{\partial \mu}{\partial Q}\right)_e \cdot Q + \left(\frac{\partial^2 \mu}{\partial Q^2}\right)_e \cdot \frac{Q^2}{2!} + \left(\frac{\partial^3 \mu}{\partial Q^3}\right)_e \cdot \frac{Q^3}{3!} + \dots$$

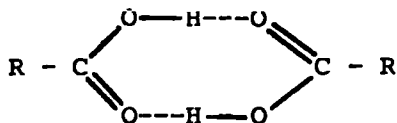
where  $Q$  is a normal coordinate. If the quadratic and higher terms are important, the dipole moment is not proportional to the displacement implied by a particular normal coordinate.

The term anharmonic coupling is used to describe the process whereby the force constant for the X-H motion becomes dependent on the X---Y distance when a hydrogen bond is formed, and thus the  $\nu_g(\text{XH})$  and  $\nu_g(\text{XH}---\text{Y})$  modes become coupled.

Further background and discussion of these theories are provided in the chapters by Hofacker, Maréchal and Ratner (39), Hadzi and Bratos (19) and Sandorfy (40) in the book of Schuster, Zundel and Sandorfy.

The theory proposed by Witkowski and Maréchal (41-43) is concerned with the  $\nu_g(\text{OH})$  mode of the acetic acid dimer in the vapour phase. Using the harmonic approximation and envisaging coupling between the  $\nu_g(\text{OH})$  and the hydrogen bond stretching ( $\nu_g(\text{OH}---\text{O})$ ) modes they were able to calculate the positions and intensities of the lines contributing to the absorption

band in the infrared spectrum and obtain reasonable agreement with the experimental data of Haurie and Novak (44) for both  $(CD_3COOH)_2$  and  $(CD_3COOD)_2$ . The compounds with deuterated methyl groups were used to avoid interferences from  $\nu(CH)$  stretching vibrations in the spectra. The model chosen assumed a planar cyclic dimer configuration ( $C_{2h}$  symmetry)



and neglected any contribution due to lower frequency bending modes of the hydrogen bond. It should be noted that the Born-Oppenheimer type of separation of the vibrational modes used in this approach is only possible when one mode ( $\nu_s$ ) is of very much higher frequency than the other ( $\nu_o$ ).

By considering the interaction between the two hydrogen bonds in the dimer, Witkowski was also able to explain the splitting of the  $\nu_o$  band in the far-infrared which had previously been observed by Ginn and Wood (45). Leviel and Maréchal (46) were later able to incorporate into the model allowance for the anharmonicity of the  $\nu_o$  mode and predicted the positions of further lines in the spectra. This approach was extended to propynoic, acrylic (47) and other carboxyl acid dimers (48) with similar agreement.

The main criticism of these spectral reconstructions is that they only predict the positions and intensities of the spectral lines and give no indication of their linewidths. When attention was turned to measuring band intensities in the solid (49) and also the gas phase (50), it was found that the ratio of the transition probabilities  $P_H/P_D$  for protium and deuterium species was found to be approximately 2 rather than the expected value of  $\sqrt{2}$  (see also ref. (39)). This was interpreted within the theory as being due, at least in part, to a combination of mechanical and possibly also electrical anharmonicity.

Certain other gas-phase complexes have also been studied. These are mostly the complexes of hydrogen chloride and hydrogen fluoride with ethers and carbonyl compounds (51,52); the hydrogen chloride-dimethyl ether complex being analysed in greater detail by Coulson and Robertson (37,53). The structure of the  $\nu_s$  (XH) band of a series of hydrogen halide-nitrile complexes was interpreted in terms of hot bands by Thompson and Thomas (18,54). The shape of the  $\nu_s$  (FH) band in the hydrogen fluoride-trimethylamine gas-phase spectrum observed by Arnold and Millen (52) was interpreted by Lascombe et al. in terms of broadening caused by rotation of the complex as a non-rigid rotor (55). The rotation of the complex causes changes in the X---Y distance and these are incorporated in the model by means of a fluctuating potential function. The model was also extended to the liquid and solid phases where the fluctuating potential takes the form of a stochastic potential representing the interactions from surrounding molecules (see also Chapter 4). Only the broadening of the central  $\nu_s$  (FH) line was considered; the same method could be applied to the other observed lines which were assumed to be due to combinations of the type  $\nu_s \pm n\nu_\sigma$ .

The second important modern theory is that of Bratos (56,57). This theory differs essentially from the previous ones in that it makes extensive use of nonequilibrium thermodynamics and correlation functions. The same type of approach has also been used to calculate infrared (58) and raman (59) band profiles in liquids. The theory describes an isolated hydrogen bonded complex of two molecules (of  $N_A$  and  $N_B$  atoms) in an inert solvent, the "internal" vibrations of the complex are described by  $3N_A + 3N_B - 12$  normal coordinates which obey the laws of quantum mechanics and the six "external" vibrations are described by stochastic functions which obey the laws of classical mechanics. The meaning of this is that the hydrogen bond takes on a character which is determined very largely

by the stochastic (i.e. random) nature of its solvent environment. The "external" vibrations can be said to be strongly coupled to the thermal bath. By setting up a Hamiltonian for the "internal" vibrations and allowing this to be perturbed by a stochastic potential, the dipole moment correlation function for the  $\nu_s$  mode is arrived at and by Fourier transformation the theoretical infrared absorption profile is obtained. The model allows for anharmonic coupling between the  $\nu_s$  and  $\nu_\sigma$  modes and in this respect can be considered similar to the theories discussed above. In order to simplify the calculation, Bratos makes the following approximation: since the observed  $\nu_s$  bands are very broad (between  $100\text{cm}^{-1}$  and  $300\text{cm}^{-1}$ ) their phase relaxation times must be very short (between  $\sim 1\text{ps}$  and  $0.03\text{ps}$ ) and since these times are much shorter than those for other dynamic processes in the liquid ( $10^{-12}\text{s}$  to  $10^{-13}\text{s}$  for "external" vibrations and  $10^{-10}\text{s}$  to  $10^{-12}\text{s}$  for translations and rotations), the time-dependence of the perturbing potential is ignored. The outcome of this is that the solvent is considered to be static for the duration of the vibrational relaxation of  $\nu_s$  (XH) oscillator. This situation may be described as the "slow modulation limit" and the resultant infrared band will consequently have a gaussian profile. It is in this aspect that this theory differs from that of Robertson (60) where provision is made for fast modulation with the result that a bandshape with lorentzian and gaussian character is predicted (see Chapter 4). When the theory of Bratos is applied to systems involving hydrogen bonds with enthalpies of formation around  $20\text{kJ mol}^{-1}$  and involving no Fermi resonance, the theory predicts an asymmetrical distorted gaussian bandshape and this is in accord with previous experimental data for the complex phenol-dibutyl ether (61).

The broadening theory of Rösch and Ratner (62) differs from the theory of Bratos in that it envisages the relaxation of the  $\nu_s$  (XH) oscillator in solution to take place directly, whereas the Bratos theory envisages

indirect relaxation via coupling to the  $\nu_g$  (X-H---Y) mode. The direct relaxation is considered to be due to electrostatic interaction between the dipole moment produced by the motion of the hydrogen bonded proton and the local electrical field set up in the solvent environment. The electric field magnitude at the proton is again taken as a stochastic variable but no slow-modulation approximation is made (cf. above). Electrical anharmonicity is ignored, as is the interaction between the environment and the atoms X and Y. Again, an expression for the dipole moment correlation function is developed and by Fourier transformation the spectral bandshape is obtained. Rosch and Ratner do not attempt to compare their theoretical predictions with experimental data but it would be expected that this mechanism be more important when a dipolar solvent is employed.

(v) Theories involving Fermi resonance

In many cases "structure" is observed (see Section 4.11) in a  $\nu_g$  infrared band profile and this is explicable not in terms of sum or difference bands but by the phenomenon known as Fermi resonance (63). This is usually caused by an interaction between the  $\nu_g$  stretching mode and the first-overtone of the  $\nu_d$  and  $\nu_g$  in-plane and out-of-plane bonding modes. It has been shown (64) that when two vibrational transitions in vibrational modes of the same symmetry have the same frequency or their frequencies lie close together, then interaction between the energy levels takes place. This interaction is due to the presence of cubic or higher terms in the potential energy function and is this caused by anharmonicity of the vibrations. The main consequences of this interaction are that the two sets of energy levels are shifted apart with the result that a minimum, or "Evan's hole" (64) is created in the absorption band and that the total intensity is shared between the two bands with the result that one becomes less intense and one more intense. In this way a very weak overtone band can acquire intensity comparable with the band with which it interacts (see also ref. 17, pp.326-331).



Effects of this type have been noted by Claydon and Sheppard in solid phenylphosphonic and dibutylarsinic acids (65) and by Claydon et al. in polycrystalline  $\alpha$ -chromous acid (66). Hall and Wood (67) noted a series of maxima and minima in the spectra of various complexes of p-substituted phenols with a series of p-substituted pyridines. The positions of the absorbance maxima and minima were found not to change with change of base for a particular phenol but did change with change of phenol. From these observations it was concluded that the Fermi resonance involves combination or overtone bands in the proton donor moiety and likely combinations and overtones were suggested. A similar effect, but producing one absorbance minimum, was observed by Dean, Masri and Wood (68) in the  $\nu_s(\text{NH})$  band of the complex cations formed when trimethylammonium perchlorate or fluoroborate is dissolved in pyridine and other heterocyclic bases.

Throughout these works there appears to be some disagreement as to whether the frequency of the absorbance maximum or the absorbance minimum should be taken to compare with the frequency of the overtone or combination band (see refs. 49 and 51). Theory (64) would suggest that the point of inflexion be taken (see also below).

Of the more modern broadening theories only that of Bratos treats the Fermi resonance problem in detail; that of Rösch and Ratner specifically excludes cases where this interaction is important. It has been suggested that the differences between observed spectra and the reconstructions of Maréchal et al. may be explained by either Fermi resonance (69) or electrical anharmonicity.

With his broadening theory Bratos calculated absorption band profiles for  $\nu_s$  modes where Fermi resonance occurs between a broad continuum and either sharp or diffuse overtone or combination bands. The difference between the frequency of the overtone or combination band and the frequency at which absorbance minimum occurs is accounted for by the theory and thus

provides much clarification of the problem mentioned above. Robertson (70) has now developed a model which includes the effects of Fermi resonance but which is not confined to the slow modulation limit.

CHAPTER TWO

INSTRUMENTATION AND COMPUTATIONAL METHODS

## 2.1 Introduction

In this chapter the instrumentation, experimental techniques and computer methods used to obtain data over a spectral range of  $4000\text{cm}^{-1}$  to about  $2\text{cm}^{-1}$  are described. The higher wavenumber regions were covered by use of a Perkin-Elmer Model 577 dispersive infrared spectrometer and the low wavenumber regions were investigated by means of a Beckman-R.I.I.C. FS-720 interferometric spectrometer which was subject to modification in order to improve its performance and extend its low wavenumber limit. The spectral regions in which these instruments were used will be called, for convenience, the mid- and far-infrared respectively.

## 2.2 The Perkin-Elmer Model 577 spectrometer

The Perkin-Elmer Model 577 is of the conventional double-beam type employing the 'optical-null' method of recording the ratio of the intensities of the sample and reference beams. The source is a ceramic tube heated by an internal wire to a temperature of about  $1200^{\circ}\text{C}$ . In the  $4000\text{cm}^{-1}$  to  $2000\text{cm}^{-1}$  region (the principal region of interest in this work) the second order of a  $1000\text{ lines mm}^{-1}$  dispersion grating is used, the radiation of this order being separated from other orders by means of optical filters automatically brought in and out of use at certain pre-determined frequencies. The detector is a thermocouple. Further details of the instrument may be obtained from the manufacturer's instrument manual (71).

If accurate spectral data are to be obtained, the instrumental parameters must be chosen with care and the particular combinations used will now be discussed.

The spectrometer has seven slit "programmes" and the spectral slitwidth for each "programme" over the range  $4000\text{cm}^{-1}$  to  $2000\text{cm}^{-1}$  is shown as a function of wavenumber in Figure 2.1. Because the source does not emit

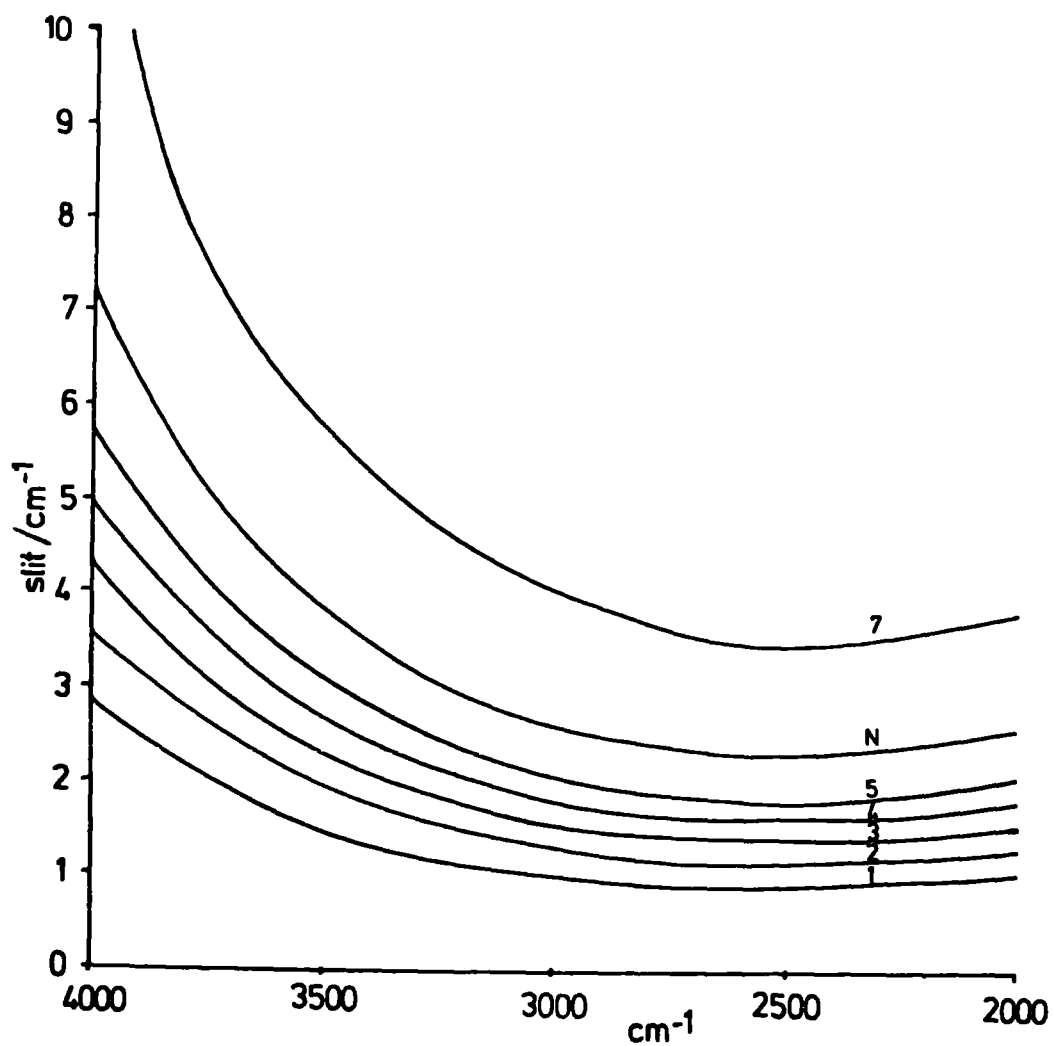


Figure 2.1 The spectral slitwidth (in  $\text{cm}^{-1}$ ) as a function of wavenumber for each of the seven slit "programmes" (1-5, N and 7) of the Perkin-Elmer Model 577 Spectrometer.

constant energy at all frequencies the slit is constructed to change as the spectrometer scans in order to maintain approximately constant energy at the detector. In this way approximately constant pen response and signal-to-noise ratio throughout the entire range of the spectrometer is achieved. From the figure it can be seen that this opening effect is greatest near to  $4000\text{cm}^{-1}$  and is smaller on the narrower slit programme.

When bandshape analysis is to be performed on the spectrum it is desirable to record the spectrum with a constant slitwidth, or at least to ensure that the slitwidth always remains small compared with the halfwidth of the band being recorded (72) and that any change in the slitwidth through the spectrum is minimised. For these reasons and in order to maintain reasonable energy throughput to the detector the slit programme "2" was chosen.

Once the slitwidth to be used is decided upon, the time constant and scanning speed can then be fixed. The maximum scanning speed for accurate recording of the spectral bandshape in  $\text{cm}^{-1} \text{ s}^{-1}$  is often obtained from the following empirical relationship:

$$\text{maximum scan speed} = \frac{1}{2} \times \frac{\text{spectral slitwidth (cm}^{-1}\text{)}}{\text{time constant (s)}} \quad (2.1)$$

In the  $4000\text{cm}^{-1}$  to  $2000\text{cm}^{-1}$  region the Perkin-Elmer Model 577 has scanning speeds of  $1.67\text{cm}^{-1} \text{ s}^{-1}$  ("X5" scale),  $0.833\text{cm}^{-1} \text{ s}^{-1}$  ("X10" scale) and  $0.167\text{cm}^{-1} \text{ s}^{-1}$  ("X25" scale) available. On slit programme "2" the slitwidth has a minimum value of  $\sim 1.2\text{cm}^{-1}$  and with a time constant of 1s ("Auto" position) this gives a maximum scanning speed of  $\sim 0.6\text{cm}^{-1}$ . In order that a large number of spectra be recorded in a reasonable time, the speed of  $0.833\text{cm}^{-1} \text{ s}^{-1}$  was used. This was considered reasonable in view of the width of the broadened  $\nu_s(\text{OH})$  and  $\nu_s(\text{OD})$  bands to be recorded (at least  $80\text{cm}^{-1}$ ).

The time constant chosen was the shortest available to give the truest indication of noise (i.e. random errors) in the spectrum. This is of prime importance in the analysis of the data (see Chapter 4).

In summary the slitwidth was narrowed to remove as much effect of the "programmed" slit as possible and the scan speed was chosen to be approximately that given by Equation 2.1 with regard to the need to collect data within a reasonable period of time.

The final instrumental parameter, the gain, was chosen to provide a compromise between noise in the spectrum and adequate pen response. This was taken as being when the pen returned to its rest position with little oscillation in about 2s after the removal of an opaque object which had been placed in the sample beam.

### 2.3 The digitising system

The spectrometer was provided with an output which gives between zero and 10mV according to the position of the pen on the transmittance scale of zero to 100% transmittance. This output was connected to a Solatron data transfer unit operating a Solatron LM1450 digital voltmeter with a zero to 10mV scale. The voltage output from the spectrometer was "read" at predetermined time intervals (usually of 4s) by the data transfer unit and displayed on the voltmeter and punched onto paper tape along with the elapsed time by a Westrex model ASR-33 Teletype.

The photometric accuracy of the spectrometer was checked periodically using a set of Beckman LD-6200 rotating sectors. The results obtained on two different occasions are shown in Table 2.1 and it can be seen that the measured millivolts readings are always close to the manufacturer's  $\pm 1\%$  of the values given for the Beckman sectors. The long-term variation can also be seen to be reasonable.

Table 2.1 The photometric accuracy of the spectrometer and digitising system. The readings "A" and "B" are on two occasions separated by about 21 months

transmittance value of rotating sector	expected voltmeter reading (mV)	A		B	
		voltmeter reading (mV)	discrepancy (mV)	voltmeter reading (mV)	discrepancy (mV)
71%	7.10	6.97	-0.13	7.03	-0.07
50.1%	5.01	4.84	-0.17	4.95	-0.06
25.1%	2.51	2.40	-0.11	2.47	-0.04
12.6%	1.26	1.19	-0.07	1.29	+0.03
6.3%	0.63	0.54	-0.09	0.60	-0.03

The accuracy of the zero to 10mV scale compared with the position of the pen on the transmittance scale was also checked periodically. This was done in the following manner. With an attenuator (Beckman AT-04) placed in the sample beam in the fully open position and the reference beam clear the spectrometer was set at  $2600\text{cm}^{-1}$  and switched to 'TD1' scan which allowed the wavenumber to remain fixed and for the chart to move at  $2.5\text{cm min}^{-1}$ . The particular wavenumber was chosen because this region is free from absorption by atmospheric water vapour and carbon dioxide, the presence of which could slow down pen response. (In order to minimise any such effects in other spectral regions the sample compartment was flushed with dry nitrogen gas at a rate of  $\sim 150\text{cm}^3\text{ s}^{-1}$ ). The pen was set on the "100%" line by means of the "100%" control which simply drives a comb into the sample beam. The reading of the voltmeter was noted and the procedure repeated for other positions of the pen achieved by closing the attenuator. Typical readings are shown in Table 2.2 and the agreement with the indicated pen position and also the long-term reproducibility can both be seen to be good.



Table 2.2 The accuracy of the zero to 10mV scale on the spectrometer. The readings "A" and "B" are on two occasions separated by about 21 months

A				B			
chart transmittance value	voltmeter reading expected 1 (mV)	voltmeter reading observed 1 (mV)	discrepance (mV)	chart transmittance value	voltmeter reading expected (mV)	voltmeter reading observed (mV)	discrepance (mV)
100.1%	10.01	9.93	-0.08	100.2%	10.02	9.99	-0.03
90.0%	9.00	8.92	-0.08	90.2%	9.02	9.01	-0.01
79.8%	7.98	7.92	-0.06	79.9%	7.99	7.99	-
70.2%	7.02	6.99	-0.03	70.0%	7.00	6.98	-0.02
59.6%	5.96	5.91	-0.05	60.1%	6.01	5.98	-0.03
48.7%	4.87	4.84	-0.03	50.0%	5.00	4.97	-0.03
40.2%	4.02	3.91	-0.03	40.1%	4.01	3.98	-0.03
30.0%	3.00	2.88	-0.12	30.1%	3.01	2.95	-0.06
20.0%	2.00	1.88	-0.12	20.0%	2.00	1.97	-0.03
10.1%	1.01	0.89	-0.11	10.0%	1.00	0.97	-0.03

The baseline was checked for the effect of stray light by placing a highly absorbing sample in the sample beam (carbon tetrachloride at  $770\text{cm}^{-1}$ ) and confirming that the pen lay on the 0% transmittance line. The balance of the ratioing amplifier was ensured by placing an opaque object in both beams and checking that the pen showed a constant position with time.

#### 2.4 Computer programmes and computing methods used

The computer processing of the data obtained from the Perkin-Elmer spectrometer was achieved using the Northumbrian Universities Multiple-Access Computer ("NUMAC"), an I.B.M. model 370/168. The Fortran IV programmes were compiled and "run" and the various files manipulated under the Michigan Time-Sharing System ("MTS").

The paper tapes with time and millivolts data encoded upon them by the Teletype (see Section 2.3) were "read-in" to the computer and various superfluous characters removed by the programme 'DCL99JAK, and the basic time and millivolts data were printed as card images into a file on a "private" magnetic disk pack. One of the series of programmes IRINT1 to IRINT6 (73) was used to perform the following functions:

- (i) the subtraction of the baseline or background;
  - this could be provided by data on a second paper tape
  - or could be a series of linearly interpolated transmittance values between the first and last data points of the sample tape,
- (ii) the calculation of the (naparian) logarithmic absorbance at each point and
- (iii) the interpolation, using the subroutine INTPOL (74) of absorbance values and conversion to output points at whole wavenumber intervals.

The output data from this programme were stored in a new file location on the magnetic disk pack from where they could be outputted onto punched cards, listed by means of a lineprinter or used as input for other programmes. One such programme was GPLOT7 which was a modified version of GPLOT3 (75) and could be used to plot the absorbance data on the I.B.M. 1627 plotter attached to the NUMAC system at Durham. The modifications in particular allowed for more absorbance scales (zero to 0.1, 0.2 or 0.5) and for the plotting of several sets of data of different lengths with different starting wavenumbers on the same chart. The implications of the choice of baseline or background are discussed further in Section 4.10.

## 2.5 Sampling methods and techniques used in the mid-infrared

One of the chief objects of this work was to obtain the profile of the  $\nu_s$  (OH) or  $\nu_s$  (OD) absorption band of phenol and its deuterated analogue  $C_6H_5OD$  when the phenol is in a hydrogen-bonded complex with various bases in a solvent. In order to perform a detailed analysis of the bandshape it must be accurately defined: the absorbance must be determined at as many wavenumbers as possible, the spectral background must be accurately subtracted to remove the effects of any other bands in the solvent or base in the same region and to give an accurate bandshape in the spectral "wings" and the bandshape must also be free from any distortion produced by a finite spectral slitwidth.

There are basically two sampling methods appropriate; these will be called Method A and Method B. It was hoped to find the better method in terms of experimental convenience and accuracy and precision of results.

Method A. In this method two solutions are made up; one contains the sample (in this case phenol with excess base in the solvent) and the other is a background solution (containing in this case base and solvent). Using two cells (for details see below) with spacers matched

to give as near as possible the same pathlength in each cell, the spectrum is recorded with a cell containing sample solution in the sample beam and the cell containing reference solution in the reference beam.

Method B. Using the two solutions as before but with only one cell the spectrum of each solution in turn is recorded. Any absorptions present in the base or solvent can be ratioed out using the computer programme described above.

The disadvantages of Method A are that the cell pathlengths must be matched almost exactly (this is fairly easily achieved at relatively long pathlengths (over 100 $\mu$ m) but can be very difficult at very short (e.g. 10 $\mu$ m) pathlengths) and also that a baseline must be introduced in order to compute absorbance values. The baseline can be either interpolated between the "ends" of the band, as described above, or can be provided by a second paper tape which contains transmittance values obtained when the spectrometer is scanned over the region of interest with the "background" solution in both sample and reference beams. The main advantages are that if the "computed" background is used, the time to obtain a spectrum is halved relative to Method B and also that short term variations in the accuracy of the spectrometer or recording system are not so important as in Method B. This is the chief disadvantage of Method B; any change in the spectrometer system (for example the moisture present in the cell-box through which both beams pass) between the recording of the two spectra will result in an error in the computed absorption band profile.

Standard Beckman F-01 cells were used throughout; these are of a demountable type and were fitted with potassium bromide or calcium fluoride windows and employed "teflon" or "melinex" spacers.

## 2.6 Introduction to far-infrared spectroscopy

The far-infrared region of the electromagnetic spectrum can be defined as that region of frequencies between  $500\text{cm}^{-1}$  ( $20\mu\text{m}$ ,  $15\text{THz}$ ) and  $3\text{cm}^{-1}$  ( $3 \times 10^5\mu\text{m}$ ,  $90\text{GHz}$ ). Both these limits are extremely arbitrary, the higher one is approximately the lower limit of the range of conventional "infrared" grating spectrometers and the lower one the lower limit of the interferometric spectrometers which are often used in this far-infrared region. There is much to be gained by extending this lower limit towards the "microwave" region (see Section 2.10).

The far-infrared spectral region is of great importance in the study of hydrogen bonded systems because it is in this region that the intermolecular modes of vibration of a hydrogen bonded complex may be expected to occur for all but very strongly bonded complexes (see Section 1.2).

In the far-infrared region instrumental factors very severely influence the design of an efficient spectrometer. Sources which emit the major part of their radiation in this region are unknown and detectors are of the type which react to the total power of all radiation falling upon them. For these, and other, reasons an interferometric spectrometer is very often used for investigations in this spectral region. These instruments are basically Michelson interferometers and consist of a source the radiation from which is divided into two beams by a beamsplitter and, after reflection by two plane mirrors, interference between the two beams takes place and the recombined beam is presented to the detector (see Figure 2.2). By variation of the difference between the paths of the two beams an interferogram (see Figure 2.3) as a plot of intensity against path-difference can be obtained and by Fourier transformation a plot of intensity against frequency for the radiation reaching the detector can be produced.

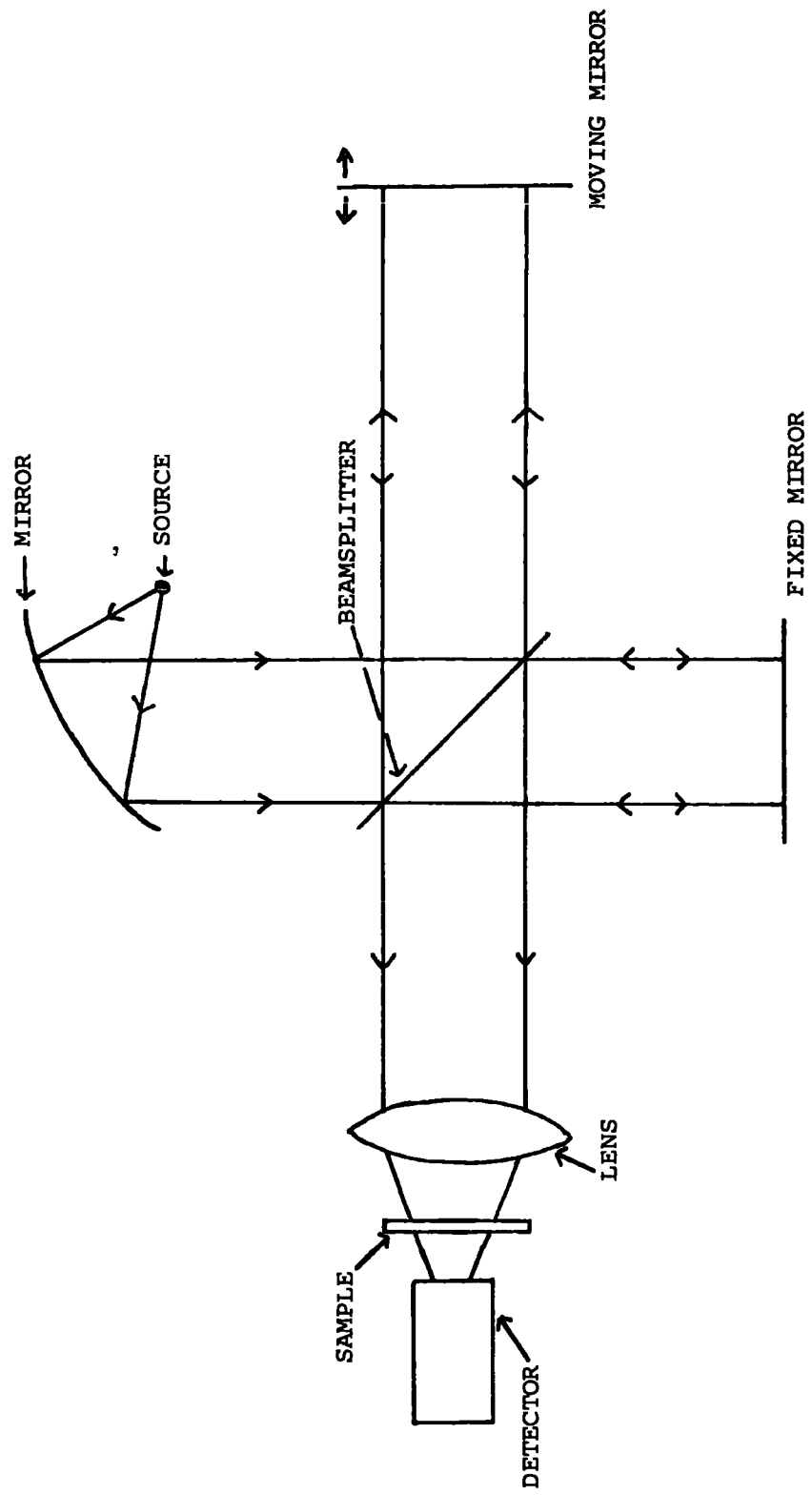


Figure 2.2 A schematic diagram of a spectrometer based on a Michelson interferometer.

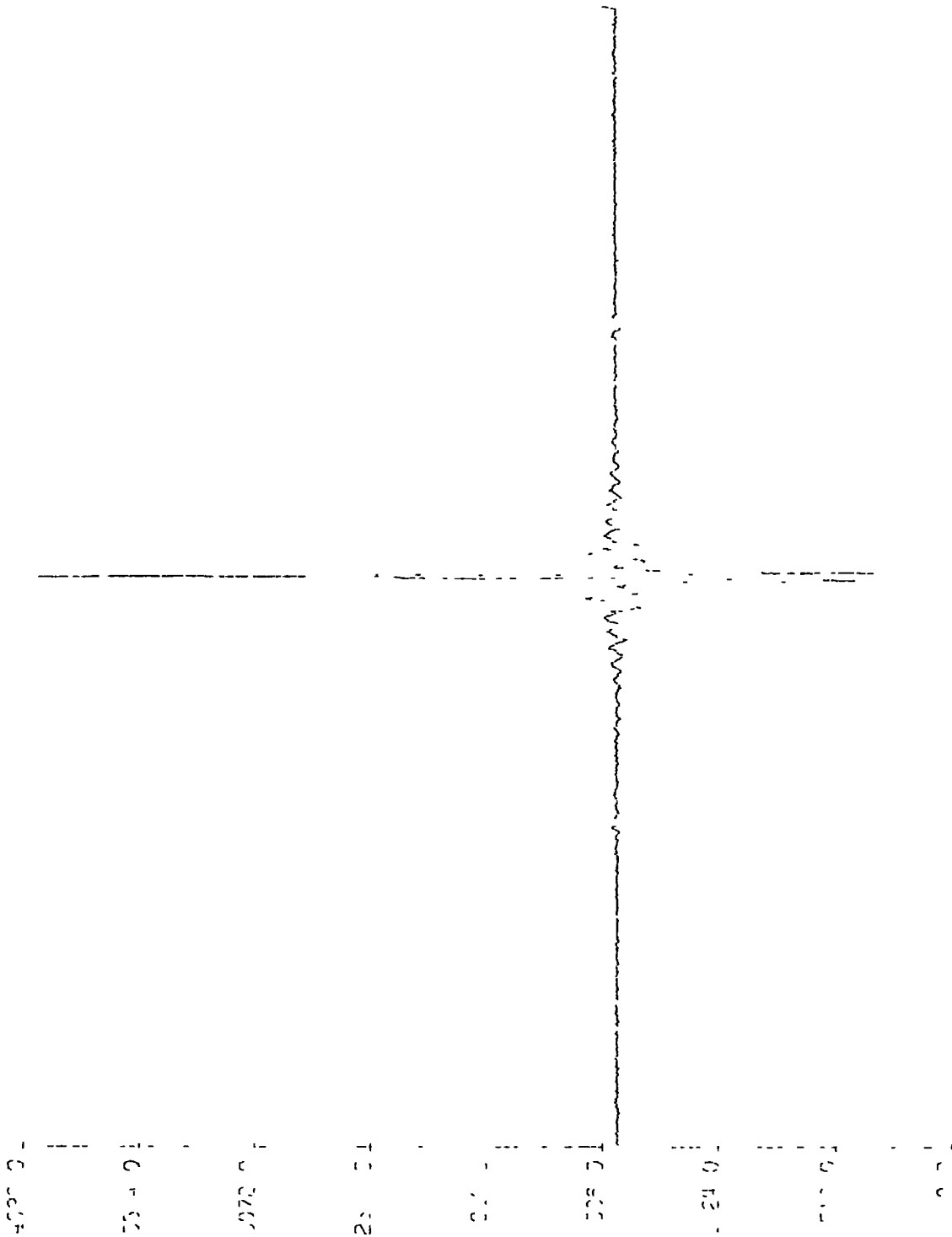


Figure 2.3 A typical interferogram. A vertical axis represents intensity of radiation reaching the detector and the horizontal axis represents mirror movement. The maximum intensity corresponds to zero path difference.

In simple terms, the polychromatic radiation reaching the detector is analysed for its intensity at each frequency by the process of division by the beamsplitter, variation of the path-difference between the divided beams and recording and finally Fourier transforming an interferogram. The mathematics of the process have been dealt with in all books on the subject, particularly those by Bell (76), Möller and Rothschild (77) and Chantry (78) and elsewhere (75,79). No attempt will be made here to reproduce this theory but in the following sections the particular interferometer used to obtain far-infrared spectra will be described and various points in the theory with important experimental implications will be emphasised.

## 2.7 The Beckman-R.I.I.C. FS-720 interferometric spectrometer

The Beckman-R.I.I.C. FS-720 spectrometer is basically a Michelson interferometer. The source is a mercury discharge lamp which emits broadband radiation between  $\sim 2\text{cm}^{-1}$  and  $\sim 1000\text{cm}^{-1}$ , the beamsplitter is made from polyethylene terephthalate ("melinex"), the optical path-difference is varied by moving one mirror with an electric motor and the sample is placed immediately before the detector which is a Golay cell. A full description is given in the manufacturer's manual (79). The peripheral equipment comprised a Beckman FS-200/7 electronics package and an Addo paper-tape punch. This has also been described elsewhere (75). The interferometric data were recorded on paper tape at fixed increments of path-difference and were read-in to the NUMAC computer where they could be stored on magnetic disk as card images.

The Fourier transformation and various other data-manipulation operations were carried out using the computer programme FTRAN5 which was a development of the programme FTRAN4 (75) and functioned in essentially the same manner.



## 2.8 Aspects of interferometry theory with important experimental implications

### (i) Beamsplitter considerations

The melinex sheets used as beamsplitters varied in thickness between  $3.5\mu\text{m}$  (15 gauge) and  $100\mu\text{m}$  (400 gauge). This material is chosen because it has the property of transmitting approximately 50% and reflecting approximately 50% of the incident radiation. However, these beamsplitters have the disadvantage that thin-film interference takes place within them (this is not to be confused with the interference which occurs between the recombined beams) and the energy reaching the detector has maxima and minima at particular frequencies. These "hooping" patterns are shown in Figure 2.4. Obviously this effect is of crucial importance when obtaining spectra since each beamsplitter will have certain frequencies at which little or no energy is allowed to reach the detector. The frequency range over which absorbance data are required must be first considered and often two or more beamsplitters must be used to obtain data over a complete range of frequencies.

These problems were to some extent eliminated when the instrument was converted to operate as a polarising interferometer (see Section 2.10).

### (ii) Aliasing

The interferogram output from the Beckman FS-720 instrument was digitised and punched onto paper tape at particular intervals of mirror movement ranging from  $4\mu\text{m}$  to  $64\mu\text{m}$  (for precise details see ref. (75)). It can be shown mathematically (see ref. (76), Chapter 7) that if the sampling interval is  $\Delta\delta$  (in cm) the computed spectrum will repeat every  $\Delta\sigma$   $\text{cm}^{-1}$ , where  $\Delta\sigma = (\Delta\delta)^{-1}$ . When negative frequency values are considered (they are mathematically as significant as positive values) the problem also arises that the negative values of one spectrum may overlap with the positive

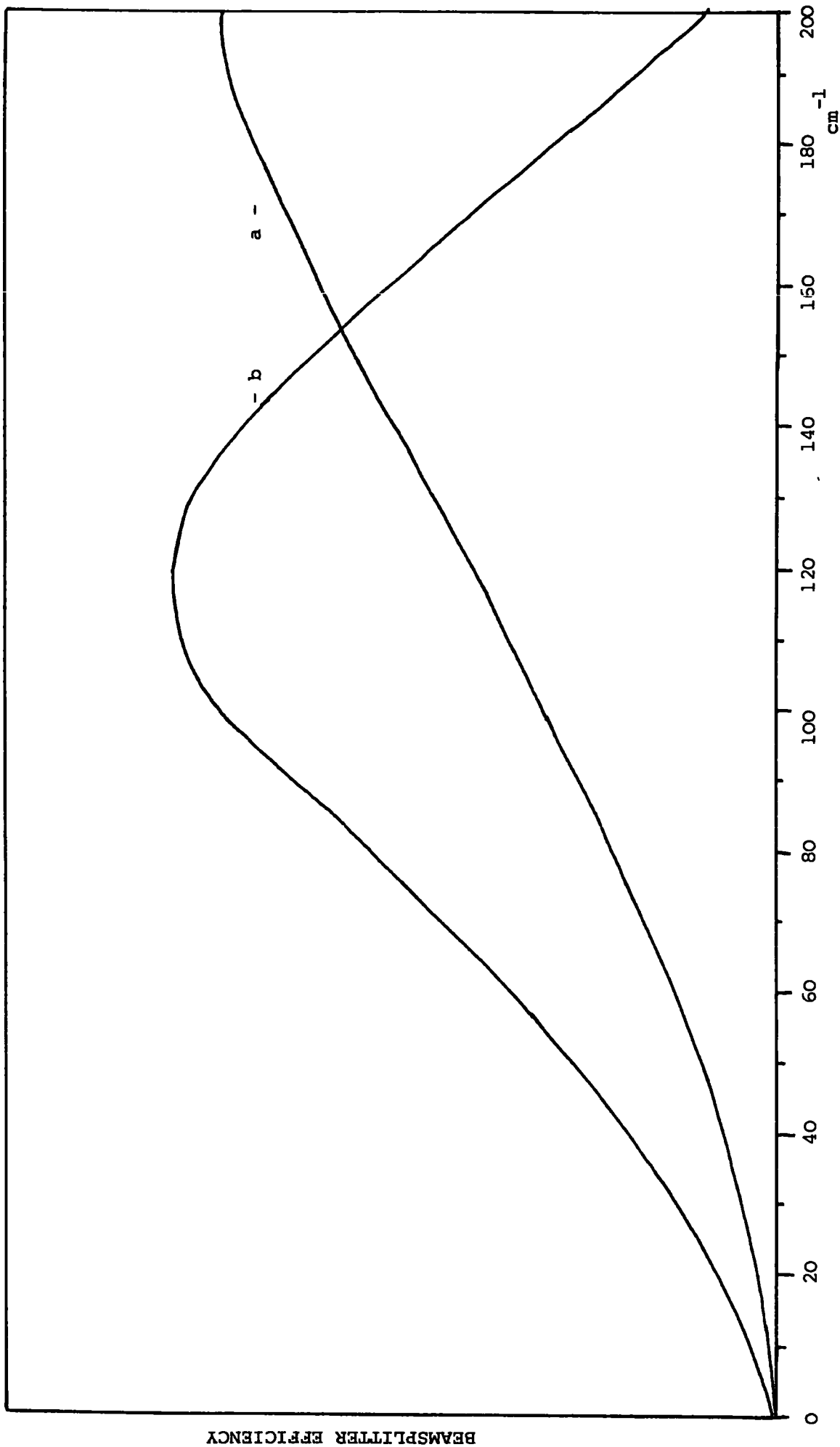


Figure 2.4 Theoretical "hooping" patterns for the interferometer beamsplitters. The two curves are for (a) a 25 gauge (6μm) and (b) a 50 gauge (12μm) beamsplitter.

values of the adjacent spectrum. This phenomenon whereby the spectrum repeats every  $\Delta\sigma$  wavenumbers is known as aliasing. The problem must be avoided by preventing radiation of frequency greater than  $\sigma_{\max}$ , where  $\sigma_{\max} = \frac{1}{2} \Delta\sigma$ , from reaching the detector. This prevents any frequencies, positive or negative, from higher-order spectra interfering with the real spectrum in the region 0 to  $\sigma_{\max} \text{ cm}^{-1}$ . The frequency  $\sigma_{\max}$  is called the aliasing frequency and if the sampling interval is increased the aliasing frequency decreases.

When interferograms were recorded these high frequencies were eliminated by use of various filters. A thin sheet of polyethylene impregnated with carbon black was used to eliminate frequencies above  $625 \text{ cm}^{-1}$  (the aliasing frequency for a sampling interval of  $8 \mu\text{m}$ ) and various other filters could also be used for lower cut-off frequencies.

#### (iii) Autocorrelation, resolution and apodisation

When the interferogram is digitised it is very unlikely that a data point will fall precisely at the grand maximum of the interferogram and the digitised interferogram will therefore be very likely to be asymmetric. This is corrected by autocorrelation, i.e. convolution of the interferogram with itself. This has the effect of symmetrising the data. The cosine Fourier transformation is then performed on one half of this interferogram and the theoretical resolution (R) obtained can be shown (see ref. (76), Chapter 6) to be given by  $R = (2L)^{-1}$  where L is the mirror movement corresponding to the number of points which are contained in the half-interferogram which is transformed. The computer programme FTRAN5 can deal only with interferograms of  $2^N$  points so tapes of approximately 256, 512, 1024 etc. points were produced and the programme could "pad" or truncate these as necessary.

The resolution actually obtained was poorer than that given above because an operation called apodisation is also performed upon the digitised interferogram. This is necessary because in practice data can only be collected over finite mirror movements (whereas theory assumes infinite movement) and no matter how small the modulation in the interferogram is at the extremes this truncation of data produces the equivalent of a "spike" at each end of the interferogram which if transformed would lead to spurious features in the absorbance spectrum. To overcome this problem a convolution with an apodising or smoothing function is employed and the particular one used by FTRAN5 is

$$\text{APOD}(k) = \cos^2(k\pi/N)$$

where  $N$  is the total number of points in the interferogram and  $k$  takes values from unity to  $N$  in an order such that the function  $\text{APOD}(k)$  decays smoothly from unity at the interferogram maximum ( $k = N/2$ ) to zero in each wing ( $k = 1$  and  $N$ ). The effect of apodisation is also to worsen the resolution somewhat, a factor of two is often assumed (see ref. (77), p.135).

## 2.9 Advantages and disadvantages of interferometric over grating spectrometers

Because of the limitations imposed by the sources and detectors available in the far-infrared (see above) and because of the difficulties in scattering long wavelength radiation grating spectrometers for this region tend to have poor performance. For this reason the interferometric technique is generally adopted, especially since digital computers have become faster and cheaper. The interferometric method however has two inherent advantages over the dispersive; these are known as the Fellgett Advantage and the Jacquinot Advantage.

The first term relates to the fact that a Michelson interferometer is a multiplex system, that is, all spectral frequencies are observed for the whole observation time and therefore (see ref. (78), p. 15) an

improvement in signal-to-noise ratio by a factor of  $\sqrt{N}$  ( $N$  = number of spectral elements equal to the resolution) results. It is important to note that this is true only if the instrument is detector-noise limited (i.e. the origin of most noise is the detector and not the source); if the instrument is source-noise limited the dispersive system is better because only noise at the frequency of observation at any time will be of significance.

The second term relates to the fact that an interferometer has a high energy throughput; it is not limited by the narrow dimensions of the spectral slit in a grating instrument. The size of the beams is limited only by the mirror size (about 7cm in the FS-720) and so large solid-angles at source and detector are possible.

The outcome is that an interferometer can provide high quality spectra in the far-infrared, low noise and high signal being provided as explained above. The resolution can be very high (see ref. (75), pp. 93-112) and can be varied by changing the maximum path-difference employed.

The disadvantages are due to the computation time and expense and the fact that the absorbance spectrum cannot be observed as the instrument records data. Recent developments in small computers could very well significantly reduce all these disadvantages very soon.

#### 2.10 Modifications made to the standard FS-720 interferometer

The instrument used to obtain the far-infrared spectra described in Chapter 5 had been modified in certain ways chiefly to improve its performance at low frequencies. The standard Golay detector has a low frequency limit of about  $20\text{cm}^{-1}$  and in order to obtain spectra at lower frequencies than this it could be replaced by an antimony-doped single crystal germanium bolometer which operated at 1.5K. This temperature was obtained by housing the bolometer below an Oxford Instrument MD800 detector

cryostat which was filled with liquid helium, the pressure over which was reduced to about  $4.8 \times 10^2 \text{ Nm}^{-2}$ . Full details can be found elsewhere (75,80), but it should be noted that the instrument gave much improved spectra over a range from  $\sim 5\text{cm}^{-1}$  to  $\sim 200\text{cm}^{-1}$ .

The instrument could also be adapted to operate as a polarising interferometer in the way originally described by Martin and Puplett (81). Full details can again be found elsewhere (80) and it should be sufficient to say here that the energy throughput is improved by using a wire-grid beamsplitter which eliminates to some extent the problem of "hooping" described above and also the energy wastage in a conventional interferometer where one half of the source energy is reflected straight back to the source by the dielectric beamsplitter.

The polarising system when used in conjunction with the low-temperature detector provided an instrument with a useful range of  $\sim 2\text{cm}^{-1}$  to  $\sim 100\text{cm}^{-1}$ . An instrument background is shown in Figure 2.5.

In order to take advantage of the low frequency performance of the interferometer the electronic system was modified to provide sampling intervals of  $16\mu\text{m}$ ,  $32\mu\text{m}$  and  $64\mu\text{m}$ , giving aliasing frequencies of  $313\text{cm}^{-1}$ ,  $156\text{cm}^{-1}$  and  $78\text{cm}^{-1}$  respectively. Suitable filters were used in each case to absorb energies above the particular aliasing frequency.

### 2.11 Sampling methods and techniques used in the far-infrared

Since an interferometric spectrometer is by nature a single-beam instrument, ratioed spectra can only be obtained by one method (cf. Section 2.5). The "sample" and "background" single-beam spectra are recorded separately with the whole instrument evacuated to remove interferences from atmospheric water vapour and carbon dioxide. They are then ratioed by the computer programme FTRANS after Fourier transformation etc. At this stage the effects of the beamsplitter's absorption spectrum and any filters are ratioed-out. The output data of absorbance values and wavenumbers could

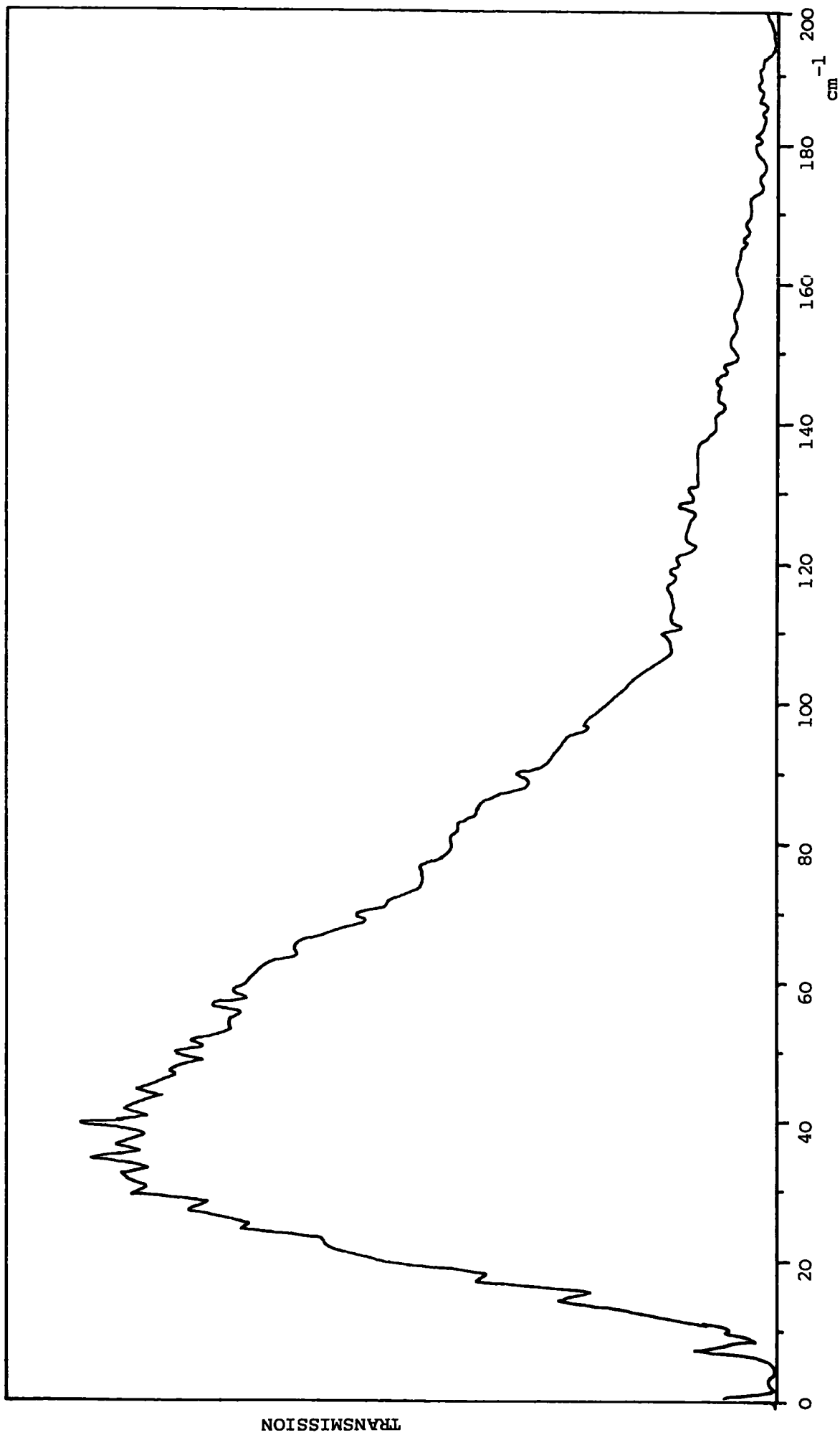


Figure 2.5 The instrument background for the polarising interferometer (computed at Queen Mary College, London).

be outputted on punched cards or stored as card images on the private magnetic disk pack. A computer programme, DCHO512, was available to calculate band intensities and provide data output at whole wavenumber intervals (FTRAN5 provides output at intervals of fractions of the spectral resolution).

Standard Beckman FS-03 demountable cells fitted with "polythene" windows and "teflon" spacers were used throughout.



CHAPTER THREE

THEORY OF VIBRATIONAL RELAXATION IN A HYDROGEN BONDED  
COMPLEX

### 3.1 Introduction

In this chapter the theory developed by Robertson and Yarwood (60) to explain the broadening on hydrogen bond formation of  $\nu_s$  (XH) bands in the infrared is described in some detail. The spectral data obtained are analysed in terms of this model in Chapter 4 and Chapter 5.

This particular model was chosen chiefly for the following reasons. Firstly, the predicted infrared absorption band can have both gaussian and lorentzian character and this is in concordance with the observed bandshapes which are demonstrably (60) of intermediate bandshape. The reason for this prediction is that the model makes no "slow modulation limit" approximation as does the model of Bratos (see Section 1.3) with which it shares several common features. Secondly, the chosen model is described by parameters which should be sensitive to chemical and physical changes (deuteration, change of solvent, temperature and so on) and which can be obtained from the experimentally-obtained band profile by least-squares fitting. One further advantage is that predictions about the far-infrared absorption of a complex (due to the  $\nu_\sigma$  (XH---Y) mode) may be made along with the effect of the hydrogen bonding on the neutron inelastic scattering spectrum of the proton donor and acceptor molecules.

An attempt was made to relate the Rösch and Ratner (46) model to experimental data for the phenol-acetonitrile complex in carbon tetrachloride with varying concentrations of acetonitrile. This proved unfruitful largely because certain parameters in the model have no ready physical interpretation. If further work on this problem were to yield meaningful results the comparison with the model of Robertson and Yarwood would be very interesting.

### 3.2 A description of the hydrogen bonding model

The model is of a semi-classical type and assumes that the phase relaxation of the  $\nu_s(XH)$  mode of the complex takes place indirectly through coupling with the  $\nu_\sigma(XH---Y)$  mode which is in close energetic contact with its solvent environment. It is therefore an indirect relaxation model similar to that of Bratos (56) rather than one involving direct relaxation as is the model of Rbsch and Ratner (62).

For a linear complex of the type X-H---Y coupling between the  $\nu_s(XH)$  and  $\nu_\sigma(XH---Y)$  modes is proposed and, if Fermi resonance is excluded and in the absence of other strong interaction between the X-H---Y system and other parts of the complex and the solvent, the hamiltonian for the system in the harmonic oscillator approximation can be written as:

$$\hat{H}_0 = \hat{H}_1 + \hat{H}_2 + V_{12} \quad (3.1)$$

where

$$\hat{H}_1 = \frac{p_1^2}{2m_1} + \frac{1}{2} m_1 \omega_1^2 r_1^2 \quad (3.2)$$

and

$$\hat{H}_2 = \frac{p_2^2}{2m_2} + \frac{1}{2} m_2 \omega_2^2 r_2^2 \quad (3.3)$$

that is, as a sum of a kinetic energy term and a potential energy term.

In these expressions  $p$  represents momentum,  $m$  reduced mass,  $\omega$  angular frequency and  $r$  a normal coordinate. The subscripts "1" and "2" refer to the  $\nu_s(XH)$  and  $\nu_\sigma(XH---Y)$  vibrational modes respectively. The coupling term  $V_{12}$  is given by

$$V_{12} = K_{112} r_1^2 r_2 \quad (3.4)$$

where  $K_{112}$  is an anharmonic force constant.

By taking advantage of the large difference in the periods of vibration of the two modes which are coupled the two modes may be adiabatically separated and for an isolated gas-phase complex the absorption spectrum may be calculated (53,82). This is achieved by averaging the rapid motion over the period of oscillation of the slow motion. In the liquid phase this is no longer appropriate because Fourier transformation of observed infrared absorption bands of complexes has indicated (60) a transition dipole correlation time of about 0.2ps for the  $\nu_s(XH)$  vibrational mode. This is similar to the period of vibration of the  $\nu_\sigma(XH---Y)$  mode and therefore the phase coherence of the  $\nu_s(XH)$  mode is not preserved for a sufficiently long time for this averaging to be appropriate. The model therefore assumes that the nature of the low frequency mode is determined by its interaction with the solvent rather than by coupling. The  $\nu_\sigma(XH---Y)$  mode is therefore described as an oscillator undergoing brownian motion and which perturbs a quantum-mechanical harmonic oscillator which represents the  $\nu_s(XH)$  vibrational mode.

According to the theory of brownian motion (83,84) it is assumed that the displacement coordinate  $r_2$  for the  $\nu_\sigma(XH---Y)$  mode obeys the Langevin equation

$$\ddot{r}_2 + \gamma \dot{r}_2 + \omega_2^2 r_2 = m_2^{-1} F(t) \quad (3.5)$$

where  $\gamma$  is a damping parameter which ought to be related to the nature of the solvent and  $F(t)$  is a random force which the complex experiences. Following the method of Kubo (85) it is taken to be a gaussian random variable. In other words the coordinate  $r_2$ , and therefore  $\omega_2$ , varies in a random fashion with time and through the cubic coupling term,  $V_{112}$ ,  $\hat{H}_1$  becomes time-dependent.

By making certain assumptions (60) it is then possible to obtain an expression for the molecular dipole moment autocorrelation function,  $\phi(t)$ , which is:

$$\phi(t) = \exp \left\{ -a^2 \langle r_2^2 \rangle \omega_2^{-2} \left[ \gamma t + \omega_2^{-2} \left( (\gamma^2 - \omega_2^2) (e^{-\frac{1}{2}\gamma t} \cos \bar{\omega}^2 t - 1) + (\gamma/2\bar{\omega}) (\gamma^2 - 3\omega_2^2) e^{-\frac{1}{2}\gamma t} \sin \bar{\omega} t \right) \right] \right\} \quad (3.6)$$

where

$$\bar{\omega}^2 = \omega_2^2 - \gamma^2/4$$

in the periodic case. In accordance with the fluctuation-dissipation theorem (86) an expression for the bandshape,  $I(\omega)$ , of the  $\nu_s$  (XH) absorption band can now be obtained by Fourier transformation of Equation 3.6:

$$I(\omega) = (\omega/2\pi) [1 - \exp(-h\omega/kT)] \int_{-\infty}^{\infty} \exp[i(\omega - \omega_1)t] \phi(t) dt \quad (3.7)$$

### 3.3 The prediction of a slow and a rapid modulation limit

The model described above is a particular example of frequency modulation of an oscillator by a gaussian random process and such processes have been discussed in general terms by Kubo (85). Following Kubo's theory two new parameters are now defined: the first is  $\Delta$ , the amplitude of modulation, which is in this case the root mean square variation of the randomly fluctuating angular frequency of the low frequency vibrational mode. The second parameter is  $\tau_c$ , called the characteristic time of the modulation and is given by the expression

$$\tau_c = \int_0^{\infty} \phi(t) dt. \quad (3.8)$$

In this particular case it can be shown that  $\Delta$  is given by

$$\Delta = a \langle r_2^2 \rangle^{1/2} \quad (3.9)$$

where

$$a = K_{112}/m_1 \omega_1 \quad (3.10)$$

and  $\tau_c$  is given by

$$\tau_c = \gamma/\omega_2^2 \quad (3.11)$$

The expression developed for  $\phi(t)$  may be approximated at short times to

$$\phi(t) = \exp\left(-\frac{1}{2} \Delta^2 t^2\right) \quad (3.12)$$

and at long times to

$$\phi(t) \approx C \exp(-\Delta^2 \tau_c t) \quad (3.13)$$

where  $C$  is a constant. Following the method of Kubo it can be shown that on Fourier transformation the above expressions generate functions,  $I(\omega)$ , which show respectively a gaussian and a lorentzian bandshape. Moreover, these expressions for  $\phi(t)$  will be good approximations for all times if the conditions  $\tau_c \Delta \gg 1$  and  $\tau_c \Delta \ll 1$  respectively are satisfied.

The damping of the  $\nu_\sigma$  (XH---Y) motion is controlled, in the terms of this model, by the quantity  $\gamma/2\omega_2$ ; overdamping occurs when  $\gamma > 2\omega_2$ , underdamping when  $\gamma < 2\omega_2$  and the situation when  $\gamma = 2\omega_2$  corresponds to critical damping. On a molecular level overdamping can be envisaged as the case when the interaction between solvent and complex is strong and the  $\nu_\sigma$  (XH---Y) mode is severely perturbed by the solvent. In this situation the random force of the Langevin equation is large. Underdamped motion corresponds to a situation where the solvent interacts little with the complex and the limit when  $\gamma = 0$  would correspond to an isolated, gas-phase, complex. It must be understood that the model does not attempt to describe this situation and the previous assumptions made would be inappropriate to a gas-phase complex.

Returning now to consider the shape of the predicted absorption band; the overdamped and critically damped cases will be examined first. In this situation Kubo's theory may be used in its original form and  $\tau_c$  may be considered as a genuine correlation time and not as the more general "characteristic" time mentioned above (see refs. (60) and (85)). The quantity  $\tau_r$  is now introduced as the transition dipole moment relaxation time of the  $\nu_s$  (XH) oscillator and it is given by

$$\tau_r^{-1} = \tau_c \Delta^2 \quad (3.14)$$

According to Kubo the expression (4.4) applies at all times if  $\tau_c \Delta \gg 1$  and this corresponds to the case where  $\tau_c \gg \tau_r$  (for small  $\Delta$ ). In other words the relaxation time of the oscillator is very short compared with the correlation time of the stochastic modulation. During the relaxation time of the oscillator the solvent environment is effectively static and the bandshape predicted for the  $\nu_s$  (XH) absorption band reflects not the dynamics of the environment but only the quasi-static distribution of the molecules. The bandshape is thus gaussian since this is the distribution first assumed and the situation is called the slow modulation limit.

If  $\tau_c \Delta \ll 1$ , corresponding to  $\tau_c \ll \tau_r$ , the relaxation time of the oscillator is long compared with the correlation time of the modulation and during the period of relaxation the solvent environment no longer remains static. The dynamics of the solvent environment are reflected in the bandshape which is lorentzian. This is the rapid modulation limit which is also known as the situation of "motional narrowing". (See also Figures 3.1 and 3.2.)

It should also be noted that the slow modulation limit could arise from strong coupling between the  $\nu_s$  (XH) and  $\nu_\sigma$  (XH---Y) modes. This can be shown to be true by writing (3.11) as

$$\tau_c \Delta = \gamma \Delta / \omega_2^2 \quad (3.15)$$

or as

$$\tau_c \Delta = (\gamma / 2\omega_2) (2\Delta / \omega_2) \quad (3.16)$$

Thus, for a given damping situation with  $\gamma$  and  $\omega_2$  fixed,  $\tau_c \Delta$  can only be large if  $\Delta$  is large and via (3.9) and (3.10) the mode-mode coupling constant is large.

It is when the underdamped case is considered that it becomes necessary to refer to the quantity  $\tau_c$  as a characteristic time of modulation because here Kubo's theory can not be applied exactly. This is because although the expressions (3.12) and (3.13) are valid at short and long times

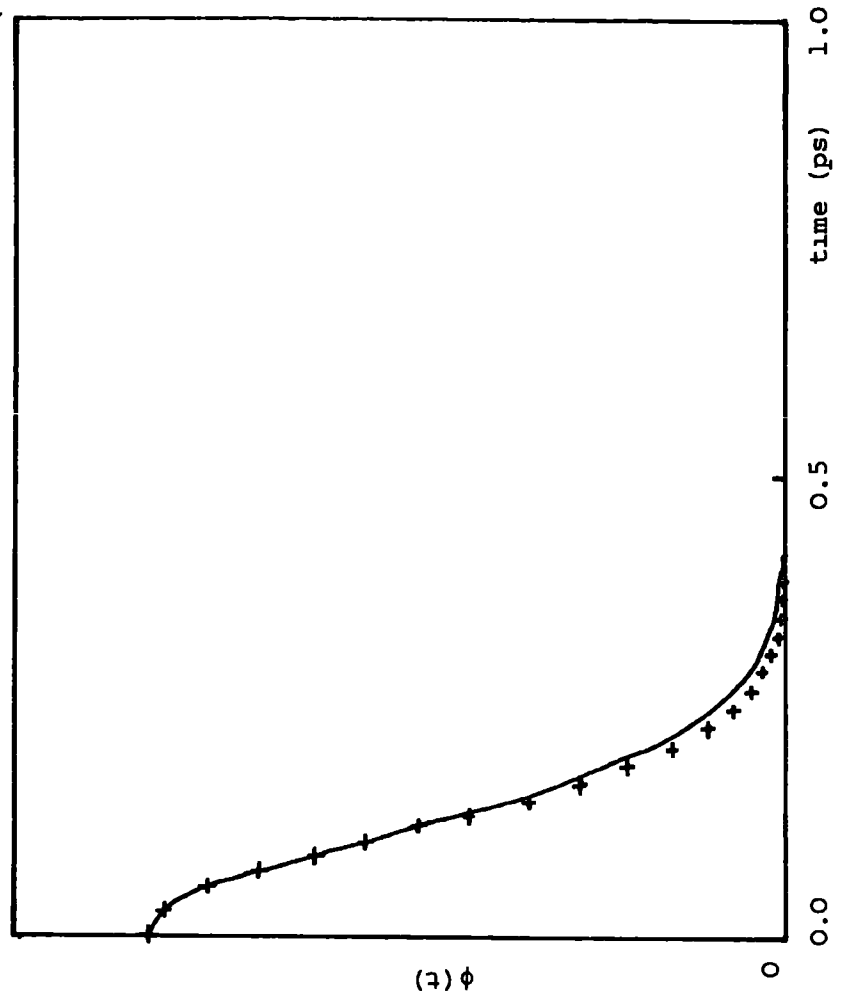


Figure 3.1b

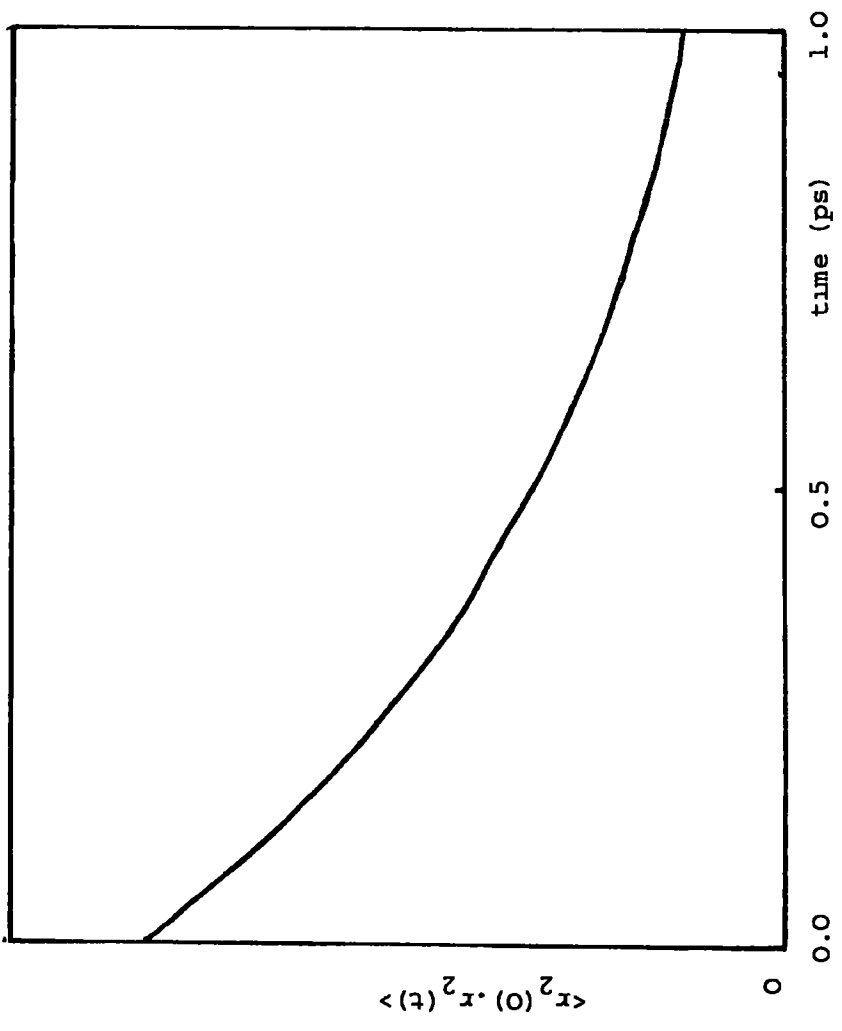


Figure 3.1a



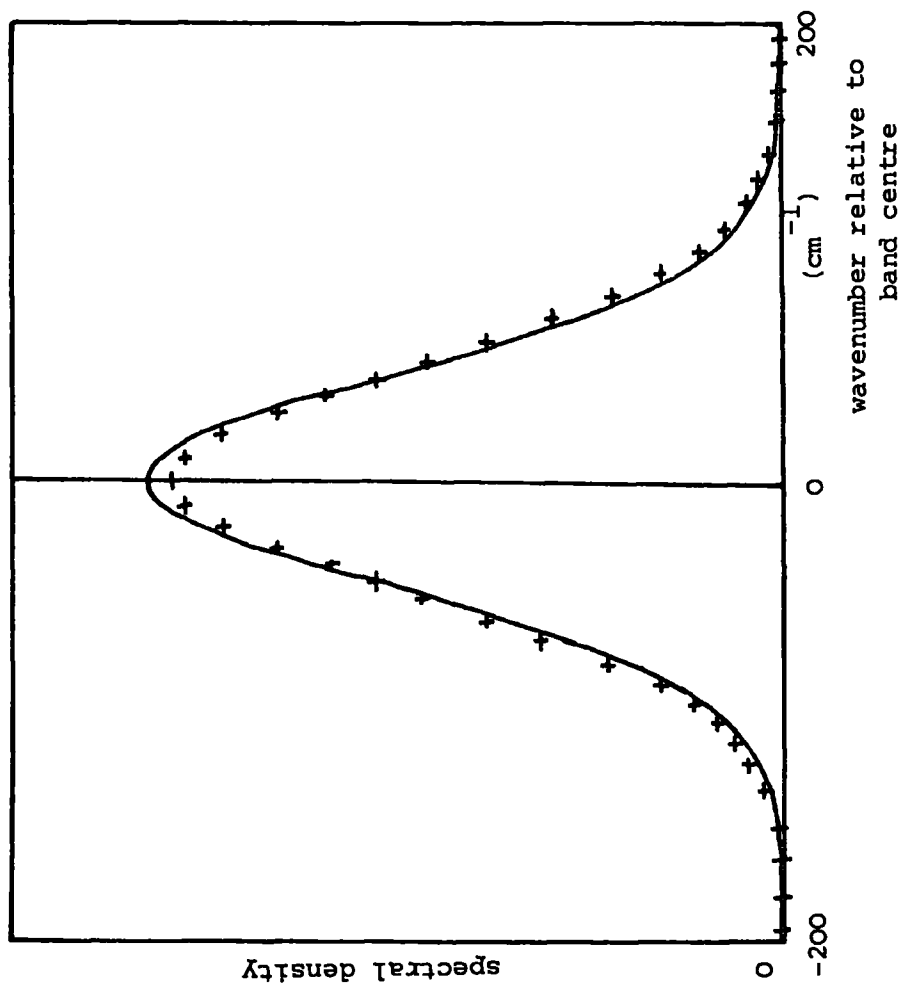


Figure 3.1c

Figure 3.1

Figures 3.1a, 3.1b and 3.1c show respectively the autocorrelation function  $\langle r_2(0) \cdot r_2(t) \rangle$  of the  $\nu_g(XH---Y)$  displacement coordinate, the autocorrelation function  $\phi(t)$  of the  $\nu_s(XH)$  transition dipole moment and the spectral density of  $\phi(t)$ . A gaussian function is shown for comparison in (b) and (c) by crosses. In this case the  $\nu_g(XH---Y)$  motion is heavily overdamped with  $\gamma_g/2\omega_g = 5$  and  $\tau_c \Delta = 5$ . It can be seen that the autocorrelation function in (b) decays much more quickly than in (a) and that the spectral density is almost gaussian.

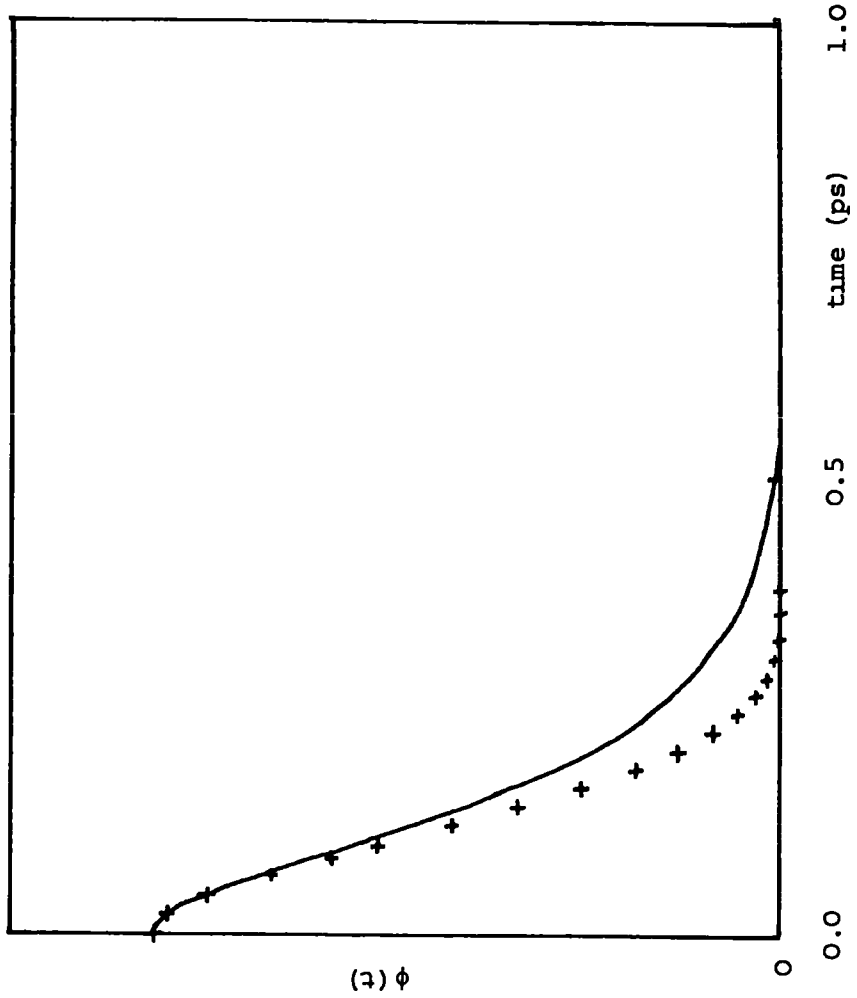


Figure 3.2b

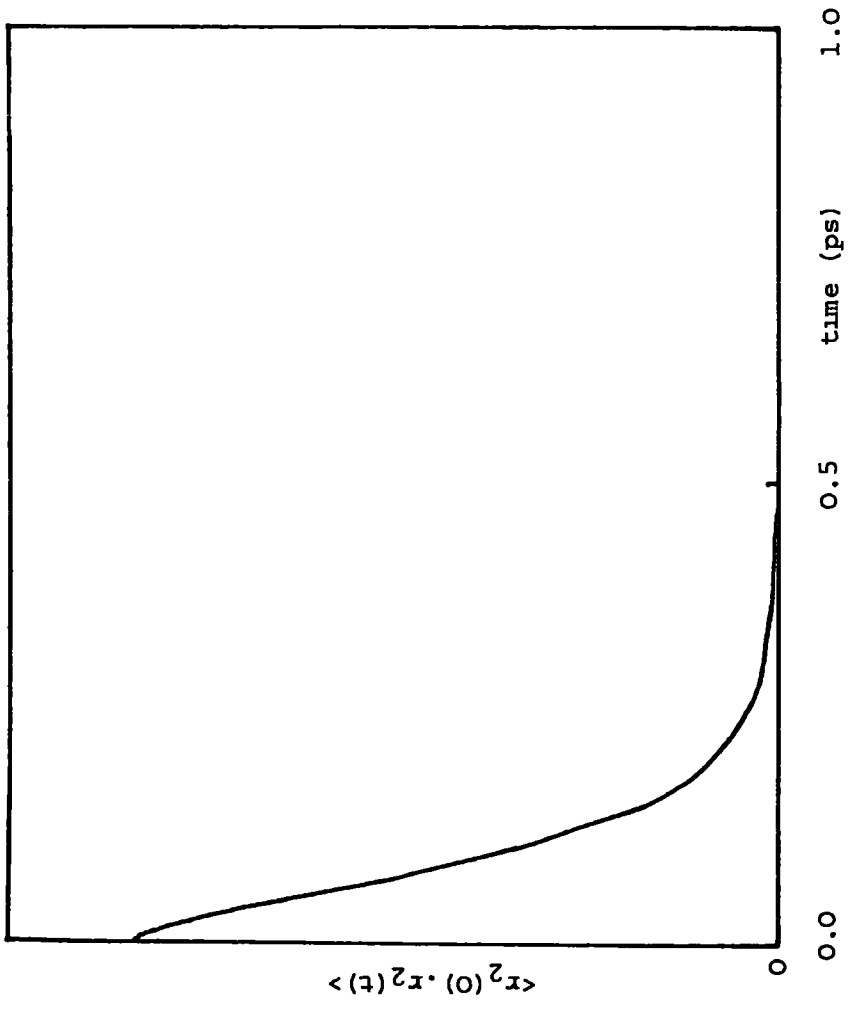


Figure 3.2a

Figure 3.2 Figures 3.2a, 3.2b and 3.2c show the same functions as Figure 3.1 with the  $\nu_{\sigma}$  (XH---Y) motion critically damped and  $\gamma/2\omega_2 = 1$  and  $\tau_c \Delta = 1$ . It can be seen that the two autocorrelation functions decay at similar rates and that the spectral density deviates considerably from the pure gaussian.

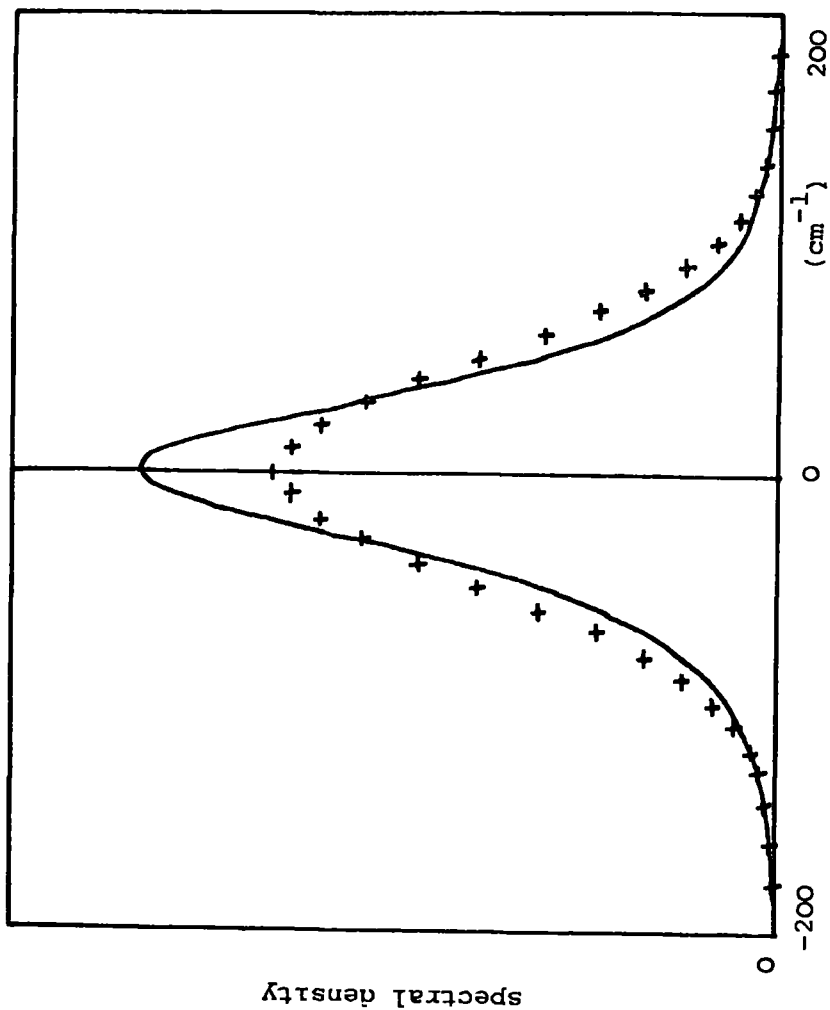


Figure 3.2(c) wavenumber relative to band centre

respectively there is an intermediate region during which the function  $\phi(t)$  does not decay smoothly and does in fact contain Fourier components of  $\omega_2$ . The corresponding  $I(\omega)$  spectrum has shoulders corresponding to frequencies  $\omega_1 \pm \omega_2$ ,  $\omega_1 \pm 2\omega_2$  etc. which when  $\gamma$  becomes very small appear as partially-resolved sub-bands and when  $\gamma = 0$  are actually present as separate spectral lines which have intensity relative to the central line determined by the value of  $\Delta/\omega_2$ . This situation is similar to that considered in the theory of Maréchal and Witkowski (41-43, 47, 48) but as emphasised above the theory described here is not applicable to a complex in the gas phase and moreover this is a semi-classical theory and that of Maréchal and Witkowski is fully quantum mechanical.

Aside from the prediction of these satellite lines the theory of Robertson and Yarwood does predict a gaussian bandshape in the underdamped case when  $\tau_c \Delta$  is large and as  $\gamma/2\omega_2$  decreases at constant  $2\Delta/\omega_2$  an initial change to a lorentzian shape can be observed before any shoulders or sub-bands begin to appear. (See also Figure 3.3.)

If the criterion for slow modulation  $\tau_c \Delta \gg 1$  is rewritten as

$$(\gamma/2\omega_2) (2\Delta/\omega_2) \gg 1 \quad (3.17)$$

or for rapid modulation

$$(\gamma/2\omega_2) (2\Delta/\omega_2) \ll 1 \quad (3.18)$$

it can be seen that the possible cases are:

(i) if the motion is overdamped ( $\gamma/2\omega_2 > 1$ ) then slow modulation can occur if  $\Delta$  is large or moderate, rapid modulation is only possible if  $2\Delta/\omega_2$  is small, corresponding to very weak mode-mode coupling.

(ii) for overdamped motion ( $\gamma/2\omega_2 < 1$ ) rapid modulation is possible if  $2\Delta/\omega_2$  is small or moderate but slow modulation is only possible if  $2\Delta/\omega_2$  is large, corresponding to very strong mode-mode coupling.

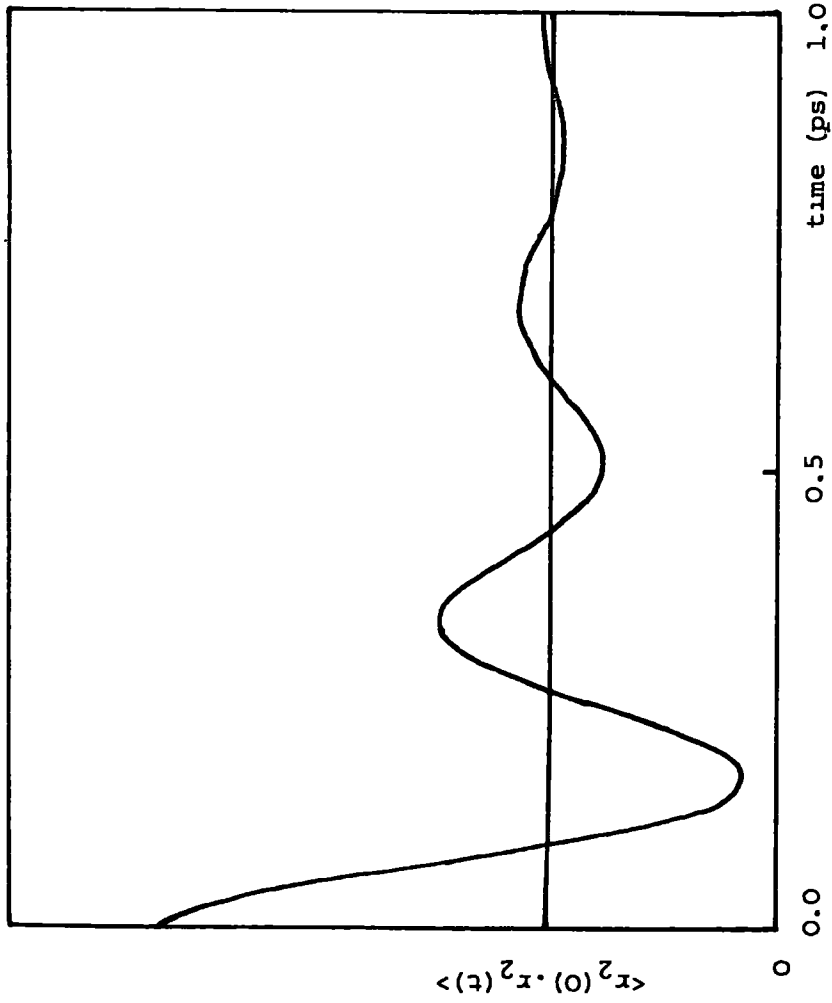


Figure 3.3a

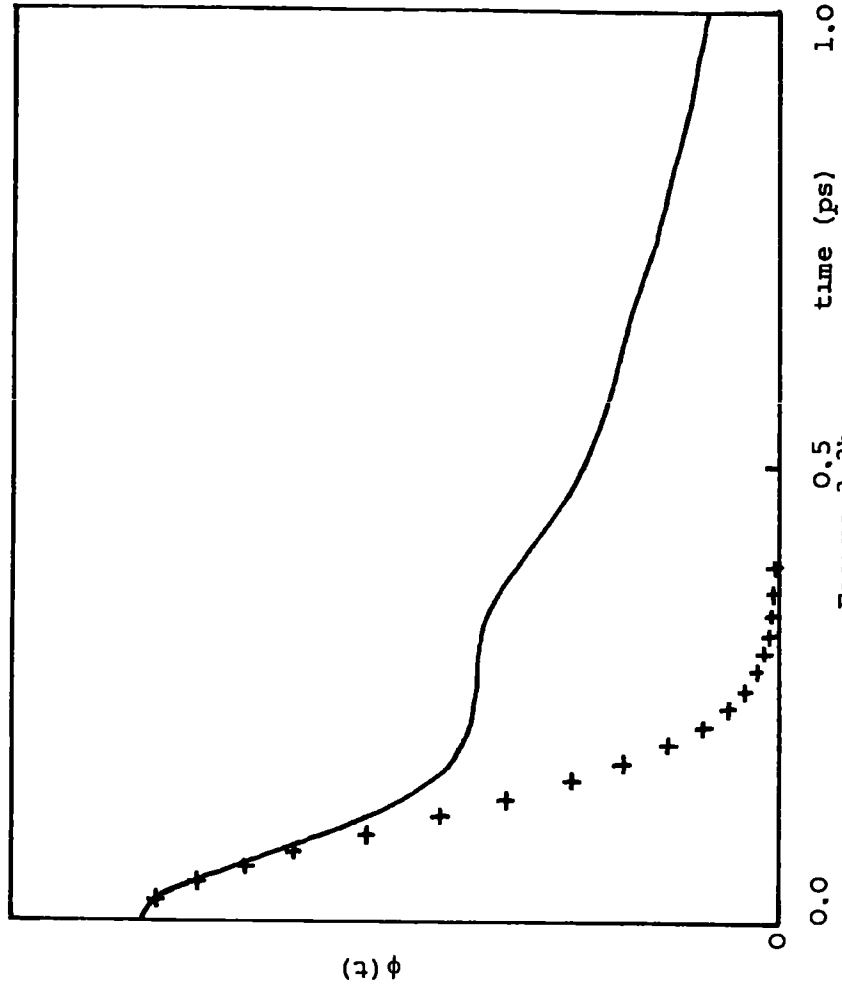


Figure 3.3b

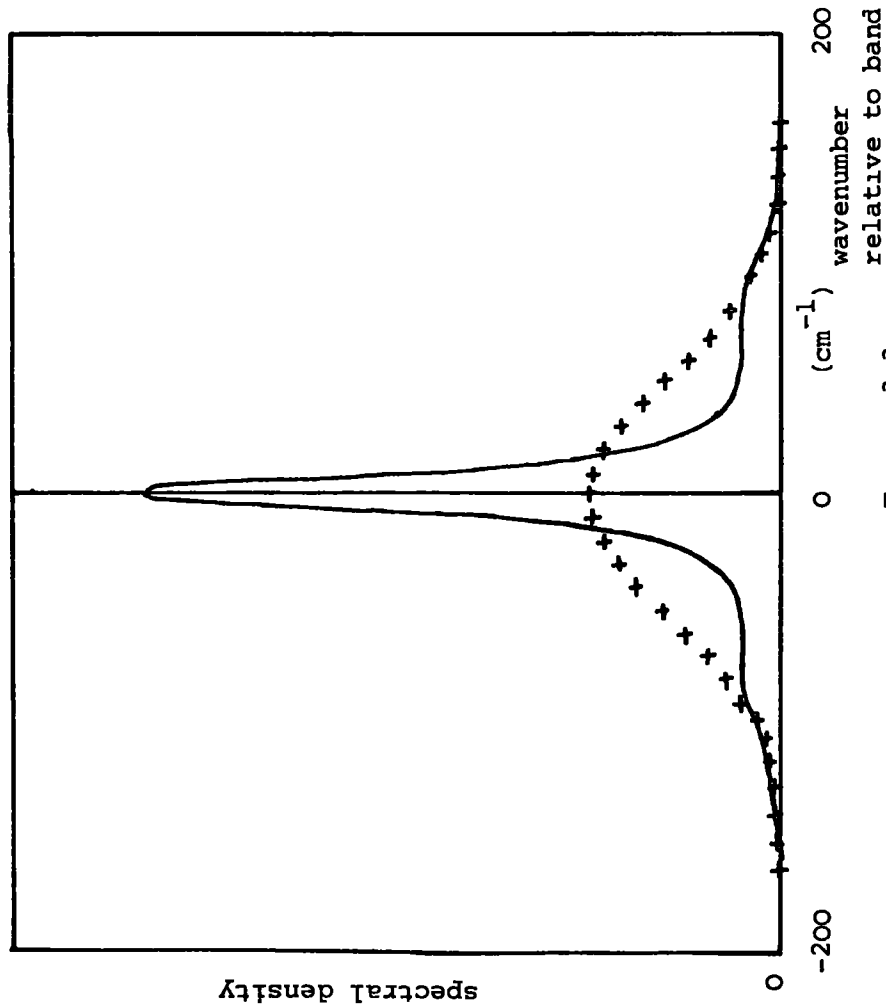


Figure 3.3c

Figure 3.3 Figures 3.3a, 3.3b and 3.3c show the same functions as Figure 3.1 with the  $\nu_{\sigma}$  (XH---Y) motion underdamped and  $\gamma/2\omega_2 = 0.2$  and  $\tau_c \Delta = 0.2$ . It can be seen that the function  $\phi(t)$  oscillates before reaching a region of smooth decay, the function  $\langle r_2(0) \cdot r_2(t) \rangle$  also oscillates and the spectral density has distinct shoulders at  $\pm \omega_2$ .

It is assumed throughout the above that  $\omega_2$  remains almost constant (a value of  $100-150\text{cm}^{-1}$  being typical).

It is unlikely, by this theory, that combination bands of the type  $\nu_s(\text{XH}) \pm \nu_\sigma(\text{XH}---\text{Y})$  are seen in solution. Because these bands must be narrow, the condition  $\tau \Delta \ll 1$  must be satisfied but at the same time the  $\Delta/\omega_2$  must be large for the lines to have appreciable intensity. Only if  $\gamma/2\omega_2$  were very small would these bands be resolved and, as stressed before, the model is invalid for the case where  $\gamma$  is very small, which might be thought of as the situation present in the gas phase.

#### 3.4 The effect of deuteration

When the proton which participates in the hydrogen bond is replaced by a deuteron the angular frequency,  $\omega_1$ , of the  $\nu_s(\text{XH})$  mode will change because the reduced mass,  $m_1$ , changes. The angular frequency,  $\omega_2$ , of the  $\nu_\sigma(\text{XH}---\text{Y})$  mode will remain constant, at least to a first approximation, and  $\gamma$  should similarly be unaffected since the solvent is unchanged.

It follows from (3.9) and (3.10) that

$$\Delta = \frac{K_{112}}{m_1 \omega_1} \langle r_2^2 \rangle^{1/2} \quad (3.19)$$

and assuming that the harmonic oscillator condition

$$\frac{\omega_1^{\text{H}}}{\omega_1^{\text{D}}} = \sqrt{\frac{m_1^{\text{D}}}{m_1^{\text{H}}}} \quad (3.20)$$

is satisfied it follows that since  $m_1^{\text{D}} = 2m_1^{\text{H}}$  (or very nearly)

$$\omega_1^{\text{H}} = \sqrt{2} \omega_1^{\text{D}} \quad (3.21)$$

and from (3.19) that

$$\frac{\Delta^{\text{H}}}{\Delta^{\text{D}}} = \frac{m_1^{\text{D}} \omega_1^{\text{D}}}{m_1^{\text{H}} \omega_1^{\text{H}}} \quad (3.22)$$

or

$$\frac{\Delta^H}{\Delta^D} = \frac{2m_1^H \omega_1^D}{m_1^H \omega_1^H} = \frac{2m_1^H \omega_1^D}{m_1^H \sqrt{2}\omega_1^D} = \frac{2}{\sqrt{2}}$$

that is

$$\Delta^H = \frac{2}{\sqrt{2}} \Delta^D = \sqrt{2} \Delta^D \quad (3.23)$$

The effect that this has on the bandshape depends on whether the slow or the rapid modulation limit is applicable. In the former case, from (3.12), it can be shown that the halfwidth,  $(\Delta\omega)_{\frac{1}{2}}$ , for a purely gaussian band is given by

$$(\Delta\omega)_{\frac{1}{2}} = 2\Delta(2\ln 2)^{\frac{1}{2}} \quad (3.24)$$

where  $(\Delta\omega)_{\frac{1}{2}}$  is in units of angular frequency. In the latter case, from (3.13)

$$(\Delta\omega)_{\frac{1}{2}} = 2\Delta^2 \tau_c \quad (3.25)$$

for a purely lorentzian band.

The effect of a change in  $\Delta$  on the bandwidth will therefore be different in the two limits. In the slow modulation limit the halfwidth is proportional to  $\Delta$  and will therefore decrease as  $\Delta$  decreases. Since  $\omega_1$  changes in the same way as  $\Delta$  on deuteration (see Equations (3.21) and (3.23)) the halfwidth will decrease as  $\omega_1$  decreases. In the rapid modulation limit the halfwidth is proportional to  $\Delta^2$  and the decrease in width on deuteration will depend on  $\omega_1^2$ . The experimental value for the decrease in halfwidth will give an indication of which modulation limit is applicable.

### 3.5 The effect of change of solvent

The friction constant ( $\gamma$ ) of the Langevin equation is, in principle at least, a property of the solvent and change of solvent should obviously affect the value of this constant. Provided that the change of solvent does not change the electronic structure of the complex  $\Delta$  and  $\omega_2$  should not



be affected since the force constant  $K_{112}$  should not change. A change in  $\gamma$  will change  $\tau_c$  according to Equation (3.11) and therefore the Kubo parameter  $\tau_c \Delta$  will change with a resultant change in bandshape because the degree of approach to either modulation limit will change. This will be true in all cases except the extreme slow modulation limit where, according to Equation (3.12) the value of  $\tau_c$  has no effect on the bandshape. This may be identified with the situation where the  $\nu_s(XH)$  oscillator relaxes so quickly compared with the time scale of the solvent motions that the nature of the solvent molecules has no effect on bandshape associated with the oscillator.

### 3.6 The effect of change of temperature

Variation of the temperature is another means which may be used to test the validity of the model. The parameters which are to be expected to change with temperature are  $\Delta$  and  $\gamma$ . Of these two,  $\Delta$  is proportional to the root-mean-square amplitude of the harmonic oscillator which represents the  $\nu_\sigma(XH---Y)$  motion since Equation (3.9) is

$$\Delta = \alpha \langle r_2^2 \rangle^{1/2}$$

The mean-square amplitude of a harmonic oscillator is given (87) in the quantum mechanical limit by:

$$\langle r_2^2 \rangle = (\hbar/2m_2\omega_2) [\coth(\hbar\omega_2/2kT)] \quad (3.25)$$

Now, making the abbreviations  $\alpha = \hbar/2m_2\omega_2$  and  $\beta = \hbar\omega_2/2k$ , it follows that

$$\langle r_2^2 \rangle^{1/2} = \alpha^{1/2} [\coth(\beta/T)]^{1/2} \quad (3.26)$$

and so  $\Delta$  is proportional to  $[\coth(\beta/T)]^{1/2}$  if  $\omega_2$  may be considered to be constant with changing temperature.

In the classical or high-temperature limit of the theory  $\Delta$  is proportional to simply  $\sqrt{T}$  and this can be shown as follows. From (3.26):

$$\langle r_2^2 \rangle^{1/2} = \alpha^{1/2} \left\{ \frac{\exp(\beta/T) + \exp(-\beta/T)}{\exp(\beta/T) - \exp(-\beta/T)} \right\}^{1/2}$$

If  $T$  is large the exponentials may be approximated each to the first two terms of a Taylor series and so

$$\begin{aligned} \langle r_2^2 \rangle^{1/2} &= \alpha^{1/2} \left\{ [1 + (\hbar\omega_2/2kT) + 1 - (\hbar\omega_2/2kT)] / \right. \\ &\quad \left. [1 + (\hbar\omega_2/2kT) - 1 + (\hbar\omega_2/2kT)] \right\}^{1/2} \\ &= \alpha^{1/2} (T/\beta)^{1/2} \\ &= (kT/m_2\omega_2^2)^{1/2}. \end{aligned}$$

In Figure 3.4 the function  $(\langle r_2^2 \rangle / \alpha)^{1/2}$  is plotted, assuming a value of  $150\text{cm}^{-1}$  for  $\bar{\nu}_2 (= \omega_2/2\pi c)$ , for the quantum mechanical limit where

$$(\langle r_2^2 \rangle / \alpha)^{1/2} = [\coth(\beta/T)]^{1/2} \quad (3.27)$$

and for the classical approximation where

$$(\langle r_2^2 \rangle / \alpha)^{1/2} = (T/\beta)^{1/2}. \quad (3.28)$$

The figure shows the difference in the functions at low temperatures and indicates that a study on a complex at a low temperature would be of some interest. At any temperature a change in  $\Delta$  would be expected to affect the value of  $\tau_c \Delta$  and therefore a change in bandshape would be expected.

In the simplest sense the damping constant  $\gamma$  of the Langevin equation (3.5) can be identified with the macroscopic viscosity of the solvent (usually designated  $\eta$ ). The change of viscosity with temperature is somewhat complicated and various expressions containing empirical constants such as

$$\eta = A \exp(b/RT)$$

(88) where  $A$  and  $b$  are constants (assumed to be independent of temperature) have been proposed. When the temperature dependence of  $b$  is considered (89) the following expression is obtained (90).

$$\eta = K - \frac{3.42}{R} \ln T + \frac{1080}{RT}$$

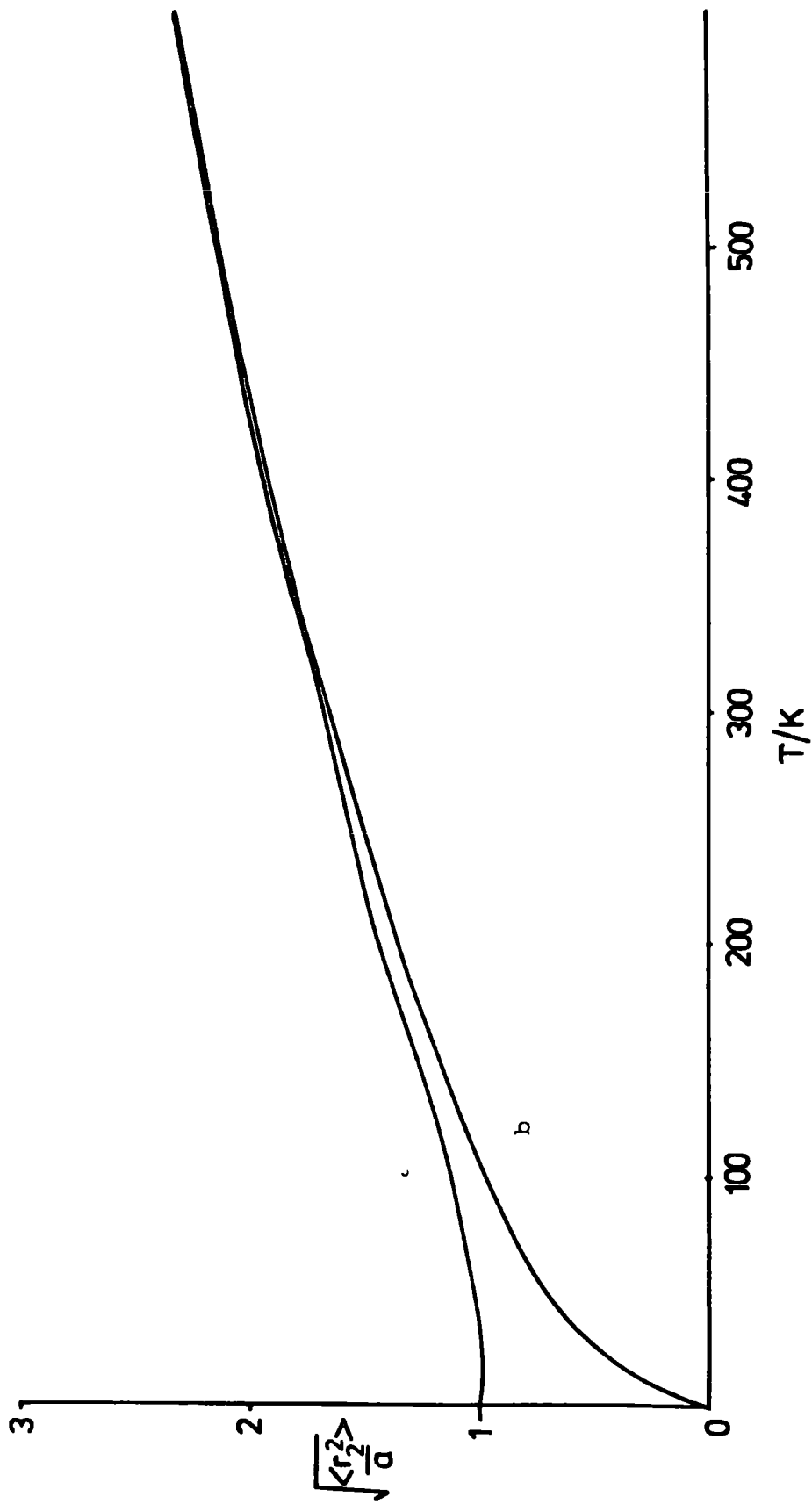


Figure 3.4 The function  $(\langle r^2 \rangle / a)^{1/2}$  plotted in (a) the quantum mechanical limit and (b) the classical approximation as a function of temperature (see text for details).

(the numerical constants being appropriate to c.g.s. units). In any event these equations are only valid for non-polar liquids and polar liquids show considerable deviations from the predicted behaviour.

The overall conclusion is that  $\eta$  decreases in an approximately exponential manner with increasing temperature and  $\gamma$  would be expected (if it is related to  $\eta$ ) to decrease in some similar way. However, experimental data (see Section 4.9) suggest that  $\eta$  and  $\gamma$  are not related in this simple way.

The effect of change in  $\gamma$  is to change  $\tau_c$  (via Equation (3.11)) and therefore to change the bandshape in all but the case of the extreme slow modulation limit.

The total effect of temperature on the system via the parameters  $\Delta$  and  $\gamma$  is evidently rather complicated but it is true to say that, unless opposing factors cancel out fortuitously, some change in bandshape is to be expected.

### 3.7 The far-infrared and inelastic neutron scattering spectra

The theory of Robertson and Yarwood has an important advantage over most others because it includes expressions for the far-infrared and inelastic neutron scattering spectra. The far-infrared absorption profile is simply given by the Fourier cosine transform of the autocorrelation function of the Ornstein-Uhlenbeck stochastic process (i.e. the variation of  $r_2$  in a random manner with time) mentioned in Section 3.2 (see also refs. (60) and (83)). The expression obtained for the intensity as a function of angular frequency,  $\omega$  is

$$I(\omega) = C\gamma\omega^2 [1 - \exp(-\hbar\omega/kT)] / [(\omega^2 - \omega_2^2)^2 + \gamma^2 \omega^2] \quad (3.29)$$

where  $C$  is a constant arising from the Fourier transformation. The factor  $[1 - \exp(-\hbar\omega/kT)]$  represents a correction for stimulated emission from the

second (i.e. upper) vibrational level. It is interesting to note that the maximum of the absorption profile is not necessarily at  $\omega_2$  and the shift from  $\omega_2$  depends upon the value of  $\gamma$ . In the case of underdamped motion the shift is small but in the critically damped case the maximum is at  $0.58\omega_2$  and as the damping increases the shift becomes even greater.

This treatment is less useful if it is found that other vibrational or rotational modes absorb in the same spectral region and in particular bending modes of the complex may in fact interfere (see Chapter 5).

The expressions for the inelastic neutron scattering spectrum of the complex will not be discussed in detail here but efforts have been made to obtain the inelastic (91) neutron scattering spectrum of the complex methanol-pyridine using a triple-axis neutron spectrometer at A.E.R.E. Harwell.

CHAPTER FOUR

RESULTS IN THE MID-INFRARED REGION AND THEIR

INTERPRETATION

#### 4.1 Introduction

In this chapter the experimental data and results obtained for the complexes of phenol with the bases acetonitrile, 1,4-dioxan and pyridine in the mid-infrared region will be described. Far-infrared data will be presented in Chapter 5 and the manner in which the data were obtained is described in Chapter 2. Also included here is a description of some work which attempted to investigate the hydrogen-bonding interactions in liquid water and reasons why this system could not be described and analysed in terms of the Robertson-Yarwood model.

#### 4.2 The $\nu_s$ (OH) absorption band of the phenol-acetonitrile complex

This complex was investigated in carbon tetrachloride solution and in the dipolar solvent chloroform-d (see Section 4.5). The changes that take place when the hydrogen bonded proton is replaced by a deuteron were also investigated.

The absorption spectrum in carbon tetrachloride was obtained by Method A (see Section 2.5), the concentrations used were phenol 0.0257M and acetonitrile 2.51M. All substances used here and throughout the experimental work were "spectroscopic" or "analytical" grade and the liquids were dried over type 4A molecular sieves and in no case gave spectroscopic evidence of containing moisture. The complex formed has an equilibrium constant measured as  $5.0 \pm 0.2 \text{ dm}^3 \text{ mol}^{-1}$  at 298K (92) and the stoichiometry has been shown to be 1 : 1 by Horak et al. (93).

The Beckman F-01 cells were fitted with teflon spacers of approximately 500 $\mu\text{m}$  thickness and the windows were of potassium bromide polished using a slurry of ethanol and Beckman polishing rouge (PK6) on a "Selvyt" polishing cloth stretched over a glass plate. After assembly the interference fringes produced by internal reflections in the cells (94) were recorded and in this way it could be seen whether the windows were

reasonably flat and parallel, or otherwise. Because of the method used to analyse the data (see Section 4.6) it was not necessary to obtain absolute intensity values and so the pathlength was not required accurately although it could have been measured from the interference fringe pattern in the usual manner (94).

The spectra were recorded at the temperature of the spectrometer beam, measured to be  $\sim 313\text{K}$  with a thermocouple, the cell being allowed to come to thermal equilibrium with the beam before any measurements were taken. The data transfer unit (see Section 2.3) was set to "take" millivolt readings at 4s intervals and this produced a wavenumber interval of  $3.33\text{cm}^{-1}$  with a scan rate of  $0.833\text{cm}^{-1}\text{ s}^{-1}$ . The spectrum was recorded from  $3800\text{cm}^{-1}$  to approximately  $3130\text{cm}^{-1}$ , the starting wavenumber having been set by the spectrometer wavenumber marker (and therefore all wavenumber values are subject to at least the inaccuracy of this marker, measured to be better than  $\pm 1\text{cm}^{-1}$  by comparison with the wavenumbers of water vapour lines (95)). A "background" tape was produced in an exactly similar manner but with both cells containing the acetonitrile solution. The entire procedure was repeated ten times to obtain ten independent spectra to enable the necessary statistical analysis to be performed.

The data collected in the above manner were transferred to magnetic disks as described in Section 2.4. A range of computer techniques were available to calculate the absorbance spectrum and particular attention was paid to the effect each of these had on the bandshape obtained because this is of considerable importance for the band-fitting procedure. The model to which the data were fitted is very sensitive to the bandshape in the spectral wings, the region of the spectrum which is most greatly affected by different background subtraction techniques. The different methods will now be described.



Using the programme IRINT1 the absorbance spectrum was calculated between  $3800\text{cm}^{-1}$  and  $3127\text{cm}^{-1}$  first with a background of linearly interpolated transmittance values between the values at the wavenumbers given above and then with the background provided by the tape obtained when acetonitrile solution was placed in both cells. These methods were designated "computed" and "real" background methods respectively. The same procedure was repeated for each of the ten individual "runs" and the mean absorbance value at each wavenumber was calculated by use of the programme MEANSPEC3 (96) which also calculated the weighting factors used in the fitting procedure (see Section 4.6).

Although the situation is physically meaningless it does sometimes happen in the spectral wings that the transmittance in the sample spectrum is greater than that in the background spectrum. This can be due, for example, to the noise fluctuations in the spectra or to slight changes in the photometric accuracy of the spectrometer between the recording of the two spectra. When the interpolated, "computed", background is used, the particular noise level at the terminal data points can lead to the same effect in the wings. This effect is also produced if the transmittance values of the "sample" spectrum increase between the terminal data points and the transmittance minimum (see Figure 4.1). When the programme IRINT1 encounters such a point it sets the absorbance value to zero on the grounds that negative values have no meaning. When the mean of ten sets of data is calculated this practice can lead to an error because over the ten spectra the mean absorbance value at a particular point may be positive when some individual values are negative. In order to overcome this difficulty the programme IRINT6 allows negative absorbance values in the individual spectra and these values are carried through MEANSPEC3 and finally outputted and plotted. The effect on the fitting procedure is discussed in Section 4.7.

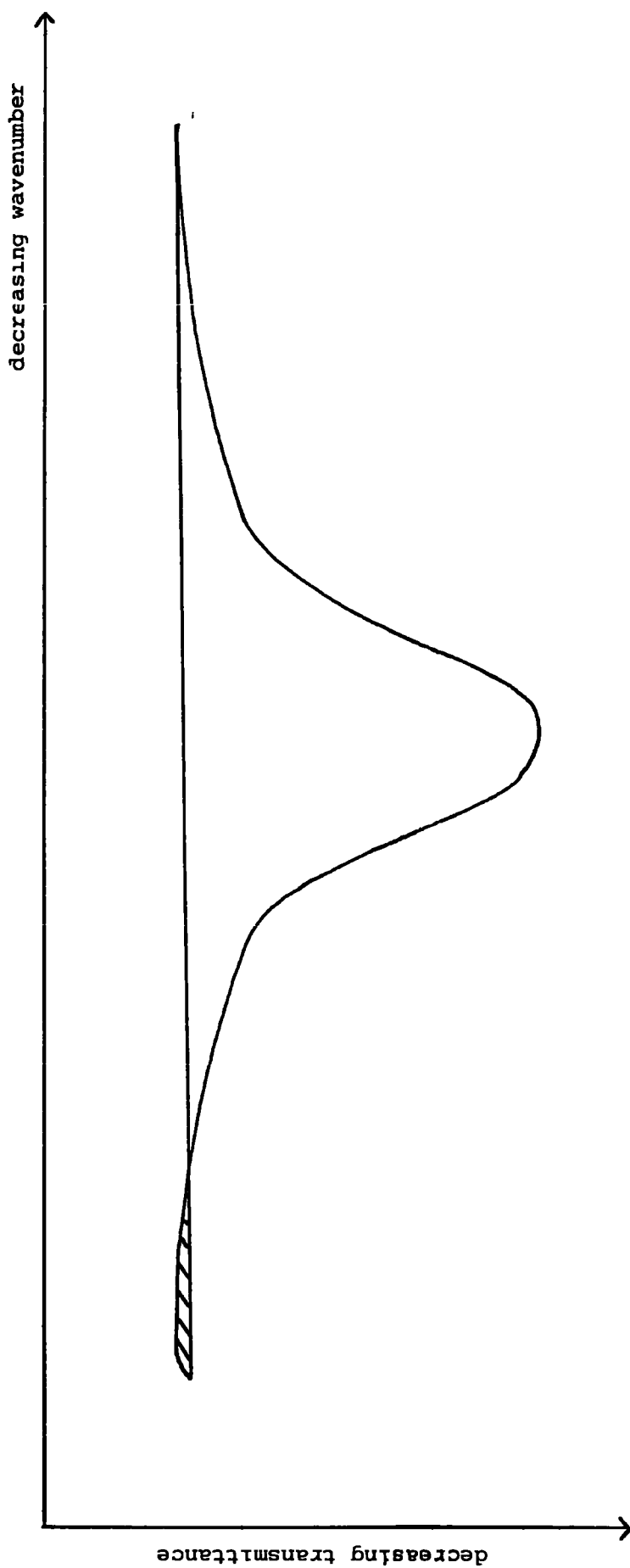


Figure 4.1 Showing a band on a transmittance scale. At the high wavenumber end of the band the transmittance has begun to decrease and the "computed" background, having been "drawn" between the terminal data points, creates negative absorbance values over the range of the hatched portion.

The transmittance spectra recorded for the "sample" and "background" solutions are shown in Figure 4.2; Figures 4.3 and 4.4 each show a single "run" computed with IRINT1 using a "computed" and a "real" background respectively. Ten independent spectra are shown in Figures 4.5 and 4.6, computed with IRINT6 and using "computed" and "real" backgrounds respectively. The spectra of mean absorbance values calculated by MEANSPEC3 with output data from IRINT6 are shown in Figures 4.7 and 4.8 for the "computed" and "real" backgrounds respectively, and comparison with Figure 4.2 or 4.3 shows the decrease in noise in the spectrum on averaging.

In order to investigate the effect of deuteration at the hydroxyl proton of the phenol the procedure described above was repeated for the  $\nu_s$  (OD) band of  $C_6H_5OD$ . A solution containing the deuterated phenol was prepared by dissolving phenol ( $\sim 1.6g$ ) in deuterium oxide ( $\sim 15cm^3$ ) and after allowing it to stand for about 3hrs extracting the phenol with five portions of carbon tetrachloride each of  $\sim 5cm^3$ , and finally making the solution up to  $50cm^3$  with the solvent. The resulting solution was dried over calcium chloride; it was found that type 4A molecular sieve brought about a reversion to  $C_6H_5OH$ . The solution thus obtained contains both the protium and deuterium species but since the  $\nu_s$  (OH) and  $\nu_s$  (OD) absorption bands are separated by about  $1000cm^{-1}$  the  $\nu_s$  (OD) band can be recorded without interference from the  $\nu_s$  (OH) band.

It was not necessary to know the precise concentration of the deuterium species since the band intensity and transition dipole moment correlation functions are normalised in the fitting procedure. The concentration of phenol used was, however, chosen to give similar band intensity as that of the  $\nu_s$  (OH) band. The spectroscopic data were obtained over the range  $2800cm^{-1}$  to  $2310cm^{-1}$  in the same manner as described above and were treated also in the same way. The transmittance spectra recorded



Figure 4.2 The transmittance spectra recorded for the "sample" and "background" solutions for the complex phenol-acetonitrile in carbon tetrachloride.

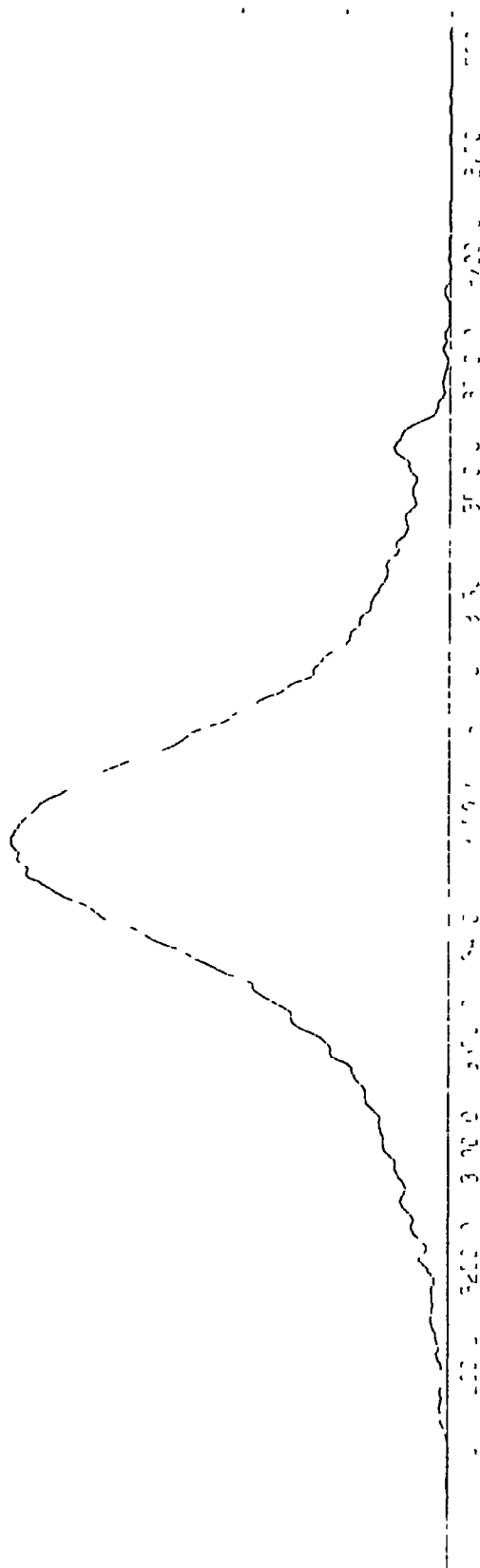


Figure 4.3 A single spectral "run" for the complex phenol-acetonitrile in carbon tetrachloride computed with IRINT1 using a "computed" background. The absorbance scale is decadic.

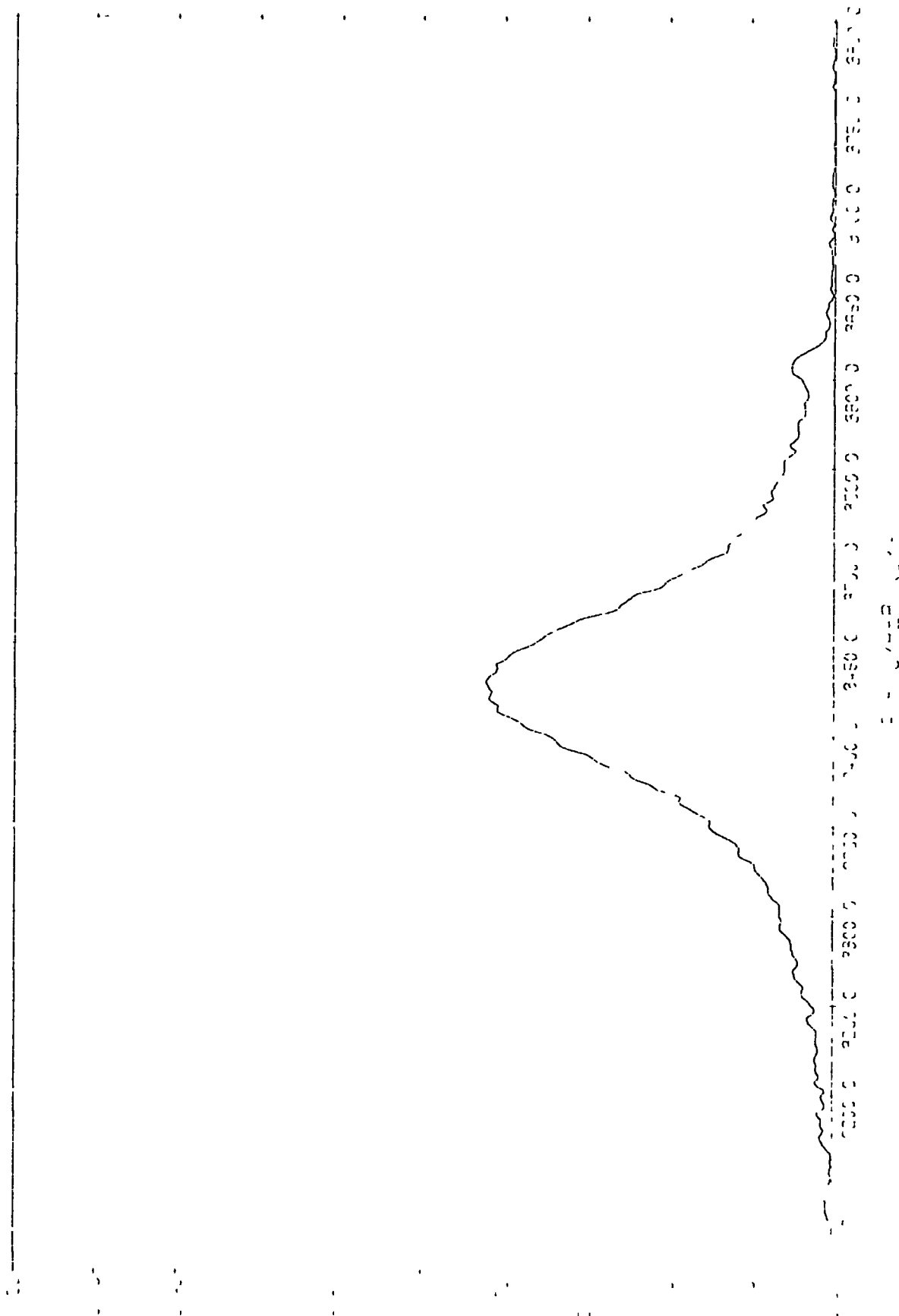


Figure 4.4 A single spectral "run" for the complex phenol-acetonitrile in carbon tetrachloride computed with IRINT1 using a "real" background. The absorbance scale is decadic.

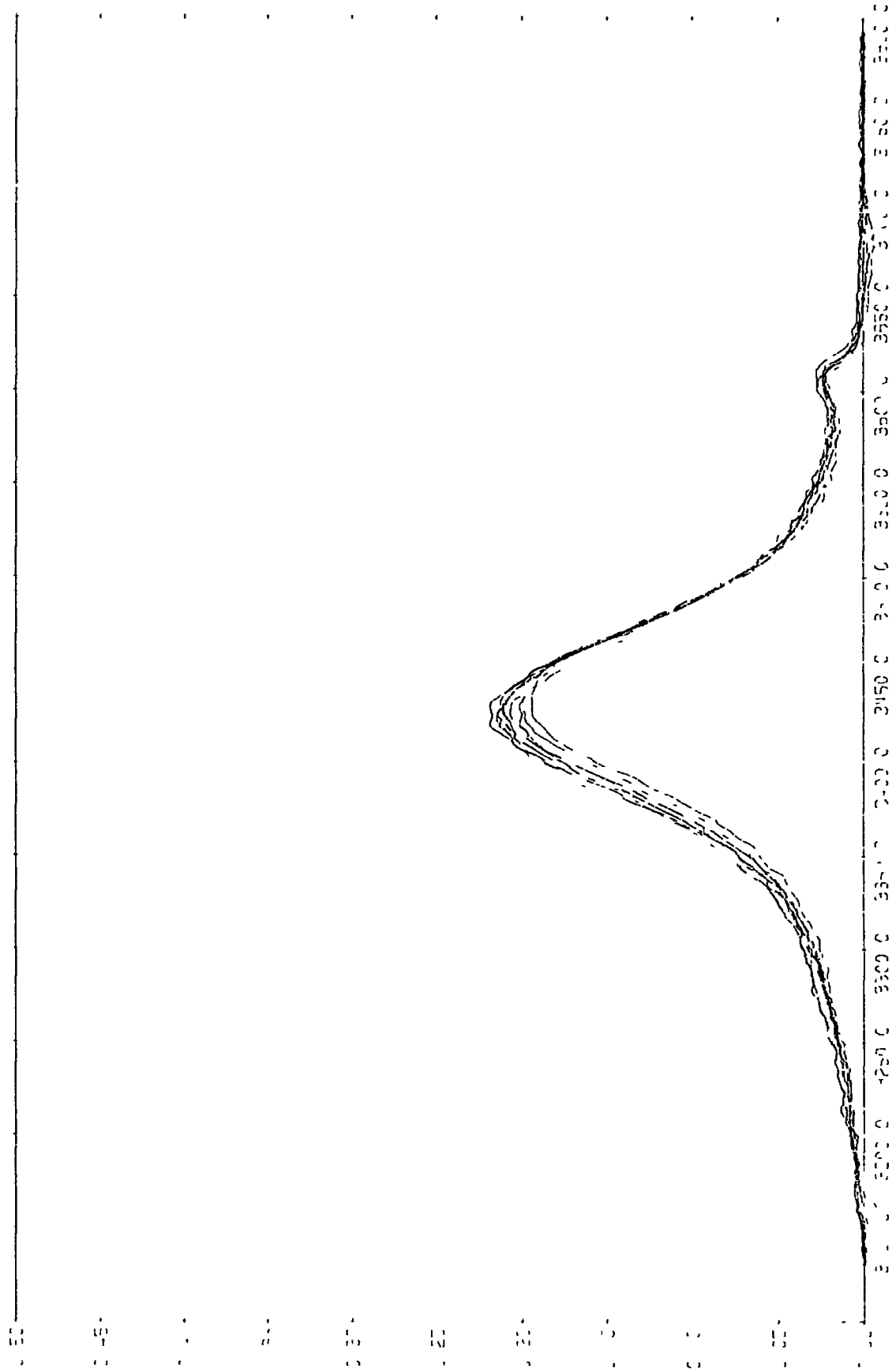


Figure 4.5 Ten independent spectral "runs" for the complex phenol-acetonitrile in carbon tetrachloride computed with IRINT6 using a "computed" background. The absorbance scale is decadic.

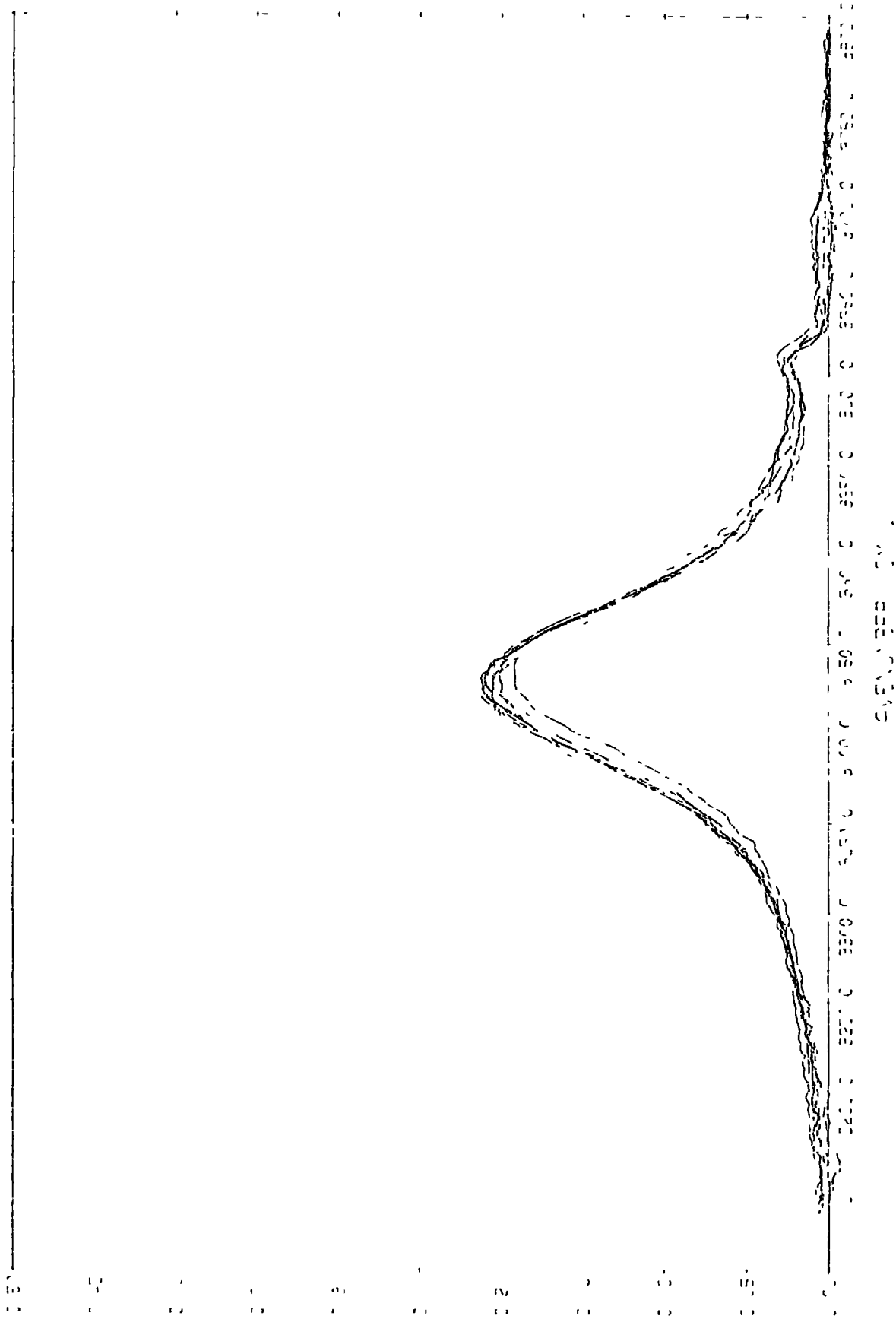


Figure 4.6 Ten independent spectral "runs" for the complex phenol-acetonitrile in carbon tetrachloride computed with IRINT6 using a "real" background. The absorbance scale is decadic.



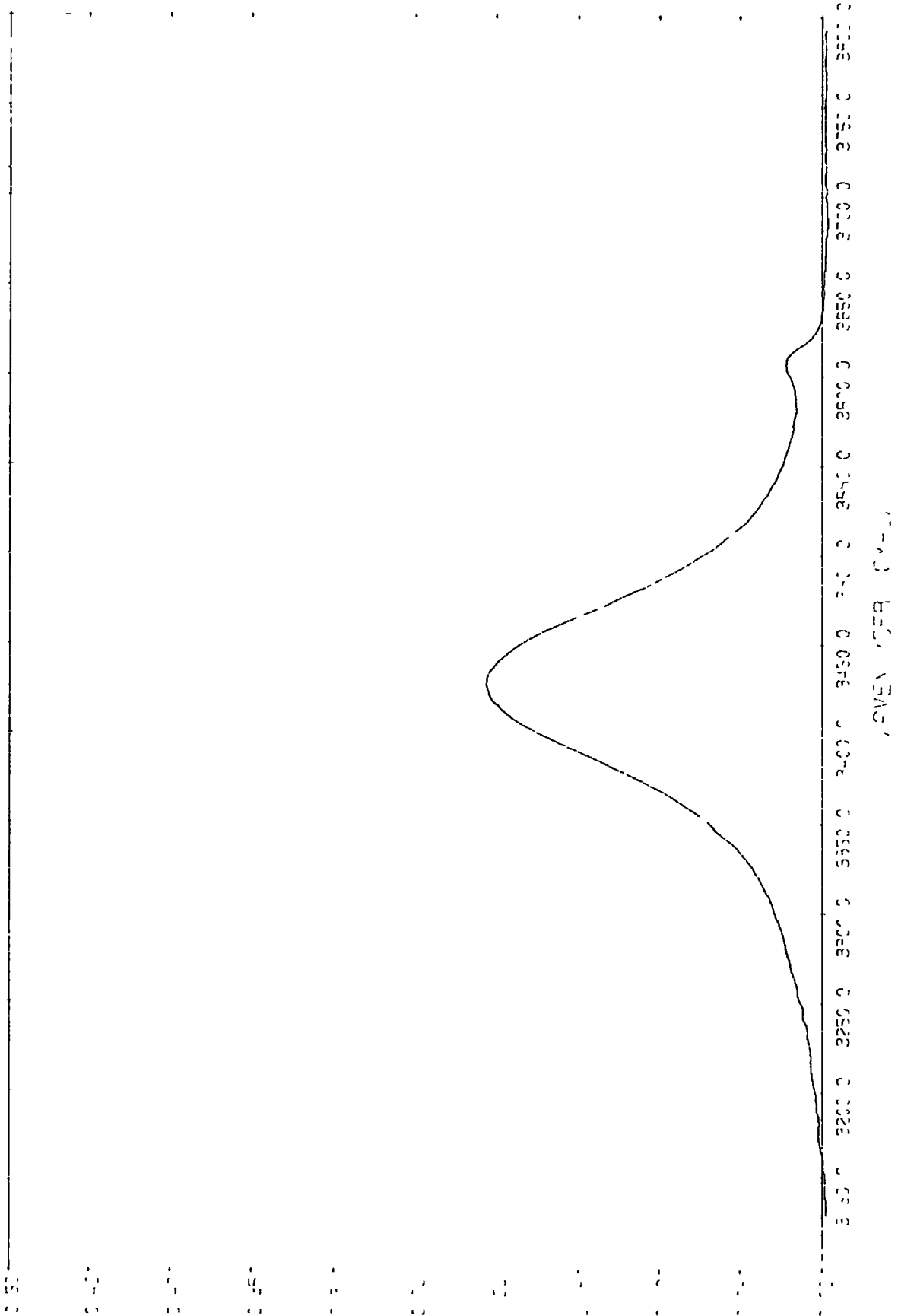


Figure 4.7 The spectrum of mean decadic absorbance values computed with IRINT6 using a "computed" background for the complex phenol-acetonitrile in carbon tetrachloride.

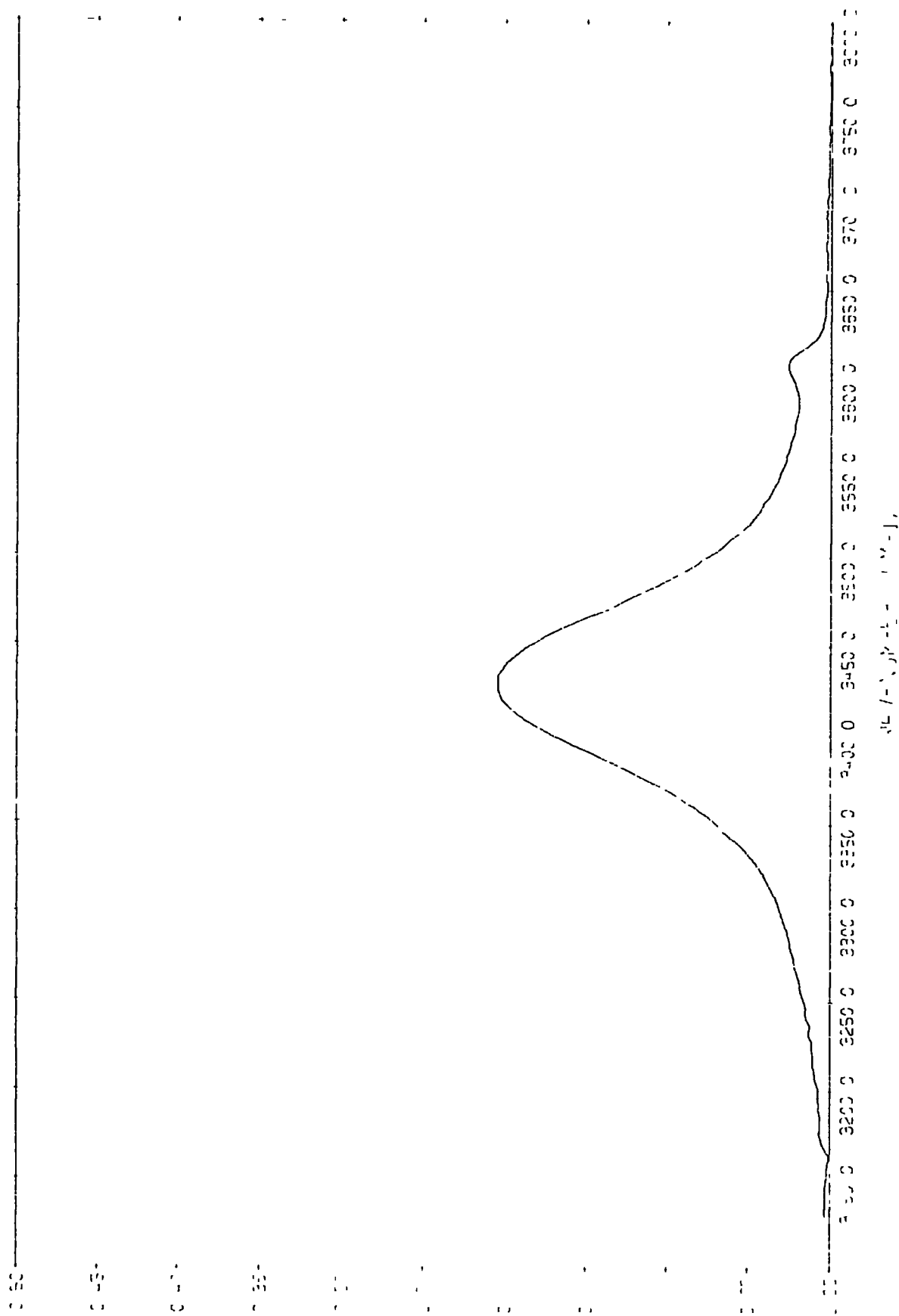


Figure 4.8 The spectrum of mean decadic absorbance values computed with IRINT6 using a "real" background for the complex phenol-acetonitrile in carbon tetrachloride.

for the "sample" and "background" solutions are shown in Figure 4.9; Figures 4.10 and 4.11 show a single "run" computed with IRINT1 using a "computed" and a "real" background respectively. The ten independently-obtained spectra computed with IRINT1 are shown in Figures 4.12 and 4.13 for "computed" and "real" backgrounds respectively. Figures 4.14 and 4.15 show the same spectra computed with IRINT6 and the spectra of mean absorbance values are shown in Figures 4.16 and 4.17 for "computed" and "real" backgrounds respectively.

The noticeably poorer precision of the data for the deuterium species compared with the protium species is probably due to changes in the equilibrium concentration of the species brought about by thermal fluctuations in the sample and the presence of very small concentrations of water.

The Figures 4.10 to 4.17 show that there is a tendency for the "computed" background versions of the spectra to produce negative absorbance values in the low frequency wing and the effect of this is discussed in Section 4.10. The difference between the "real" and the "computed" background versions of the spectra is also discussed in Section 4.10.

#### 4.3 The $\nu_s$ (OH) absorption band of the phenol-1,4-dioxan complex

The spectral data for this complex were obtained in a very similar manner to that described in Section 4.2 for the phenol-acetonitrile complex. The concentrations of phenol and 1,4-dioxan used were respectively 0.0244M and 1.34M. Deuterated phenol was prepared in the same manner as described before and the spectrum of the deuterium species was measured with the base at 1.30M. The complex formed has an equilibrium constant measured to be  $4.0 \text{ dm}^3 \text{ mol}^{-1}$  at 298K (97) and it is assumed that the large excess of base used makes the formation of any complexes of stoichiometries



Figure 4.9 The transmittance spectra recorded for the "sample" and "background" solutions for the complex phenol(OD)-acetonitrile in carbon tetrachloride.

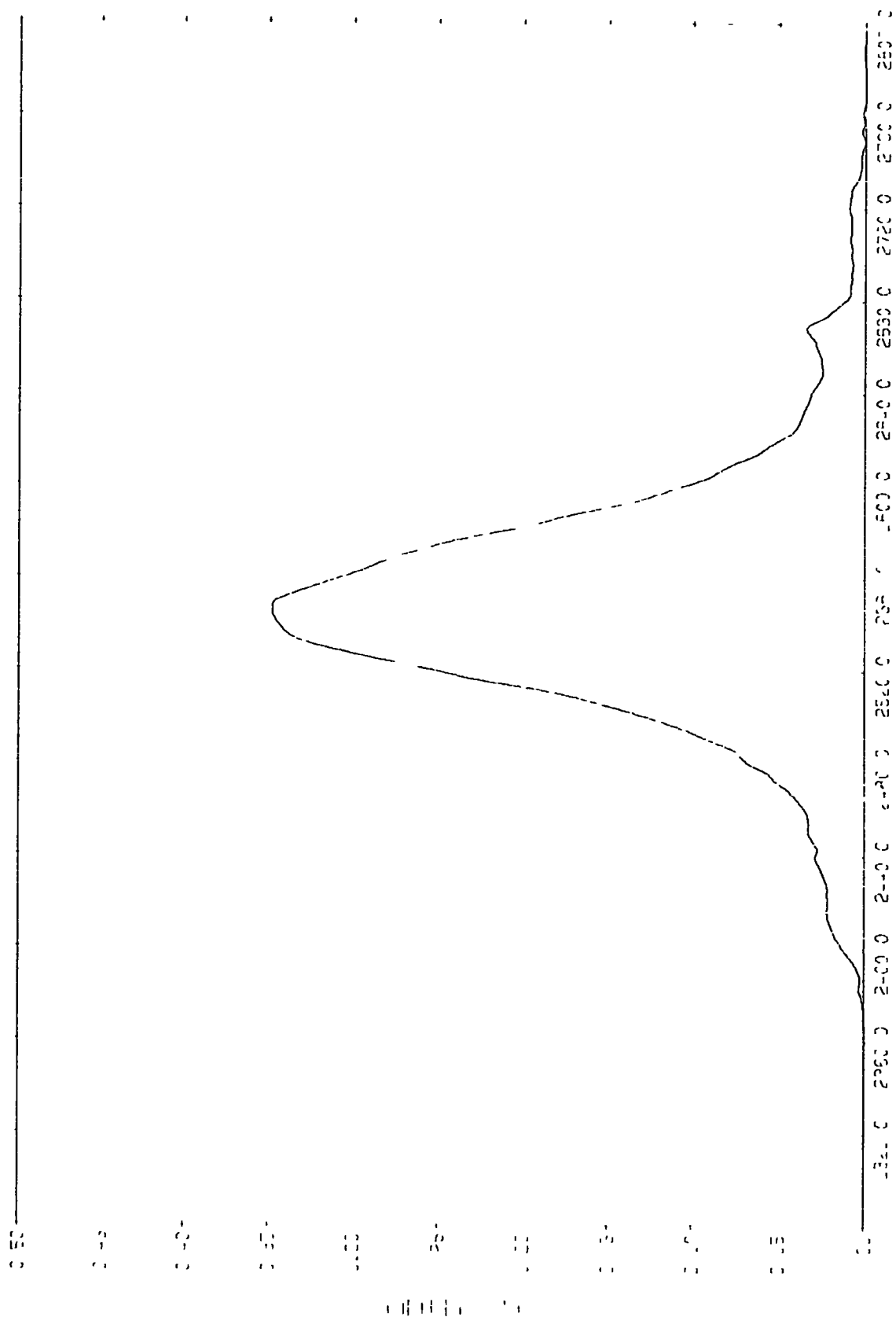


Figure 4.10 A single spectral "run" for the complex phenol (OD)-acetonitrile in carbon tetrachloride computed with IRINTL using a "computed" background. The absorbance scale is decadic.

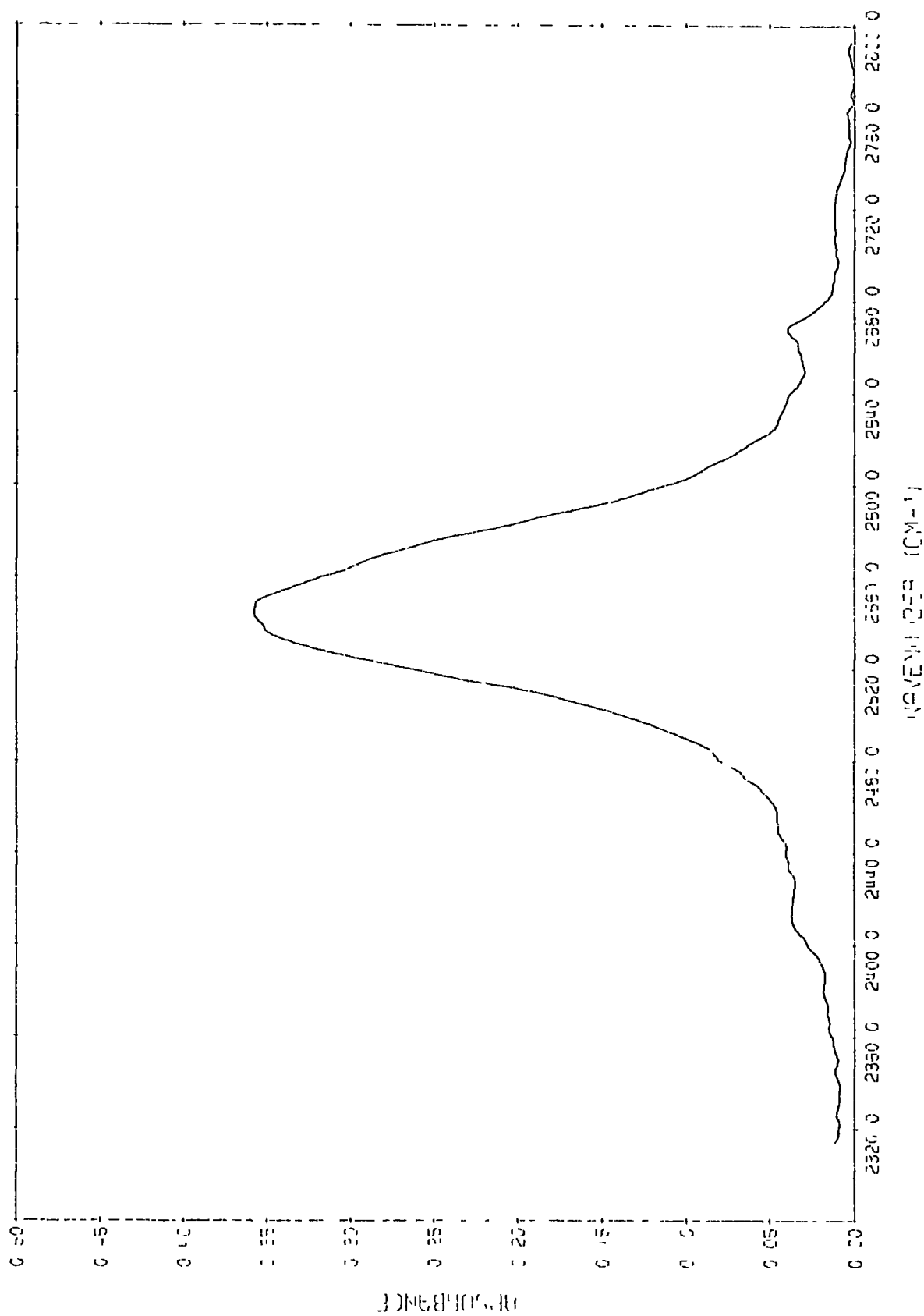


Figure 4.11 A single spectral "run" for the complex phenol (OD)-acetonitrile in carbon tetrachloride computed with IRINT1 using a "real" background. The absorbance scale is decadic.

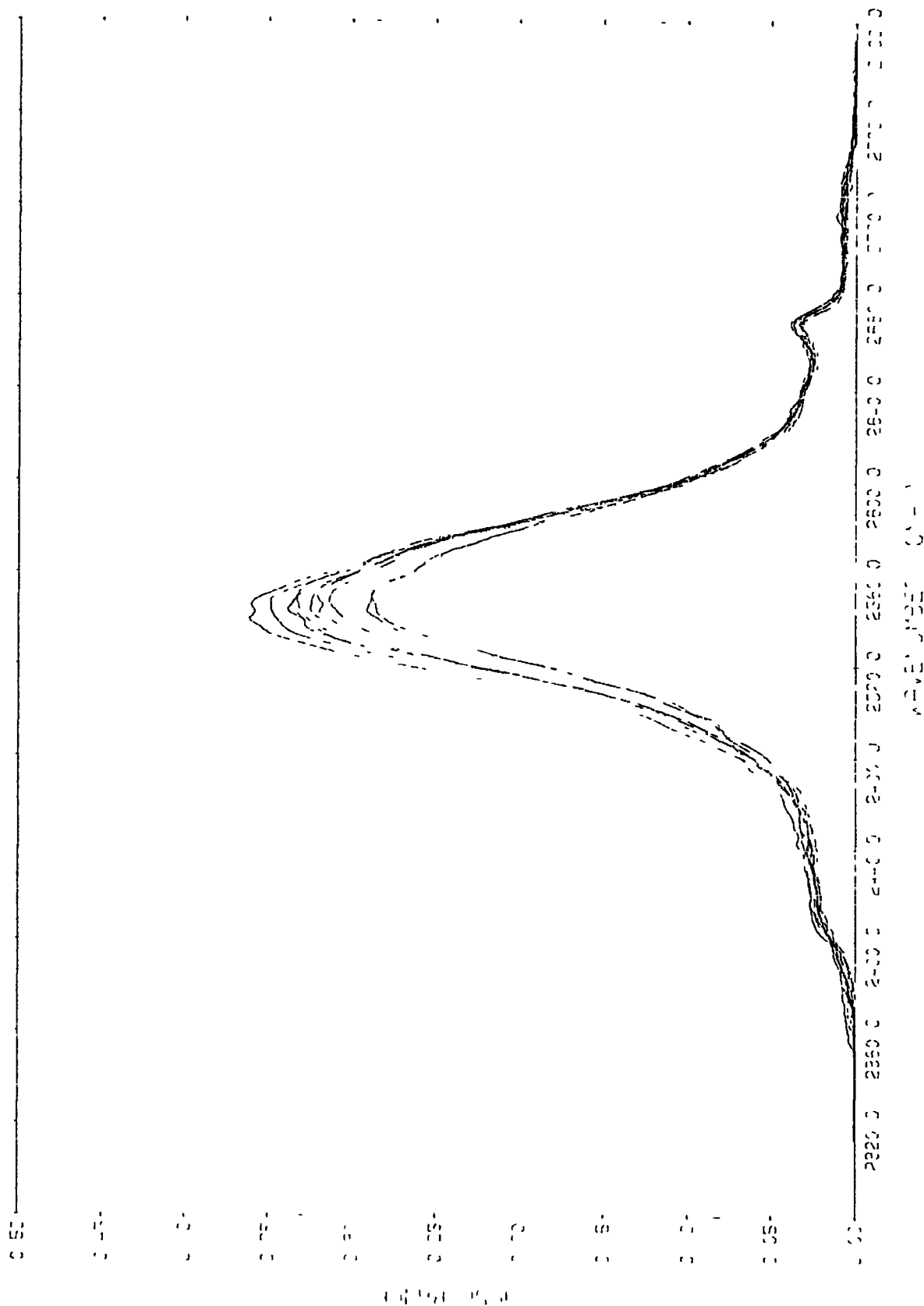


Figure 4.12 Ten independent spectral "runs" for the complex phenol(OD)-acetonitrile in carbon tetrachloride computed with IRINT1 using a "real" background. The absorbance scale is decadic.

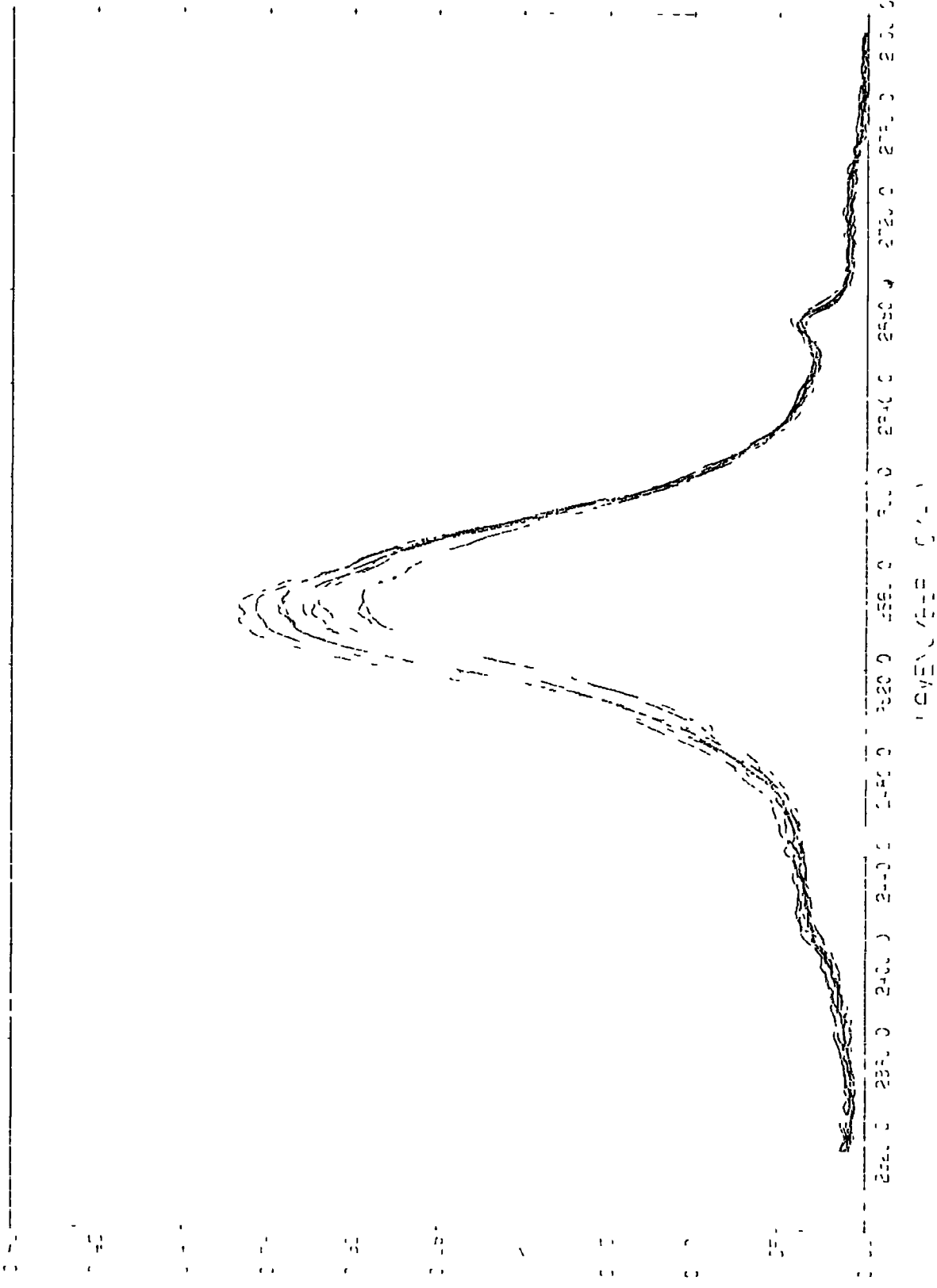


Figure 4.13 Ten independent spectral "runs" for the complex phenol(OD)-acetonitrile in carbon tetrachloride computed with IRINT1 using a "real" background. The absorbance scale is decadic.



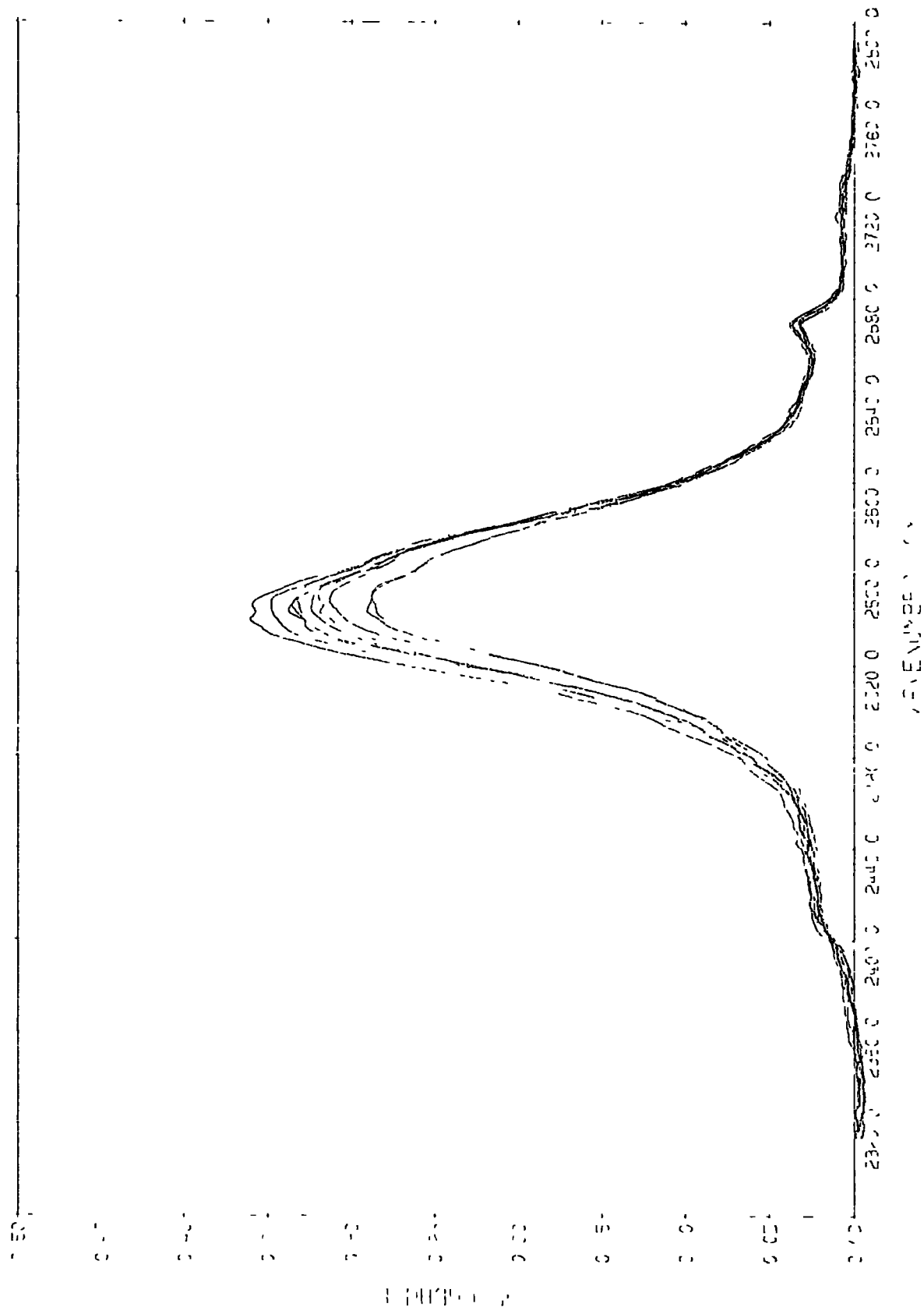


Figure 4.14 Ten independent spectral "runs" for the complex phenol(OD)-acetonitrile in carbon tetrachloride computed with IRINT6 using a "computed" background. The absorbance scale is decadic.

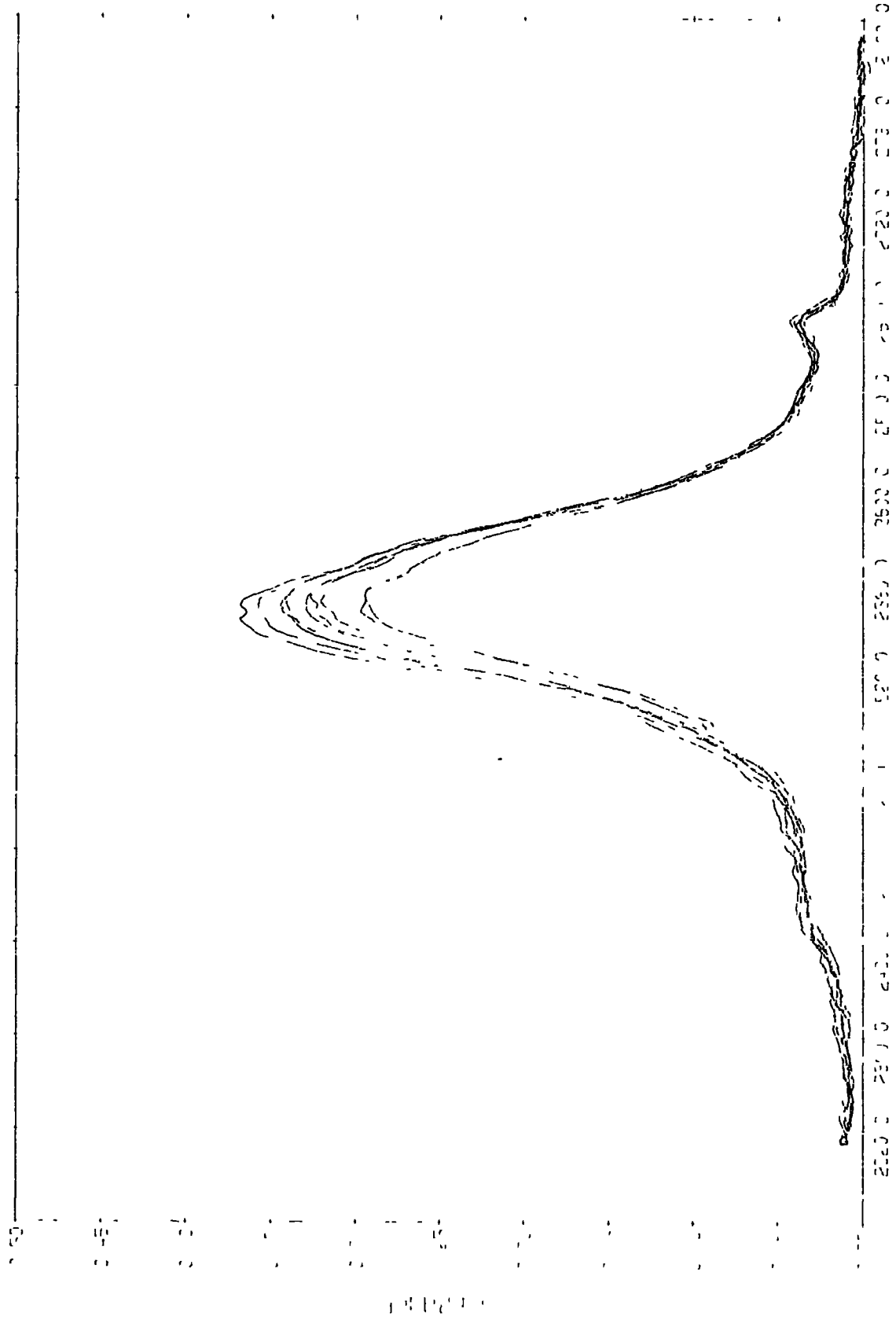


Figure 4.15 Ten independent spectral "runs" for the complex phenol(OD)-acetonitrile in carbon tetrachloride computed with IRINT6 using a "real" background. The absorbance scale is decadic.

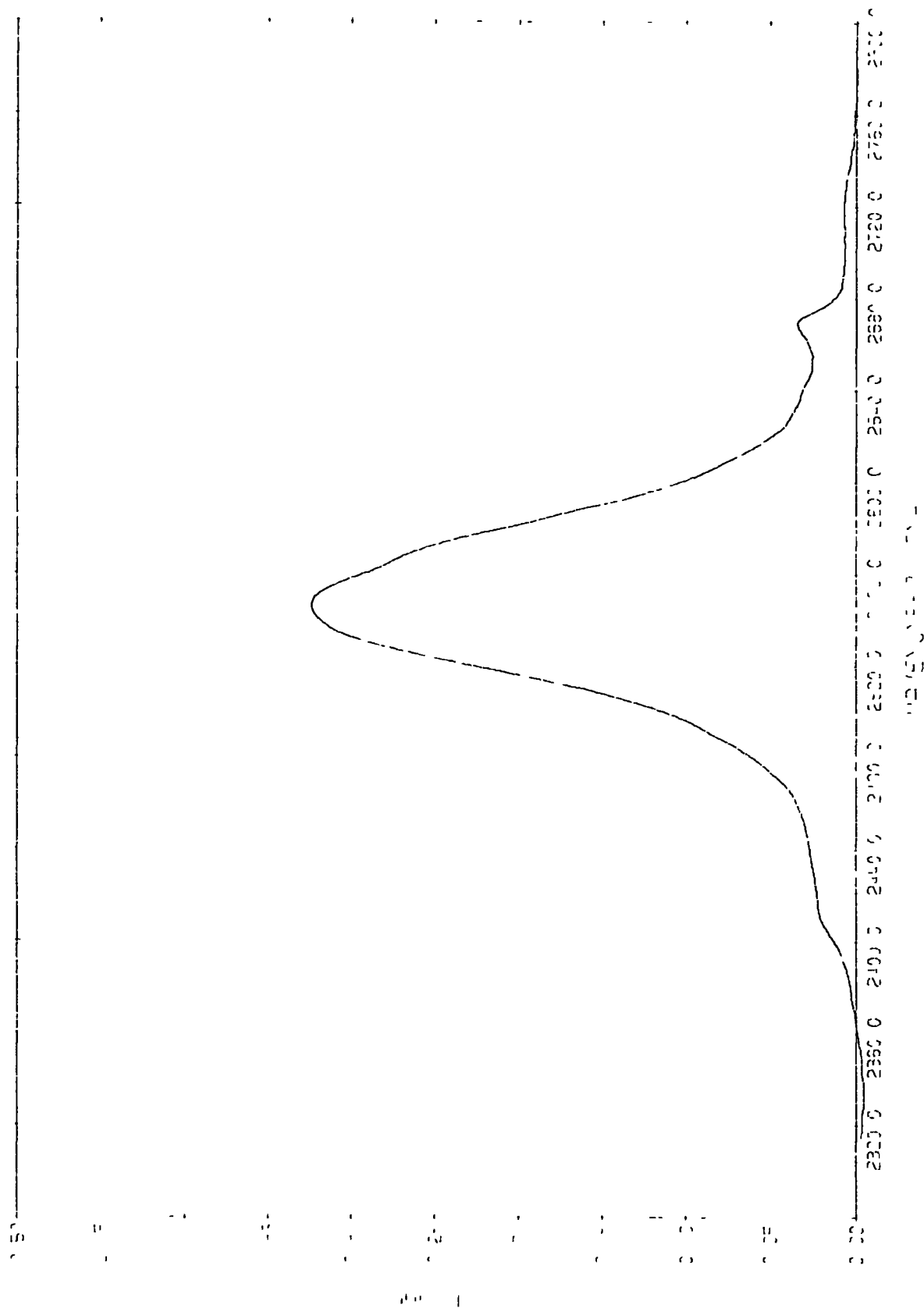


Figure 4.16 The spectrum of mean decadic absorbance values computed with IRINT6 using a "computed" background for the complex phenol(OD)-acetonitrile in carbon tetrachloride.

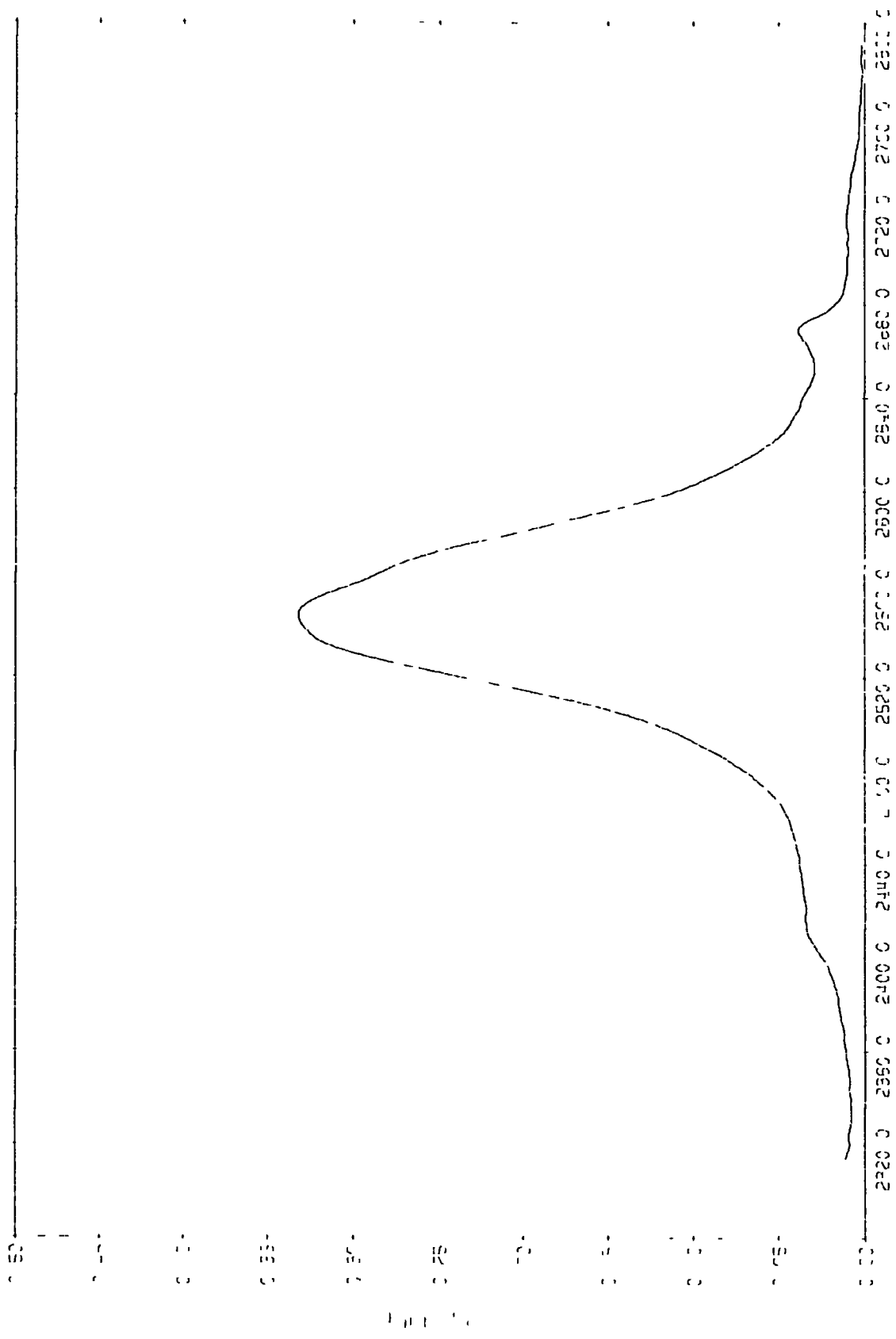


Figure 4.17 The spectrum of mean decadic absorbance values computed with IRINT6 using a "real" background for the complex phenol (OD)-acetonitrile in carbon tetrachloride.

other than 1 : 1 very unlikely. In practice, no spectroscopic evidence was found to suggest that complexes of other stoichiometries were present at measurable concentrations.

One particular problem here is that there are two very intense absorption bands in the spectrum of 1,4-dioxan at approximately  $2750\text{cm}^{-1}$  and  $2690\text{cm}^{-1}$ . When Method A of recording the data is used this leads to a lack of instrument response through these regions because the highly-absorbing substance is present in both beams of the spectrometer and therefore little energy reaches the detector. Figure 4.18 shows the approximate instrument response plotted against wavenumber, the measure of the response being obtained by placing an opaque object in the sample beam for  $\sim 2\text{s}$  and measuring the consequent pen deflection. The effect of this lack of response is to produce some pen-drift through these two regions which occur in the high-frequency wing of the band and the transmittance values there are consequently somewhat unreliable.

As before, the absorbance spectrum was calculated with both a "real" and a "computed" background using the programme IRINT6 which allows negative absorbance values and also for comparison using IRINT1 which does not. The ten spectra computed with IRINT6 are shown in Figures 4.19 and 4.20 with "computed" and "real" backgrounds for the protium system and in Figures 4.21 and 4.22 for the deuterium system. The spectra of mean absorbance values calculated by use of MEANSPEC3 are shown in Figures 4.23 to 4.26 for the protium and deuterium species and for "computed" and "real" backgrounds.

#### 4.4 The spectral data obtained for the complexes of phenol with acetonitrile and 1,4-dioxan

Tables 4.1 to 4.4 show the spectral data acquired for these complexes in carbon tetrachloride solution. Listed are the means and

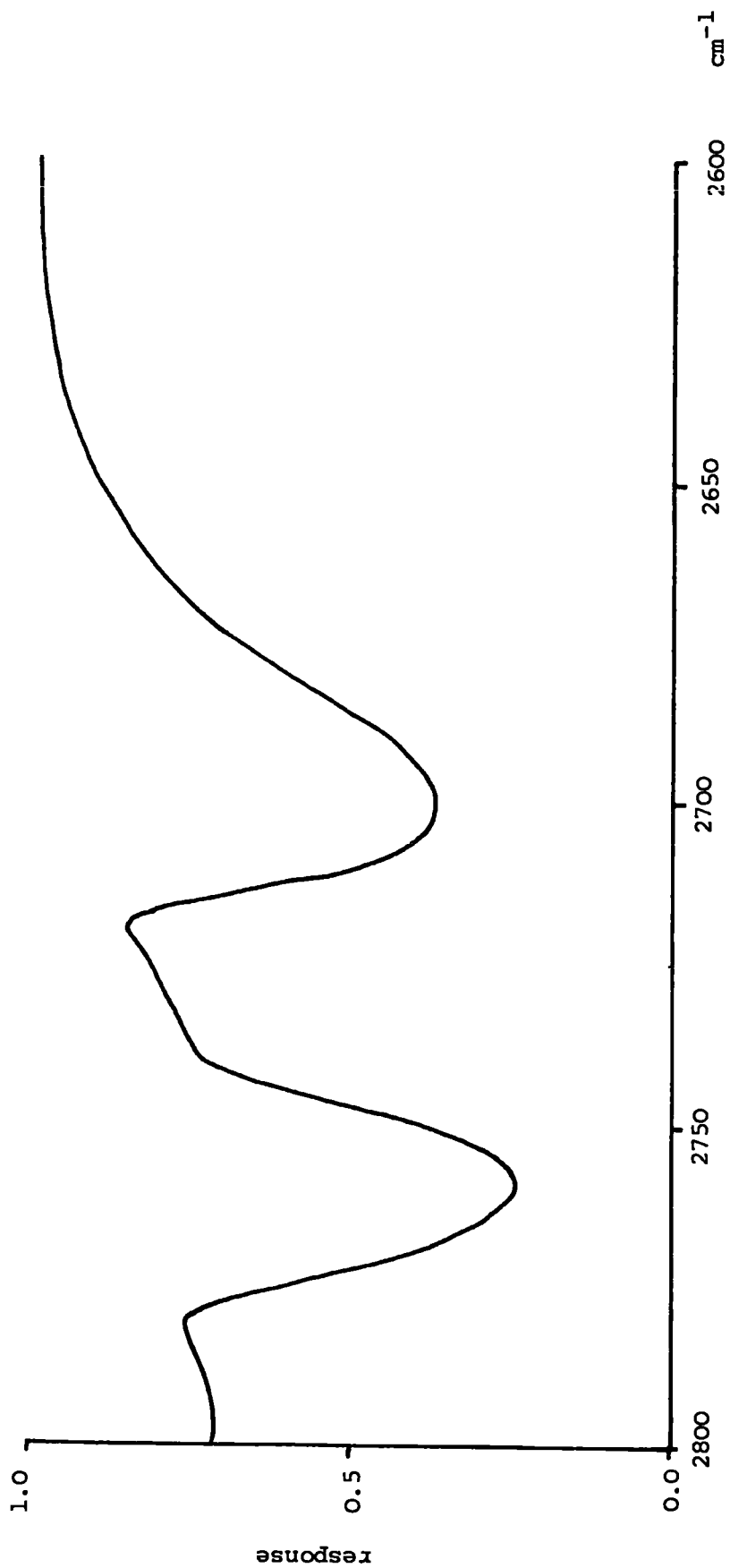


Figure 4,18 Approximate relative spectrometer response for the PhOD-1,4-dioxan in carbon tetrachloride system. The response is normalised arbitrarily at 2600cm<sup>-1</sup>

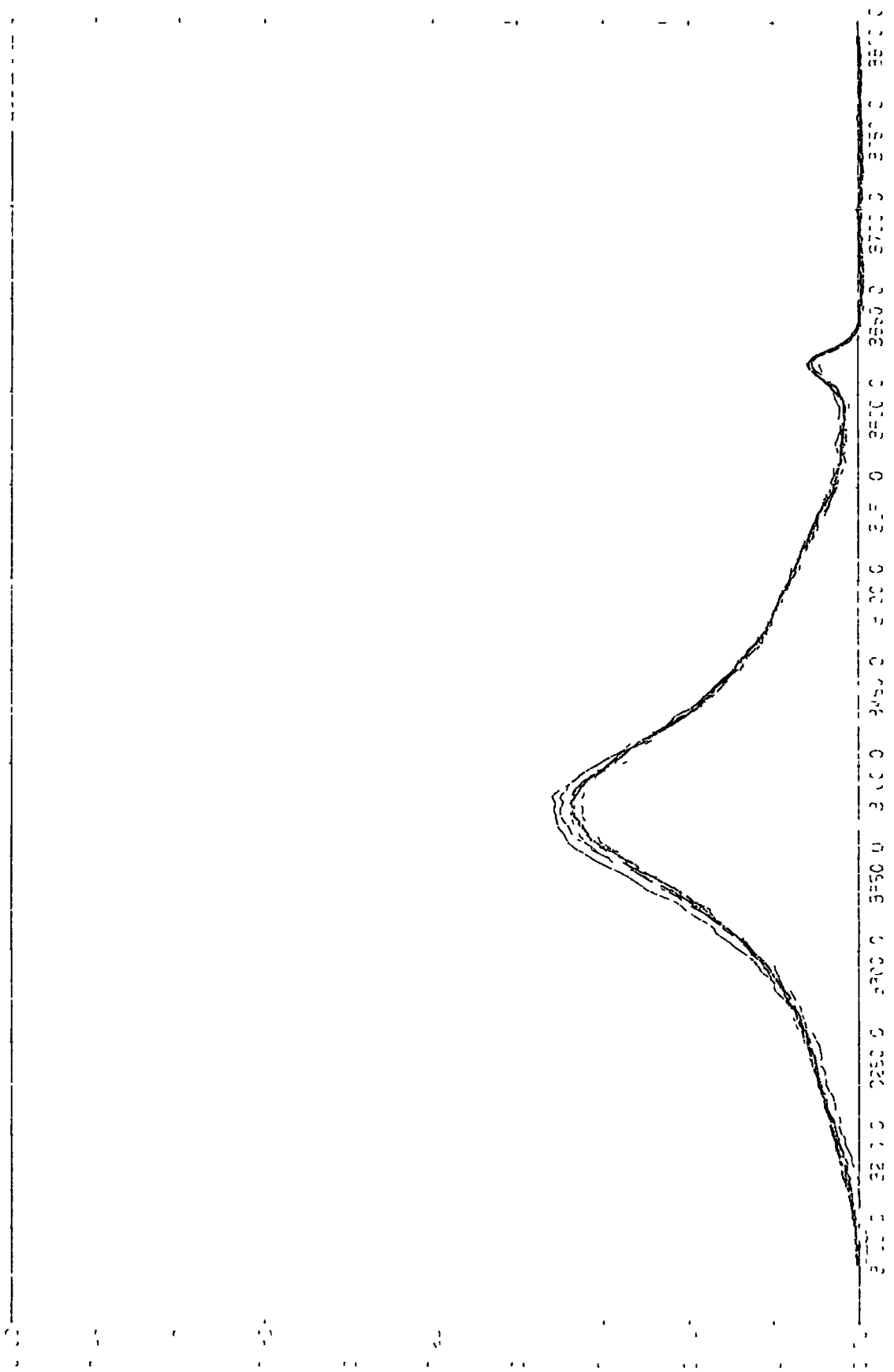


Figure 4.19 Ten independent spectral "runs" for the complex phenol-1,4-dioxan in carbon tetrachloride computed with IRINT6 using a "computed" background. The absorbance scale is decadic.

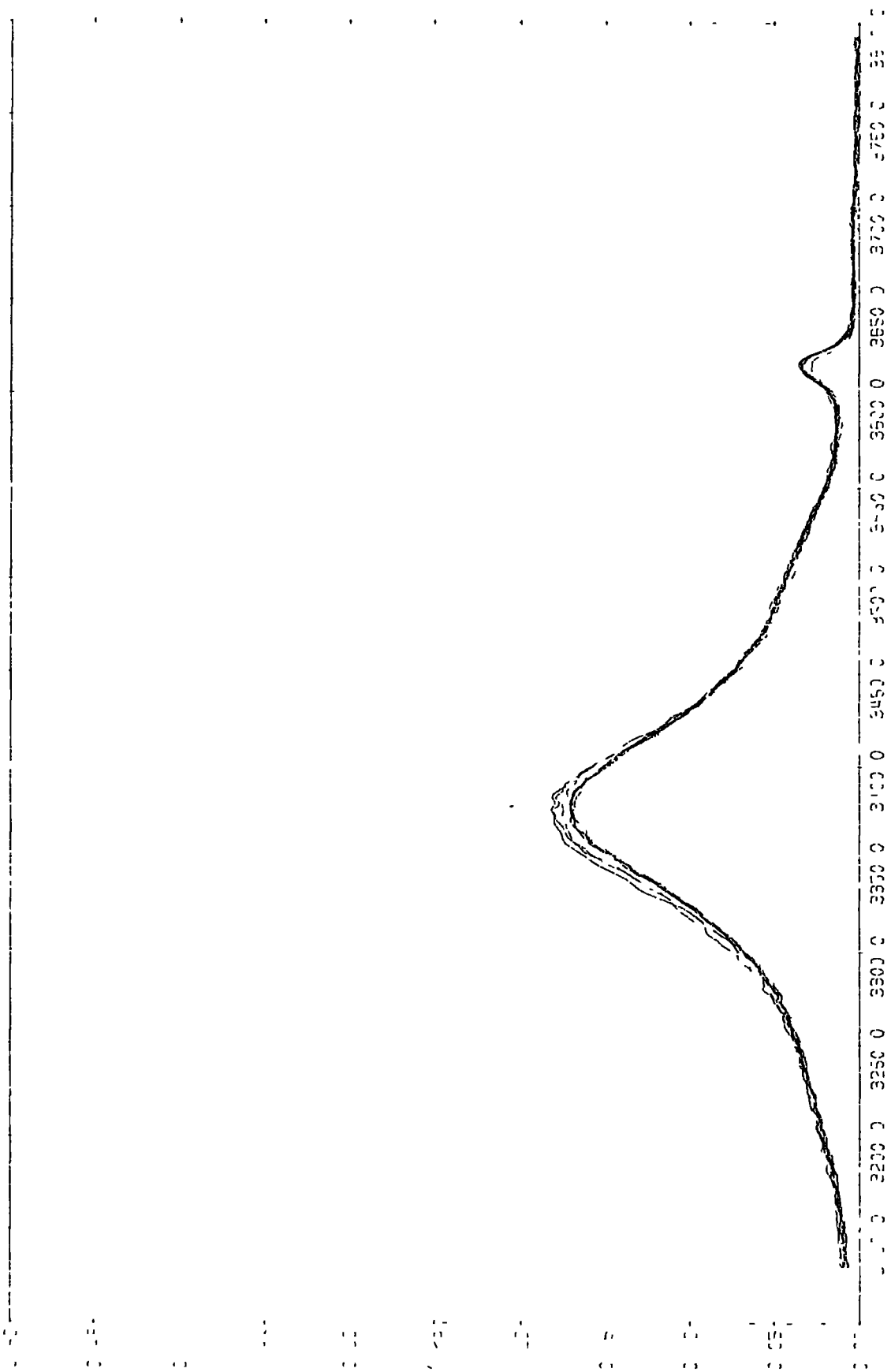


Figure 4.20 Ten independent spectral "runs" for the complex phenol-1,4-dioxan in carbon tetrachloride computed with IRINT6 using a "real" background. The absorbance scale is decadic.



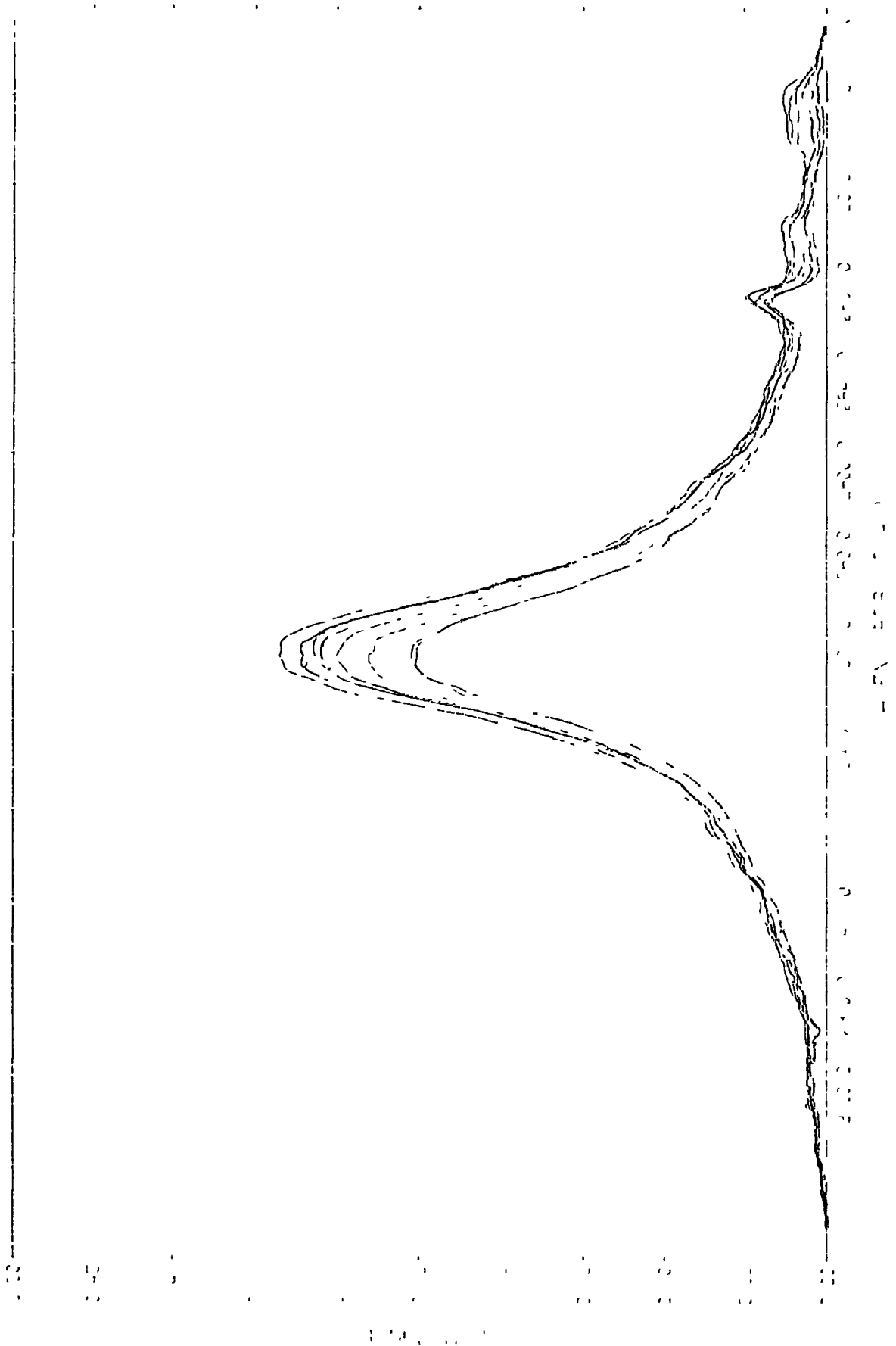


Figure 4.21 Ten independent spectral "runs" for the complex phenol (OD)-1,4-dioxan in carbon tetrachloride computed with IRINT6 using a "computed" background. The absorbance scale is decadic.

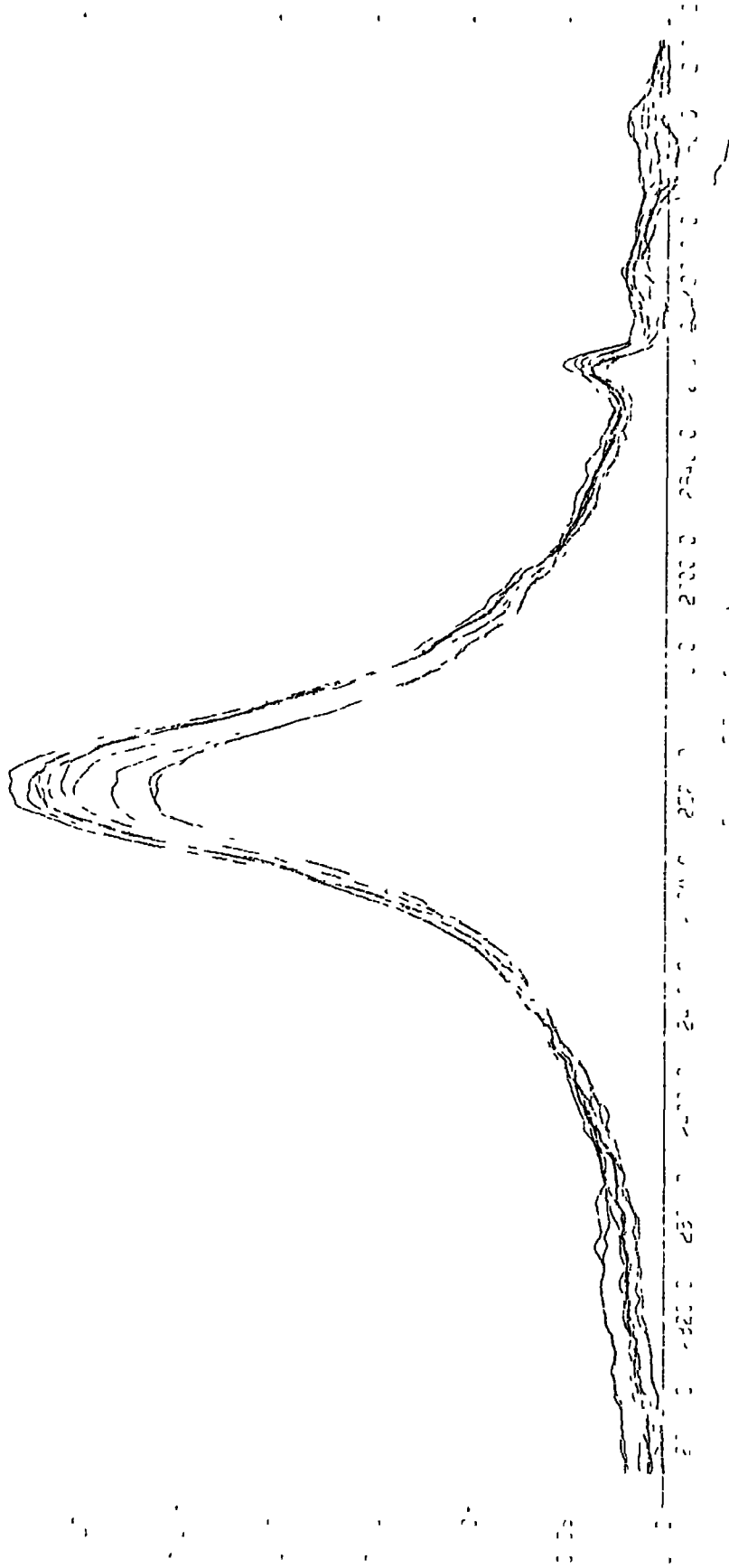


Figure 4.22 Ten independent spectral "runs" for the complex phenol(OD)-1,4-dioxan in carbon tetrachloride computed with IRINT6 using a "real" background. The absorbance scale is decadic.

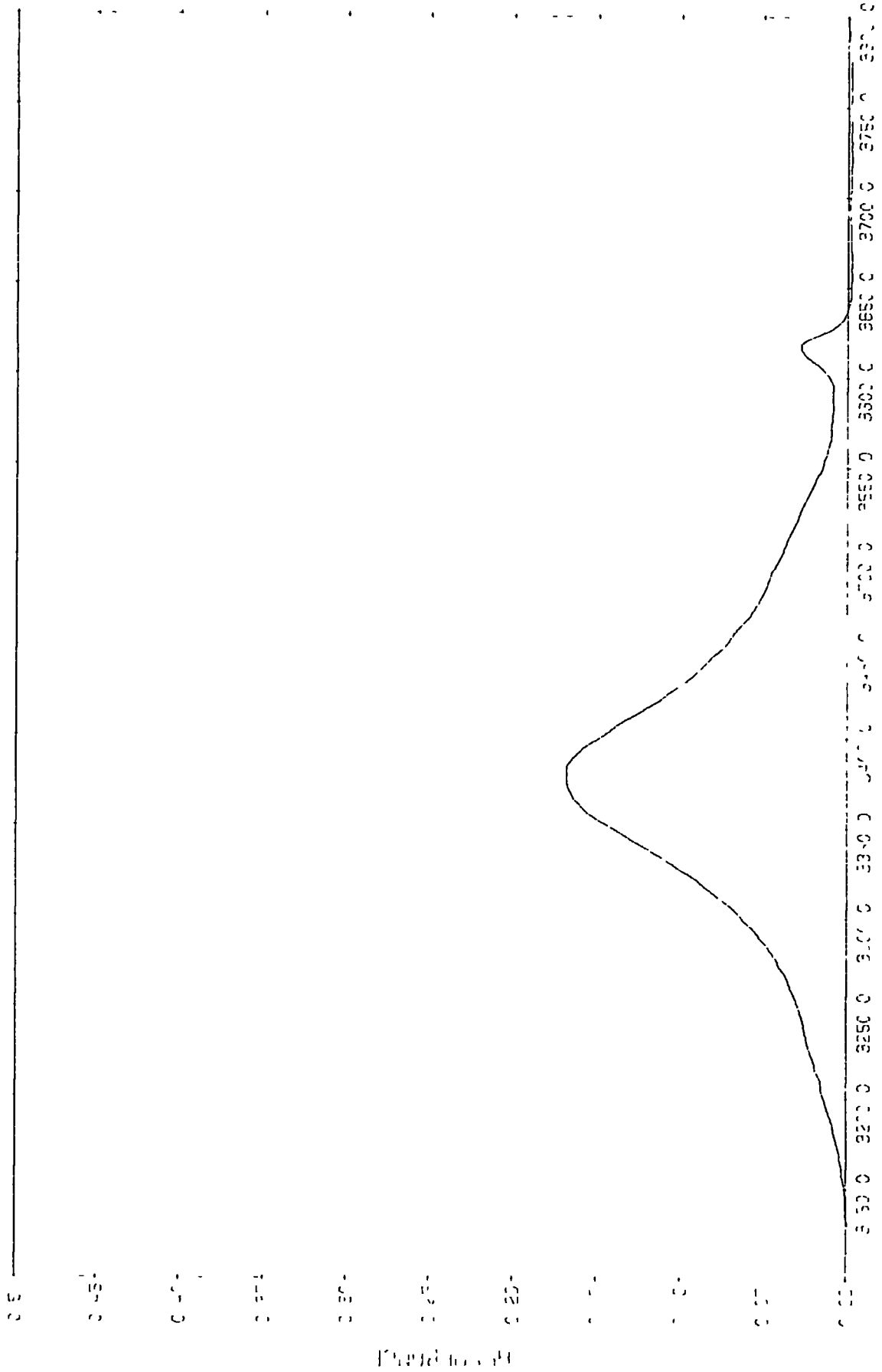


Figure 4.23 The spectrum of mean decadic absorbance values computed with IRINT6 using a "computed" background for the complex phenol-1,4-dioxan in carbon tetrachloride.

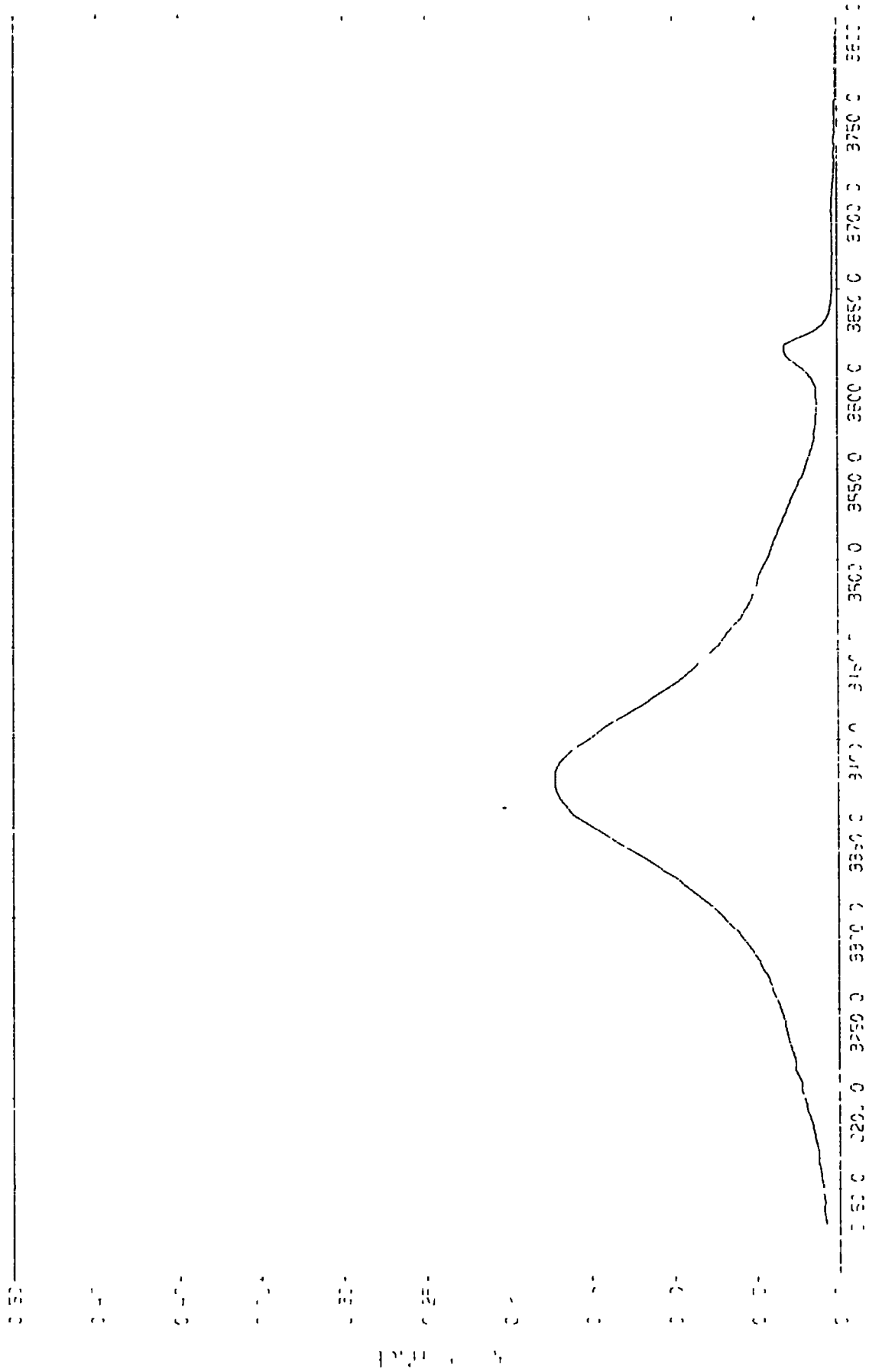
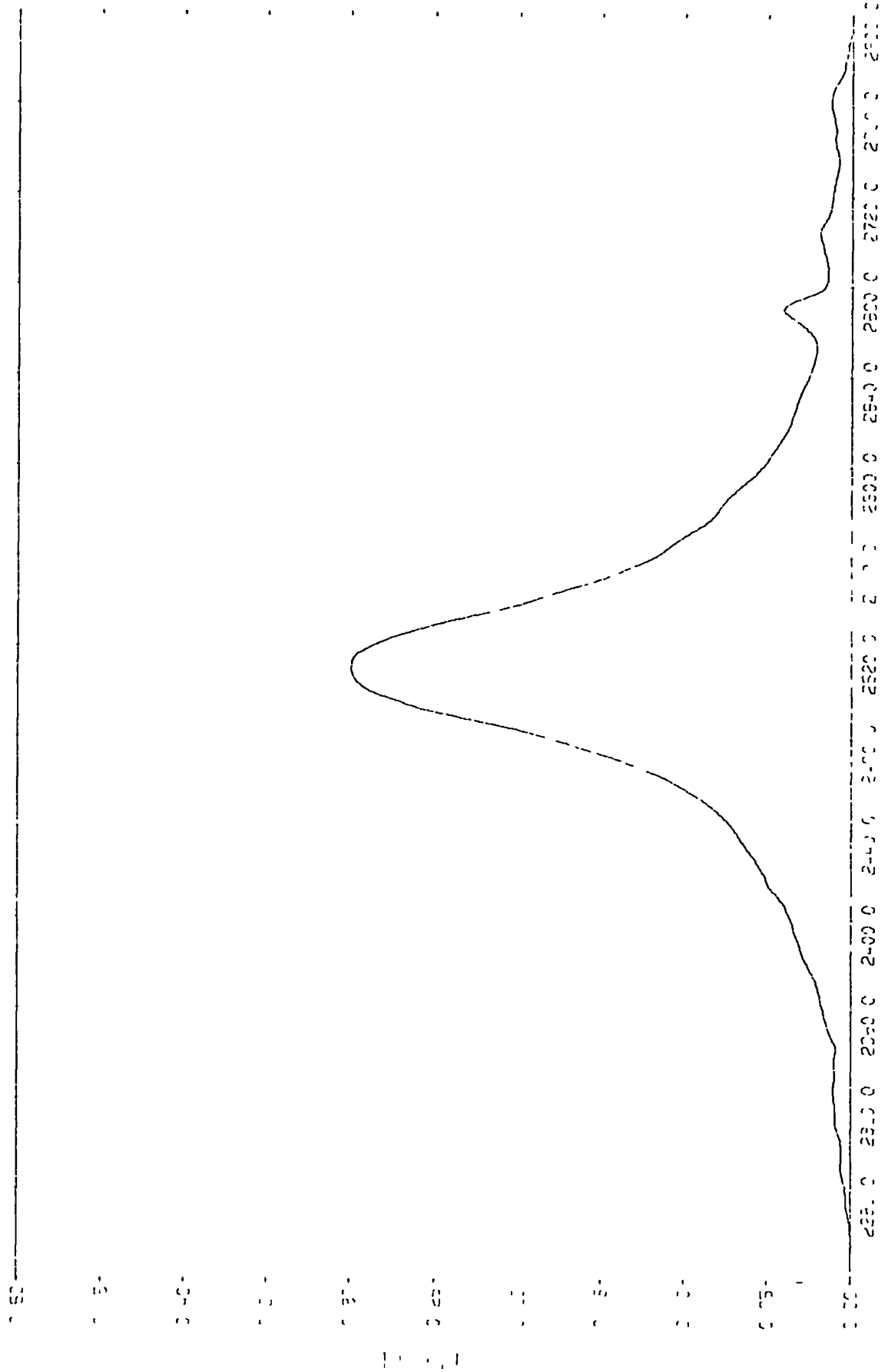


Figure 4.24 The spectrum of mean decadic absorbance values computed with IRINT6 using a "real" background for the complex phenol-1,4-dioxan in carbon tetrachloride.



2000 - 1000

Figure 4.25 The spectrum of mean decadic absorbance values computed with IRINT6 using a "computed" background for the complex phenol(OD)-1,4-dioxan in carbon tetrachloride.

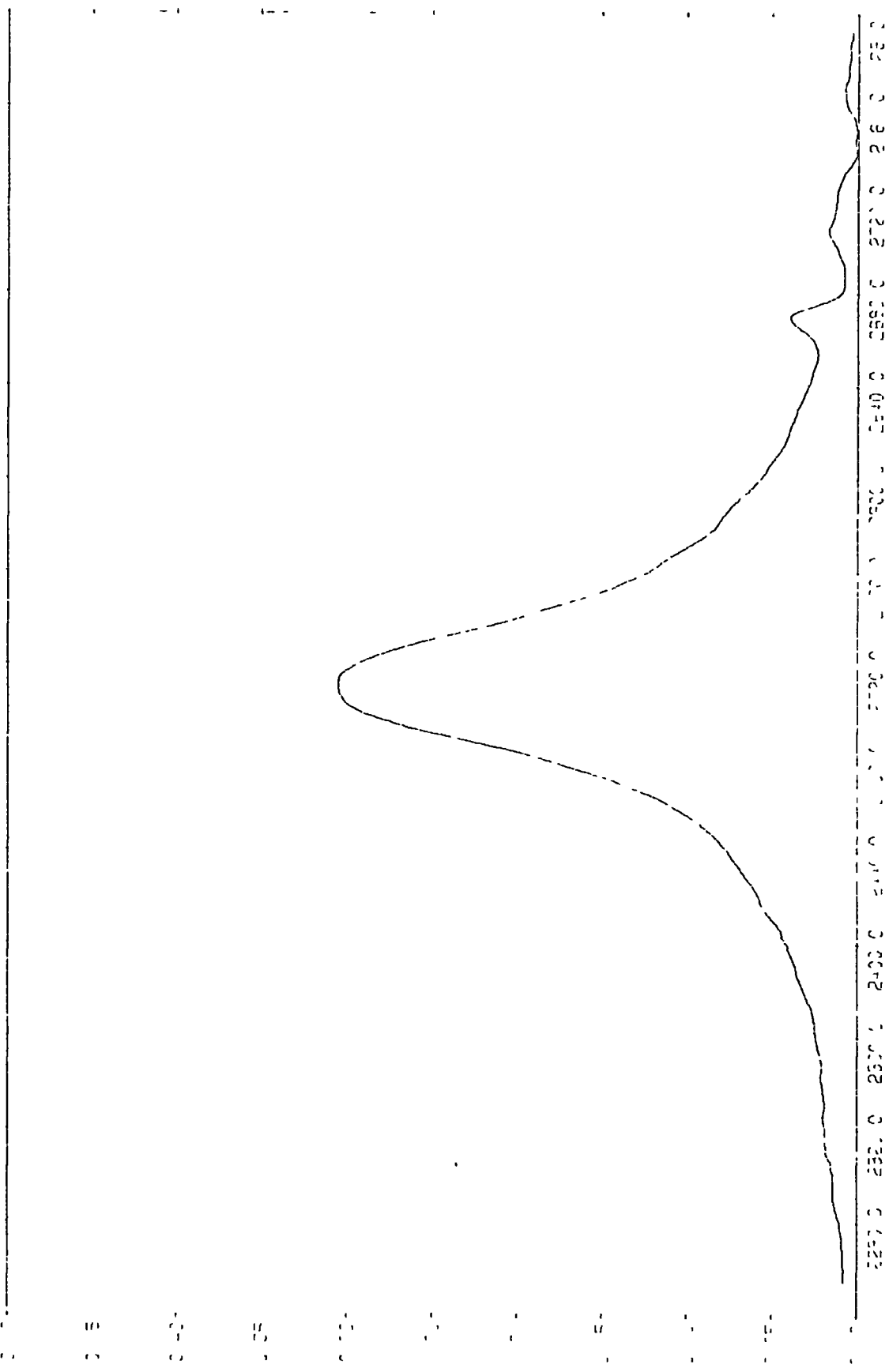


Figure 4.26 The spectrum of mean decadic absorbance values computed with IRINT6 using a "real" background for the complex phenol(OD)-1,4-dioxan in carbon tetrachloride.

Table 4.1 Spectral parameters for the  $\nu_s(\text{OH})$  band of the phenol-acetonitrile complex

in carbon tetrachloride

	maximum absorbance (decadic)	wavenumber of maximum absorbance ( $\text{cm}^{-1}$ )	halfwidth ( $\text{cm}^{-1}$ )	area (decadic)	
				IRINT1	IRINT6
"real" background ten independent spectra spectrum of mean values	0.205 $\pm 0.006$	3428 $\pm 5$	115 $\pm 2$	31 $\pm 1$	31 $\pm 2$
	0.205 $\pm 0.002$	3427	115	-	-
"computed" background ten independent spectra spectrum of mean values	0.209 $\pm 0.008$	3428 $\pm 4$	116 $\pm 1$	30 $\pm 1$	30 $\pm 1$
	0.208 $\pm 0.002$	3428	115	-	-

Table 4.2 Spectral parameters for the  $\nu_s$  (OD) band of the phenol(OD)-acetonitrile complex  
in carbon tetrachloride

	maximum absorbance (decadic)	wavenumber of maximum absorbance ( $\text{cm}^{-1}$ )	halfwidth ( $\text{cm}^{-1}$ )	area (decadic) ( $\text{cm}^{-1}$ )	
				IRINT1	IRINT6
"real" background	0.332	2546 $\pm$ 3	79 $\pm$ 1	35 $\pm$ 2	35 $\pm$ 2
	$\pm 0.024$				
spectrum of mean values	0.331	2547	80	-	-
"computed" background	0.325	2546 $\pm$ 3	78 $\pm$ 1	32 $\pm$ 2	31 $\pm$ 2
	$\pm 0.023$				
spectrum of mean values	0.323	2546	79	-	-
	$\pm 0.008$				



Table 4.3 Spectral parameters for the  $\nu_s$  (OH) band of the phenol-1,4-dioxan complex  
in carbon tetrachloride

	maximum absorbance (decadic)	wavenumber of maximum absorbance ( $\text{cm}^{-1}$ )	halfwidth ( $\text{cm}^{-1}$ )	area (decadic) ( $\text{cm}^{-1}$ )	IRINT1 IRINT6
"real" background	ten independent spectra	0.173 $\pm 0.005$	3376 $\pm 3$	127 $\pm 2$	30 $\pm 1$ 30 $\pm 1$
	spectrum of mean values	0.172 $\pm 0.002$	3377	127	-
"computed" background	ten independent spectra	0.170 $\pm 0.004$	3378 $\pm 3$	125 $\pm 3$	27 $\pm 1$ 27 $\pm 1$
	spectrum of mean values	0.168 $\pm 0.001$	3380	125	-

Table 4.4 Spectral parameters for the  $\nu_5$  (OD) band of the phenol(OD)-1,4-dioxan complex  
in carbon tetrachloride

	maximum absorbance (decadic)	wavenumber of maximum absorbance ( $\text{cm}^{-1}$ )	halfwidth ( $\text{cm}^{-1}$ )	area (decadic) ( $\text{cm}^{-1}$ )
				IRINT1
"real" background	ten independent spectra	2510 $\pm$ 3	79 $\pm$ 1	36 $\pm$ 3
	spectrum of mean values	2511	78	-
"computed" background	ten independent spectra	2511 $\pm$ 2	77 $\pm$ 2	34 $\pm$ 4
	spectrum of mean values	2510	78	-

their standard errors for the ten individual runs for each of the maximum absorbance (in decadic logarithmic units), the wavenumber at which it occurs, and the half bandwidth (full width at half maximum absorbance), all calculated by IRINT6. The mean areas of the absorption bands calculated with IRINT6 (allowing negative absorbance values) and with IRINT1 (setting negative absorbance values equal to zero) are also shown along with their standard errors (98). The parameters for the absorption band made up of mean absorbance values at each interpolated wavenumber are also shown. The close agreement in all cases between the parameters for this band and the mean values for the ten individual bands indicates good agreement between the individual bands, especially in terms of wavenumber precision where poor precision would result in a band with a lower maximum absorbance than the mean of the individual spectra. This is because the ten values contributing to the maximum of the "MEANSPEC3" band would not all be maxima of their individual bands.

#### 4.5 The $\nu_s$ (OH) absorption band of the complex phenol-acetonitrile in chloroform-d

In order to investigate the effect of a polar solvent on the  $\nu_s$  (OH) bandshape of the phenol-acetonitrile complex the absorbance spectrum when chloroform-d was used as solvent was recorded. This particular solvent was chosen because of its "structural" relationship to carbon tetrachloride and the deuterated compound was used to avoid the possibility of any interference in the spectrum from the  $\nu_s$  (CH) absorptions which would be present in the region  $3100\text{cm}^{-1}$  to  $2900\text{cm}^{-1}$  if the protium compound were used. Method B was used to obtain the absorbance data in an attempt to assess the Methods A and B for experimental ease, precision of data etc. The concentrations used were phenol 0.0562M and acetonitrile 3.49M. The cell pathlength was again approximately  $500\mu\text{m}$  and potassium bromide windows

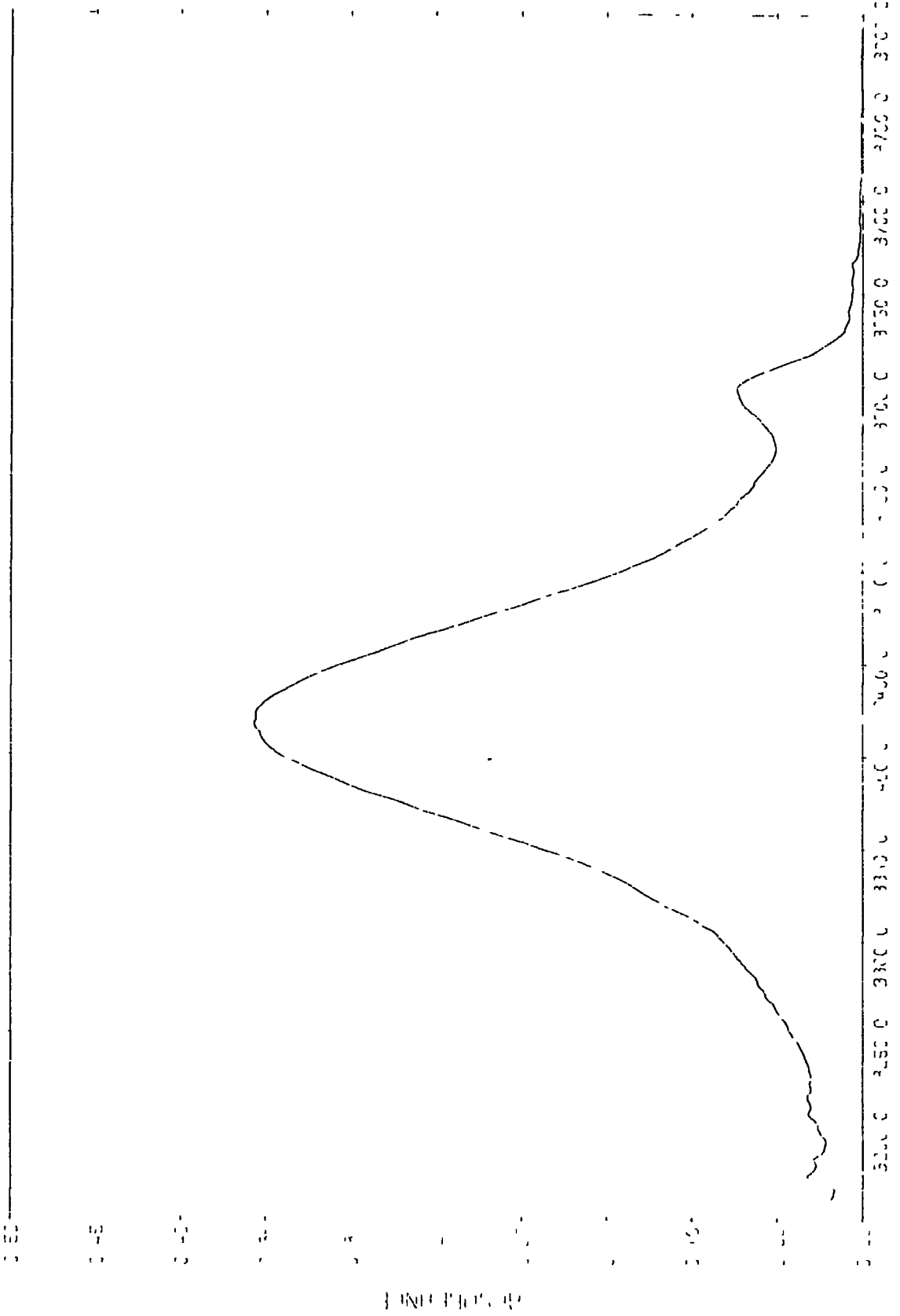


Figure 4.27 The spectrum of mean decadic absorbance values computed with IRINT6 for the complex phenol-acetonitrile in chloroform-d.

were used, the temperature was the spectrometer beam temperature,  $\sim 313\text{K}$ . The "sample" and "background" tapes for each of the ten runs were ratioed in order to obtain absorbance values using the programme IRINT6 and the spectrum of mean absorbance values was calculated using MEANSPEC3. The data so obtained are shown in Table 4.5 and Figure 4.27 shows the spectrum of mean absorbance values calculated by MEANSPEC3.

Table 4.5 Spectral parameters for the  $\nu_s(\text{OH})$  band of the phenol-acetonitrile complex in chloroform-d

	maximum absorbance (decadic)	wavenumber of maximum absorbance ( $\text{cm}^{-1}$ )	halfwidth ( $\text{cm}^{-1}$ )	area (decadic) ( $\text{cm}^{-1}$ )
ten independent spectra	$0.357 \pm 0.005$	$3416 \pm 1$	$141 \pm 1$	$147 \pm 3$
spectrum of mean values	$0.357 \pm 0.005$	3417	141	

#### 4.6 The method of fitting the experimental spectrum to the theoretical bandshape function

In this section the method used to fit the experimentally-obtained spectrum to the bandshape function predicted by the Robertson-Yarwood model will be described; further detail can be obtained from Appendix 1. The principle used is first to assume that the vibrational phase relaxation of the  $\nu_s(\text{OH})$  oscillator is fully described by the model described in Chapter 3; in other words that the absorbance data are fully described by the Fourier transform of Equation 3.6, the expression for the theoretical autocorrelation function. When the model parameters have been obtained by non-linear least-square fitting to this function, the extent to which the model describes the

experimental data can be assessed by application of variance-ratio tests. The model validity may also be tested by changing the temperature, solvent or molecular nature of the complex, for example by deuteration at the hydrogen-bonded proton.

The theoretical autocorrelation function was Fourier transformed using the Cooley-Tukey algorithm and the function obtained was fitted to the mean experimental spectrum using Fletcher's modification of Marquardt's non-linear least-squares method (99). The weighting factors used were calculated by the programme MEANSPEC3 (see Section 4.2) and were equal to the reciprocal of the square of the standard errors on the mean absorbance values. If in the following,  $v$  represents variance,  $\sigma$  standard deviation,  $s$  standard error,  $w$  the weighting factor and  $n$  the number of independent determinations (in this case usually ten)

$$w = s^{-2} = n/\sigma^2 = n/v \quad (4.1)$$

since

$$v = \sigma^2 \text{ and } s = \sigma/n^{1/2}$$

During the fitting procedure the points are weighted according to  $w^{1/2}$ , that is, inversely as the square root of their variances.

The four independent parameters used in the fitting procedure were  $\omega_1$ ,  $\omega_2$ ,  $\Delta$  and  $\Delta^2\tau_c$ , where  $\omega_1$  and  $\omega_2$  are the angular frequencies of the high and low frequency modes of vibration respectively,  $\Delta$  is the amplitude of modulation of the high frequency,  $\nu_s$  (XH), mode and  $\tau_c$  is the characteristic (or if appropriate correlation) time of the low frequency,  $\nu_o$  (XH---Y), mode. These parameters were previously defined in Sections 3.2 and 3.3. The reason for the use of  $\Delta^2\tau_c$  rather than simply  $\tau_c$  is because of its appearance in Equation 3.13 and therefore because its value determines the bandshape near the maximum (the "long-time" part), the bandshape in the wings (the "short-time" part) is determined by the value



of  $\Delta$  itself. As implied by the terms "long-time" and "short-time" the parameters  $\Delta^2 \tau_c$  and  $\Delta$  determine the value of the transition dipole moment autocorrelation function at long and short times respectively.

The fitting procedure used allowed a correction for "background-slope" to be made: as explained in Sections 2.4 and 2.5 the experimental baseline is difficult to obtain and considerable effort was made to find out which of the alternative methods (Method A or B, "real" or "computed" backgrounds) gave the best results. The correction procedure is described in Appendix 1 and amounts basically to subtracting a linear trend from the experimental absorbance data if a baseline slope can be shown to be present in the data.

The procedure also gave provision for "zero-weighting" certain parts of the experimental spectrum. This means that certain regions which were known to contain inaccurate or inappropriate data could be made to have no influence on the values of the fitted parameters obtained. Examples of such regions are where the phenol which remains uncomplexed at equilibrium with the base, despite the use of a large excess of the latter, absorbs and also where lack of pen response makes the absorbance values unreliable (see Section 4.3).

#### 4.7 The fitted parameters obtained for the complexes of phenol with acetonitrile and with 1,4-dioxan

Table 4.6 shows the estimates of the parameters  $\omega_1$ ,  $\omega_2$ ,  $\Delta^2 \tau_c$  (see Section 4.6) which were obtained from the fitting procedure. Also shown are values for  $\bar{\nu}_1$  ( $= \omega_1/2\pi c$ ) and  $\bar{\nu}_2$  ( $= \omega_2/2\pi c$ ), the values for  $\bar{\nu}_1$  compare well with those obtained by inspection of the absorbance data (see Tables 4.1 to 4.5). The data used were obtained with the early version (IRINT1) of the background ratioing and interpolating programme in which negative absorbance values are set equal to zero in the computation of each

Table 4.6 Estimated parameters for the complexes of phenol with acetonitrile and with 1,4-dioxan

complex	solvent	$\omega_1$ (rad ps <sup>-1</sup> )	$\omega_2$ (rad ps <sup>-1</sup> )	$\Delta$ (ps <sup>-1</sup> )	$\Delta^2 \tau_c$ (ps <sup>-1</sup> )	$\bar{\nu}_1$ (cm <sup>-1</sup> )	$\bar{\nu}_2$ (cm <sup>-1</sup> )	variance ratio	regions zero-weighted (cm <sup>-1</sup> )	
									uncomplexed $\nu_g$ (OH)	other interferences
PhOH- acetonitrile	CCl <sub>4</sub>	644 88 ± 0.06	25.1±0.9	14.1±0.9	11.3±0.3	3424.1±0.3	133±5	19.2	3580-3620	- -
PhOD- acetonitrile	CCl <sub>4</sub>	479 60 ± 0.06	25.1	10.4±0.7	6.6±0.1	2546.1±0.3	133	17.8	2655-2685	2570-2590 2390-2440
PhOH- 1,4-dioxan	CCl <sub>4</sub>	636 03 ± 0.04	29.0±0.4	19.0±0.6	10.2±1.0	3376.6±0.2	154±2	12.9	3580-3620	- -
PhOD- 1,4-dioxan	CCl <sub>4</sub>	473.13 ± 0.04	27.9±0.4	14.7±0.6	6.8±0.4	2511.8±0.2	148±2	1.02	2650-2793	- -
PhOH- acetonitrile	CDCl <sub>3</sub>	643.30 ± 0.04	23.9±1.7	15.1±0.1	16.1±0.5	3415.2±0.2	127±9	5.5	3580-3620	- -



individual spectral run. The fitting was repeated for certain systems with data obtained from the later version (IRINT6) which allows the negative absorbance values to be carried through to the final spectrum of mean absorbances but the effect on the parameter estimates was found to be negligible.

The choice of "real" or "computed" background was made for each system with a view to using the background with least slope. This meant that "computed" backgrounds were used for  $C_6H_5OH$  and  $C_6H_5OD$  with acetonitrile in carbon tetrachloride solution and that "real" backgrounds were used when 1,4-dioxan was the base. The phenol-acetonitrile complex in chloroform-d solution was obtained by Method B and so no "computed" background was possible. Background slope corrections were necessary for  $C_6H_5OD$  with acetonitrile and with 1,4-dioxan in carbon tetrachloride and for the phenol-acetonitrile complex in chloroform-d. Also shown in Table 4.6 are internal-external variance ratios (see Appendix 1). These are equal to unity when the discrepancies between the data and the model are caused only by random errors and rise to higher values if the model does not account entirely for the experimental data. It must be noted that only in one case ( $C_6H_5OD$ -1,4-dioxan in carbon tetrachloride) is the variance ratio close to unity; this is despite apparently good agreement between the experimental spectrum and that calculated from the fitted parameters.

The regions in which the absorbance data were zero-weighted to avoid interferences as described above are also shown in Table 4.6. In order to obtain reasonable parameter estimates for the system  $C_6H_5OD$ -acetonitrile in carbon tetrachloride it was necessary to zero-weight the data in three regions: 2655 to  $2685\text{cm}^{-1}$  corresponding to absorption by uncomplexed phenol, 2570 to  $2590\text{cm}^{-1}$  where there is an obvious shoulder on the absorption band and 2390 to  $2440\text{cm}^{-1}$  where there is a third irregularity in the bandshape. The last of these three interferences may be due to lack

of pen response due to absorption at  $\sim 2410\text{cm}^{-1}$  in acetonitrile in both spectrometer beams but the region  $2570$  to  $2590\text{cm}^{-1}$  corresponds to no absorption band in either base or solvent and therefore the possibility of a weak Fermi resonance-type effect cannot be ruled out. In order to aid the fitting procedure for this system the value of  $\bar{\nu}_2$  ( $133\text{cm}^{-1}$ ) obtained from the protium species complex was inputted to the fitting procedure. The value of  $\bar{\nu}_2$  (corresponding to  $\nu_\sigma(\text{XH}---\text{Y})$  or  $\nu_\sigma(\text{XD}---\text{Y})$ ) is expected to change only by a small amount of deuteration since the motion in question only involves the proton or deuteron by a small amount.

#### 4.8 The change in the fitted parameters on deuteration

As mentioned before, the  $\nu_s(\text{OH})$  frequency decreases on deuteration by a factor of approximately  $2^{1/2}$  and this was in fact observed (see Tables 4.1 to 4.4). This relationship is only approximate because it applies only in the harmonic oscillator approximation and it also assumes that the ratio of the reduced masses (and not the masses) is equal to two. In the harmonic approximation there should be no change in the  $\nu_\sigma(\text{XH}---\text{Y})$  frequency ( $\omega_2$ ) on deuteration. The change in the amplitude of modulation parameter,  $\Delta$ , can be found as follows. From Equations 3.9 and 3.10:

$$\Delta = \frac{K_{112} \langle r_2^2 \rangle^{1/2}}{m_1 \omega_1} \quad (4.2)$$

now, in the harmonic oscillator approximation

$$\frac{m_1^H}{m_1^D} = \frac{[\omega_1^D]^2}{[\omega_1^H]^2} \quad (4.3)$$

from Equation 4.2

$$\frac{\Delta^H}{\Delta^D} = \frac{m_1^D \omega_1^D}{m_1^H \omega_1^H} \quad (4.4)$$

so

$$\frac{\Delta^H}{\Delta^D} = \frac{[\omega_1^H]^2 \omega_1^D}{[\omega_1^D]^2 \omega_1^H} \quad (4.5)$$

or

$$\frac{\Delta^H}{\Delta^D} = \frac{\omega_1^H}{\omega_1^D} \quad (4.6)$$

assuming that  $K_{112}$  and  $r_2$  do not change on deuteration. The damping parameter of the Langevin equation,  $\gamma$ , should show no change on deuteration since it is, at least in principle, a property of the solvent. The characteristic time of the stochastic modulation,  $\tau_c$ , should vary only if  $\omega_2$  changes since (from Equation 3.11)

$$\tau_c = \gamma/\omega_2^2$$

The transition dipole moment relaxation time,  $\tau_r$ , which is given by (from Equation 3.14)

$$\tau_r^{-1} = \tau_c \Delta^2$$

should change as  $1/\Delta^2$ , that is, as  $1/\omega_1^2$ .

Table 4.7 shows the changes in both the fitted and derived parameters on deuteration and the expected changes for comparison.

It can easily be seen that the transition dipole moment relaxation time,  $\tau_r$ , for the  $\nu_s$ (OH) oscillator is increased on deuteration because  $\Delta$  is decreased and therefore the modulation of the  $\nu_s$ (OH) mode by the solvent environment is decreased. The value for  $\tau_c \Delta$  is also smaller in the deuterated complexes showing them to have a more nearly lorentzian bandshape.

As explained in Section 3.4 the halfwidths of the absorption bands should show a deuteration ratio of between 2 (in the rapid modulation limit) and  $2^{1/2}$  (in the slow modulation limit) unless one modulation limit is applicable; this is shown to be as expected in Table 4.7 and is consistent with values for  $\tau_c \Delta$  of around 0.6.

Table 4.7 Changes in parameters on deuteration for the complexes of phenol with acetonitrile and with 1,4-dioxan  
in carbon tetrachloride

complex	$\frac{\bar{\nu}_1^H}{\bar{\nu}_1^D}$	$\frac{\Delta^H}{\Delta^D}$	$\left[ \frac{(\tau_c^H)^2}{(\tau_c^D)^2} \right]^{1/2}$	$\frac{\Delta \bar{\nu}_1^H}{\Delta \bar{\nu}_1^D}$	$\gamma$	$\tau_c$	$\gamma/2\omega_2$	$\tau_c \Delta$
phenol- -OH	1.3448	1.36±0.01	1.31±0.02	1.55±0.05	35.7±2.3	0.057±0.002	0.71±0.04	0.80±0.03
acetonitrile -OD	±0.002				38.4±0.8	0.061±0.002	0.77±0.02	0.64±0.02
phenol- -OH	1.3443	1.29±0.01	1.23±0.07	1.61±0.05	23.9±0.4	0.028±0.001	0.41±0.01	0.54±0.01
1,4-dioxan -OD	±0.002				24.2±0.5	0.031±0.001	0.44±0.01	0.46±0.01
expected change	$\sqrt{2}$	as $\frac{\bar{\nu}_1^H}{\bar{\nu}_1^D}$	as $\frac{\bar{\nu}_1^H}{\bar{\nu}_1^D}$	between $\sqrt{2}$ and 2	none	only if $\omega_2$ changes	only if $\omega_2$ changes	as $\frac{\bar{\nu}_1^H}{\bar{\nu}_1^D}$

#### 4.9 The change in the fitted parameters on change of solvent

The change in halfwidth from  $115\text{cm}^{-1}$  to  $141\text{cm}^{-1}$  and a downward shift in frequency from  $3428 \pm 5\text{cm}^{-1}$  to  $3416 \pm 1\text{cm}^{-1}$  when the phenol-acetonitrile complex is dissolved first in carbon tetrachloride and then in chloroform-d can be seen from Tables 4.1 and 4.5. There are two possible explanations of these changes:

(i) following the work of Bellamy et al. (100) there is some specific interaction between solvent and complex leading to a strengthening of the complex in the polar solvent, or

(ii) following the work of Buckingham (101) and of Horak et al. (93,102) the more polar solvent causes a lowering of the self-energy of the  $v = 0$  and  $v = 1$  states by differing amounts and produces a shift in the frequency of the absorption maximum.

The first mechanism may be considered to be a "chemical" interaction and the second mechanism is a "medium" effect. The broadening can be explained in terms of the Robertson-Yarwood model as follows:

(i) a change in the electronic structure of the complex strengthens the hydrogen bond and thus the anharmonic coupling constant  $K_{112}$  is increased and the force constant for the stretching of the O-H band is decreased. Both these effects bring about an increase in  $\Delta$ , the amplitude of stochastic modulation.

In the case (ii) the variance of the random force in the Langevin equation (Equation 3.9) is greater and  $\gamma$  must increase if  $m_2$ ,  $r_2$  and  $\omega_2$  do not change. The value of  $\tau_c$  is thus affected (Equation (3.11)) and the band-shape becomes broader except in the slow modulation limit (see Equations 3.24 and 3.25).

From Table 4.6 the values for  $\bar{\nu}_2$  (corresponding to  $\nu_0(\text{XH}---\text{Y})$ ) are  $133 \pm 5\text{cm}^{-1}$  and  $127 \pm 9\text{cm}^{-1}$  for phenol-acetonitrile in

carbon tetrachloride and chloroform-d solution respectively. These values provide no evidence that the hydrogen bond strength is altered in the polar solvent, largely on account of the large standard errors associated with them. In order to make a better comparison between the data the two systems were re-analysed with the value of  $\bar{\nu}_2$  being fixed at  $133\text{cm}^{-1}$  in the fitting procedure. The real and computed backgrounds were used for the complex in carbon tetrachloride and the real version for the chloroform-d system, the data for which were obtained by Method B, and so no computed background was available. The estimated and derived parameters obtained in this way are shown in Table 4.8.

It can be seen from Table 4.8 that the value for  $\Delta$  is increased somewhat in the polar solvent but because of the standard errors associated with the parameter values and the discrepancy between the real and computed background versions of the complex in carbon tetrachloride solution the effect is rather inconclusive. The data in Table 4.8 do, however, show that  $\gamma$  certainly increases from carbon tetrachloride solution to chloroform-d solution and therefore the characteristic time of the stochastic modulation also shows a marked increase. The increase in  $\tau_c \Delta$  indicates a move towards the slow modulation limit and hence a more gaussian bandshape which appears broader.

Although the change in  $\gamma$  can be associated with an increase in the random force in the Langevin equation it must be noted that the macroscopic viscosity of the two solvents does not change in the same manner as the value of  $\gamma$ . The viscosity of chloroform-d is  $4.59 \times 10^{-4} \text{kgm}^{-1} \text{s}^{-1}$  and of carbon tetrachloride is  $7.38 \times 10^{-4} \text{kgm}^{-1} \text{s}^{-1}$  (103). These figures illustrate the danger of associating the bulk properties of a liquid with processes which take place at a molecular level as is often done (see, for example ref. 104). For the same reason it would not be possible to determine  $\gamma$  by means of the Stokes-Einstein relationship (105)

Table 4.8 Solvent effects on the phenol-acetonitrile complex

Solvent	Background	$\Delta\bar{\nu}_2$ ( $\text{cm}^{-1}$ )	$\bar{\nu}_1$ ( $\text{cm}^{-1}$ )	$\Delta$ ( $\text{ps}^{-1}$ )	$\tau_c \Delta^2$ ( $\text{ps}^{-1}$ )	$\tau_c$ (ps)	$\gamma$ ( $\text{ps}^{-1}$ )	$\tau_c \Delta$	variance ratio
$\text{CDCl}_3$	real	148	$3414.3 \pm 0.2$	$15.1 \pm 0.1$	$16.3 \pm 0.3$	$0.072 \pm 0.001$	$45.0 \pm 0.9$	$1.08 \pm 0.02$	5.4
$\text{CCl}_4$	computed	116	$3423.9 \pm 0.3$	$14.2 \pm 0.1$	$11.1 \pm 0.3$	$0.055 \pm 0.001$	$34.7 \pm 0.8$	$0.78 \pm 0.02$	18.0
$\text{CCl}_4$	real	116	$3425.0 \pm 0.2$	$14.9 \pm 0.1$	$10.1 \pm 0.2$	$0.046 \pm 0.001$	$28.6 \pm 0.4$	$0.68 \pm 0.01$	5.0

for a particle in a viscous fluid. Apart from it having been indicated (see above) that  $\gamma$  probably does not follow the macroscopic viscosity value, the Stokes-Einstein relationship only describes the situation of a spherical particle in a fluid of molecules much smaller than the particle under consideration.

4.10 Conclusions drawn from the application of the Robertson-Yarwood model to the complexes of phenol with acetonitrile and with 1,4-dioxan

The Robertson-Yarwood model has been shown to account for the shape of the  $\nu_s$  (XH) absorption band very well indeed for the  $C_6H_5OD$  - 1,4-dioxan complex in carbon tetrachloride solution and to give a very reasonable description for the other systems studied. The conclusion can be drawn that the vibrational phase relaxation of the  $\nu_s$  (XH) mode takes place very largely through anharmonic coupling to the  $\nu_g$  (XH---Y) mode which can be well-described by an Ornstein-Uhlenbeck stochastic process. The discrepancies between model and observation may be due to the influence of other relaxation processes but these would be expected to affect all the complexes studied equally with the possible exception of  $C_6H_5OD$ -acetonitrile where Fermi-resonance effects may influence the bandshape. Among these other relaxation processes which may influence the bandshape is rotational relaxation which has been shown to be important in the interpretation of the infrared absorption spectrum of simple diatomic and polyatomic molecules (58). The probable reason for the lack of influence here is that the vibrational relaxation time is very short (between 0.062 and 0.15ps) and the vibrational phase coherence is completely lost during the period of reorientation of the complex. This period would in any event be expected to be rather long due to the large size of the complex.



Because an adiabatic separation of the modes (see Section 3.2) was originally made and the model produced can then describe the observed bandshape, it can be said that vibrational energy relaxation (106) must take place at a much slower rate than vibrational phase relaxation. Otherwise, the modes would be expected to interact energetically during the period of the vibrational phase relaxation and the adiabatic approximation would then break down.

The discrepancy between the model and the observed data found for all but one system (see variance ratio values in Table 4.6) tends to suggest that systematic errors are of considerable importance. The aim of testing the "real" and "computed" background was not entirely achieved since the better of the two versions of each spectrum had a considerably high variance ratio in each case. There did not, however, appear to be a distinct tendency for either "real" or "computed" backgrounds to give a better agreement with the model. Likewise, the method of obtaining the background (Methods A and B of Section 2.5) did not have any particularly striking effect on the variance ratios obtained although the value (5.5) obtained for phenol-acetonitrile in chloroform-d by this method was relatively low although not so good as that for  $C_6H_5OD$ -1,4-dioxan obtained by Method A.

The choice between the "real" and the "computed" backgrounds is very difficult to make. The "real" background should in principle be a straight line of constant transmittance value if it is unaffected by factors such as variable pen response, photometric non-reproducibility, difference in reflection-losses in the two cells and, probably most importantly, variations in temperature. If the transmittance at both "ends" of the band are equal (as they should be if no other absorption takes place in the neighbouring region of the spectrum) the computed background should also be a line of constant transmittance values. In this ideal situation the two backgrounds would be identical apart from

the presence of noise in the "real" background and the "computed" background could be considered preferable on account of its requiring much less time in data collection. All this requires that the factors listed above can be maintained constant and this is a very difficult situation to achieve in practice. Probably the largest single source of error here is the variation in the temperature during the running of a spectrum and from one spectrum to another. An attempt was made to repeat some measurements using a Beckman Instruments VLT-2 variable temperature unit (107) and a TEM-1C temperature controller (108). Severe problems were encountered because the jacket of the cell-holder contained a vacuum space in the sample beam which was not matched in the reference beam and absorption in the reference beam by residual carbon dioxide and water vapour in the cell-box, despite flushing with dry nitrogen (see Section 2.3), created interference in the recorded spectrum.

Of the remaining factors the different reflectance losses in the two cells cannot be avoided since they depend on the contents of the cells but careful polishing can help to minimise them. The pen response and photometric precision can not be changed particularly since they are functions of the chemical nature of the system under study and the spectrometer itself.

The Method B produced reasonably precise data but problems can arise through changes in wavenumber accuracy between recording of sample and background resulting in sharp absorption bands not ratioing out precisely. Overall, however, there does not seem to be any particular advantage to either Method A or Method B and the lack of precision in the data arises largely from factors which cannot be avoided by use of either method.

A third method, that of calculating the background transmittance level from the mean of the first twenty or thirty data points in the sample, was also used and this is discussed in Section 4.11 where the analysis of data for the phenol-pyridine complex is described.

4.11 The  $\nu_s$  (OH) absorption band of the phenol-pyridine complex  
in carbon tetrachloride

This complex has been studied previously by Hall and Wood (67) and it was observed that the bandshape shows considerable "structure" in the form of a series of sub-maxima on the low-wavenumber side of the band. This effect has been attributed to Fermi-resonance type interaction taking place between the  $\nu_s$  (OH) vibration and certain overtone or combination modes of the phenol. In view of the fact that a model was being developed (70) to account for these effects without resort to a "slow-modulation limit" approximation (56) it was thought useful to attempt to obtain digital data for this absorption band in the same manner as was done for the phenol-acetonitrile and phenol-1,4-dioxan complexes.

The main difference between the phenol-pyridine system and those described before (see Sections 4.2 and 4.3) is that the  $\nu_s$  (OH) absorption band extends to as low as  $2300\text{cm}^{-1}$  and therefore "covers" the area of  $\nu_s$  (CH) absorptions in both phenol and pyridine. It must therefore be attempted to "ratio-out" these absorptions and obtain the true  $\nu_s$  (OH) band profile. This is only possible if the  $\nu_s$  (CH) absorptions are unperturbed on complex formation and their effects on the complex spectrum can be removed by using the spectral data from the uncomplexed components. Preliminary investigations showed immediately that this was not the case and so the study was continued using pyridine- $d_5$  in which the  $\nu_s$  (CD) absorptions are shifted to  $2220\text{--}2400\text{cm}^{-1}$  which is below the region of principal interest. It was also found that the  $\nu_s$  (CH) vibrations of phenol are perturbed on complexation but the expense of  $C_6D_5OH$  precluded the use of this compound to remove the effects of  $\nu_s$  (CH) absorption in  $C_6H_5OH$  in a similar manner. The region in which these absorptions affect the spectral profile must be zero-weighted in any subsequent analysis by a fitting procedure.

Because the equilibrium constant for the phenol-pyridine complex has a value of about 40 (109,110) sufficient concentration of complex can be obtained with a relatively low base concentration. It was therefore proceeded with phenol and pyridine-d<sub>5</sub> concentrations of 0.0709M and 0.0923M respectively giving a complex concentration given by:

$$\begin{aligned} [\text{complex}] &= K[\text{C}_6\text{H}_5\text{OH}][\text{C}_5\text{D}_5\text{N}] \text{ at equilibrium} \\ &\approx 0.00355 \text{ mol dm}^{-3} \end{aligned}$$

The spectrum of a solution containing both components at the above concentrations was recorded in the manner described for Method B (see Section 2.5) over the range 3800cm<sup>-1</sup> to approximately 2100cm<sup>-1</sup> using a cell with a nominal 500µm teflon spacer and potassium bromide windows. A sampling interval of 4s was used corresponding to 3.33cm<sup>-1</sup>. This procedure was then repeated using solutions first of phenol and then of pyridine-d<sub>5</sub> each at the same molarity as used for the mixture. The two background spectra computed separately using the "computed background" version of IRINT6 are shown in Figures 4.28 and 4.29.

It was first attempted to subtract both the phenol and the pyridine absorptions from the spectrum of the complex by using a computer programme that added together the absorbances in the two "background" spectra, using the "computed background" method, and then subtracted the sum from the complex spectrum computed in the same way. This was found to be rather unsatisfactory because in the regions of the spectrum away from the chief ν<sub>s</sub>(CH) and ν<sub>s</sub>(CD) absorptions there is some absorption (≈ 0.02 naperian units), because the "baseline" is not completely level, and when these absorptions were summed they became rather appreciable and produced an unwanted effect on the spectrum obtained after subtraction.

It was therefore considered better to proceed in the following way. A value for the baseline transmittance for the complex and for the pyridine-d<sub>5</sub> was obtained by taking the mean of the first thirty data points

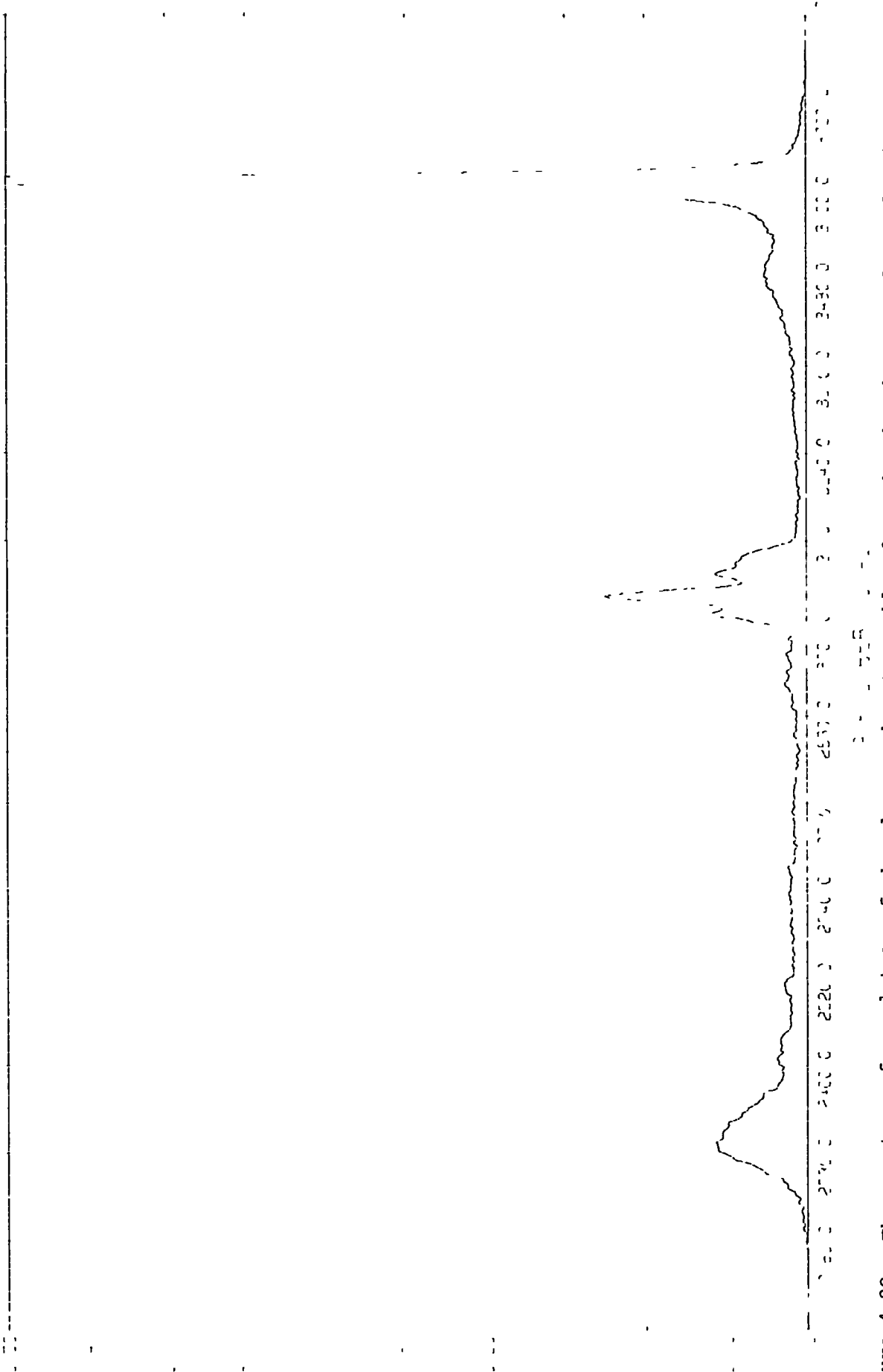


Figure 4.28 The spectrum of a solution of phenol in carbon tetrachloride. The absorbance scale is decadic.

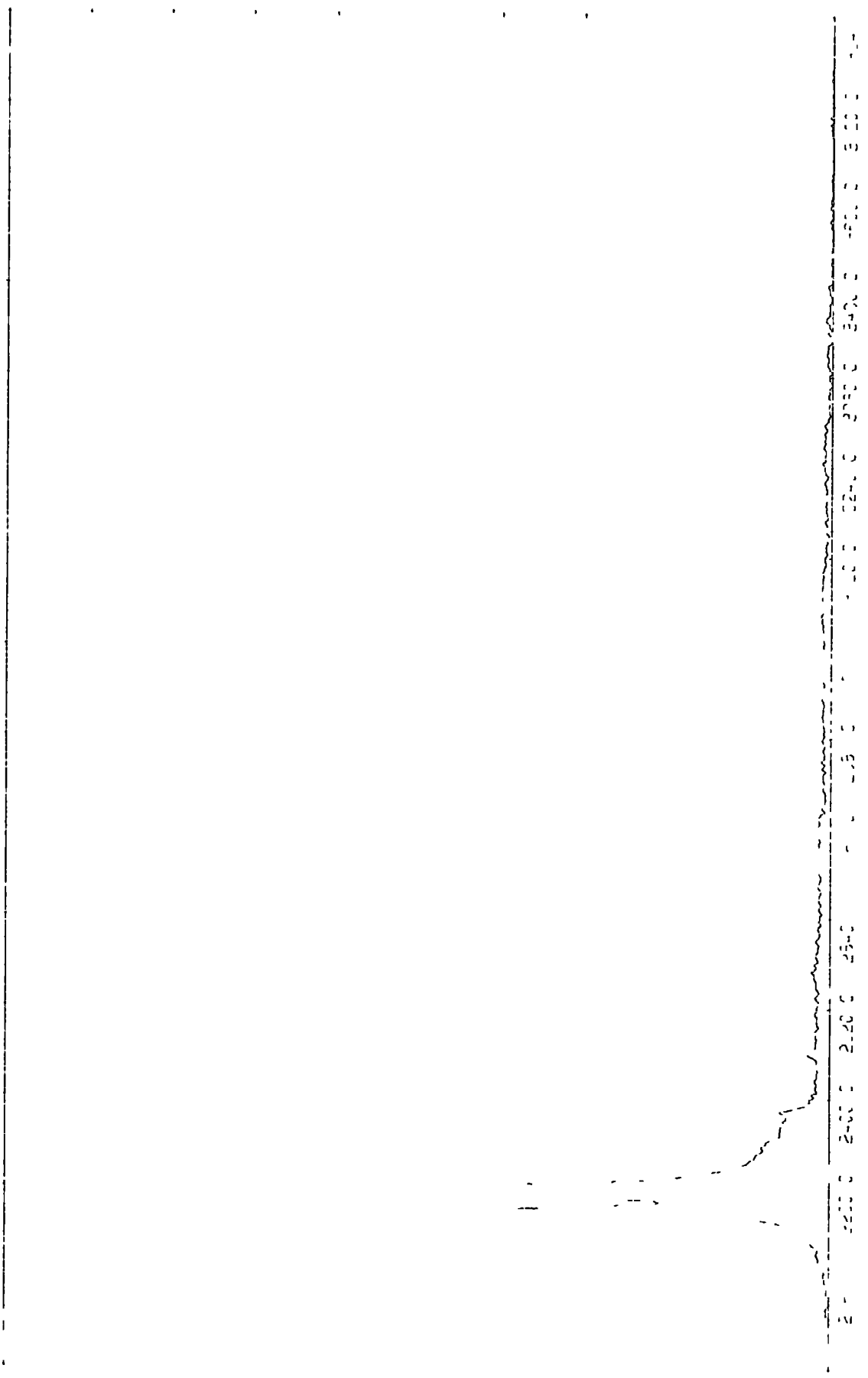


Figure 4.29 The spectrum of a solution of pyridine-d<sub>5</sub> in carbon tetrachloride. The absorbance scale is decadic.

(i.e.  $3800\text{cm}^{-1}$  to  $\sim 3700\text{cm}^{-1}$ ) and using this value of  $T_0$  to calculate the absorbances according to

$$A = \ln(T_0/T)$$

For the phenol spectrum a baseline was calculated by taking the mean of twenty data points from  $\sim 3263\text{cm}^{-1}$  to  $\sim 3200\text{cm}^{-1}$  and absorbance values were calculated as above. These absorbances were added to the absorbances for the pyridine- $d_5$  solution only over the region of  $\nu_s(\text{CH})$  absorption ( $\sim 3263\text{cm}^{-1}$  to  $\sim 2813\text{cm}^{-1}$ ) and the total background absorbance was finally subtracted from the sample absorbance. A computer programme, derived from IRINT6, was specially developed to deal with these spectra only and was called PYRINT. After calculation of the absorbance at each data point the interpolation procedure to intervals of  $1.0\text{cm}^{-1}$  was carried out as with the programme IRINT6. The programme MEANSPEC3 could then be used to calculate mean absorbance values and Figure 4.30 shows a spectrum so obtained from six individual sets of three spectra. The regions which would have to be zero-weighted in a fitting procedure are as follows:

- $\sim 3100\text{cm}^{-1}$  to  $\sim 3520\text{cm}^{-1}$  where uncomplexed phenol absorbs,  $\sim 3110\text{cm}^{-1}$  to  $\sim 2950\text{cm}^{-1}$  where the  $\nu_s(\text{CH})$  absorptions of phenol, which are perturbed on complex formation, do not subtract-out exactly and  $\sim 2400\text{cm}^{-1}$  to  $\sim 2200\text{cm}^{-1}$  where  $\nu_s(\text{CD})$  absorptions of pyridine- $d_5$  likewise fail to subtract-out.

These data await analysis using the model extended to include Fermi-resonance effects.

#### 4.12 The $\nu_s(\text{OH})$ and $\nu_s(\text{OD})$ absorption bands of isotopically dilute water solutions

An isolated water molecule possesses  $C_{2v}$  symmetry and a group theoretical treatment shows that the molecule has three infrared active modes of vibration. These are a symmetric and an asymmetric H-O-H stretching mode,  $\nu_1$  and  $\nu_3$  respectively, and a H-O-H bending mode which is designated  $\nu_2$ .

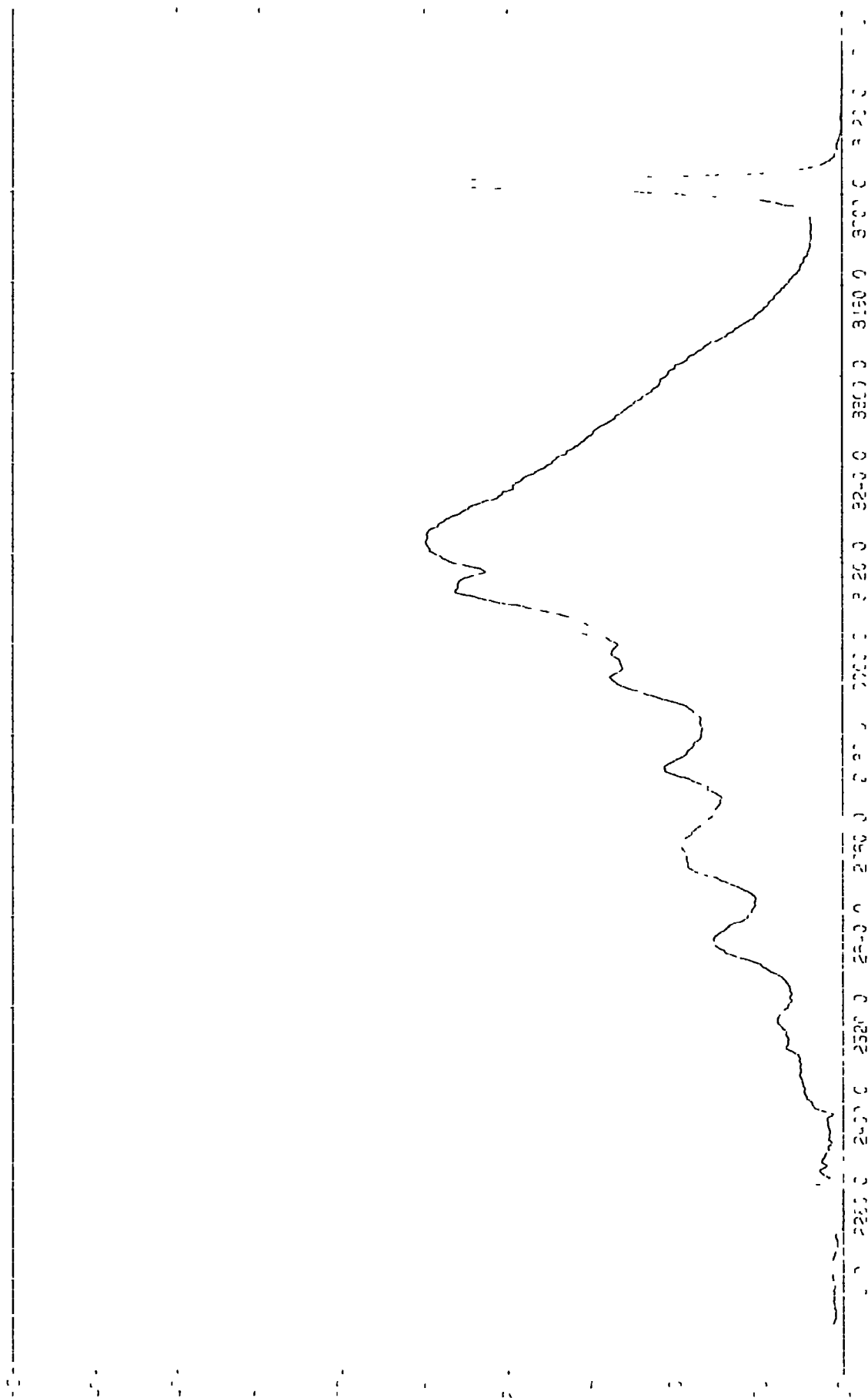


Figure 4.30 The spectrum of mean decadic absorbance values for the complex phenol-pyridine-d<sub>5</sub> in carbon tetrachloride computed by use of the programme PYRINT.



The frequencies, extinction coefficients, and halfwidths of these bands in liquid water and deuterium oxide have been tabulated (111) along with details of other intramolecular modes which are infrared or Raman active.

Two main problems are encountered when it is attempted to record and analyse the infrared spectrum of liquid water in the O-H "stretching region". These are first that the absorption band is very intense, necessitating the use of a very short cell pathlength, and second that the  $\nu_1$  and  $\nu_3$  modes of vibration are coupled and the corresponding absorption bands occur very close together to produce a broad band with two maxima at  $\sim 3280\text{cm}^{-1}$  and  $\sim 3490\text{cm}^{-1}$  in  $\text{H}_2\text{O}$  and at  $\sim 2450\text{cm}^{-1}$  and  $\sim 2540\text{cm}^{-1}$  in  $\text{D}_2\text{O}$  (112). These problems are usually circumvented by studying dilute solutions of  $\text{H}_2\text{O}$  in  $\text{D}_2\text{O}$  and of  $\text{D}_2\text{O}$  in  $\text{H}_2\text{O}$ . In each case an equilibrium quantity of HDO molecules is produced and the decoupled  $\nu_s(\text{OH})$  vibration can be studied in the first case and the decoupled  $\nu_s(\text{OD})$  vibration in the latter case. These absorption bands also have somewhat lower extinction coefficients (113) and it is possible to record the infrared spectrum of a  $\sim 10\%$  by volume solution using a pathlength of  $\sim 10\mu\text{m}$ .

The infrared spectra of isotopically dilute water solutions have been recorded before (112-116) but it was necessary to repeat previous work to obtain spectra in a digitised form if analysis by an extended Robertson-Yarwood model was to be achieved.

Solutions of  $\text{H}_2\text{O}$  in  $\text{D}_2\text{O}$  and of  $\text{D}_2\text{O}$  in  $\text{H}_2\text{O}$  were made up using freshly distilled water and deuterium oxide supplied by Fluorochem Ltd having a stated purity of 99.83 atom percent. In each case two different mixtures were used giving HDO concentrations of 4.06M and 6.62M for the  $\nu_s(\text{OH})$  band and 6.85M and 11.7M for the  $\nu_s(\text{OD})$  band. The concentrations being calculated from the known value of the equilibrium constant (117). A Beckman F-01 cell fitted with calcium fluoride windows and a spacer specially cut from "Mylar" sheet was used. The cell pathlength was

measured by the interference fringe method (94) and was approximately 12 $\mu$ m. The spectra were recorded by "Method B" (see Section 2.5) at a scan rate of 0.83cm<sup>-1</sup> s<sup>-1</sup> using a slit setting of "3" (see Figure 2.1). The ranges used were 4000cm<sup>-1</sup> to ~ 2825cm<sup>-1</sup> for the  $\nu_s$ (OH) band and 2900cm<sup>-1</sup> to ~ 2190cm<sup>-1</sup> for the  $\nu_s$ (OD) band. The background was recorded with pure water or deuterium oxide in the cell as appropriate. The temperature was ~ 313K. Each spectrum was repeated ten times, the absorbance data for each individual run were calculated using IRINT6 and the mean absorbances and weighting factors were calculated using MEANSPEC3. Table 4.9 shows the maximum absorbances obtained and their wavenumbers and the half bandwidths along with literature values (111). Figures 4.31 to 4.34 show the spectra of mean absorbance values calculated by MEANSPEC3 for respectively  $\nu_s$ (OH) for HDO at 4.06M and 6.62M and  $\nu_s$ (OD) for HDO at 6.85 and 11.7M.

The structure of liquid water has been the subject of much controversy and investigation. There is no agreement, from evidence obtained from infrared and Raman spectra, on whether there exists a mixture of distinct species with differing hydrogen bond lengths and angles or whether there is a continuum of species (for further discussion see refs. (118-120)). There is also considerable controversy over whether or not there exist non-hydrogen bonding -OH groups in the structure of water and if there are, what proportion of the total number of -OH groups are "free" (see ref. (120)). It should be plain to see that the Robertson-Yarwood model cannot in its present form accurately describe either of these situations since it cannot cope with a continuum of species and a mixture of species could not be analysed in the manner here described. It may, however, be possible to analyse an absorption band for a continuum of species by incorporating an appropriate radial distribution function into the model.

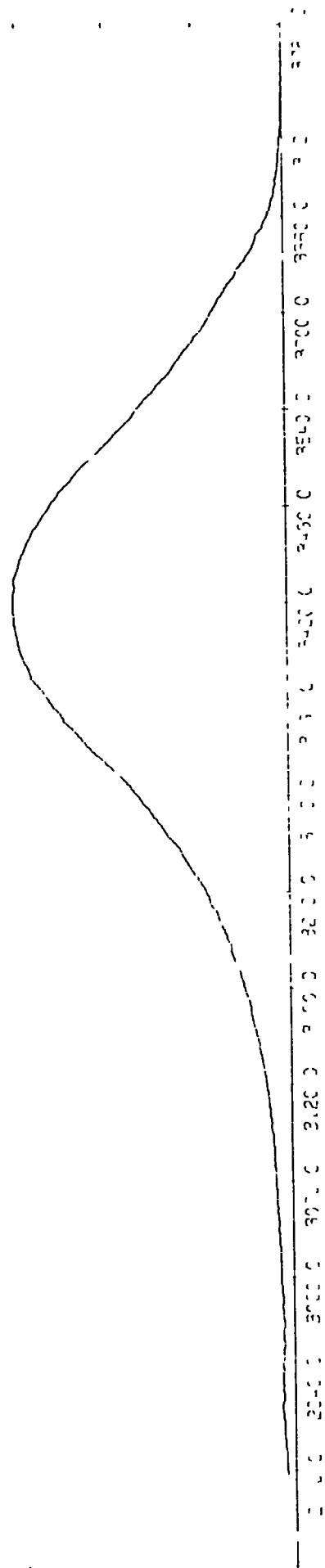


Figure 4.31 The decoupled  $\nu_s(\text{OH})$  absorption band of HDO 4.06M in  $\text{D}_2\text{O}$ . The absorbance scale is decadic.

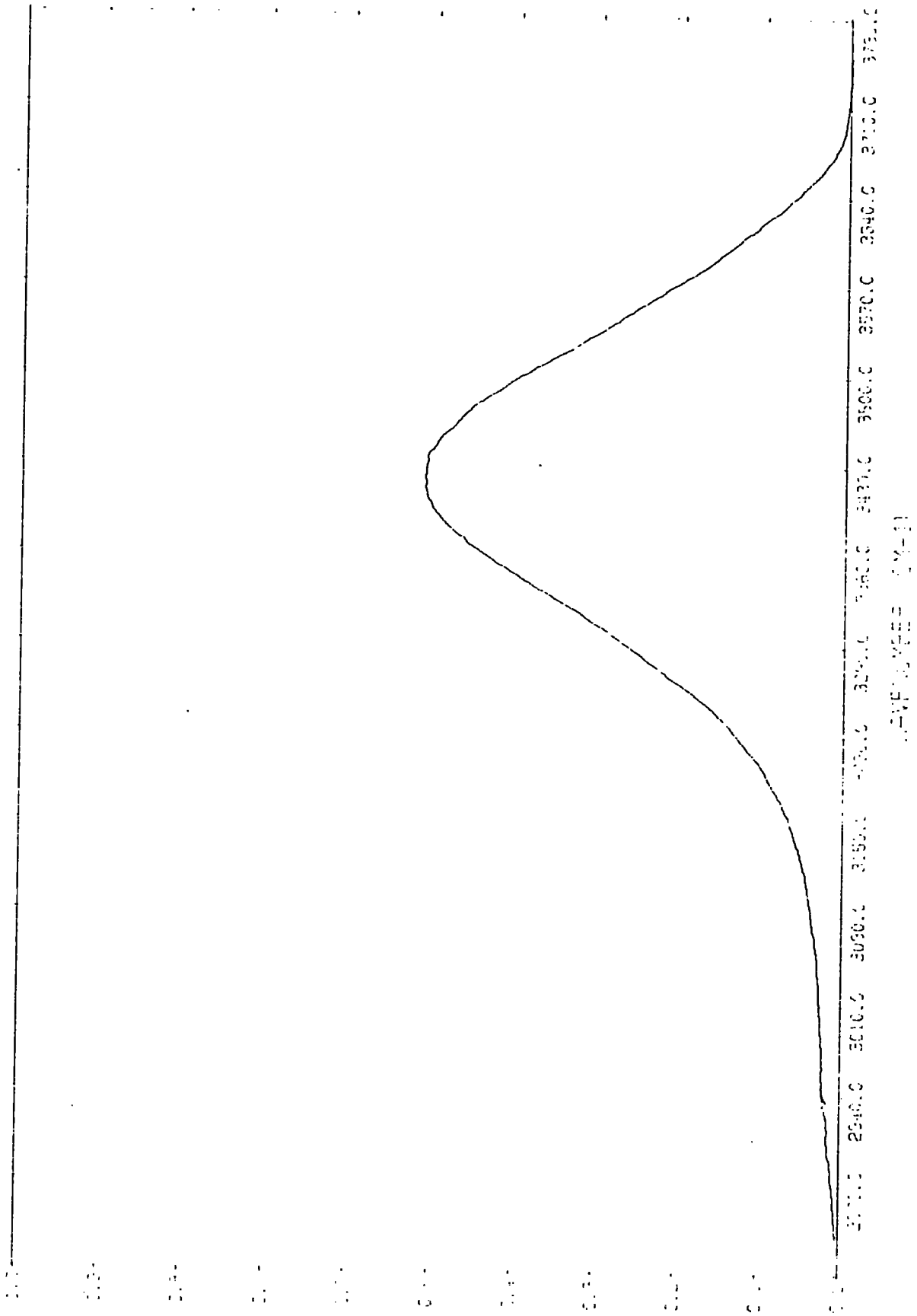


Figure 4.32 The decoupled  $\nu_s(\text{OH})$  absorption band of HDO 6.62M in  $\text{D}_2\text{O}$ . The absorbance scale is decadic.

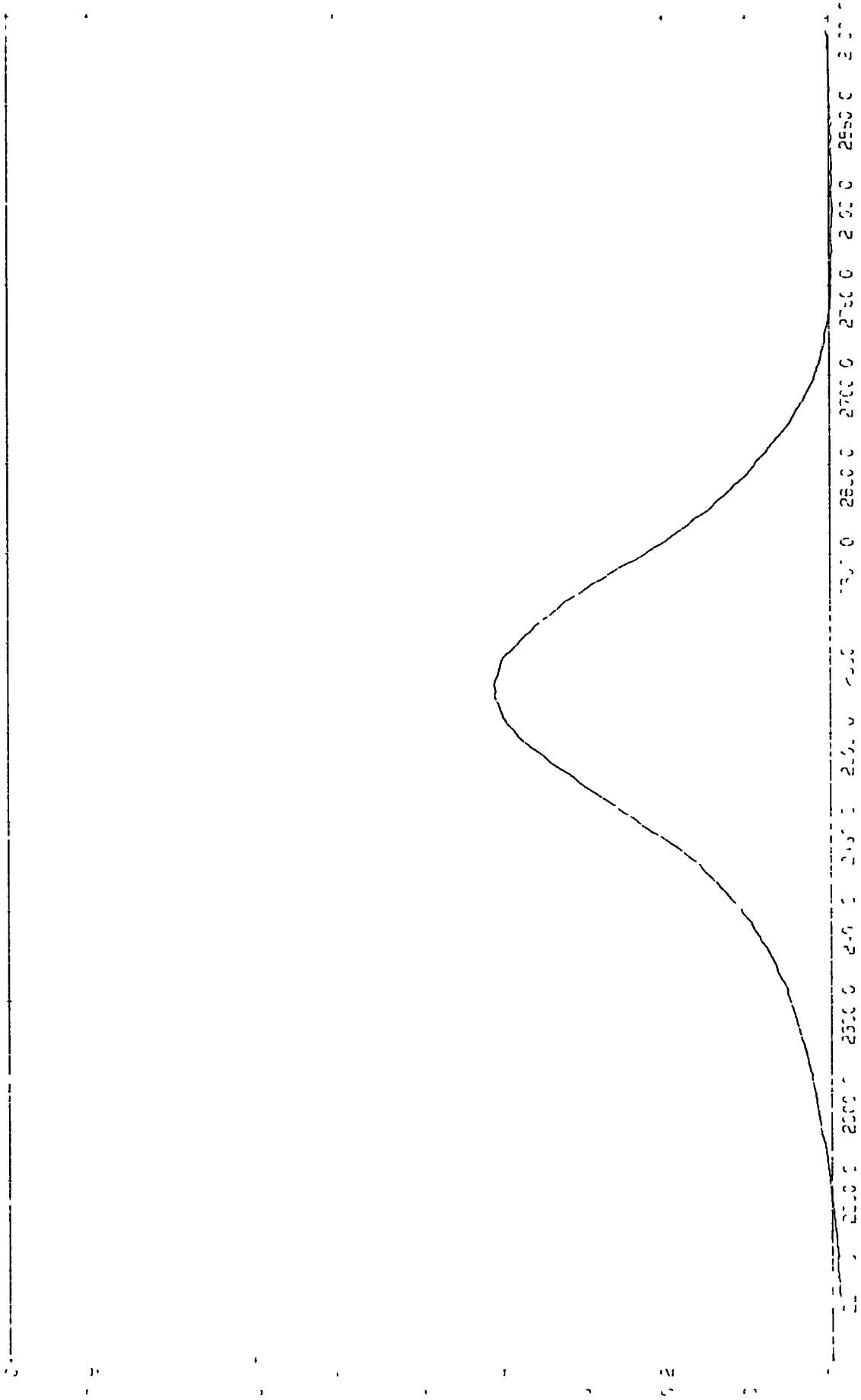


Figure 4.33 The decoupled  $\nu_s$  (OD) absorption band of HDO 6.85M in  $H_2O$ . The absorbance scale is decadic.

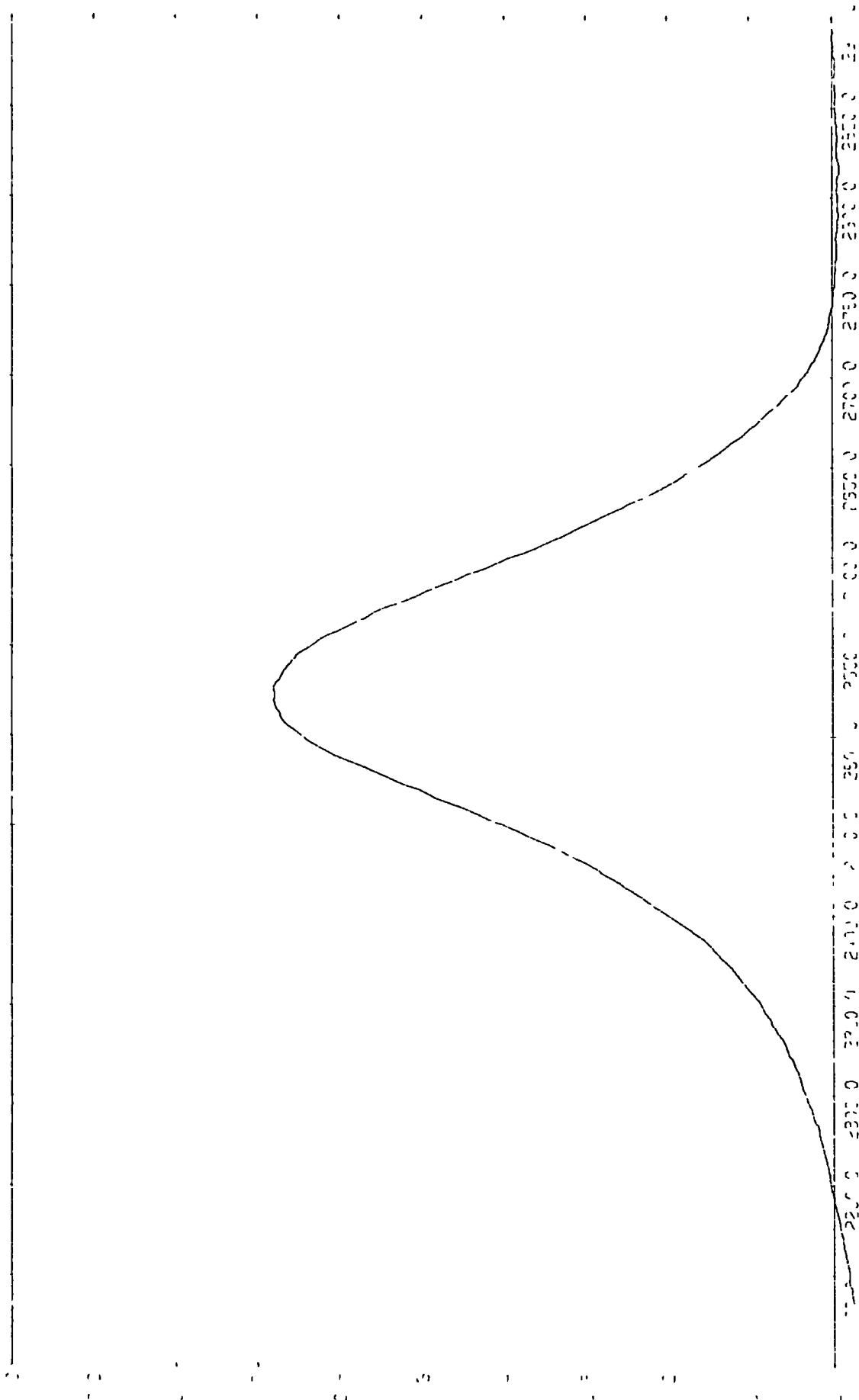


Figure 4.34 The decoupled  $\nu_s$  (OD) absorption band of HDO 11.7M in  $\text{H}_2\text{O}$ . The absorbance scale is decadic.

Table 4.9 Spectral parameters for the  $\nu_s$  (OH) and  $\nu_s$  (OD) bands of isotopically dilute water solutions; the experimental data are the values for the spectrum of mean absorbance values

system	maximum absorbance (decadic)	wavenumber of maximum absorbance ( $\text{cm}^{-1}$ )	halfwidth ( $\text{cm}^{-1}$ )	temperature
HDO in 4.06M	0.308	3420	266	~313K
D <sub>2</sub> O 6.62M	0.511	3417	250	~313K
HDO in 6.85M	0.406	2526	163	~313K
H <sub>2</sub> O 11.7M	0.679	2526	171	~313K
literature value for HDO in D <sub>2</sub> O	-	3400	255±5	295K
literature value for HDO in H <sub>2</sub> O	-	3460	270±5	393K
	-	2500	160±5	295K
	-	2550	180±5	393K

CHAPTER FIVE

RESULTS IN THE FAR-INFRARED REGION AND THEIR INTERPRETATION



## 5.1 Introduction

In this chapter the spectral data obtained in the far-infrared region will be presented and analysed. These data are complementary to those presented and analysed in Chapter 4 for two main reasons:

(i) If a value for  $\omega_2$  is obtained from far-infrared spectroscopy it can be used as an input parameter in the fitting procedure for the mid-infrared absorption for the same complex and so reducing the number of parameters to be estimated from four to three with a consequent improvement in their reliability.

(ii) Since the Robertson-Yarwood model makes predictions about the  $\nu_{\sigma}(\text{XH}---\text{Y})$  mode of a complex which gives rise to a band in the far-infrared region experimental data in this region would be very useful as a means of checking the model validity.

## 5.2 Far-infrared studies of the complexes of phenol with acetonitrile and with 1,4-dioxan

All attempts to obtain the far-infrared spectrum of the phenol-acetonitrile complex proved fruitless. This was because of the absorption associated with acetonitrile in this region. The high concentration of acetonitrile which it was necessary to use in order to provide a measurable concentration of the complex (the equilibrium coefficient has a value of  $5.0 \pm 0.2 \text{ dm}^3 \text{ mol}^{-1}$  at 298K (92)) produces a very intense absorption which allows very little energy to reach the detector in this region. The signal-to-noise ratio obtained is therefore very poor and the  $\nu_{\sigma}(\text{XH}---\text{Y})$  absorption, which is expected to be broad and weak, is very difficult to observe. This absorption in acetonitrile in dilute solution has been used to study the molecular dynamics of the molecule by several workers (see refs. (121) and (122) for some recent work).

A far-infrared spectrum for the phenol-1,4-dioxan complex in carbon tetrachloride solution was obtained by using the Beckman- R.I.I.C. FS-720 interferometric spectrometer with the cooled bolometer detector, as described in Section 2.10, and a conventional optical system. A 25-gauge beamsplitter was used giving useful energy above  $\sim 30\text{cm}^{-1}$  and a maximum at  $234\text{cm}^{-1}$  (75), the sampling interval was  $16\mu\text{m}$  and a quartz filter was used to absorb radiation above  $\sim 140\text{cm}^{-1}$  which is considerably lower than the aliasing frequency of  $313\text{cm}^{-1}$ . A half-interferogram of 256 points was transformed producing a theoretical resolution of  $2.44\text{cm}^{-1}$  (neglecting apodisation). The concentrations of phenol and 1,4-dioxan used were 0.507M and 0.935M respectively, these being somewhat different from those used to obtain the  $\nu_s(\text{OH})$  absorption spectrum. The pathlength was 1.01mm. It was found necessary to use a high phenol concentration to obtain a band of significant intensity and too high a base concentration would produce unwanted absorption in both sample and background spectra with the same effect on signal-to-noise ratio as described above for acetonitrile.

The spectrum thus obtained is shown in Figure 5.1; two separate "runs" are shown to give an indication of the precision of the data. The "background" absorption was removed by ratioing the "sample" spectrum against one of a solution of 1,4-dioxan in carbon tetrachloride at the same molarity. The low frequency part of the absorption was also obtained using the polarising optical system and the cooled bolometer detector. This combination provided spectra over the range  $\sim 3\text{cm}^{-1}$  to  $\sim 80\text{cm}^{-1}$ . Figure 5.2 shows a spectrum in duplicate. The conditions were the same as above except that the polarising system allowed a pathlength of 2.56mm to be used and the improvement in signal to noise ratio is still evident. The absorbance scale in Figure 5.2 has been chosen to provide continuity with Figure 5.1.

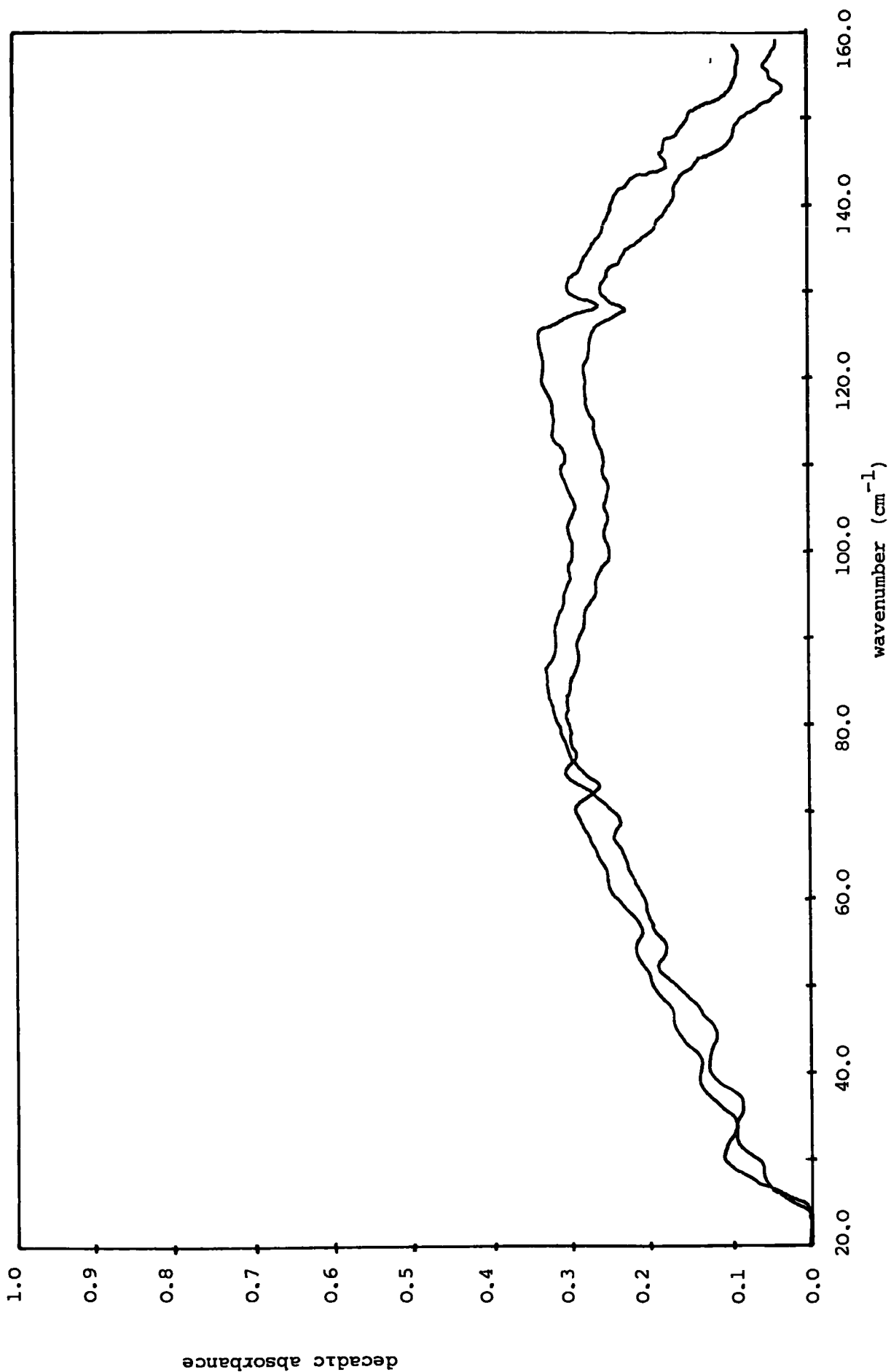


Figure 5.1 The absorbance spectrum for the phenol-1,4-dioxan complex in carbon tetrachloride over the range 20-160cm<sup>-1</sup>

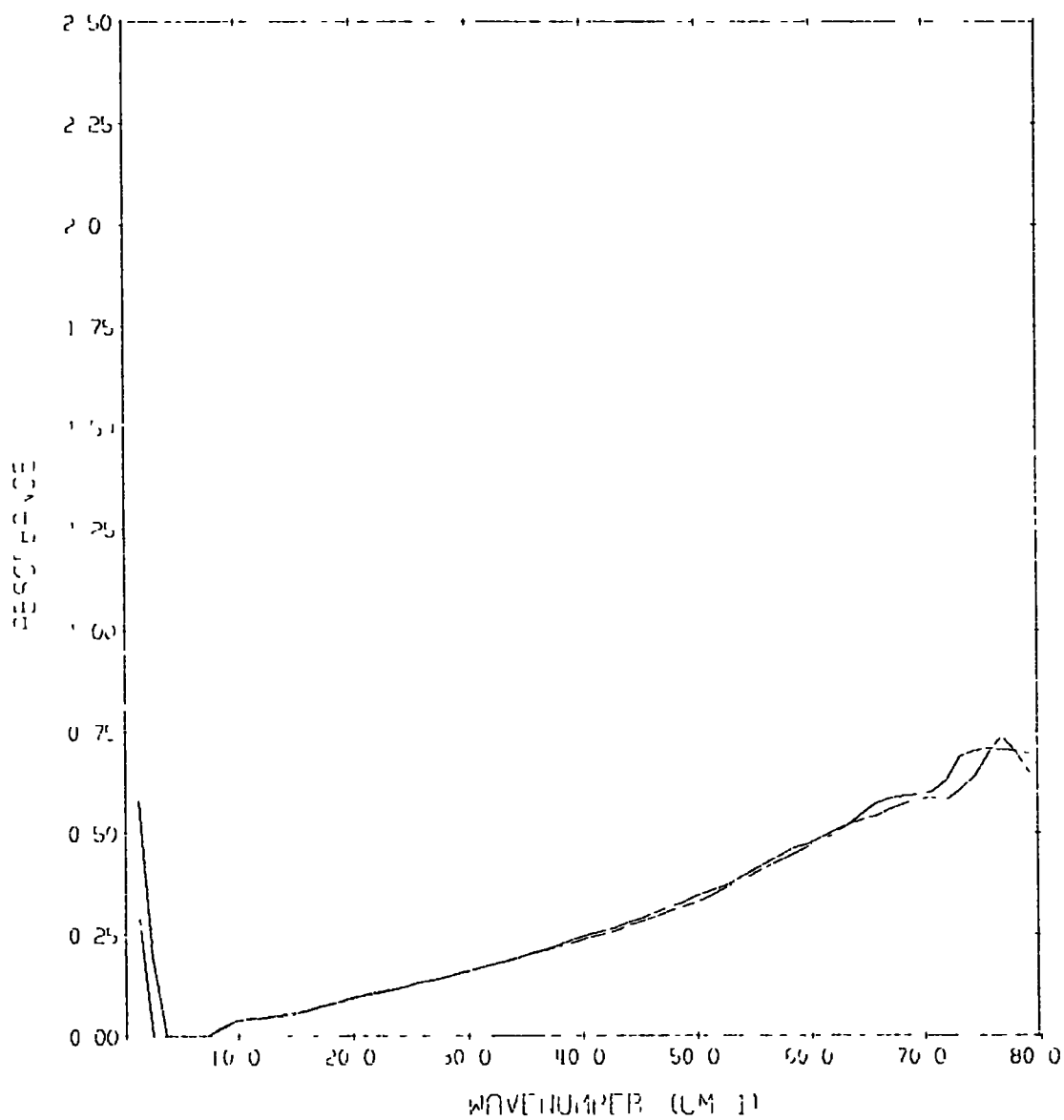


Figure 5.2 The decadic absorbance spectrum for the phenol-1,4-dioxan complex in carbon tetrachloride over the range 10-80cm<sup>-1</sup>.

The spectra shown in Figures 5.1 and 5.2 clearly show two broad, overlapping bands with maxima at  $\sim 80\text{cm}^{-1}$  and  $\sim 125\text{cm}^{-1}$ . The interpretation of this spectrum is rather difficult because of the poor state of knowledge of the collisional, reorientational and vibrational processes that take place in the liquid phase at these frequencies and give rise to absorption in this spectral region. It should be noted that the lifetime of this complex is certainly very short. Some idea of the lifetime can be gained by assuming that the rate of complex formation is equal to rate of molecular translations (i.e. it is diffusion controlled) and then by taking the equilibrium constant to be equal to the ratio of the rate constants for complex formation and destruction the rate of destruction can be deduced. The equilibrium constant in this case has been measured to be  $4.0\text{dm}^3\text{mol}^{-1}$  at 298K (97) and therefore the rates of complex formation and destruction must be very nearly equal. The complex lifetime must thus be similar to the period of molecular translations, that is approximately  $10^{-11}\text{s}$ .

It is well-known that 1,4-dioxan absorbs in the 20 to  $200\text{cm}^{-1}$  region of the spectrum with a peak at  $\sim 70\text{cm}^{-1}$  (123) and this absorption has been attributed to collision-induced dipole fluctuations in the liquid. Although 1,4-dioxan has only a very small dipole moment (0.45 D) (103), which may be due to the presence of a small number of molecules in the "boat" conformation or to a deviation from  $D_{3h}$  symmetry of chair conformers caused by molecular collisions, a dipole may be induced in either conformer by interaction with the quadrupole or octopole moments of other molecules in the liquid. It is the variation of these induced dipoles due to translational motions that is thought to give rise to the far-infrared absorption.

The possible explanations of the spectrum observed for the complex may be summarised as follows:

(i) The band at  $\sim 80\text{cm}^{-1}$  may be due to a perturbation of the 1,4-dioxan absorption at  $\sim 70\text{cm}^{-1}$ . The change would be due to the rate of translational motions being altered by the formation of a complex.

(ii) The same absorption may be due to a combination of the re-orientational motions of the phenol and the 1,4-dioxan molecules. This explanation would be appropriate if the lifetime of the complex were shorter than the period of reorientational motion of the molecules.

(iii) A low-frequency bending mode (see Section 1.2) of the complex may contribute to the absorption in this region.

(iv) The absorption at  $\sim 125\text{cm}^{-1}$  may be due to the  $\nu_{\sigma}(\text{XH}\cdots\text{Y})$  mode of the complex.

(v) At the concentrations used effects due to 2:1 phenol-1,4-dioxan complexes may be important.

Any combination of the above processes could give rise to the observed absorption spectrum but it seems likely that a  $\nu_{\sigma}(\text{XH}\cdots\text{Y})$  vibrational mode does at least contribute to the absorption in the  $125\text{cm}^{-1}$  region; otherwise it is difficult to explain why a perturbation of the low frequency 1,4-dioxan spectrum should lead to a distinct second maximum in the absorption profile at this frequency.

### 5.3 Far-infrared studies of the complex of phenol with pyridine

The phenol-pyridine complex has been studied in the far-infrared region by Wood et al. (32,124,125) who observed an absorption band with a maximum at  $\sim 134\text{cm}^{-1}$  and a half-width somewhere in the region of  $35\text{cm}^{-1}$ .

In order to obtain more accurate data in a digitised form the complex was re-investigated using the Beckman-R.I.I.C. FS-720 interferometric spectrometer. Ten independent spectra were obtained and after making a baseline correction using DCHO512 (see Section 2.11) and interpolating to an interval of  $1\text{cm}^{-1}$  the spectra were averaged using MEANSPEC3 (see Section 4.2) and at the same time weighting factors and standard errors

were also calculated. The concentrations used were phenol 0.460M and pyridine 1.09M. The pathlength of the cell was approximately 2.56mm. These concentrations differ considerably from those used to obtain the mid-infrared spectrum of phenol complexed with pyridine-d<sub>5</sub> (see Section 4.11) but it was necessary to use such a high phenol concentration to obtain appreciable intensity in the far-infrared at a practicable pathlength. A longer pathlength would result in stronger solvent absorption in both sample and background which would necessitate the use of high amplifier gains and result in a considerable worsening of the signal-to-noise ratio of the spectrum. It is indeed an inherent problem with these complexes that due to grossly different intensities in the mid- and the far-infrared and because of certain instrumental factors it is very difficult to obtain data in both spectral regions with the species at similar concentrations.

The interferometer was used with a conventional optical system and a golay detector, a 25-gauge beamsplitter gave useful energy transmission above  $\sim 30\text{cm}^{-1}$  and had maximum transmission at  $234\text{cm}^{-1}$  (75), the sampling interval used was  $8\mu\text{m}$  which produces an aliasing frequency of  $625\text{cm}^{-1}$ ; radiation of frequencies above this value was eliminated by use of a thin black polythene filter.

The spectra produced by ratioing the phenol-pyridine mixture against pyridine at the same concentration in carbon tetrachloride are shown in Figure 5.3 and the spectrum of mean absorbance values is shown in Figure 5.4. The improvement in signal-to-noise ratio of the averaged spectrum compared with an individual spectrum can be clearly seen.

The spectrum shows an absorption band with a maximum at  $\sim 132\text{cm}^{-1}$  and a full-width and half maximum absorbance of  $\sim 27\text{cm}^{-1}$ . This compares with the parameters of Wood et al. of  $134 \pm 1\text{cm}^{-1}$  and  $\sim 35\text{cm}^{-1}$  (32,125) respectively. The disagreement is not surprising considering the relative unsophistication of the dispersive spectrometer of Wood et al. It is also

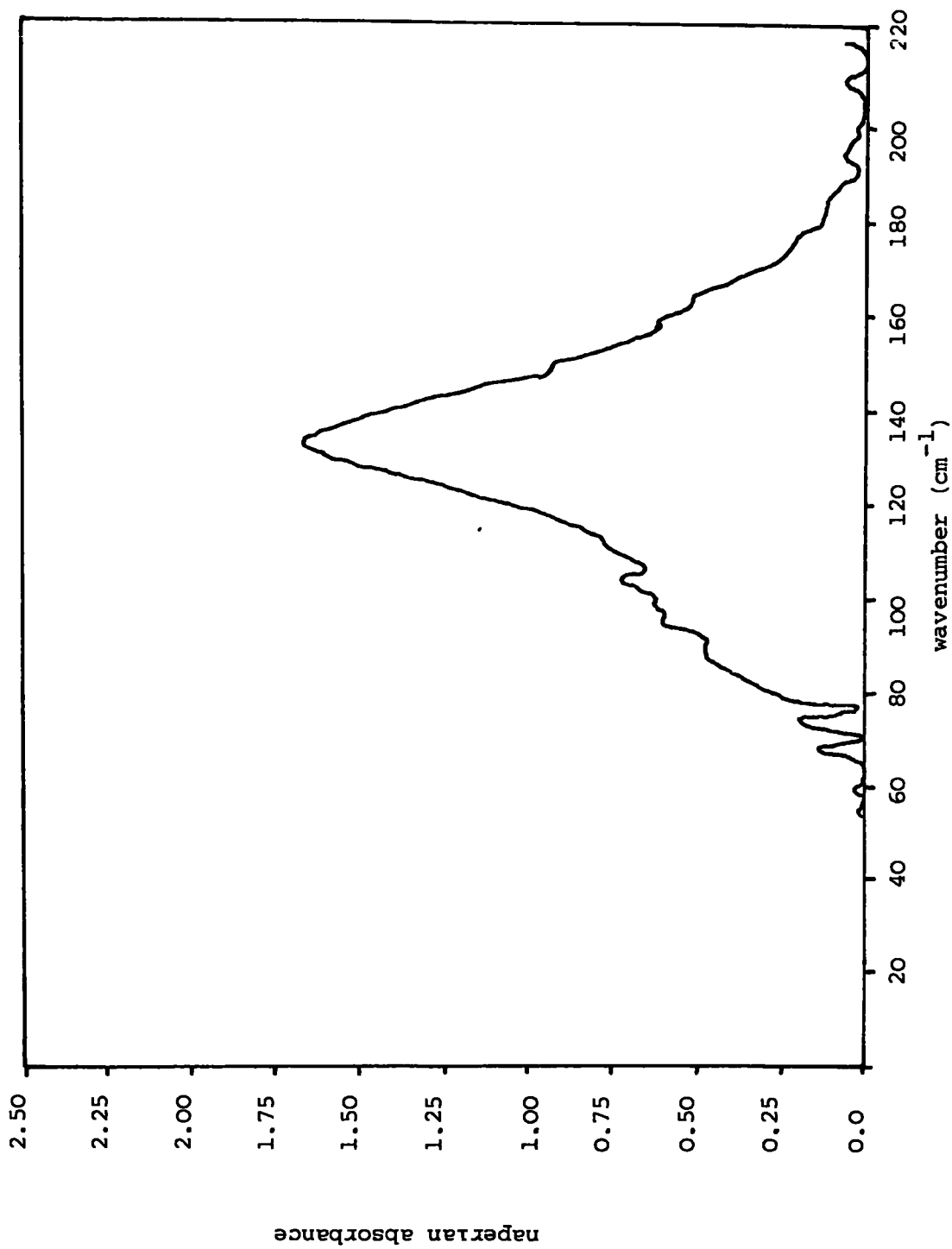
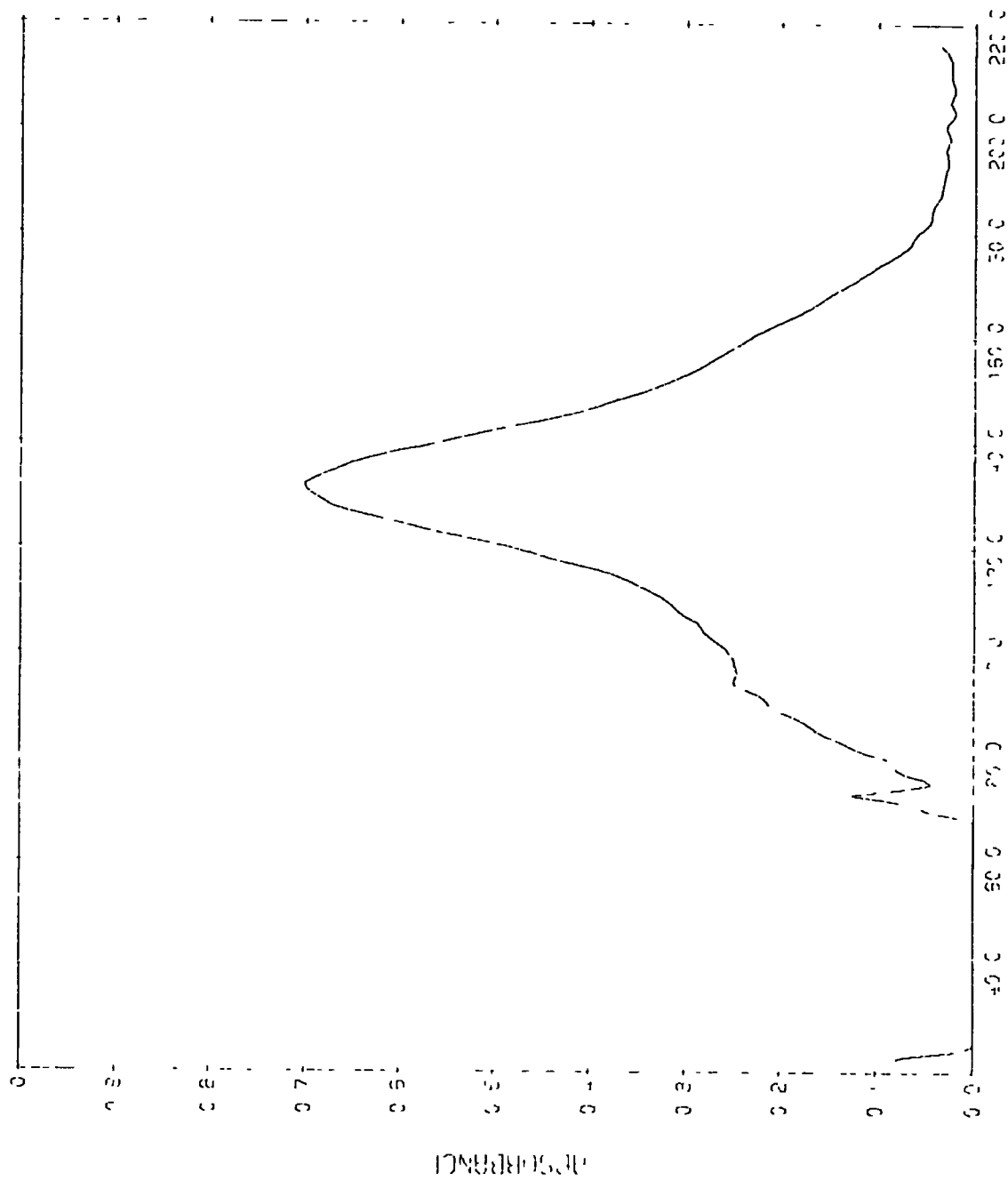


Figure 5.3 The absorbance spectrum for a single spectral "run" for the complex phenol-pyridine in carbon tetrachloride computed with FTIRAN5.





APR 1952 (1-1)

Figure 5.4 The spectrum of mean absorbance values for the complex phenol-pyridine in carbon tetrachloride. The absorbance scale is decadic.

clear from the spectra obtained that a second band at a lower frequency of  $\sim 95\text{cm}^{-1}$  appears as a shoulder on the main absorption. This feature was not observed by Wood et al. because of the range and sensitivity of their spectrometer. Since the band at  $\sim 132\text{cm}^{-1}$  has been satisfactorily assigned to the  $\nu_{\sigma}$  (XH---Y) mode of the complex by Ginn and Wood (32) the lower frequency band must be due to some other process. As was explained in Section 5.2 for the phenol-1,4-dioxan complex it is very difficult to make an unambiguous interpretation of these low-frequency absorptions. However, some investigations were made to attempt to eliminate some possibilities.

It is well-known (126) that many polar and non-polar molecules absorb in the  $70\text{cm}^{-1}$  region and this absorption has been assigned to the libration of the pyridine molecule in a Poley-Hill type process (127, 128). In the same way as for the phenol-1,4-dioxan system the problem is to distinguish between absorption due to perturbation of this type of process and absorption due to vibrational modes of the hydrogen-bonded complex, in this case bending and torsional modes.

In order to investigate the effect of complexation with phenol on the low frequency absorption of pyridine in carbon tetrachloride solution spectra were obtained using the cooled bolometer detector and the polarising optical system over the range 3 to  $80\text{cm}^{-1}$ , first of pyridine in carbon tetrachloride and then of pyridine complexed with phenol. The molarities used were pyridine 0.418M and phenol 0.929M and a pathlength of  $\sim 2.56\text{mm}$  was employed. A sampling interval of  $16\mu\text{m}$  gave an aliasing frequency of  $313\text{cm}^{-1}$  which was well above the upper frequency limit of the detector and therefore no spectral filtering was necessary. The spectral resolution was  $2.44\text{cm}^{-1}$  (neglecting apodisation) since a half-interferogram of 256 points was transformed. The background solutions, against which the sample solutions were ratioed, were pure carbon tetrachloride and phenol at 0.929M

respectively. The spectra obtained, each was duplicated to check on the reproducibility, are shown in Figure 5.5. As can be seen, the addition of phenol has very little effect on the absorption due to pyridine, at least over the frequency range available with this instrumental arrangement. This is rather surprising, especially in view of the fact that the complex is thermodynamically fairly stable and would therefore be expected to have a considerable lifetime. A spectrum of the complex (phenol 0.372M, pyridine 1.05M) over the 3 to  $80\text{cm}^{-1}$  range obtained in a similar manner is shown in Figure 5.6 and here it can be seen that there is very little absorption in this region, what absorption there is may be due to some perturbation of the pyridine spectrum on complexation (the background solution is pyridine at 1.05M) or to the reorientational motion of the phenol molecules themselves.

In the light of this evidence it seems best that the low-frequency shoulder be tentatively assigned to a bending or torsional mode of the complex, most probably the  $\nu_{\gamma}$  in-plane bending mode of the hydrogen bond which would be expected to be the highest in frequency of the bending and torsional modes (see Section 1.2).

A preliminary analysis of this spectrum was made by fitting the experimental bandshape to the expression (Equation 3.29) obtained for the far-infrared absorption profile over the range 27 to  $206\text{cm}^{-1}$ . The fitted spectrum is compared with the experimental spectrum in Figure 5.7. The fitting is fairly good on the high frequency side of the band but on the low frequency side the shoulder at  $\sim 95\text{cm}^{-1}$  prevents a good fit from being made. It may be possible to perform a decomposition of the observed band into two bands and then improve the quality of fit to the high frequency band. Zero-weighting the points below  $\sim 100\text{cm}^{-1}$  would be another, but less satisfactory, expedient.

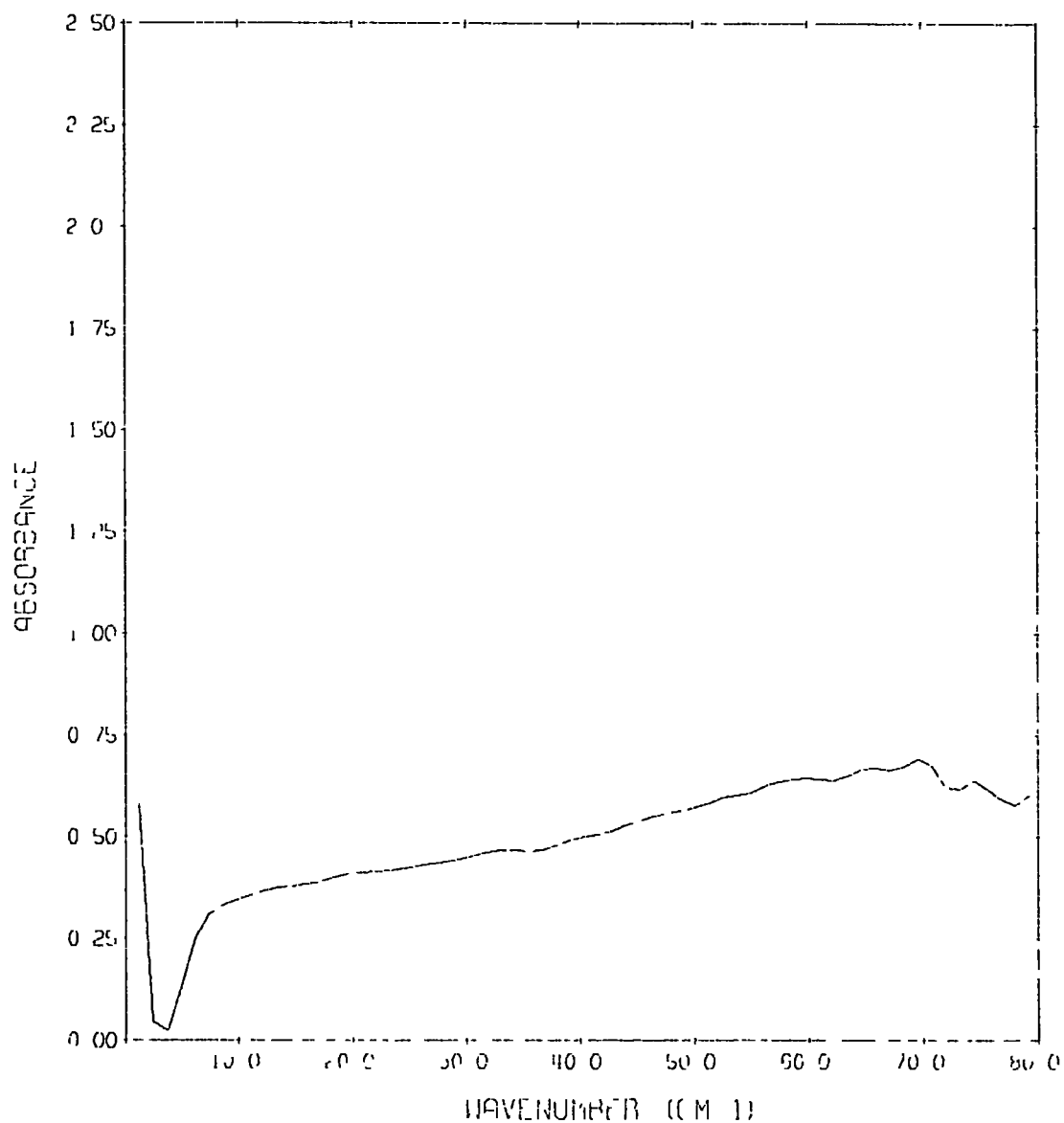


Figure 5.5a The low frequency absorption spectrum of a solution of pyridine in carbon tetrachloride. The absorbance scale is naperian.

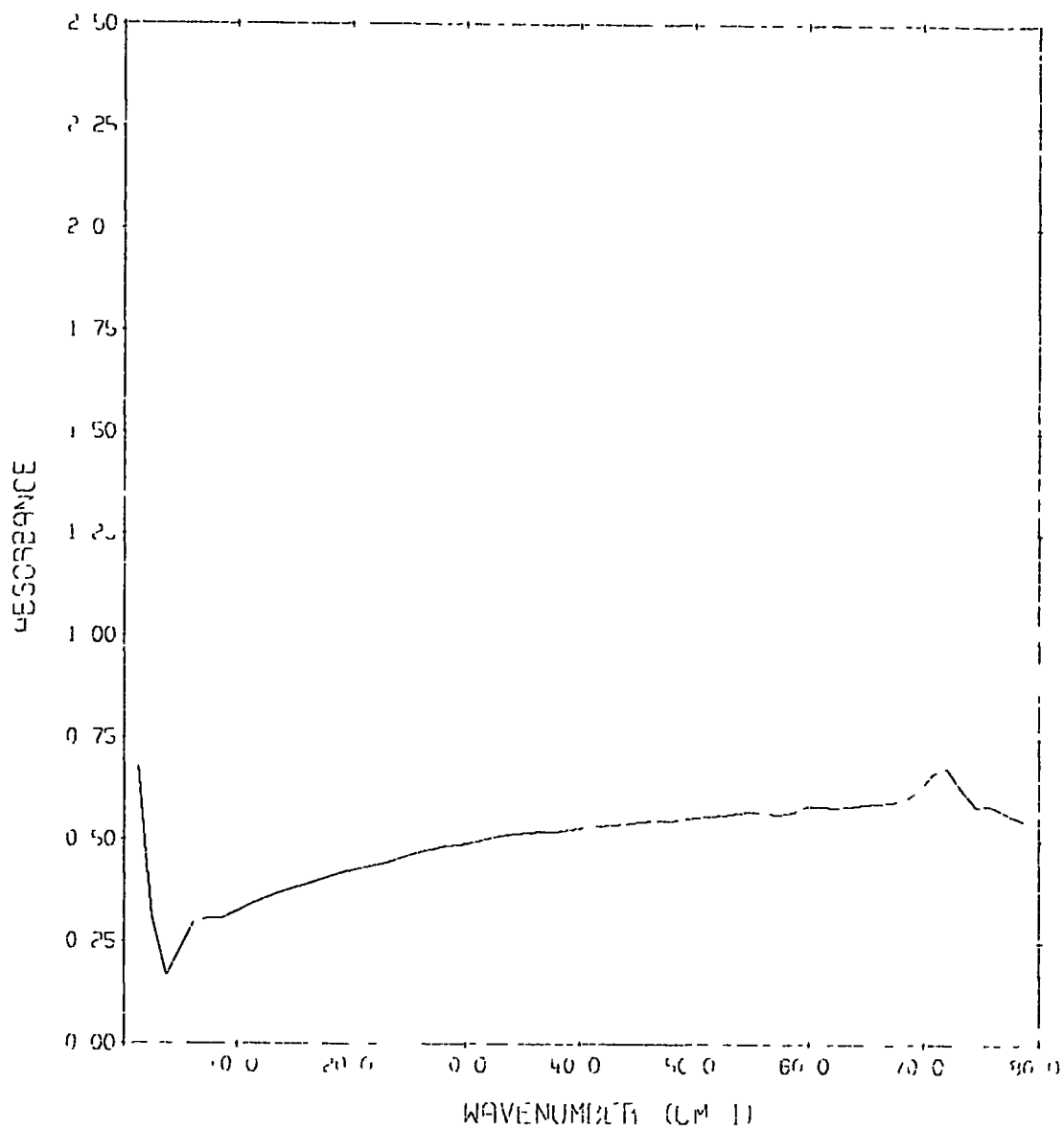


Figure 5.5b The low frequency absorption spectrum of a solution of pyridine in carbon tetrachloride in the presence of phenol. The absorbance scale is napierian.

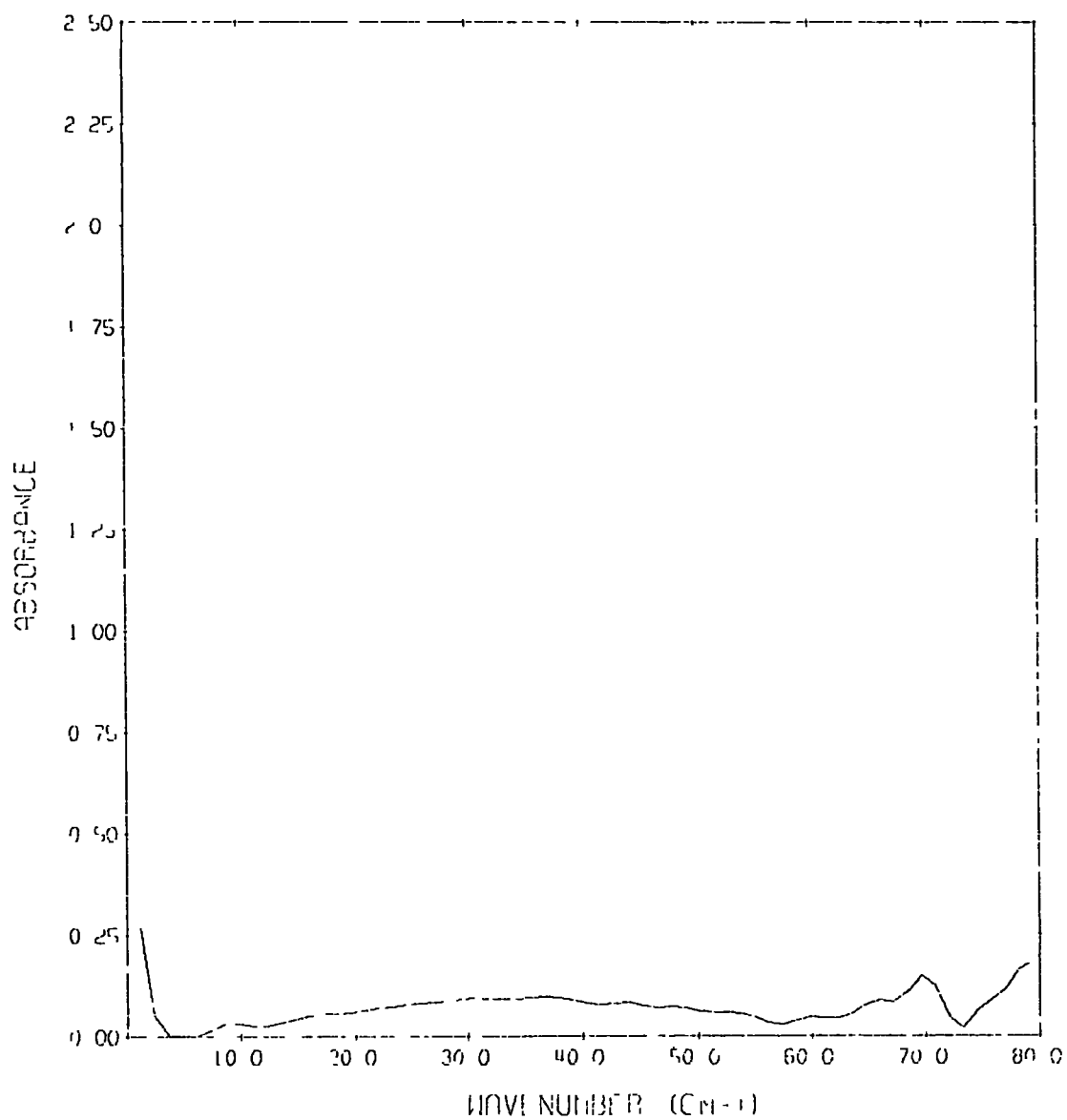


Figure 5.6 The low frequency absorption spectrum of the complex phenol-pyridine in carbon tetrachloride solution. The absorbance scale is naperian.

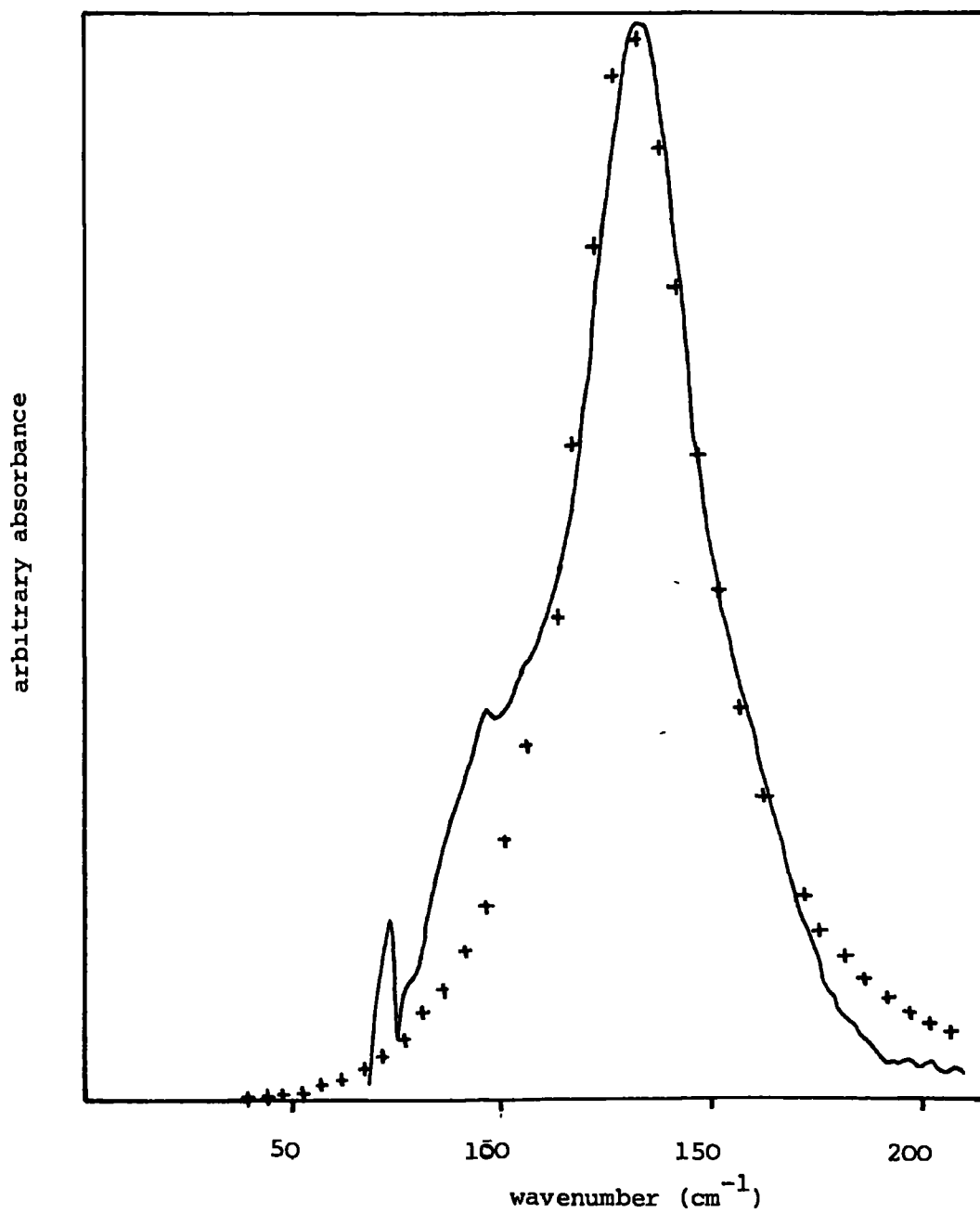


Figure 5,7 The spectrum of mean absorbance values (solid line) for the phenol-pyridine complex in carbon tetrachloride compared with the spectrum computed from the fitted parameters.

The fitted parameters obtained are shown in Table 5.1 along with their standard deviations. The value of  $\bar{\nu}_2$  is  $130.5 \pm 0.3 \text{ cm}^{-1}$  which is in the region expected (the band maximum need not necessarily coincide with  $\bar{\nu}_2$ , see Equation (3.29)). The value of  $\gamma/2\omega_2$  is  $0.143 \pm 0.003$  and this means that  $\gamma$  has a value of  $(7.030 \pm 0.007) \times 10^{12} \text{ s}^{-1}$ . The value of the

Table 5.1 Fitted parameters obtained for the far-infrared absorption for the phenol-pyridine complex in carbon tetrachloride

$\omega_2$ ( $\text{s}^{-1}$ )	$\bar{\nu}_2$ ( $\text{cm}^{-1}$ )	$\gamma/2\omega_2$	C
$(2.458 \pm 0.006) \times 10^{13}$	$130.5 \pm 0.3$	$0.143 \pm 0.003$	$1.49 \pm 0.02$

proportionality constant in Equation (3.29) is estimated to be  $1.49 \pm 0.02$ . It should be noted that the estimate for  $\gamma$  found here is much lower than for the complexes described in Chapter 4 although the solvent is carbon tetrachloride in both cases. This result indicates the danger of regarding  $\gamma$  purely as a property of the solvent (see also Section 4.9). This low value of  $\gamma$  could be explained by the fact that the phenol-pyridine complex is much stronger than the complexes with acetonitrile and 1,4-dioxan and is therefore more rigid. It is thus much less affected by the stochastic nature of the solvent environment and so the value of  $\gamma$  which can only be obtained for the solvent indirectly by the effect on the hydrogen bonded complex is much lower.

If  $\gamma$  could be obtained from the mid-infrared spectrum it would be very interesting to compare the two values. This would be possible using an extended model that allows for Fermi resonance effects (70).



CHAPTER SIX

A RAMAN SPECTRAL STUDY OF VIBRATIONAL RELAXATION IN A  
HYDROGEN BONDED COMPLEX

## 6.1 Introduction

In this chapter a Raman spectroscopic study of the complex acetonitrile-methanol- $d_4$  will be described. The experimental work was carried out at the Institut für Physikalische Chemie der Technischen Universität, Braunschweig in West Germany.

In this study attention was concentrated on a vibrational mode of acetonitrile, namely  $\nu_1$ , corresponding to symmetric stretching of the C-H bonds, which does not involve the displacement of atoms directly participating in the formation of the hydrogen bond. Acetonitrile was chosen because much work has been done on its molecular dynamics using Raman spectroscopy (129-131) but despite this they are far from being fully understood and information in a situation where the intermolecular forces are supposedly well-known (i.e. a hydrogen bond) would be very useful. Methanol was chosen since it forms a well-defined ground state complex with acetonitrile having an equilibrium constant of  $\sim 2.6 \text{ dm}^3 \text{ mol}^{-1}$  (132) and is readily available in a completely deuterated form to enable the  $\nu_1$  mode of acetonitrile to be studied without interference from vibrational modes of methanol. Furthermore the molecule is also amenable to quasi-elastic neutron scattering studies of hydrogen bonding because the compound  $\text{CD}_3\text{OH}$  may be prepared and the motion of the hydrogen-bonded proton can then be studied without effects from the methyl group protons being present. In this way information from both techniques and also infrared and far-infrared spectroscopy can be combined to give the best chance of a unique interpretation.

A group theoretical treatment of the acetonitrile molecule (point group  $C_{3v}$ ) shows that it should display eight Raman active vibrational modes. These eight modes are also infrared active and four of them belong to the symmetry class  $A_1$  and four to the class E. These latter are each doubly degenerate thus giving the twelve normal modes of

vibration expected for a non-linear molecule of six atoms. The  $A_1$  modes correspond to totally symmetric vibrations and therefore for these the isotropic part of the scattered intensity can be obtained and hence the vibrational relaxation function, the manner of decay of which is central to the interpretation of the Raman bandshape (see below). Of these four modes  $\nu_2$  and  $\nu_4$  are complicated by the presence of hot bands of the type  $(\nu_2 + \nu_8 - \nu_8)$  and  $(\nu_4 + \nu_8 - \nu_8)$  (133) although this has only recently been realised and previously "structure" was attributed to the presence of clusters of acetonitrile molecules (134) which were thought to persist even in dilute solution. The analysis of the shapes of these bands is made difficult for this reason but such an analysis is in progress (135). The  $\nu_3$  band is weak but has recently (129) been studied in some detail in both the liquid and in dilute solution. The remaining band,  $\nu_1$  (at  $\sim 2940\text{cm}^{-1}$ ) is well-suited to study (129, 136), is intense and complicated only by the presence of the E band  $\nu_5$  (at  $\sim 3003\text{cm}^{-1}$ ) in the high frequency wing. This interference can be avoided by using only the low frequency half of the  $\nu_1$  band. The  $\nu_1$  mode is of interest here because it gives information about the extent to which the onset of hydrogen bonding interactions affects the parts of molecules remote from the actual interaction (see Section 4.11 for a discussion of similar effects in the phenol-pyridine complex). The analysis of the data will follow closely the methods used by Yarwood, Arndt and Döge (129).

## 6.2 Instrumentation, experimental method and computation

The spectra analysed here were obtained using a Coderg LRT800 laser Raman spectrometer which features a triple monochromator, and a Spectra Physics 171-06 argon ion laser with a Spectra Physics 270 exciter. The laser provided up to 6W of power at 514.5nm wavelength; of this power  $\sim 2.5\text{W}$  was available at the sample. The laser beam was plane polarised

before reaching the sample and an analyser after the sample could be rotated to allow components of the scattered light polarised parallel ( $I_{VV}$ ) to the plane of polarisation of the incident light or perpendicular ( $I_{VH}$ ) to it to enter the monochromator.

The spectrometer allowed the bandshape to be recorded in digitised form by employing a stepping motor and direct photon counting. A counting period of 5s at  $0.25\text{cm}^{-1}$  intervals was used to record the  $\nu_1$  band of acetonitrile and the total photon counts at each wavenumber point were punched directly onto paper tape by means of a Facit 4070 punch. The bandshape was also displayed on a Servoscribe chart recorder whilst the spectrum was being recorded.

The sample was contained in a standard glass UV cell of  $\sim 1\text{cm}^2$  cross-section into which it was possible to distil material directly. The temperature was controlled (usually to  $15.0^\circ\text{C}$ ) by a Haake FS temperature controller and water circulating through a brass block surrounding the cell. "Spectroscopic" grade carbon tetrachloride and acetonitrile were used and the methanol- $d_4$  was supplied by CIBA-Geigy. All the materials were distilled before use to exclude dust which if present in the sample causes additional noise in the spectrum because light scattering from the dust particles slightly attenuates the laser beam in a random manner.

For  $\nu_1$  of acetonitrile data were recorded from  $2900\text{cm}^{-1}$  to  $\sim 6\text{cm}^{-1}$  beyond the band maximum at  $\sim 2940\text{cm}^{-1}$ , the laser power (at the laser) was between 2W and 3W depending on the acetonitrile concentration being used. The spectral slitwidth was  $0.84\text{cm}^{-1}$  and was equal to  $\sim 16\%$  of the apparent bandwidth. Normally the polarised ( $I_{VV}$ ) spectrum was recorded twice for each solution and the depolarised ( $I_{VH}$ ) spectrum once. This enabled two values of the isotopic scattering function to be obtained for each solution.

The digital data were analysed in Braunschweig using the ICL/1906S computer installation there. The programme "NUE1" (137) had been developed

there especially for the analysis of the  $\nu_1$  band of acetonitrile. The programme performed the following operations.

(i) The background for each spectrum was removed by using a baseline calculated from the mean of the first twenty data points (cf. Section 4.11).

(ii) The band maximum was found after interpolation between the  $0.25\text{cm}^{-1}$  data points had been effected.

(iii) The points beyond the maximum were removed, leaving the low frequency half of the band.

(iv) After normalisation the isotropic part of the scattered intensity (see Section 6.3) was calculated from the formula

$$I_{\text{iso}} = I_{\text{VV}} - \frac{4}{3} I_{\text{VH}} \quad (6.1)$$

(v) After integration of the bandshape to obtain the total intensity the depolarisation ratio (see Section 6.3) and band second moment (138) were calculated. This latter quantity,  $\langle \omega^2 \rangle$ , is given by the formula

$$\langle \omega^2 \rangle = \frac{\int (\omega - \omega_0)^2 I(\omega - \omega_0) d\omega}{\int I(\omega - \omega_0) d\omega} \quad (6.2)$$

where  $\omega_0$  is the band centre.

(vi) A Fourier transformation was performed on  $I_{\text{iso}}$  to obtain the correlation function  $\phi_{\text{iso}}(t)$  which is equal to the product of the vibrational (or at least non-reorientational) relaxation function and a gaussian correlation function appropriate to the spectral slitwidth used, i.e.:

$$\phi_{\text{iso}}(t) = \phi_{\text{V}}(t) \phi_{\text{S}}(t) \quad (6.3)$$

Finally, correction for the finite spectral slitwidth was made and thus  $I_{\text{V}}(t)$  was obtained from which the correlation time  $\tau_{\text{V}}$  (see below) was obtained by integration:

$$\tau_{\text{V}} = \int_0^{t_{\text{L}}} \phi(t) dt \quad (6.4)$$

where  $t_{\text{L}}$  is the time limit expected from the spectral resolution (139),

### 6.3 Theory of vibrational relaxation processes

It can be shown (140) that for a Raman line the depolarisation ratio for plane polarised incident light,  $\rho_\ell$ , is given by

$$\rho_\ell = \frac{I_{VH}}{I_{VV}} = \frac{3\beta^2}{45\alpha + 4\beta} \quad (6.5)$$

where  $\alpha$  is the spherical part of the change of polarisability tensor,  $\beta$  is a measure of the anisotropy and  $I_{VH}$  and  $I_{VV}$  are respectively the components of the scattered light perpendicular to and parallel to the plane of polarisation of the incident light. It can be also shown (141, 142) that the isotropic,  $I_{iso}(\omega)$ , and anisotropic,  $I_{aniso}(\omega)$ , parts of the scattered intensity are given by

$$I_{iso}(\omega) = I_{VV} - \frac{4}{3} I_{VH} \quad (6.6)$$

and

$$I_{aniso}(\omega) = I_{VH}(\omega) \quad (6.7)$$

When a Fourier transformation into the time domain is made, the following correlation functions are obtained if instrumental resolution effects are assumed to have been removed,

$$\phi_V^{iso}(t) \propto \frac{\int I_{iso}(\omega) \exp(-i\omega t) d\omega}{\int I_{iso}(\omega) d\omega} \quad (6.8)$$

and

$$\phi_V^{aniso}(t) \cdot \phi_{2R}(t) \propto \frac{\int I_{aniso}(\omega) \exp(-i\omega t) d\omega}{\int I_{aniso}(\omega) d\omega} \quad (6.9)$$

Thus a vibrational (or non-reorientational) correlation function,  $\phi_V^{iso}(t)$ , is obtained from  $I_{iso}(\omega)$  and from  $I_{aniso}(\omega)$  the product of a vibrational and a reorientational,  $\phi_{2R}(t)$ , correlation function. Fourier transformation

of an infrared absorption band yields

$$\phi_V^{IR}(t) \cdot \phi_{1R}(t) \propto \frac{\int I_{IR}(\omega) \exp(-i\omega t) d\omega}{\int I_{IR}(\omega) d\omega}$$

where the function  $I_{IR}(\omega)$  represents the intensity of the infrared band and  $\phi_{1R}(t)$  is another reorientational correlation function.

It is often assumed (143), with no particular justification (144), that  $\phi_V^{iso}(t) = \phi_V^{aniso}(t) = \phi_V^{IR}(t)$  in order to obtain  $\phi_{1R}(t)$  and  $\phi_{2R}(t)$ . It should also be noted that for a non-totally symmetric vibration where  $\alpha = 0$  and  $\rho_\ell$  has a value of  $3/4$   $\phi_{iso}(t)$  cannot be found because  $I_{VH} = 3/4 I_{VV}$  and so in Equation (6.6)

$$I_{iso}(\omega) = I_{VV} - \frac{4}{3} \left( \frac{3}{4} I_{VV} \right) = 0 \quad (6.10)$$

It is therefore not possible to obtain  $\phi_V^{iso}(t)$  by this method and some other method must be used (142).

For the  $\nu_1$  mode of acetonitrile the value of  $\rho_\ell$  is very small and so  $\phi_{iso}(\omega)$  can be calculated from Equation (6.5) and thus  $\phi_{iso}(t)$  can be obtained by Fourier transformation. This function will be regarded as being equal to a non-reorientational correlation function,  $\phi_V(t)$ , which is also called a vibrational relaxation function. It is in fact influenced by all non-reorientational relaxation processes going on in the liquid (145, 146). If these processes are divided into pure energy relaxation processes and phase relaxation processes and it is assumed that the two groups are statistically uncorrelated. Thus

$$\phi_V(t) = \phi_E(t) \cdot \phi_{pp}(t) \quad (6.11)$$

where the function  $\phi_{pp}(t)$  can be regarded to consist of other uncorrelated processes

$$\phi_{pp}(t) = \prod^K \phi_{pp}^K(t) \quad (6.12)$$

It must be noted that this separation of  $\phi_v(t)$  into an energy relaxation part and a phase relaxation is only justified if energy relaxation takes place very much more slowly than phase relaxation. Although there is evidence in favour of this assumption (106,143,147) it has been found that energy relaxation can in some cases, for example  $\nu_1$  of iodomethane (148), be taking place on a similar time-scale to pure phase relaxation. In the treatment here it will be assumed that for acetonitrile pure energy relaxation is very much slower than pure phase relaxation and indeed calculations (131) have suggested a factor of  $10^{-6}$  to  $10^{-8}$  in the magnitudes of the correlation times for the two processes.

The various vibrational relaxation processes which could influence the bandshape for a given Raman active vibrational mode have been classified by Rothschild (146) in the following way:-

(i) Vibrational energy transfer to the lattice via rotational and translational degrees of freedom.

(ii) Vibrational energy redistribution between internal modes of the molecule.

(iii) Resonance vibrational energy transfer by coupling, for example through transition dipole-transition dipole interactions, to neighbouring molecules.

(iv) Loss of phase coherence of the excited molecules because there is a range of transition frequencies due to interactions with surrounding molecules.

Of these processes (i) and (ii) are considered to be energy relaxation processes and (iii) and (iv) are considered to be phase relaxation processes. It will now be assumed that energy relaxation is taking place very much more slowly than pure phase relaxation for the  $\nu_1$  mode of acetonitrile. The possibility that the pure phase relaxation times calculated may be influenced by energy relaxation processes cannot be absolutely ruled out.



For each contributing vibrational phase relaxation process that involves long-range forces and leads to a distribution of vibrational frequencies (dipole-dipole, transition dipole-transition dipole etc.) a vibrational relaxation function of the type

$$\phi_{pp}(t) = \exp\{-\langle\omega^2\rangle[t\tau_c + \tau_c^2 \exp(-t/\tau_c) - 1]\} \quad (6.13)$$

can be written using Kubo's theory (85) as shown by Döge (149) and others (142,146,150). In Equation (6.13) the correlation time,  $\tau_c$  and the second moment of the band,  $\langle\omega^2\rangle$ , are parameters that characterise the phase relaxation process caused by the particular intermolecular potential involved. Equation (6.13) approximates to a gaussian decay of  $\phi_{pp}(t)$  at short times ( $t \ll \tau_c$ ) and to an exponential decay of  $\phi_{pp}(t)$  at long times ( $t \gg \tau_c$ ). For short times, or at any time in the slow modulation limit when  $\langle\omega^2\rangle^{1/2}\tau_c \gg 1$  Equation (6.13) gives:

$$\phi_{pp}(t) = \exp\left(-\frac{1}{2}\langle\omega^2\rangle t^2\right) \quad (6.14)$$

At long times, Equation (6.13) gives:

$$\phi_{pp}(t) = \exp(-\langle\omega^2\rangle t\tau_c + \langle\omega^2\rangle\tau_c^2) \quad (6.15)$$

and in the rapid modulation limit when  $\langle\omega^2\rangle^{1/2}\tau_c \ll 1$  this gives:

$$\phi_{pp}(t) = \exp(-\langle\omega^2\rangle\tau_c t) \quad (6.16)$$

From Equation (6.16) it can be seen that a graph of  $\ln\phi_{pp}(t)$  against time is a straight line with a long time slope of  $-\langle\omega^2\rangle\tau_c$ . This slope is related (129) to a correlation time which will be called  $\tau_v^S$  as follows:

$$1/\tau_v^S = \langle\omega^2\rangle\tau_c \quad (6.17)$$

Where  $\tau_v^S$  can be regarded as a vibrational relaxation time because vibrational phase relaxation is assumed to be taking place very much more quickly than energy relaxation and thus the nature of the phase relaxation process determines the total vibrational relaxation function. The gaussian limit represents the situation where the molecules oscillate with

random phases in a quasi-static environment. The lorentzian limit represents the case of extreme motional narrowing and here the parameter  $\tau_c$  is the time constant for the modulation of the molecular environment around any one molecule. In this limit the vibrational relaxation function shows exponential decay. The parameter  $\langle \omega^2 \rangle$  is a measure of the second moment of the observed Raman band (see Section 6.2) and can be obtained either by direct integration from the bandshape or from a graph of  $\ln \phi_{pp}(t)$  against  $t^2$  for the short-time (gaussian) part of  $\phi_{pp}(t)$  (see Equation 6.14).

From Equations (6.14) and (6.15) it can be seen that the model described above depends upon the parameter  $\langle \omega^2 \rangle$  in the slow-modulation limit and upon  $\langle \omega^2 \rangle$  and  $\tau_c$  in the rapid-modulation limit, and in the rapid-modulation limit the vibrational relaxation rate,  $\tau_v^{-1}$ , is given by Equation (6.17).

For molecular interactions which are principally of a long-range type, dipole-dipole, transition dipole-transition dipole etc.,  $\tau_c$  is directly proportional to the dynamic viscosity (151) and therefore inversely proportional to the absolute temperature. Since the second moment, which describes the distribution of molecules around an "active" molecule, is proportional to the number density, it follows that:

$$\tau_v^{-1} \propto \rho \eta / T \quad (6.18)$$

It should be noted that in the models that depend for phase or energy relaxation upon isolated binary collisions (152,153) or upon short-range repulsive forces and hard collisions (154)  $\tau_c$  is equivalent to a time between collisions ( $\tau_J$  in the extended diffusion model (155)) and the rate of vibrational relaxation is inversely proportional to  $\tau_c$ . When the temperature is increased, and therefore the viscosity and the density decrease, the time between collisions increases (compare the time between collisions in the gas phase and in the liquid phase) and therefore since

$$\tau_V^{-1} \propto 1/\tau_C \quad (6.19)$$

and

$$\tau_C \propto 1/\eta \quad (6.20)$$

it follows that both types of model give the same viscosity and density dependence for the rate of vibrational relaxation ( $\tau_V^{-1}$ ). The correlation time  $\tau_C$  should, however, be proportional to the viscosity of the medium for a model based on long-range interactions (151) and inversely proportional for a short-range potential model (Equation (6.20)). In the former case  $\tau_C$  can be identified with a reorientational correlation time,  $\tau_{1R}$ , (associated with  $\phi_{1R}(t)$  in Equation (6.10)), and in the latter case with a time between collisions ( $\tau_J$ ).

#### 6.4 Experimental results and their interpretation

The experimental data acquired fall into four groups, as follows.

(1) Keeping a constant molar ratio of acetonitrile to carbon tetrachloride the mole fraction of methanol- $d_4$  in the liquid mixture was increased from zero to  $\sim 0.5$ . The effect of this on the vibrational relaxation function for the  $\nu_1$  mode of acetonitrile was expected to give a measure of the effect of the presence of methanol- $d_4$  on the  $\nu_s$  (CH) vibration of acetonitrile compared with the effect of the presence of carbon tetrachloride molecules which had been studied previously (129).

(ii) Keeping a constant molar ratio of acetonitrile to methanol- $d_4$  carbon tetrachloride was added until its mole fraction was  $\sim 0.35$ . These measurements were expected to give a measure of to what extent an acetonitrile-methanol- $d_4$  "complex" is disrupted by the addition of carbon tetrachloride.

(iii) The effect of increasing the concentration of acetonitrile in methanol- $d_4$  was studied, the acetonitrile mole fraction being increased from  $\sim 0.06$  to  $\sim 0.4$ . This was expected to give an indication of the extent to which an acetonitrile molecule remains in an environment of methanol- $d_4$  molecules when the number of "other" acetonitrile molecules is increased.

Table 6.1 The addition of methanol-d<sub>4</sub> to a fixed molar ratio of acetonitrile to carbon tetrachloride

mole fractions		mole ratios		$\langle \omega \rangle^2$ (rad <sup>2</sup> s <sup>-2</sup> )	$\tau_V^1$ (ps)	$\tau_V^S$ (ps)	$\tau_C^1$ (ps)	$\tau_C^S$ (ps)	estimated viscosity (kg m <sup>-1</sup> s <sup>-1</sup> )	band centre (cm <sup>-1</sup> )
CH <sub>3</sub> CN	CD <sub>3</sub> OD	CCl <sub>4</sub> : CH <sub>3</sub> CN	CD <sub>3</sub> OD: CH <sub>3</sub> CN							
0.113	-	0.886	-	1.34x10 <sup>24</sup>	2.36	2.28	0.318	0.329	0.963x10 <sup>-3</sup>	2941.5
0.101	0.109	0.790	1.08	1.46x10 <sup>24</sup>	2.22	2.03	0.308	0.337	0.929x10 <sup>-3</sup>	2941.3
0.0878	0.238	0.674	2.71	1.60x10 <sup>24</sup>	2.07	1.98	0.303	0.317	0.887x10 <sup>-3</sup>	2941.5
0.0750	0.350	0.576	4.67	1.77x10 <sup>24</sup>	2.01	1.95	0.283	0.291	0.853x10 <sup>-3</sup>	2941.4
0.0588	0.490	0.451	8.33	2.35x10 <sup>24</sup>	1.90	1.65	0.226	0.261	0.807x10 <sup>-3</sup>	2941.4

(iv) The effect of temperature on the  $\nu_1$  band for a solution of acetonitrile in methanol- $d_4$  of mole fraction 0.120 was studied and found to be very small.

These sets of data will now be considered each in turn.

(1) The experimental data are shown in Table 6.1, Figure 6.1 shows polarised ( $I_{VV}$ ) and depolarised ( $I_{VH}$ ) parts of a typical spectrum and Figure 6.2 shows the plot of  $\ln\phi_{pp}(t)$  against time obtained. The  $\tau_V$  values were calculated both by integration ( $\tau_V^1$ ) (via Equation (6.4)) and from the long-time slope of the  $\ln\phi_{pp}(t)$  against time plot ( $\tau_V^S$ ) (Equation 6.16)). The corresponding  $\tau_c^1$  and  $\tau_c^S$  values were calculated from Equation (6.17) using values of the second moment of the  $\nu_1$  band obtained by integration (see Section 6.2). The values shown are in each case the mean of the two values obtained from the two polarised spectra (see Section 6.2). It can be seen that the  $\tau_V^1$  and  $\tau_V^S$  values follow the same trend but the  $\tau_V^1$  values are consistently somewhat higher. The value of  $\tau_V^1$  is plotted against the molar ratio  $CD_3OD:CH_3CN$  in Figure 6.3 and it can be seen that the correlation time decreases as the concentration of methanol- $d_4$  is increased (i.e. the rate of vibrational relaxation ( $\tau_V^{-1}$ ) increases). This trend may be interpreted as indicating that the methanol- $d_4$  molecules when added become preferentially associated with the acetonitrile molecules. This would be expected from consideration of the equilibrium of formation of the acetonitrile-methanol- $d_4$  complex alone since an increase in the methanol- $d_4$  concentration would lead to a decrease in the concentration of uncomplexed acetonitrile molecules. The effect observed appears to be a general medium effect and not just the effect of the formation of more complexes since the trend to a lower  $\tau_V^1$  continues to cases where the methanol- $d_4$  concentration is well in excess of that of acetonitrile. A similar study for the  $\nu_2$  mode of acetonitrile which involves the stretching of the  $C\equiv N$  bond (which is "directly complexed") should yield further information.

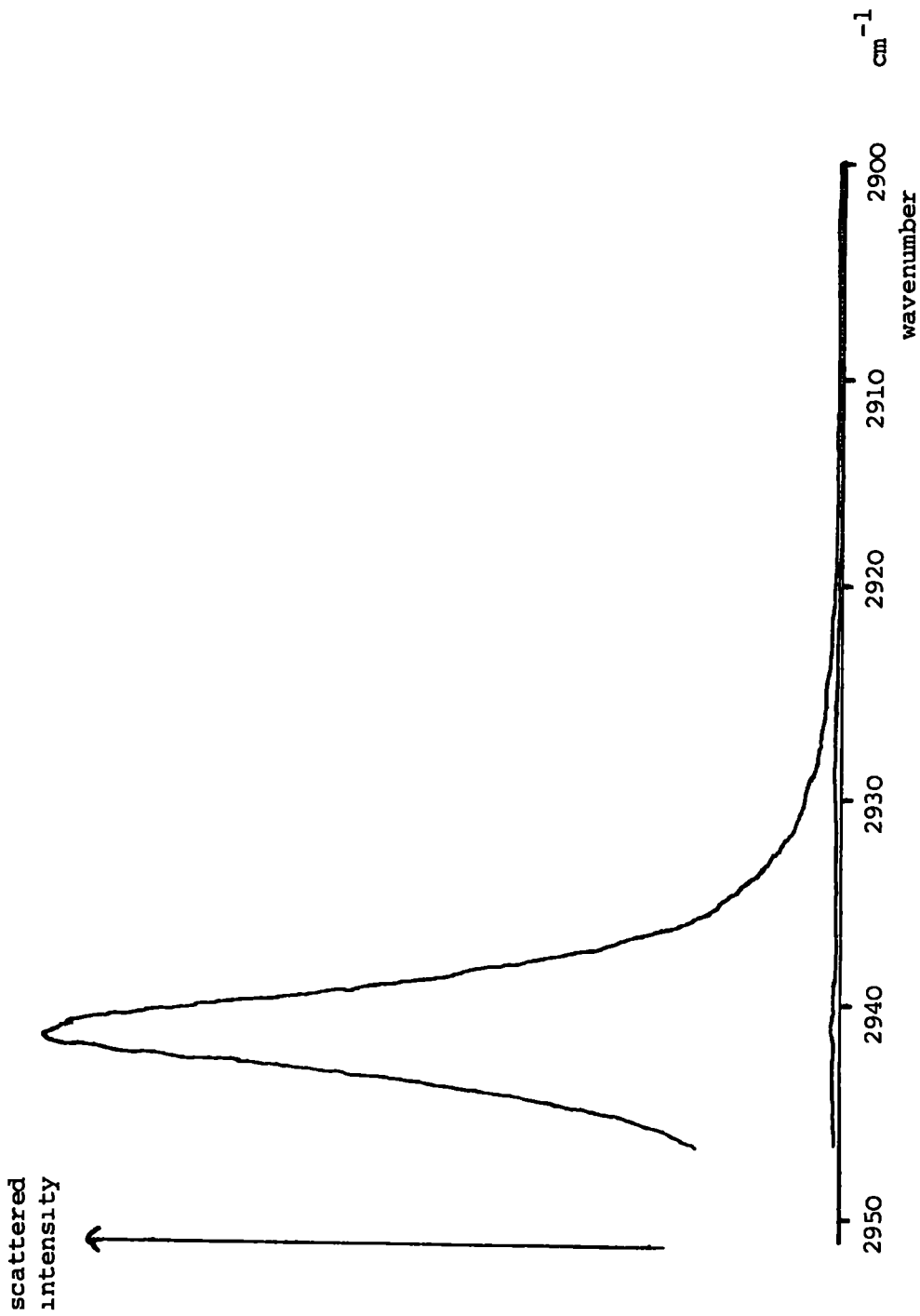


Figure 6.1 The  $\nu_1$  band of acetonitrile (0.101 m.f.) in a solution containing methanol- $d_4$  (0.109 m.f.) and carbon tetrachloride (0.790 m.f.). The polarised ( $I_{VV}$ ) and depolarised ( $I_{VH}$ ) parts are shown.

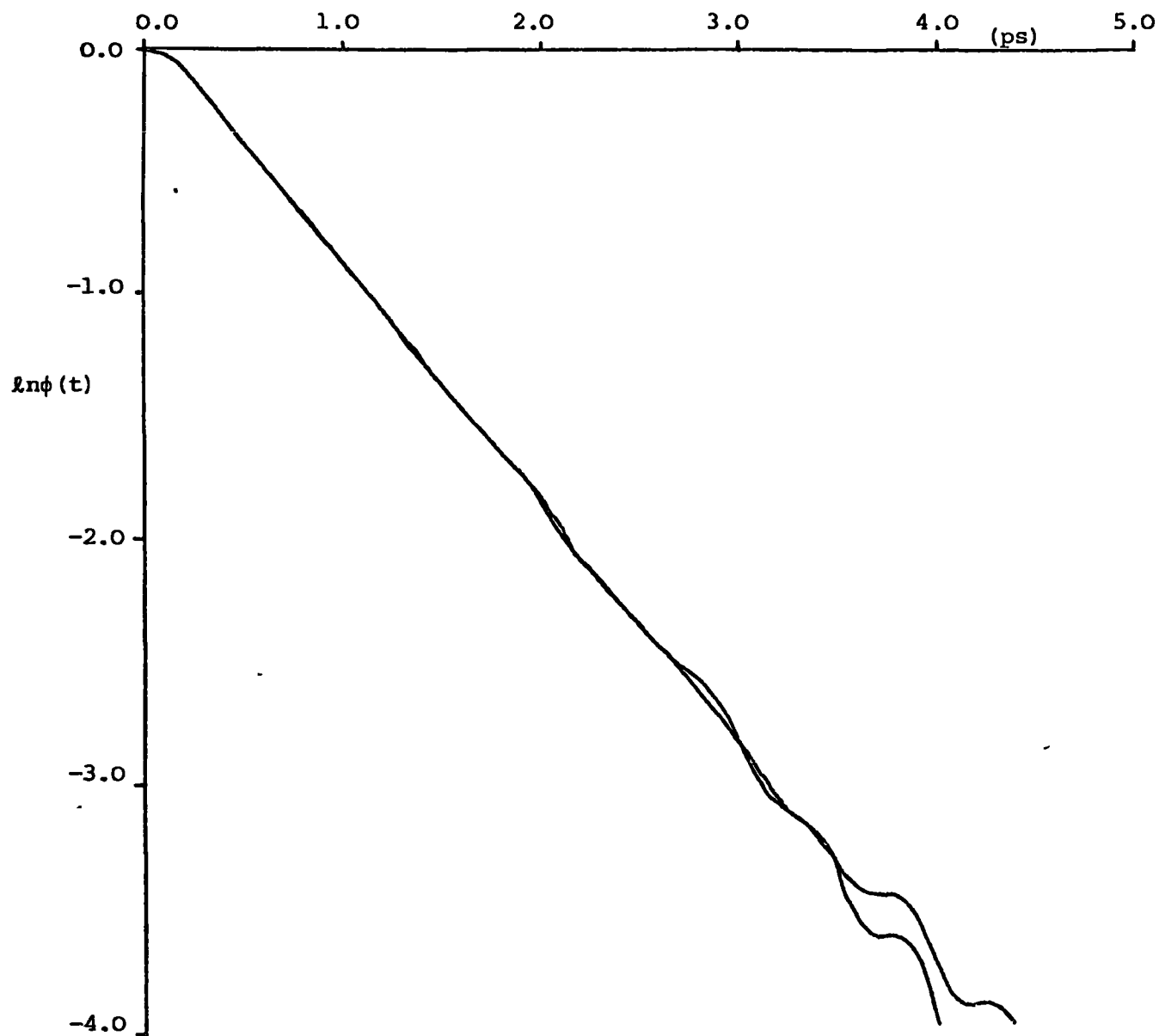


Figure 6.2 Plots of the function  $\ln\phi(t)$  against time for the spectra shown in Figure 6.1. The two curves were computed by using each of the pair of polarised spectra (only one of which is shown in Figure 6.1) recorded along with the depolarised spectrum shown.

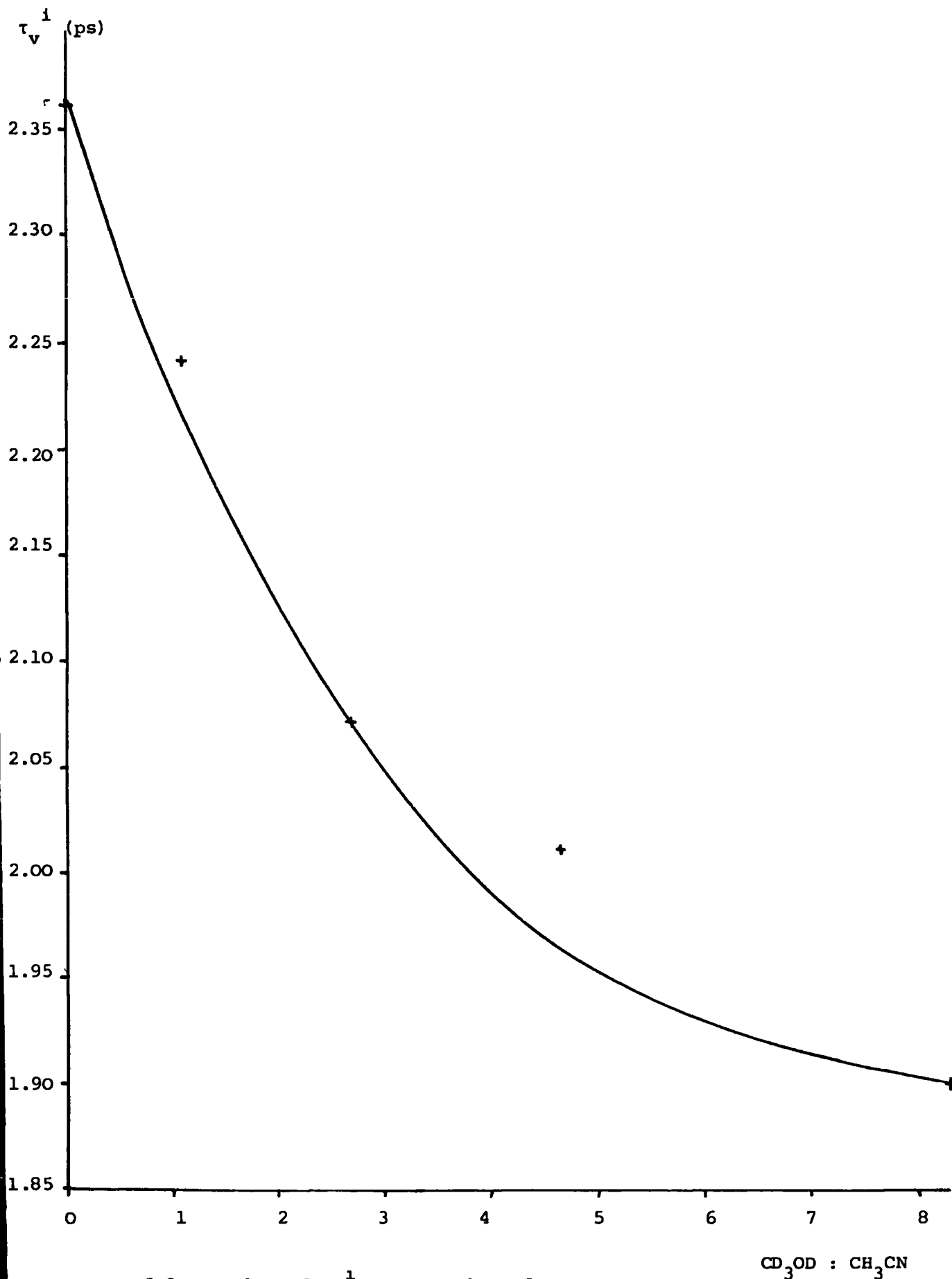


Figure 6.3 A plot of  $\tau_v^1$  against the molar ratio  $\text{CD}_3\text{OD} : \text{CH}_3\text{CN}$  for the addition of methanol- $\text{d}_4$  to a fixed molar ratio of acetonitrile to carbon tetrachloride.



The values of  $\tau_c^i$  and  $\tau_c^s$  calculated by assuming the validity of the rapid modulation limit (the bandshape is almost purely lorentzian, producing a  $\ln\phi_{pp}(t)$  against time plot which is linear at all but very short times) can also be seen to decrease in a similar fashion (the value at  $CD_3OD:CH_3CN$  of 1.08 is not a mean of two since one value of the second moment obtained was exceptionally low). Figure 6.4 shows  $\tau_c^i$  plotted against the viscosity of the solution calculated from literature values (103) assuming additivity in proportion with the mole fractions. This assumption is certainly not strictly valid but the viscosity would be expected to decrease as methanol- $d_4$  is added. The literature values are  $1.039 \times 10^{-3} \text{ kg m}^{-1} \text{ s}^{-1}$  for carbon tetrachloride and  $6.455 \times 10^{-4} \text{ kg m}^{-1} \text{ s}^{-1}$  for methanol (protium species). The figure shows a distinct increase in  $\tau_c^i$  with increase in viscosity and (see Section 6.3) this indicates that the additional vibrational phase relaxation for  $\nu_1$  of acetonitrile in the presence of methanol- $d_4$  is determined by long-range interactions. This may be interpreted as evidence in favour of the electrostatic theories of hydrogen-bonding in contrast with short-range charge transfer-type interaction theories, at least in the determination of the spectral properties of this band.

The values of the second moment increase as methanol- $d_4$  is added and in terms of this model this means that the distribution of molecules around an acetonitrile molecule increases. This effect indicates that again the methanol- $d_4$  molecules are found on average nearer acetonitrile molecules than those of carbon tetrachloride. The situation may be an acetonitrile molecule complexed by a hydrogen bond to a methanol- $d_4$  molecule and having more such molecules in the close vicinity. It may be possible that hydrogen bonds to these molecules are being made and broken as the acetonitrile molecule undergoes reorientation and translation in the liquid. The idea of a range of hydrogen bond angles and lengths seems to be consonant with this situation.

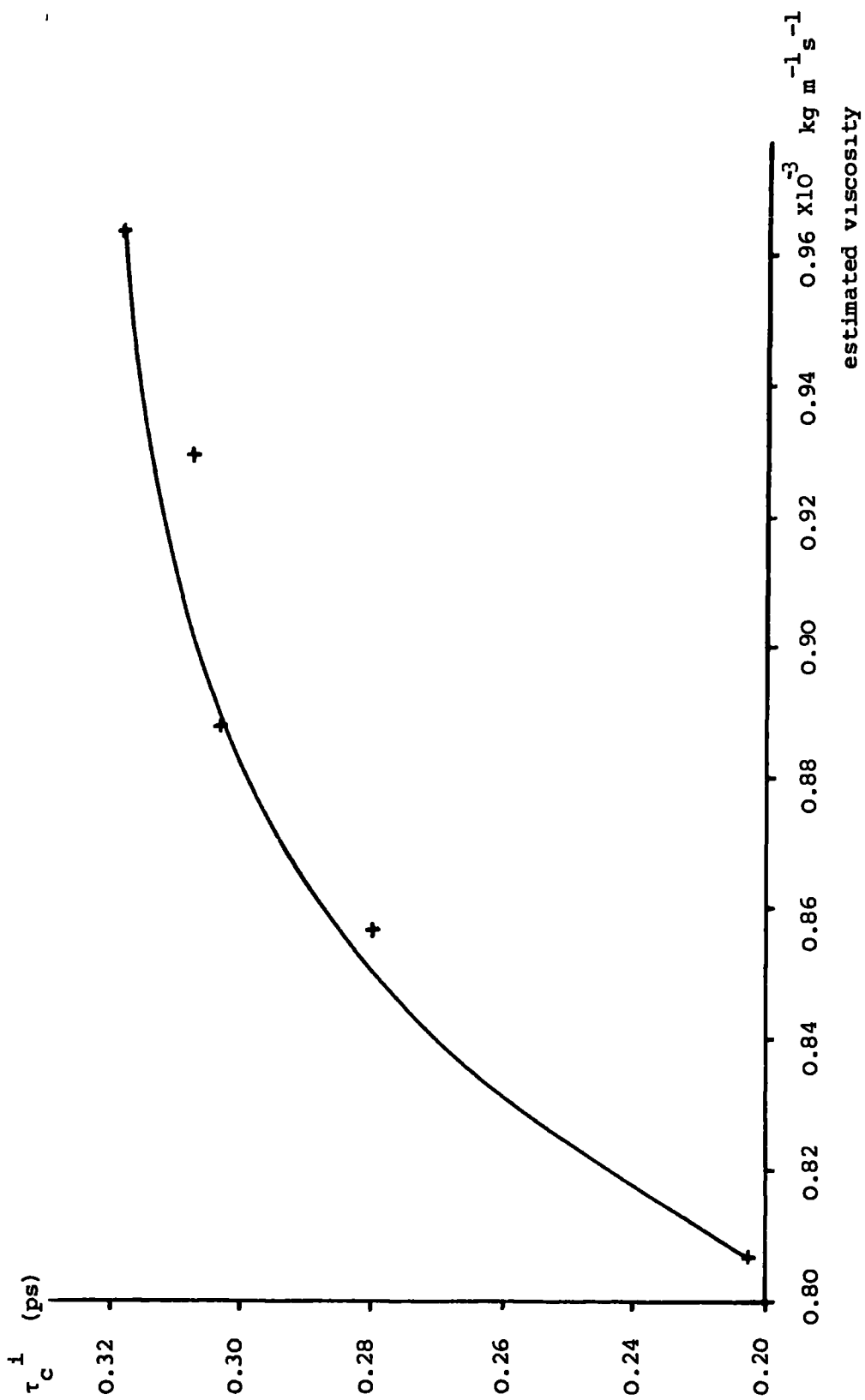


Figure 6.4 A graph of  $\tau_c^{-1}$  against estimated viscosity for the addition of methanol-d<sub>4</sub> to a fixed molar ratio of acetonitrile to carbon tetrachloride

(ii) The data for the addition of carbon tetrachloride to a fixed molar ratio of methanol-d<sub>4</sub> to acetonitrile are shown in Table 6.2.

Figure 6.5 shows polarised ( $I_{VV}$ ) and depolarised ( $I_{VH}$ ) parts of a typical spectrum and Figure 6.6 shows the plot of  $\ln\phi_{pp}(t)$  against time obtained.

Table 6.2 The addition of carbon tetrachloride to a fixed molar ratio of methanol-d<sub>4</sub> to acetonitrile

mole fractions			molar ratios		$\tau_V^1$	$\tau_V^S$	band centre
CH <sub>3</sub> CN	CD <sub>3</sub> OD	CCl <sub>4</sub>	CCl <sub>4</sub> : CH <sub>3</sub> CN	CD <sub>3</sub> OD: CH <sub>3</sub> CN	ps	ps	cm <sup>-1</sup>
0.120	0.880	-	-	7.33	1.70	1.49	2942.9
0.109	0.783	0.108	0.991	7.18	1.69	1.56	2942.7
0.0986	0.711	0.191	1.94	7.21	1.68	1.58	2942.5
0.0785	0.566	0.356	4.54	7.21	1.70	1.74	2942.1

Here the values of the second moment are not considered reliable because careful examination of the spectra reveals a weak, broad band in the low frequency wing due, presumably, to some acetone impurity. Because the value of the second moment is very sensitive to the intensity in the wings of the band (see Equation 6.2) it was considered best to discount these values. The values for  $\tau_V^1$  and  $\tau_V^S$  were, however, considered sufficiently reliable for some conclusions to be drawn. These values show that the rate of vibrational relaxation of  $\nu_1$  is essentially fairly constant as carbon tetrachloride is added. This can be interpreted as indicating that the addition of carbon tetrachloride does not upset the local solvation shell of methanol-d<sub>4</sub> molecules around acetonitrile molecules which was postulated above.

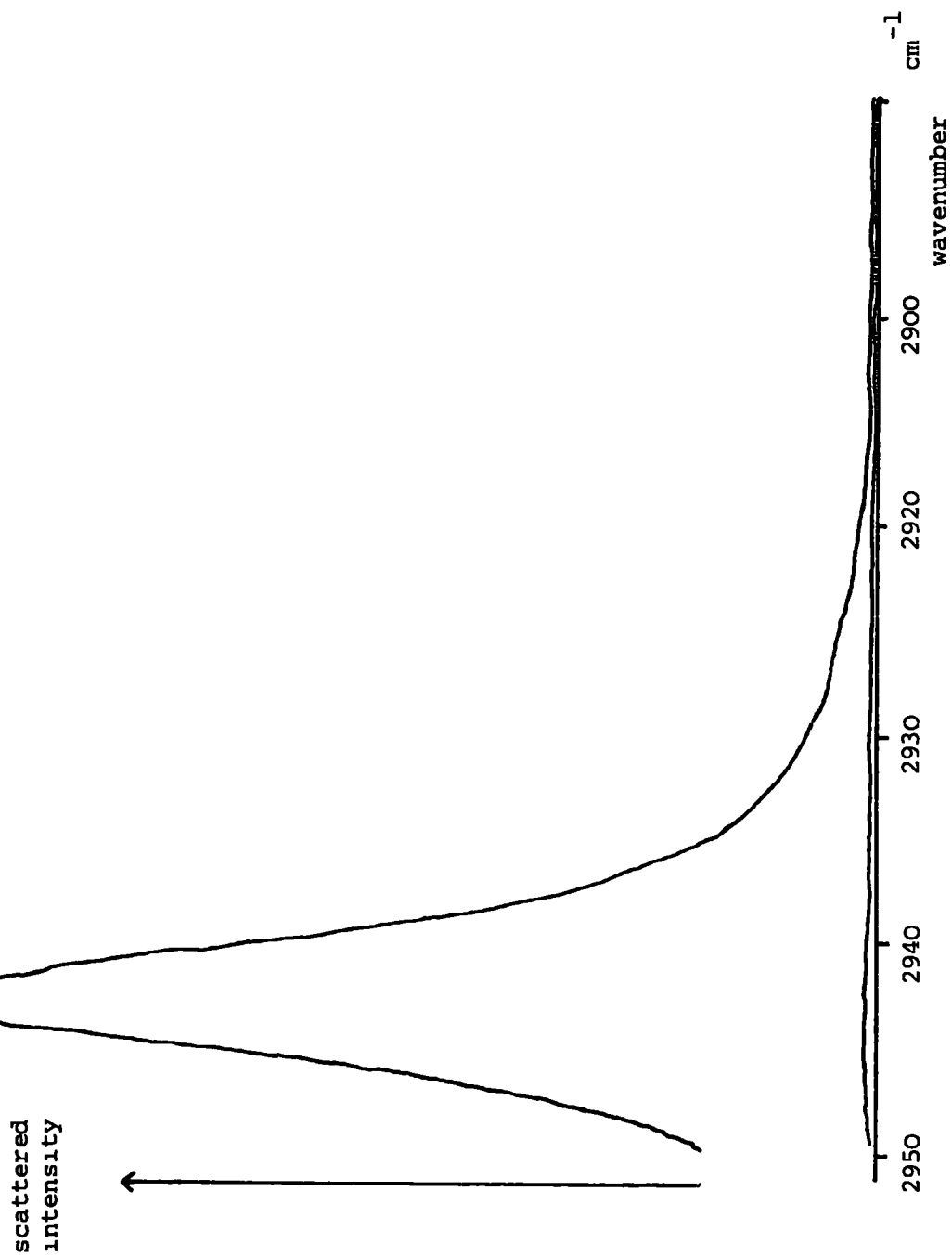


Figure 6.5 The  $\nu_1$  band of acetonitrile (0.120 m.f.) in methanol-d<sub>4</sub>.

The polarised ( $I_{VV}$ ) and depolarised ( $I_{VH}$ ) parts are shown.

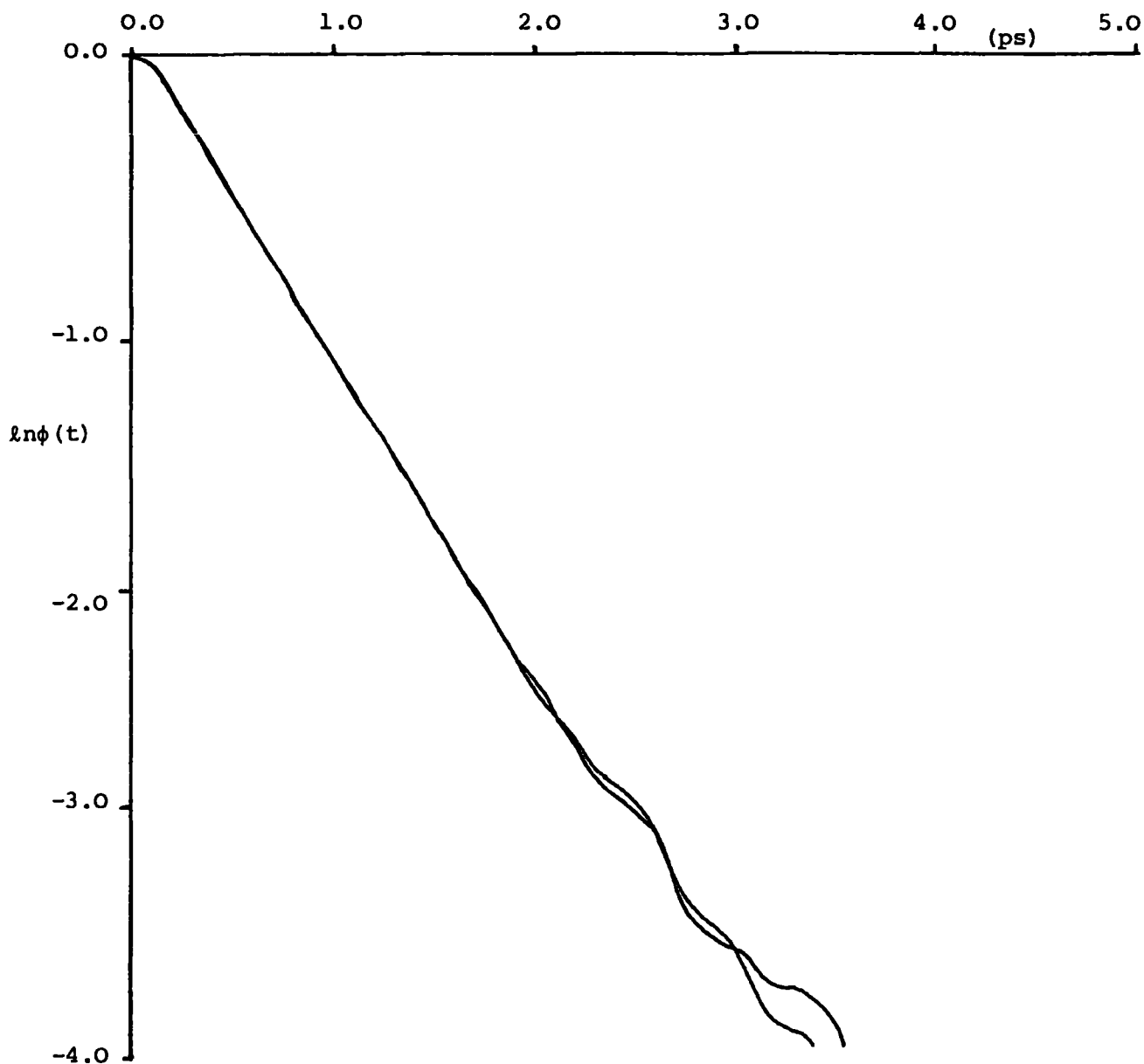


Figure 6.6 Plots of the function  $\ln\phi(t)$  against time for the spectra shown in Figure 6.5. The two curves were computed by using each of the pair of polarised spectra (only one of which is shown in Figure 6.5) recorded along with the depolarised spectrum shown.

(iii) Table 6.3 shows data for the effect of change of concentration of acetonitrile in methanol-d<sub>4</sub>. Figure 6.7 shows polarised (I<sub>VV</sub>) and depolarised (I<sub>VH</sub>) parts of a typical spectrum and Figure 6.8 shows the plot of  $\ln \Phi_{pp}(t)$  against time obtained. Here again the values of the correlation times,  $\tau_V^i$ ,  $\tau_V^s$ ,  $\tau_C^i$  and  $\tau_C^s$  show no marked trend over this concentration range.

Table 6.3 Acetonitrile in solution in methanol-d<sub>4</sub>

mole frac of CH <sub>3</sub> CN	$\langle \omega^2 \rangle$ (rad <sup>2</sup> s <sup>-2</sup> )	$\tau_V^i$ (ps)	$\tau_V^s$ (ps)	$\tau_C^i$ (ps)	$\tau_C^s$ (ps)	band centre (cm <sup>-1</sup> )
0.0651	1.91x10 <sup>24</sup>	1.69	1.54	0.310	0.340	2943.0
0.120	1.91x10 <sup>24</sup>	1.70	1.49	0.308	0.351	2941.9
0.204	1.88x10 <sup>24</sup>	1.68	1.50	0.317	0.355	2943.3
0.367	2.13x10 <sup>24</sup>	1.66	1.57	0.283	0.299	2943.2

This can be considered as evidence that the acetonitrile-methanol-d<sub>4</sub> local structure is not disrupted by the addition of further acetonitrile. Alternatively, acetonitrile-acetonitrile interactions may be considered to be similar to acetonitrile-methanol-d<sub>4</sub> interactions and so no pronounced effect is seen at these concentrations since one potential is removed and replaced by another. The values for  $\tau_V^s$  for acetonitrile in carbon tetrachloride solution are shown for comparison in Table 6.4 and it can be seen that these values are at all times higher than in methanol-d<sub>4</sub> solution, indicating that, in accordance with expectation, vibrational relaxation is faster in a polar solvent. It is not possible to say, on this evidence, how much of the observed change is due to a general "medium" effect or to specific hydrogen bonding interactions. It does seem certain that there is a tendency for the "excess" (i.e. uncomplexed) methanol-d<sub>4</sub> molecules to be found in the first coordination shell of the acetonitrile molecules.

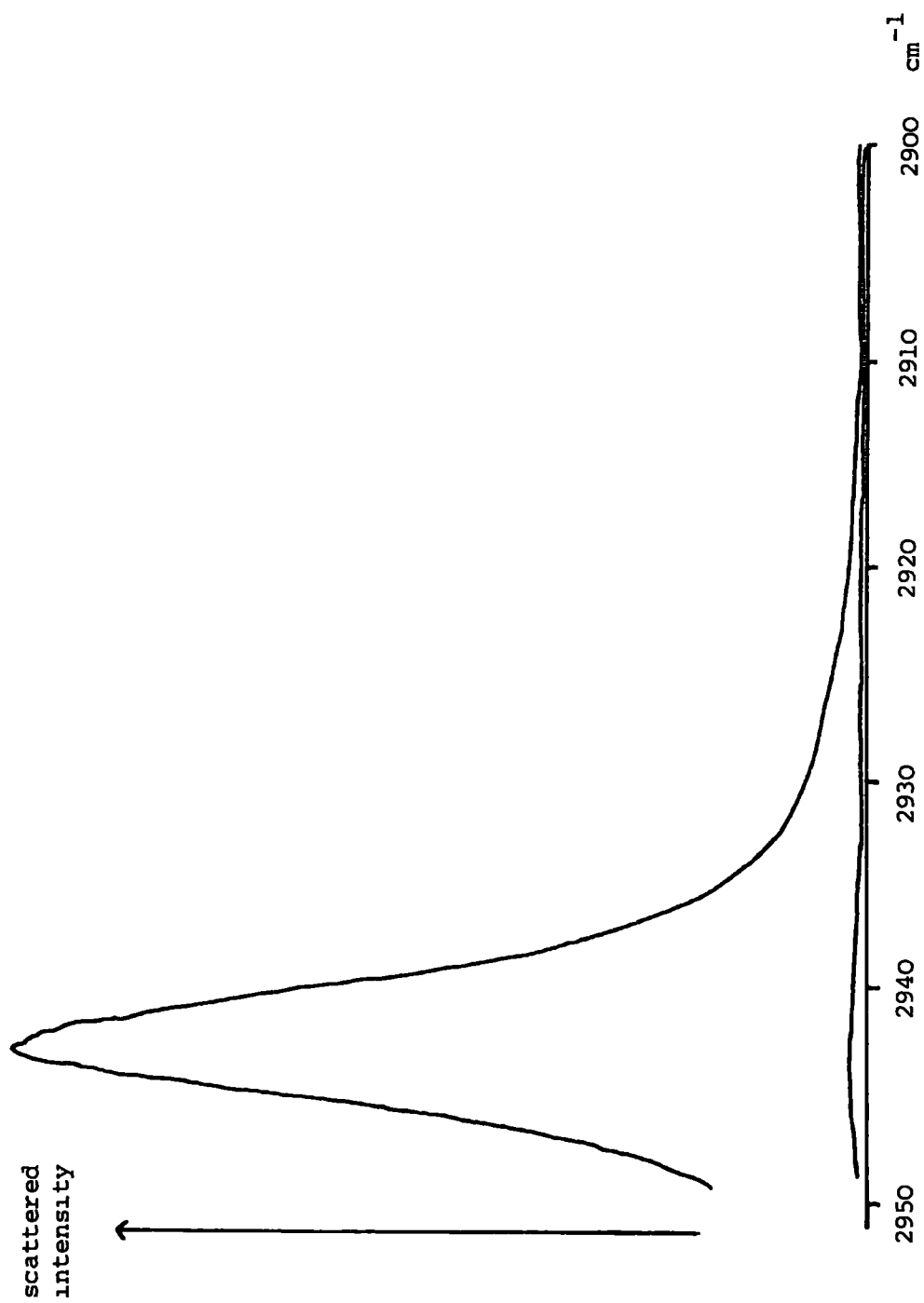


Figure 6.7 The  $\nu_1$  band of acetonitrile (0.240 m.f.) in methanol- $d_4$ .

The polarised ( $I_{VV}$ ) and depolarised ( $I_{VH}$ ) parts are shown.

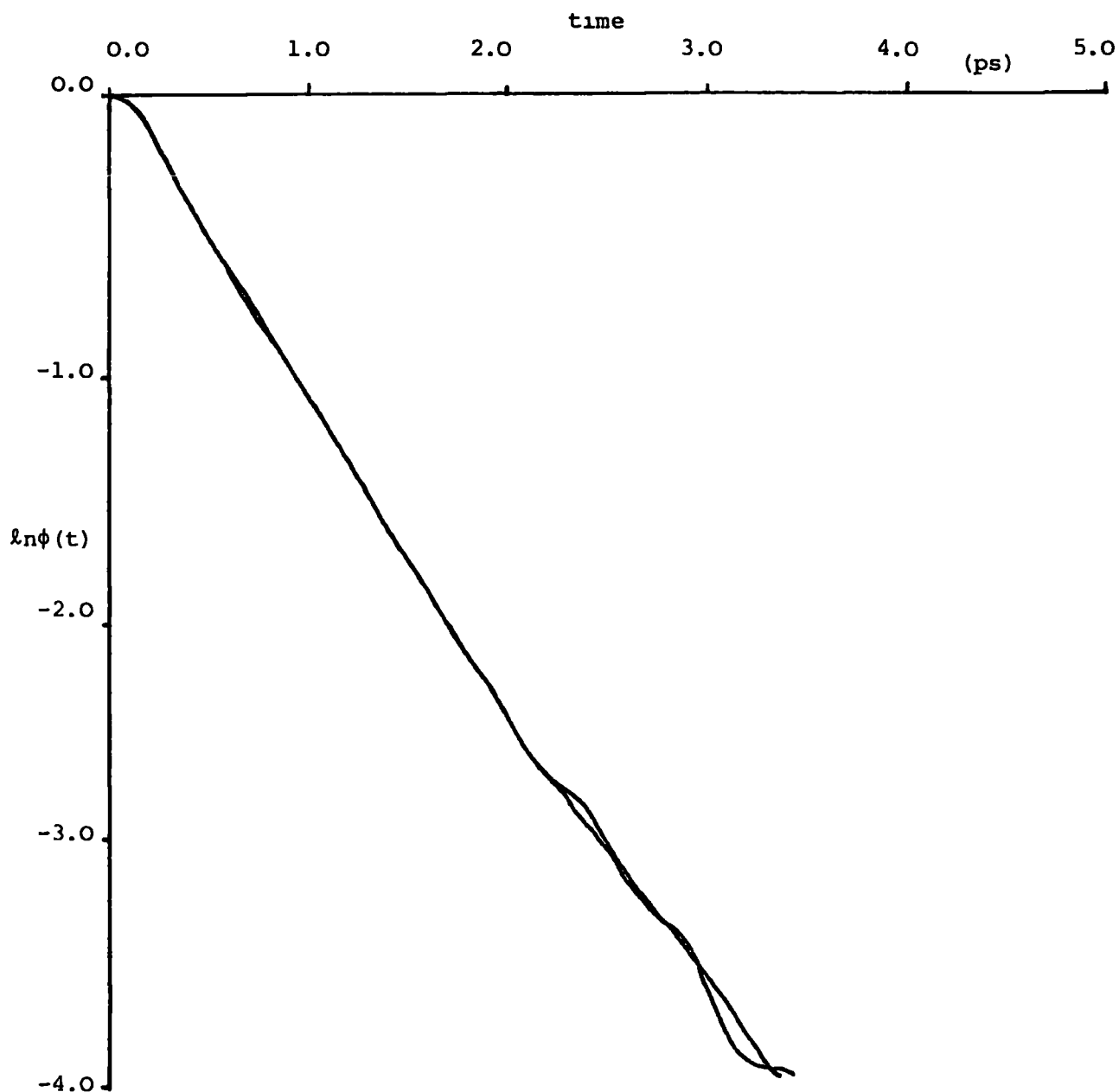


Figure 6.8 Plots of the function  $\ln \phi(t)$  against time for the spectra shown in Figure 6.7. The two curves were computed by using each of the pair of polarised spectra (only one of which is shown in Figure 6.5) recorded along with the depolarised spectrum shown.



Table 6.4 Values of  $\tau_V^s$  for acetonitrile in carbon tetrachloride  
(from ref. (129))

mole fraction of CH <sub>3</sub> CN	$\tau_V^s$ (ps)
0.64	1.86
0.37	1.97
0.16	2.16
0.06	2.41
0.03	2.60
0.01	2.71

#### 6.5 Summary and conclusions

Although it seems that the acetonitrile-methanol-d<sub>4</sub> interactions, at least those that influence the vibrational relaxation of the  $\nu_1$  mode, are of a long-range force type it cannot be said whether one or more phase relaxation process contributes to the bandshape. Dipole-dipole interactions between acetonitrile molecules and methanol-d<sub>4</sub> molecules would be expected to be weaker than between acetonitrile molecules themselves because of the smaller dipole moment (1.66D) (103) of methanol compared with that of acetonitrile (3.44D) (103). Therefore some "additional" effect would seem to be present and this could be either the effect of hydrogen bond formation transmitted to the methyl group or the effect of local dipoles of adjacent molecules surrounding the methanol-d<sub>4</sub> molecule on all sides.

The results presented here form only a very incomplete study of a system which is inherently very complicated. Much more data would be needed before very precise conclusions could be drawn and data for the bands of acetonitrile, other than  $\nu_1$ , in addition to those in spectrum of methanol

would obviously be desirable. Particularly interesting would be data for vibrations of atoms directly participating in the hydrogen bond but there are tremendous problems connected with a study of  $\nu_2$  (equivalent to C≡N stretching) of acetonitrile (see references (133) and (135) and Section 6.1).

**REFERENCES**

1. A. Werner, *Ber.*, 36, 147 (1903)
2. T.S. Moore and T.F. Winmill, *J. Chem. Soc.*, 101, 1635 (1912)
3. J.A. Ibers, *J. Chem. Phys.*, 40, 402 (1964)
4. J.S. Waugh, F.B. Humphrey and D.M. Yost, *J. Phys. Chem.*, 57, 486 (1953)
5. K.B. Whetsel and J.H. Lady, *J. Phys. Chem.*, 69, 1596 (1965)
6. S.A. Harrell and D.H. McDaniel, *J. Amer. Chem. Soc.*, 86, 4497 (1964)
7. G.C. Pimentel and A.L. McClellan, "The Hydrogen Bond", Freeman, San Francisco (1960)
8. J.D. Watson and F.H.C. Crick, *Nature*, 171, 737 (1953)
9. C.N.R. Rao, in: "Water. A Comprehensive Treatise, Vol. I." (ed. F. Franks), Plenum, New York, Chapter 3 (1972)
10. D. Eisenberg and W. Kauzmann, "The Structure and Properties of Water", Oxford University Press (1969)
11. F. Jona and G. Shirane, "Ferroelectric Crystals", Pergamon, Oxford (1962)
12. T. Di Paolo and C. Sandorfy, *Can. J. Chem.*, 52, 3612 (1974), *idem.*, *J. Med. Chem.*, 17, 809 (1974)
13. G. Trudeau, et al., *Can. J. Chem.*, 56, 1681 (1978)
14. S.N. Vinogradov and R.H. Linnel, "Hydrogen Bonding", Van Nostrand Reinhold, New York (1971)
15. M.D. Joesten and L.J. Schaad, "Hydrogen Bonding", Marcel Dekker, New York (1974)
16. P. Schuster, G. Zundel and C. Sandorfy (eds.), "The Hydrogen Bond", North-Holland, Amsterdam (1976)
17. J.L. Wood, in "Spectroscopy and Structure of Molecular Complexes", (ed. J. Yarwood), Plenum, London, Chapter 4 (1973)
18. R.K. Thomas, *Proc. Roy. Soc.*, A325, 133 (1971)
19. D. Hadzi and S. Bratos, in ref. 16, Chapter 12
20. ref. 14, Chapter 3
21. ref. 7, Chapter 3

22. A.S.N. Murthy and C.N.R. Rao, *Appl. Spectrosc. Rev.*, 2, 69 (1968)
23. G.C. Pimentel and A.L. McClellan, *Ann. Rev. Phys. Chem.*, 22, 347 (1971)
24. R.M. Badger and S.H. Bauer, *J. Chem. Phys.*, 5, 839 (1937)
25. B. Stymne, H. Stymne and G. Wettermark, *J. Amer. Chem. Soc.*, 95,  
3490 (1973)
26. R. West. et al., *J. Amer. Chem. Soc.*, 84, 3221 (1962)
27. D.A.K. Jones and J.G. Watkinson, *J. Chem. Soc.*, 2366 (1964)
28. S. Kishida and K. Nakamoto, *J. Chem. Phys.*, 41, 1558 (1964)
29. K. Fukushima and B.Z. Zwolinski, *J. Chem. Phys.*, 50, 737 (1969)
30. M. Obradovic, T. Solmajer and D. Hadzi, *J. Mol. Struc.*, 21, 397 (1974)
31. D. Hadzi, I. Petrov and M. Zitko, in "Advances in Molecular Spectroscopy,  
Vol. II", Pergamon, London, p. 794 (1962)
32. S.G.W. Ginn and J. L. Wood, *Spectrochim. Acta.*, 23A, 611 (1967)
33. D.L. Cummings and J.L. Wood, *J. Mol. Struc.*, 20, 1 (1974)
34. G.S. Landsberg and F.S. Baryshanskaya, *Izv. Akad. Nauk.SSSR, Ser. Fiz.*,  
10, 509 (1946)
35. B. I. Stepanov, *Zh. Fiz. Khim.*, 19, 507 (1945); *idem.*, *Nature*, 157,  
808 (1946)
36. S. Bratos and D. Hadzi, *J. Chem. Phys.*, 27, 991 (1957)
37. C. A. Coulson and G.N. Robertson, *Proc. Roy. Soc.*, A337, 167 (1974);  
G.N. Robertson, *J. Chem. Soc. Far. II*, 72, 1153 (1976)
38. J.A. Ketelaar and W. Vedder, *J. Chem. Phys.*, 19, 654 (1951)
39. G.L. Hofacker, Y. Maréchal and M.A. Ratner, in ref. 16, Chapter 6
40. C. Sandorfy, in ref. 16, Chapter 13
41. A. Witkowski, *J. Chem. Phys.*, 47, 3645 (1967)
42. Y. Maréchal and A. Witkowski, *J. Chem. Phys.*, 48, 3697 (1968)
43. A. Witkowski, *J. Chem. Phys.*, 52, 4403 (1970)
44. M. Haurie and A. Novak, *J. Chim. Phys.*, 62, 137, 146 (1965)

45. S.G.W. Ginn and J.L. Wood, *J. Chem. Phys.*, 46, 2735 (1967)
46. J-L. Leviel and Y. Maréchal, *J. Chem. Phys.*, 54, 1104 (1971)
47. J. Bournay and Y. Maréchal, *J. Chem. Phys.*, 55, 1230 (1971)
48. P. Excoffon and Y. Maréchal, *Spectrochim. Acta.*, 28A, 269 (1972)
49. H.R. Zelsmann and Y. Maréchal, *Chem. Phys.*, 5, 367 (1974)
50. J. Bournay and Y. Maréchal, *J. Chem. Phys.*, 59, 5077 (1973);  
idem., *Chem. Phys. Lett.*, 27, 180 (1974); idem., *Spectrochim. Acta.*, 31A, 1351 (1975)
51. J.E. Bertie and D.J. Millen, *J. Chem. Soc.*, 497, 514 (1965)
52. J. Arnold and D.J. Millen, *J. Chem. Soc.*, 503, 510 (1965)
53. C.A. Coulson and G.N. Robertson, *Proc. Roy. Soc.*, A342, 289 (1975)
54. R.K. Thomas and H. Thompson, *Proc. Roy. Soc.*, A316, 303 (1970)
55. J. Lascombe, J.C. Lassegues and P.V. Huong, *J. Phys. Chem.*, 77, 2779 (1973)
56. S. Bratos, *J. Chem. Phys.*, 63, 3499 (1975)
57. E. Maréchal and S. Bratos, *J. Chem. Phys.*, 68, 1825 (1978)
58. S. Bratos, J. Rios and Y. Guissani, *J. Chem. Phys.*, 52, 439 (1970)
59. S. Bratos and E. Maréchal, *Phys. Rev.*, A4, 1078 (1971)
60. G.N. Robertson and J. Yarwood, *Nature*, 257, 41 (1975); idem.,  
*Chem. Phys.*, 32, 267 (1978)
61. P.V. Huong and J.C. Lassegues, *Spectrochim. Acta.*, 26A, 269 (1968)
62. N. Rosch and M.A. Ratner, *J. Chem. Phys.*, 61, 3344 (1974)
63. E. Fermi, *Z. Phys.*, 71, 250 (1931)
64. J.C. Evans, *Spectrochim. Acta.*, 16, 994 (1960)
65. M.F. Claydon and N. Sheppard, *Chem. Comm.*, 1431 (1969)
66. M.F. Claydon, et al., *Chem. Comm.*, 31 (1975)
67. A. Hall and J.L. Wood, *Spectrochim. Acta.*, 23A, 1257 (1967)
68. R.L. Dean, F.N. Masri and J.L. Wood, *Spectrochim. Acta.*, 31A, 79 (1975)
69. Y. Maréchal, *J. Phys.*, B6, L188 (1973)

70. S. Bratos and G.N. Robertson, unpublished
71. "Model 577 Grating Infrared Spectrophotometer Instrument Manual",  
Perkin-Elmer Ltd., England (1971)
72. J. Yarwood in "Spectroscopy and Structure of Molecular Complexes",  
(ed. J. Yarwood), Plenum, London, p. 112 (1973)
73. Thanks are due to Dr J. Yarwood for supplying the original programme  
which was subsequently modified.
74. R.N. Jones, et al., "Computer Programs for Absorption Spectrophotometry",  
National Research Council of Canada Bulletin No. 11, Ottawa,  
p. 17 (1968)
75. C. Barker, Ph.D. Thesis, University of Durham (1977)
76. R.J. Bell, "Introductory Fourier Transform Spectroscopy", Academic  
Press, London (1972)
77. K.D. Möller and W.G. Rothschild, "Far-Infrared Spectroscopy",  
Wiley-Interscience, London (1971)
78. G.W. Chantry, "Submillimetre Spectroscopy", Academic Press, London (1971)
79. "Instruction Manual for the Fourier Spectrophotometer FS-720",  
Research and Industrial Instruments Company (now Beckman-R.I.I.C.  
Ltd) (1968)
80. P.L. James, M.Sc. Thesis, University of Durham (1976)
81. D.H. Martin and E. Pūplett, Infrared Phys., 10, 105 (1969)
82. G.N. Robertson, Phil. Trans. Roy. Soc., A286, 25 (1977)
83. G.E. Uhlenbeck and L.S. Ornstein, Phys. Rev., 36, 823 (1930)
84. M.C. Wang and G.E. Uhlenbeck, Revs. Mod. Phys., 17, 323 (1945)
85. R. Kubo, in: "Fluctuation, Relaxation and Resonance in Magnetic Systems",  
(ed. D. Ter Haar), Oliver and Boyd, Edinburgh (1962)
86. R. Kubo, Rep. Prog. Phys., 29, 255 (1966)
87. S.J. Cyvin in: "Molecular Vibrations and Mean Square Amplitudes",  
Elsevier, Amsterdam p. 75 (1968)

88. E.N. Da C. Andrade, *Nature*, 125, 309 (1930)
89. T.E. Thorpe and J.W. Rodger, *Phil. Trans. Roy. Soc.*, A185, 397 (1894)
90. E.A. Moelwyn-Hughes in: "Physical Chemistry, 2nd Edition",  
Pergamon, Oxford p. 716 (1961)
91. M.L. Bhanot, private communication
92. M.D. Joesten and R.S. Drago, *J. Amer. Chem. Soc.*, 84, 3817 (1962)
93. M. Horak, et al., *Collect. Czech. Chem. Comm.*, 31, 622 (1966)
94. W. Brügel: "An Introduction to Infrared Spectroscopy", Methuen,  
London p. 189 (1962)
95. International Union of Pure and Applied Chemistry: "Tables of  
Wavenumbers for the Calibration of Infrared Spectrometers",  
Butterworths, London (1961)
96. Thanks are due to Dr G.N. Robertson (University of Cape Town) for  
supplying a copy of this programme
97. S. Singh and C.N.R. Rao, *J. Amer. Chem. Soc.*, 88, 2142 (1966)
98. N.C. Barford: "Experimental Measurements: Precision, Error and Truth",  
Addison-Wesley, London p. 35 (1967)
99. Thanks are due to Dr G.N. Robertson (University of Cape Town) for  
developing and supplying copies of computer programmes to perform  
the fitting procedure
100. L.J. Bellamy, K.J. Morgan and R.J. Pace, *Spectrochim. Acta.*, 22, 535  
(1966); 27A, 705 (1971)
101. A.D. Buckingham, *Proc. Roy. Soc.*, A248, 169 (1958); *Trans. Faraday Soc.*,  
56, 753 (1960)
102. M. Horak, et al., *Collect. Czech. Chem. Comm.*, 36, 2757 (1971)
103. H.H. Landolt and R. Börnstein (eds.): *Eigenschaften der Materie in  
ihren Aggregatzuständen* (Vol. II of: "Zahlenwerte und Funktionen"  
etc.), Springer, Berlin (1969)



104. B.J. Berne and D. Kivelson, *Faraday Symp. Chem. Soc.* No. 11, p. 160 (1977)
105. W.J. Moore in: "Physical Chemistry", 5th Edition, Longman, London  
pp. 924 and 946 (1972)
106. A. Laubereau and W. Kaiser, *Ann. Rev. Phys. Chem.*, 26, 83 (1975)
107. "VLT-2 Variable Temperature Unit", Beckman-R.I.I.C. Ltd. Manual
108. "TEMIC Automatic Temperature Controller Instructions", Beckman-R.I.I.C.  
Ltd. Manual
109. A.E. Beezer, et al., *J. Chem. Soc. Far. I*, 73, 1326 (1977)
110. H.P. Hopkins, C.J. Alexander and S.Z. Ali, *J. Phys. Chem.*, 82, 1268 (1978)
111. see ref. 10, p. 229
112. J.G. Bayly, V.B. Kartha and W.H. Stevens, *Infrared Phys.*, 3, 211 (1963)
113. M. Falk and T.A. Ford, *Can. J. Chem.*, 44, 1699 (1966)
114. R. D. Waldron, *J. Chem. Phys.*, 26, 809 (1957)
115. C.L. van P. van Eck, H. Mendel and J. Fahrenfort, *Proc. Roy. Soc.*,  
A247, 472 (1958)
116. C.A. Swenson, *Spectrochim. Acta.*, 21, 987 (1965)
117. I. Kirshenbaum in: "Physical Properties and Analysis of Heavy Water",  
(eds. H.C. Urey and G.M. Murphy), McGraw-Hill, New York,  
Chapter 2 (1951)
118. G.E. Walrafen in "Water a Comprehensive Treatise, Vol. I", (ed. F. Franks),  
Plenum, New York, Chapter 5 (1972)
119. W.A.P. Luck, in ref. 16, Chapter 28
120. M. Falk, *Chemistry and Physics of Aqueous Gas Solutions*, The Electro-  
chemical Society, p. 19 (1975)
121. J. Yarwood, et al., *Far. Disc. Chem. Soc.* 66, paper no. 19 (1978)
122. M.W. Evans, et al., submitted for publication to *Mol. Phys.*
123. G.J. Davies, J. Chamberlain and M. Davies, *J. Chem. Soc. Far. II*, 69,  
1223 (1973)

124. S.G.W. Ginn and J.L. Wood, Proc. Chem. Soc., 370 (1964); *idem*, Chem. Comm., 628 (1965)
125. A. Hall and J.L. Wood, Spectrochim. Acta., 28A, 2331 (1972)
126. M. Davies, G.W.F. Pardoe, J.E. Chamberlain and H.A. Gebbie, Trans. Far. Soc., 63, 2605 (1967); 64, 847 (1968); 66, 273 (1970)
127. J. Ph. Poley, J. Appl. Sci., 4B, 337 (1955)
128. N.E. Hill, Proc. Phys. Soc., 82, 723 (1968); *idem.*, Chem. Phys. Lett., 2, 5 (1968)
129. J. Yarwood, R. Arndt and G. Döge, Chem. Phys., 25, 387 (1977)
130. J. Yarwood and R. Arndt in "Molecular Association Vol. 2", (ed. R. Foster), Wiley-Interscience, New York (1978)
131. J. Schroeder, et al., J. Chem. Phys., 66, 3215 (1977)
132. A. Lowenstein and Y. Margalit, J. Phys. Chem., 69, 4152 (1965)
133. G. Fini and P. Mirone, Spectrochim. Acta., 32A, 439 (1976)
134. A. Loewenschuss and N. Yellin, Spectrochim. Acta., 31A, 207 (1975); 32A, 1249 (1976)
135. J. Yarwood, R. Arndt and G. Döge, in preparation
136. J. E. Griffiths, J. Chem. Phys., 59, 751 (1973)
137. Thanks are due to Dr R. Arndt (Technische Universität, Braunschweig) for allowing the use of this programme
138. R. G. Gordon, J. Chem. Phys., 39, 2788 (1963)
139. B. Keller and F. Kneubühl, Helv. Phys. Acta., 45, 1127 (1972)
140. G. Herzberg in: "Molecular Spectra and Molecular Structure, Vol. II", Van Nostrand, Princeton, p. 248 (1945)
141. F.J. Bartoli and T.A. Litovitz, J. Chem. Phys., 56, 404 (1972)
142. L. A. Nafie and W.L. Peticolas, J. Chem. Phys., 57, 3145 (1972)
143. R.T. Bailey in: "Molecular Spectroscopy. Vol. 2", (eds. R.F. Borrow, D.A. Long and D.J. Millen), Specialist Periodical Reports of the Chemical Society, London p. 198 (1974)

144. A.M. Amanin da Costa, M.A. Norman and J.H.R. Clarke, *Mol. Phys.*, 29, 191 (1975)
145. T. Tokuhiko and W.G. Rothschild, *J. Chem. Phys.*, 62, 2150 (1975)
146. W.G. Rothschild, *J. Chem. Phys.*, 65, 455 (1976)
147. J. Keizer, *J. Chem. Phys.*, 61, 1717 (1974)
148. A. Laubereau in: "Proceedings of the Fifth International Conference on Raman Spectroscopy" (eds. E.D. Schmid, et al.), Schutz, Freiburg (1976)
149. G. Doge in: "Molecular Motions in Liquids" (ed. J. Lascombe), Reidel, Dordrecht, p. 225 (1974)
150. P.C.M. van Woerkom, et al., *Chem. Phys.*, 4, 236 (1974)
151. R.M. Lynden-Bell and G.C. Tabisz, *Chem. Phys. Lett.*, 46, 175 (1977)
152. T.A. Litovitz, *J. Chem. Phys.*, 26, 469 (1957)
153. W.M. Madigosky and T.A. Litovitz, *J. Chem. Phys.*, 34, 489 (1961)
154. S.F. Fischer and A. Laubereau, *Chem. Phys. Lett.*, 35, 6 (1975)
155. R.E.D. McClung, *J. Chem. Phys.*, 51, 3842 (1969)

**APPENDICES**

APPENDIX 1

Chemical Physics 32 (1978) 283–299  
© North-Holland Publishing Company

**VIBRATIONAL RELAXATION OF HYDROGEN-BONDED SPECIES IN SOLUTION  
II ANALYSIS OF  $\nu_s(\text{XH})$  ABSORPTION BANDS**

J YARWOOD, R ACKROYD

*Department of Chemistry University of Durham, Durham DH1 3LE UK*

and

G N ROBERTSON

*Department of Physics, University of Cape Town, Rondebosch 7700, South Africa*

Received 9 September 1977

The  $\nu_s(\text{XH})$  absorption bands of the following complexes have been recorded in digitised form phenol(OH)– and phenol(OD)– dioxan in  $\text{CCl}_4$ , phenol(OH)– and phenol(OD)– acetonitrile in  $\text{CCl}_4$ , and phenol(OH)– acetonitrile in  $\text{CDCl}_3$ . All these bands are broad and nearly featureless, and have widths at half height ranging from 75 to 148  $\text{cm}^{-1}$ . With one possible exception they appear to be free from Fermi resonances. By least-squares fitting of the theoretical bandshape function derived in part I to the experimental spectra we have been able to estimate the parameters  $\Delta$ ,  $\omega_2$  and  $\tau_c$  which characterise the theoretical autocorrelation function, and also to determine the  $\nu_s(\text{XH})$  stretching frequency very accurately. In the case of phenol(OD)–dioxan in  $\text{CCl}_4$  the discrepancies between the observed and fitted spectra can be entirely attributed to errors of observation. It is found that the Kubo parameter  $\tau_c \Delta$  is close to unity in all cases, showing that the  $\nu_s(\text{XH})$  bands are subject to partial (but not extreme) motional narrowing. The  $\nu_O(\text{XH}-\text{Y})$  vibration is always heavily damped and has a broad spectral density. The changes in the spectral profiles produced by deuteration and change of solvent are easily understood in terms of the theory. Deuteration affects the amplitude of modulation, while changing the solvent affects the value of  $\tau_c$ . In either case  $\tau_c \Delta$  changes, and the speed of modulation is altered. Since the system is far from the gaussian (slow modulation) limit, the bandshape changes markedly in consequence.

## 1 Introduction

In the preceding paper [1] we discussed in detail one particular mechanism contributing to the relaxation of the  $\nu_s(\text{XH})$  vibrational phase coherence of a hydrogen-bonded species in solution. Although other mechanisms, including rotational relaxation and vibrational relaxation produced by local field fluctuations, may also be expected to influence the shape of the  $\nu_s(\text{XH})$  absorption band, our preliminary investigations [2] have shown that the dipole transition moment autocorrelation functions obtained by Fourier transformation of various experimental absorption bands can be well represented by an expression of form I (2.26). This suggests that vibrational relaxation is the dominant broadening mechanism, as suggested originally by Bratos [3] and that the relaxation is well described by our model. Two questions arise (1) to

what extent can the profiles of experimental infrared spectra be understood in terms of this mechanism alone, and (2) what information can be obtained about the dynamics of the relaxation process by analysis of infrared spectra. The present paper attempts to answer both these questions.

Fourier cosine transformation artificially symmetrises and smooths experimental data, and thus a comparison of experimental and theoretical autocorrelation functions [2] does not constitute a satisfactory test of the theory. We therefore work directly with spectral profiles, despite the heavy computation that this involves. We neglect all other possible relaxation mechanisms and assume that the absorbance data can be represented by

$$I(\omega) = C\omega\pi^{-1} [1 - \exp(-\hbar\omega/kT)] \times \int_0^{\infty} \phi(t, P) \cos(\omega - \omega_1) dt, \quad (1.1)$$

where  $\omega_1$  is the  $\nu_s(\text{XH})$  angular frequency,  $C$  is a measure of the integrated absorbance of the band, and  $\phi(t, P)$  is the theoretical autocorrelation function of  $I$  (2.26), which depends on three parameters  $P$ . These parameters are estimated using Marquardt's non-linear least squares method [4].

There are three main ways of testing the theory (1) applying variance ratio and chi-squared goodness-of-fit tests to the least-squares analysis, (2) investigating the effects of deuterium substitution, change of solvent, and change of temperature on the parameters estimated by  $\nu_s(\text{XH})$  band profile analysis, and (3) attempting to determine the same parameters by alternative techniques such as far infrared absorption, Raman scattering, or neutron inelastic scattering spectroscopy.

In this paper we perform statistical tests and investigate the effects of isotopic substitution and change of solvent on the relaxation parameters. The particular species we have chosen to investigate are not well suited to temperature variation studies, and their far-infrared spectra are difficult to observe under the same conditions used in recording the mid-infrared spectra.

The structure of the paper is as follows. Sections 2 and 3 describe our experimental procedure and methods of data analysis. In section 4 the spectrum of the complex between deuterated phenol ( $\text{C}_6\text{H}_5\text{OD}$ ) and dioxan in solution in carbon tetrachloride is investigated in detail, and it is shown that the discrepancies between the observed and fitted spectra can be entirely attributed to errors of observation. In other cases the discrepancies are statistically significant. In section 5 it is shown that the effect on the parameters of isotopic substitution is consistent with theoretical expectations in the case of the phenol-acetonitrile and phenol-dioxan complexes. In section 6 the effect on the phenol-acetonitrile spectrum of changing the solvent from  $\text{CCl}_4$  to  $\text{CDCl}_3$  is investigated and interpreted in terms of the theory. The final section is a summary of the positive results obtained.

## 2 Experimental

The materials used were all either Analar or spectroscopic grade chemicals. All solvents were dried for several days prior to use, and there was no spectroscopic evidence of any of the solvents containing water. Samples were made up by mixing stock solutions of acid and base in the required solvent in such a way that the reference solution always contained exactly the same total amount of base as was present in the sample solution. The cells used were Beckman-RIIC Ltd standard demountable or variable temperature infrared cells with KBr windows with matched 0.5 mm spacers. The temperature was maintained constant to within  $\pm 1^\circ\text{C}$  using a Beckman temperature controller (VLT-2) and was monitored using a copper-constantan thermo couple. Spectra were recorded on either a Grubb-Parsons (model GS2A) or a Perkin-Elmer (model 577) spectrometer with a manual (constant) slit width of about  $3.5\text{ cm}^{-1}$  in the  $3600\text{--}3000\text{ cm}^{-1}$  region and  $3.0\text{ cm}^{-1}$  in the  $2800\text{--}2200\text{ cm}^{-1}$ . The amplifier gain was adjusted until the response time of the servo amplifier system was of the order of 5 s or less for full scale deflection. The signal-to-noise ratios achieved at this resolution (shown in figs 1-4) were about 50-80 for the GS2A and 100 for the PE577. The scanning speed was about  $40\text{ cm}^{-1}$  per minute. Digitised spectra were recorded using a Solartron Digital Voltmeter, Data Transfer Unit and ASR33 Teletype; the output was recorded on paper tape at intervals of about  $3\text{ cm}^{-1}$ . The transmission scales of both spectrometers were checked using a set of Beckman-RIIC Ltd linearity discs and found to be accurate to within 0.5% over the whole range. The digitising accuracy of our DVM is 0.1 mV for a dc output scale of 0-100 mV (0-100%  $T$ ) and is well within the limits of accuracy of the instrument itself. The stray light at  $3000\text{ cm}^{-1}$  was found to be negligible.

Some discussion of the way in which spectral backgrounds were recorded is appropriate since the curve-fitting procedure is sensitive to small errors in the background. As is well known, accurate quantitative infrared spectroscopy is made difficult by the fact that the background (obtained for example with an empty cell or a cell with pure solvent) often does not fit the spectral profile in the wings [5] at large values of  $(\bar{\nu} - \bar{\nu}_0)$ . It has become customary to circumvent this problem by using a "drawn-in" baseline obtained

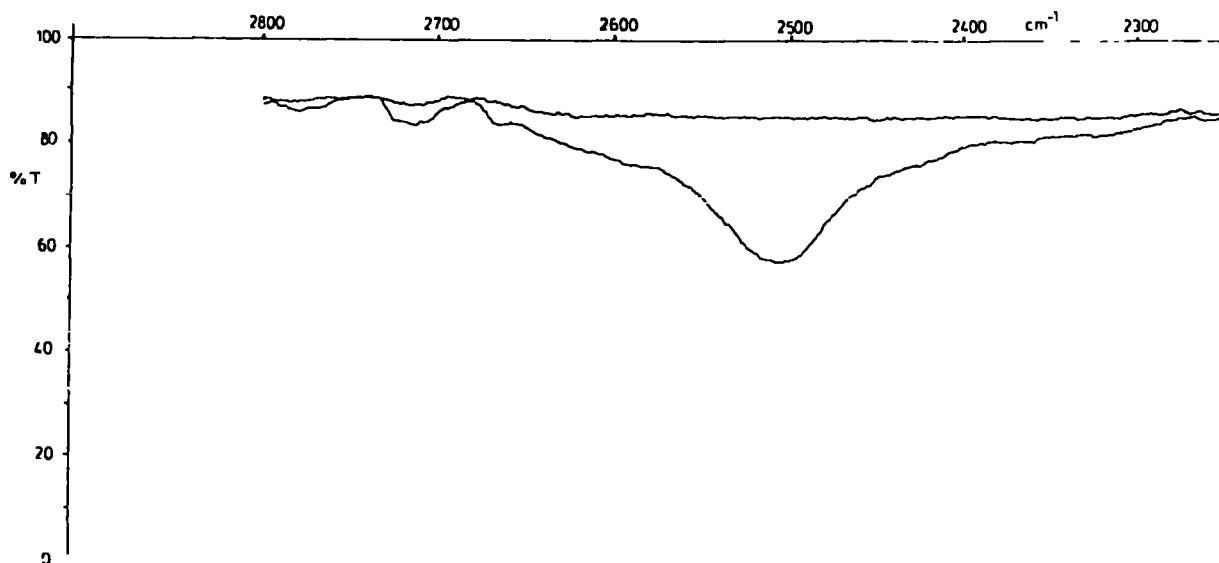


Fig 1 Observed spectrum of phenol(OD)-dioxan in  $\text{CCl}_4$  Background real, concentrations  $\text{C}_6\text{H}_5\text{OD}$ ,  $\approx 0.02$  M,  $\text{C}_4\text{H}_8\text{O}_2$ , 1.30 M  
Ordinate % transmission, abscissa wavenumber/ $\text{cm}^{-1}$

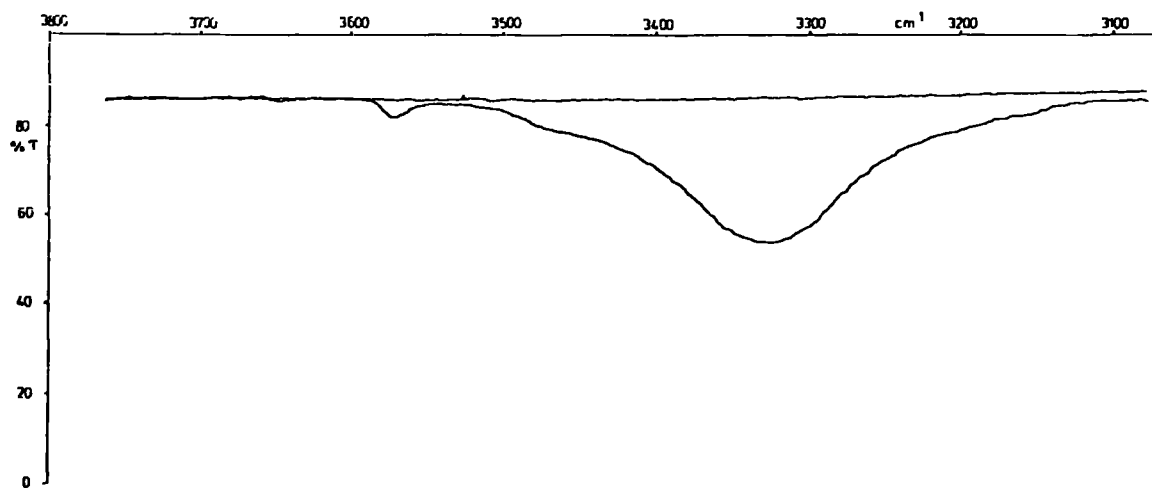


Fig 2 Observed spectrum of phenol(OH)-dioxan in  $\text{CCl}_4$  Background real, concentrations  $\text{C}_6\text{H}_5\text{OH}$ , 0.024 M,  $\text{C}_4\text{H}_8\text{O}_2$ , 1.34 M  
Ordinate % transmission, abscissa wavenumber/ $\text{cm}^{-1}$

by simply joining the ends of the recorded spectrum with a straight line [6]. This procedure is not without its drawbacks, however. In certain cases the drawn-in baseline we have obtained has a demonstrable slope, which makes the total band intensity difficult to determine accurately and complicates the analysis. Further-

more, it is difficult to determine errors of observation reliably when this method is used. Errors in the wings of the spectrum tend to be considerably underestimated.

An alternative procedure is to determine the background separately. Backgrounds such as those shown

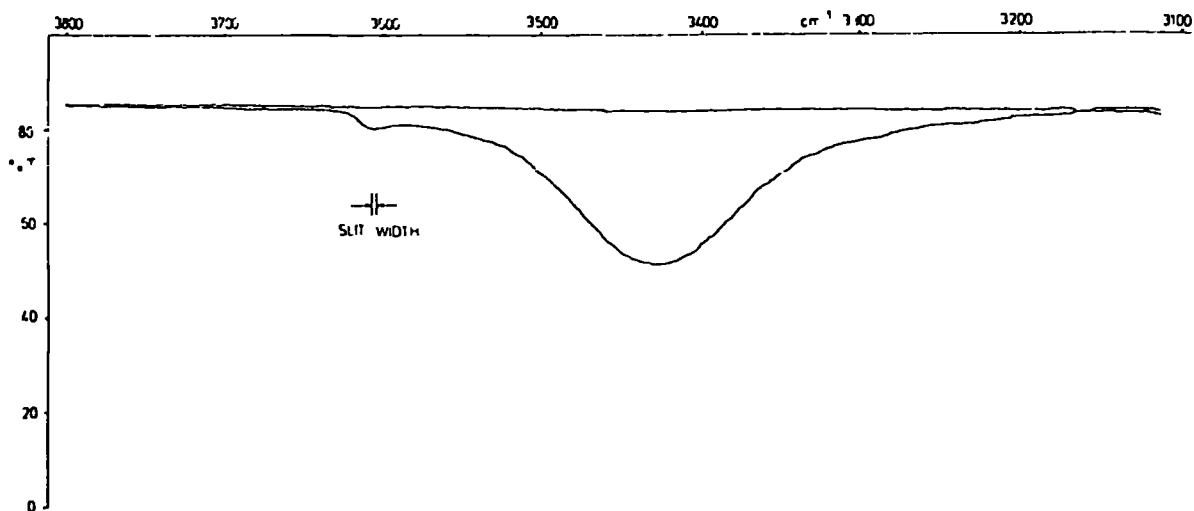


Fig 3 Observed spectrum of phenol(OH)-acetonitrile in  $\text{CCl}_4$  Background real, concentrations  $\text{C}_6\text{H}_5\text{OH}$ , 0.026 M,  $\text{CH}_3\text{CN}$ , 2.51 M Ordinate % transmission, abscissa wavenumber/ $\text{cm}^{-1}$

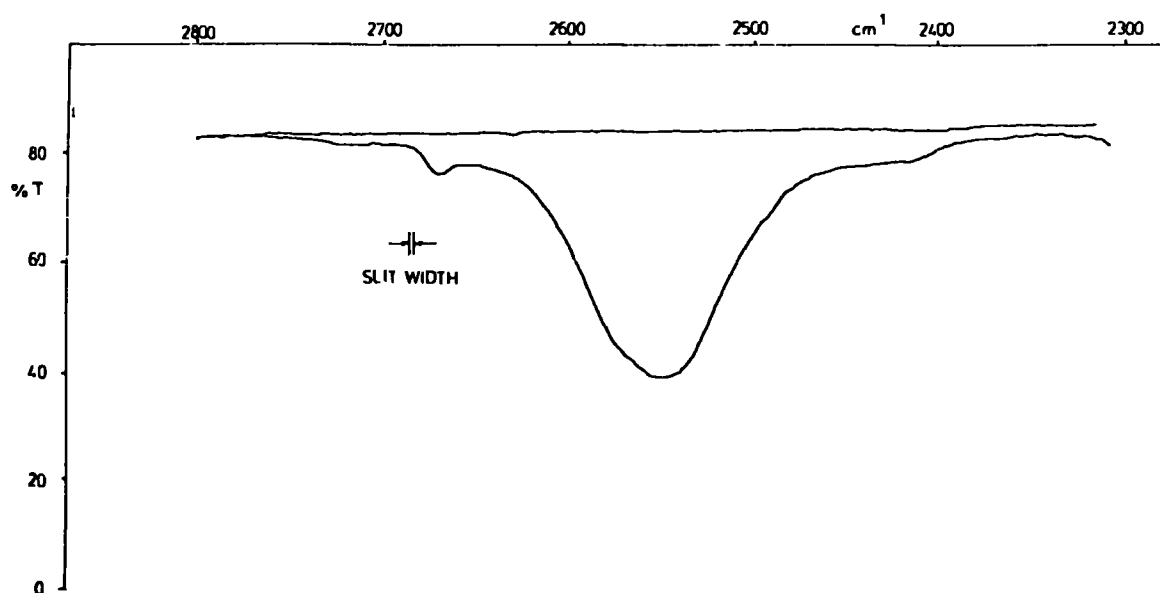


Fig 4 Observed spectrum of phenol(OD)-acetonitrile in  $\text{CCl}_4$  Background real, concentrations  $\text{C}_6\text{H}_5\text{OD}$ ,  $\approx 0.02$  M,  $\text{CH}_3\text{CN}$ , 2.71 M Ordinate % transmission, abscissa wavenumber/ $\text{cm}^{-1}$

in figs 1 to 4 have been obtained using the same reference solution in both beams of the spectrometer. This means that the spectrum and background differ only by the amount of acid present in the sample solution. The procedure avoids the problem of underestimating

the errors of observation in the wings, but leads to even greater difficulty in obtaining a baseline free from slope. Varying signal-to-noise ratio in different regions of the spectrum, absorption by the solvent or base (which affects the instrument response), and dif-



ferent temperature gradients in the sample and background solutions can all affect the baseline. The choice of method represents a compromise: in principle the real backgrounds are to be preferred, but their use is not always feasible. It must be emphasised that the absorbance data obtained by the two methods often differ by statistically significant amounts, particularly in the wings of the spectrum.

All experiments reported in this paper have been performed at ambient beam temperature (313 K). Attempts to study the  $\nu_s(\text{XH})$  spectra of complexes between phenol and organic bases in solution at low temperatures have been unsuccessful, since the solutes freeze out of solution below 240 K. In order to obtain unambiguous information about the temperature dependence of the spectra it is desirable to perform experiments at 160 K or lower, but the number of species which can be studied in solution at these temperatures is severely limited [7]. Furthermore, with conventional double-beam spectrometers it is difficult to maintain the sample and the reference cells at precisely the same low temperature unless special precautions are taken, and this can cause serious imbalances.

### 3 Method of data analysis

The data analysis proceeds in two stages. In the first stage, each spectrum is run ten times under identical conditions, and the mean absorbance and the standard deviation of the mean are calculated at each sampled frequency. In the second stage the bandshape function (1.1), obtained by Fourier transformation of the theoretical autocorrelation function using the Cooley–Tukey algorithm [8], is fitted to the averaged experimental spectrum using Fletcher's modification [9] of Marquardt's non-linear least-squares method [4]. Fortran versions of both algorithms are available in the Harwell Subroutine Library [10]. Each averaged data point is weighted inversely as the square root of its variance, this ensures that the least-squares estimate of the model parameters also represent a maximum likelihood estimate † [11]. The variance–covariance matrix of the parameters is calculated automatically by Fletcher's subroutine, the diagonal elements provide

estimates of the parameter variances, and by normalising the matrix the partial correlation coefficients of the parameter estimates can be obtained. No attempt has been made to calculate confidence regions for the parameters: owing to the appreciable parameter covariances this would be a difficult task.

We have found it convenient to determine the integrated absorbance by numerical integration prior to curve-fitting, and to use  $\omega_1$ ,  $\Delta$ ,  $\omega_2$  and  $\Delta^2\tau_c$  as the four independent parameters needed to specify the bandshape (1.1), where  $\omega_1$  and  $\Delta$  are the angular frequency and amplitude of modulation of the  $\nu_s(\text{XH})$  mode [cf. 1 (3.1)], and  $\omega_2$  and  $\tau_c$  are the angular frequency and characteristic time of the  $\nu_o(\text{XH} \cdots \text{Y})$  mode [cf. 1 (3.2)]. The reason for the choice of  $\Delta$  and  $\Delta^2\tau_c$  as independent parameters, rather than  $\Delta$  and  $\tau_c$  itself, is as follows. The short-time behaviour of the transition dipole autocorrelation function 1 (2.26) is

$$\phi(t) = \exp\left(-\frac{1}{2}\Delta^2 t^2\right), \quad (3.1)$$

so that the profile of the band in the wings is largely determined by  $\Delta$ , whereas the asymptotic form of the autocorrelation function is

$$\phi(t) \approx C \exp(-\Delta^2\tau_c t), \quad (3.2)$$

where

$$C = \exp\left[(\omega_2^2\tau_c^2 - 1)\Delta^2/\omega_2^2\right], \quad (3.3)$$

so that the band profile near its maximum is largely determined by  $\Delta^2\tau_c$ . It follows that the two parameters  $\Delta$  and  $\Delta^2\tau_c$  are relatively easy to separate, in the sense that the partial correlation coefficients of their estimated values are low. The  $\nu_s(\text{XH})$  angular frequency  $\omega_1$  on which the band is centred can be obtained with great accuracy and is not strongly correlated with other parameter estimates. The  $\nu_o(\text{XH} \cdots \text{Y})$  angular frequency  $\omega_2$  is more difficult to determine accurately, however, and tends to have a fairly high partial correlation coefficient with  $\Delta$ . The reason for this is plain. The short-time form of  $\phi(t)$  is independent of  $\omega_2$ , and the asymptotic form depends on  $\omega_2$  only through the constant  $C$  of (3.3), thus Fourier components of  $\omega_2$  can only be discerned in  $\phi(t)$  at intermediate times.

In view of the experimental difficulties encountered in determining the background (cf. section 2), it is important to check that the baseline is accurately horizontal. This can be done immediately after curve-fitting

† Strictly speaking this is only true if the data points are uncorrelated. We have assumed this to be the case.

by performing a linear regression of the residuals (i.e. the differences between the observed and fitted absorbances) on the sampled frequencies. If the gradient of this regression line differs from zero by more than two standard deviations the background slope must be regarded as significant, and a correction is indicated.

The correction is applied by subtracting a linear slope from the experimental spectrum during curve fitting. Two extra parameters are needed, and constraints are imposed on these to ensure that the corrected spectrum remains everywhere positive. The adequacy of the background correction is checked afterwards by linear regression of the residuals on the sampled frequencies. This procedure seems to be reasonably satisfactory in practice; its major disadvantage is that the need to estimate six parameters rather than four leads to increased partial correlations and thus to increased uncertainties. In particular, the partial correlation coefficient of the estimates of  $\omega_2$  and  $\Delta$  is sometimes undesirably high when six parameters are fitted. Thus the baseline correction procedure is best avoided if at all possible; the importance of an accurate experimental determination of the background cannot be overemphasised.

In cases where a baseline correction is essential, many of the above difficulties can be circumvented if an independent estimate of  $\omega_2$  is available. The number of parameters is reduced to five, and their estimates generally show no strong partial correlations. This method can give acceptable results with experimental data of relatively poor quality; the other methods all impose much more stringent requirements.

Although the experiments are performed with a large excess of base, in each case a relatively narrow absorption band due to uncomplexed phenol is visible near  $3610\text{ cm}^{-1}$  (or  $2670\text{ cm}^{-1}$  in the case of the deuterated analogue), and this overlaps the broad  $\nu_s(\text{XH})$  band of the complex (cf. figs 1–4). The problem is dealt with during the curve-fitting by zero-weighting the region of the spectrum which is subject to interference. However, the extraneous absorption band results in the estimate of the integrated absorbance being too high. Similarly, if a background slope correction is needed, the integrated absorbance must also be corrected. It is thus necessary to perform a multiple fitting procedure: after the first fitting cycle the integrated absorbance is recalculated by determining the area under the acceptable portion of the experi-

mental spectrum and adding to it the area under the fitted curve for the rejected (zero-weighted) region. If a background slope correction is attempted, a linear slope is subtracted from both the experimental and fitted spectrum before recalculating the integrated absorbance. The procedure is then repeated until the changes in the parameters determined in successive cycles are all less than one-half of their respective standard deviations. Self-consistency is usually achieved in three or four cycles.

We have also developed a version of our analytical programme which obtains the integrated absorbance by treating it as an extra parameter to be determined during the curve-fitting procedure instead of by numerical integration prior to the procedure. This is not entirely satisfactory: in general the need to determine an extra least-squares parameter leads to increased partial correlation of the other parameter estimates, particularly  $\omega_2$  and  $\Delta$ . The uncertainties are thus increased without anything definite being gained. However, the estimates of the integrated absorbance obtained in this way are in good agreement with those obtained by direct numerical integration.

#### 4 Analysis of experimental spectral profiles

The averaged experimental spectrum of PhOD-dioxan in  $\text{CCl}_4$  is shown in fig. 5 (continuous curve), the fitted spectrum is marked by crosses at intervals of  $10\text{ cm}^{-1}$ . A real background has been used (i.e. the sample and background transmission were determined separately) and a background slope correction has been applied. The data have been zero-weighted beyond  $2650\text{ cm}^{-1}$  to eliminate interferences.

The parameter estimates are

$$\bar{\nu}_1 \text{ (i.e. } \omega_1/2\pi c) = 2511.8 \pm 0.2\text{ cm}^{-1},$$

$$\bar{\nu}_2 \text{ (i.e. } \omega_2/2\pi c) = 148 \pm 2\text{ cm}^{-1},$$

$$\Delta = 14.73 \pm 0.08 \times 10^{12}\text{ s}^{-1},$$

$$\text{i.e. } \Delta/2\pi c = 78.2 \pm 0.4\text{ cm}^{-1},$$

and

$$\Delta^2\tau_c = 6.80 \pm 0.04 \times 10^{12}\text{ s}^{-1}$$

It follows that the dipole moment relaxation time  $\tau_r = 0.147 \pm 0.001\text{ ps}$ , the  $\nu_o(\text{XH} \cdots \text{Y})$  characteristic time  $\tau_c = 0.031 \pm 0.001\text{ ps}$ , and the  $\nu_s(\text{XH})$  damping

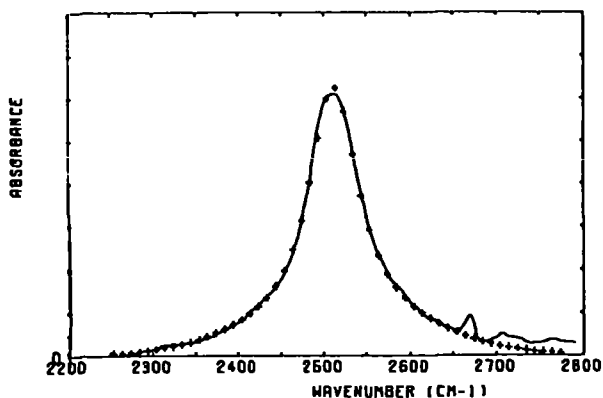


Fig 5 Observed (continuous) and fitted (crosses) spectra of phenol(OD)-dioxan in  $\text{CCl}_4$ . Background real, variance ratio 1.02

constant  $\gamma = (24.2 \pm 0.5) \times 10^{12} \text{ s}^{-1}$ . The dimensionless quantity  $\tau_c \Delta$ , used by Kubo [12] as a criterion for the validity of the slow or rapid modulation limiting approximations, is estimated to be 0.46. Clearly, neither limiting approximation is satisfactory, and the absorption band is subject to partial (but not extreme) motional narrowing. The width  $\bar{\nu}_{1/2}$  of the band at half height is about  $79 \text{ cm}^{-1}$ , so that  $2\pi c \bar{\nu}_{1/2} / \Delta$  is close to unity, in the slow modulation limit this ratio should have a value of  $(8 \ln 2)^{1/2}$  or 2.35. It is also interesting to observe that the parameter  $q = \gamma / 2\omega_2$  has a value of 0.44, showing that the  $\nu_o(\text{XH} \cdots \text{Y})$  oscillation is relatively heavily damped in solution, critical damping (i.e. aperiodic motion) would correspond to  $q = 1$ .

It is clear from fig 5 that the theoretical intensity expression allows the experimental spectrum to be fitted quite successfully. In order to make this more precise we test the null hypothesis that the theory gives a complete account of the experimental measurements and that any discrepancies are due to errors of observation. We calculate the statistic

$$R = \sum_{i=1}^N [y_i - f_i(P)]^2 / \sigma_i^2, \quad (4.1)$$

where  $y_i$  is the  $i$ th mean absorbance, with variance  $\sigma_i^2$ , and  $f_i(P)$  is the corresponding fitted absorbance. The total number of independent observations is  $N$  and the number of parameters  $P$  to be fitted is  $p$ . The er-

rors are assumed to be normally distributed and statistically independent.

According to standard theory [13], the statistic  $R$  of (4.1) is distributed as  $\chi^2$  with  $N - p$  degrees of freedom. The probability of a value of this statistic at least as great as the observed value being encountered can readily be calculated.

A somewhat cruder test is to examine  $R/(N - p)$ . This represents a ratio of two estimates of the data variance, viz. the "internal" variance (calculated from the sum of squared residuals assuming the null hypothesis to hold good) and the "external" variance, which is known. Too great a departure of this ratio from unity indicates that the null hypothesis must be rejected. It must be borne in mind, however, that these tests assume the  $\sigma_i$  to be exactly known, but that these are systematically underestimated when drawn in backgrounds are used. In the case of PhOD-dioxan in  $\text{CCl}_4$  the variance ratio  $R/(N - p)$  is found to be 1.02, and the probability of the weighted sum of squared residuals  $R$  being exceeded is 0.4. This is entirely consistent with the null hypothesis: there is no evidence at all to suppose that the model fails to account for the experimental data.

Other cases are less conclusive. The experimental and fitted spectra of PhOH-dioxan in  $\text{CCl}_4$  are shown in fig 6, a real background has been used and the data have been zero-weighted between  $3580$  and  $3620 \text{ cm}^{-1}$  to remove the free phenol absorption. There is a small,

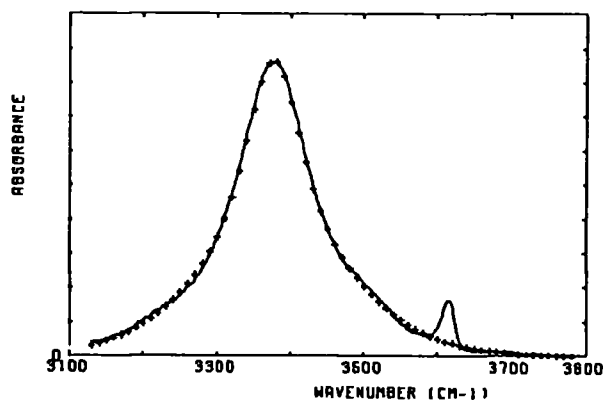


Fig 6 Observed and fitted spectra of phenol(OH)-dioxan in  $\text{CCl}_4$ . Background real, variance ratio 12.9. A strong dioxan absorption at the low-frequency end of the spectrum makes the background difficult to determine accurately.

Table 1  
Summary of parameter estimates a)

Acid	Base	Solvent	Acid conc (M)	Base conc (M)	Back ground	Slope correction	$\bar{\nu}_1$ (cm <sup>-1</sup> )	$\bar{\nu}_2$ (cm <sup>-1</sup> )	$\Delta$ (ps <sup>-1</sup> )	$\tau_c \Delta^2$ (ps <sup>-1</sup> )	Variance ratio
PhOH	C <sub>4</sub> H <sub>8</sub> O <sub>2</sub>	CCl <sub>4</sub>	0.025	1.3	real	no	3376.6 ± 0.2	154 ± 2	19.0 ± 0.6	10.2 ± 1.0	12.9
PhOD	C <sub>4</sub> H <sub>8</sub> O <sub>2</sub>	CCl <sub>4</sub>	0.025	1.3	real	yes	2511.8 ± 0.2	148 ± 2	14.7 ± 0.7	6.8 ± 0.4	1.02
PhOH	CH <sub>3</sub> CN	CCl <sub>4</sub>	0.025	2.5	drawn	no	3424.1 ± 0.3	133 ± 5	14.1 ± 0.9	11.3 ± 0.3	19.2
PhOD	CH <sub>3</sub> CN	CCl <sub>4</sub>	0.025	2.5	drawn	yes	2546.1 ± 0.3	133	10.4 ± 0.7	6.6 ± 0.1	17.8
PhOH	CH <sub>3</sub> CN	CDCl <sub>3</sub>	0.025	2.5	real	yes	3415.2 ± 0.2	127 ± 9	15.1 ± 0.2	16.1 ± 0.5	5.5

a) Temperature 313 K

but significant, background slope, no correction has been applied, however. The internal-external variance ratio is 12.9, and the probability of obtaining such a large value as a result of random errors is negligibly small, clearly the theory is not in complete agreement with experiment in this case, despite the apparently good fit (cf fig. 6). The estimated parameters are given in table 1.

In figs. 7 and 8 the spectra of PhOH-acetonitrile and of PhOD-acetonitrile in CCl<sub>4</sub> are shown. Drawn-in backgrounds have been used in both cases, as the slopes of the real backgrounds were found to be excessive, particularly in the case of the deuterated species. In fig. 7 the data have been zero-weighted between

3580 and 3620 cm<sup>-1</sup> and no background correction has been applied, although the slope is just significant. The variance ratio is 19.2, this estimate is certainly too high, since the data variances are considerably underestimated when a drawn-in background is used<sup>‡</sup>. In the case of PhOD it is necessary to zero-weight the data in three ranges in order to eliminate interferences viz. between 2390 and 2440 cm<sup>-1</sup>, between 2570 and

<sup>‡</sup> A similar analysis has been performed using a corrected real background, and the variance ratio is found to be 5.0. However, the estimates of  $\bar{\nu}_2$  and  $\Delta$  are strongly correlated, and are higher than those quoted in table 1 by statistically significant amounts.

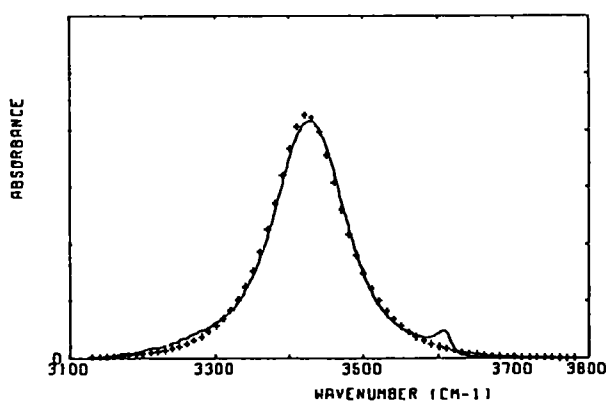


Fig. 7 Observed and fitted spectra of phenol(OH)-acetonitrile in CCl<sub>4</sub>. Background drawn, variance ratio 19.2. The estimates of the data variances in the wings of the spectrum are too low.

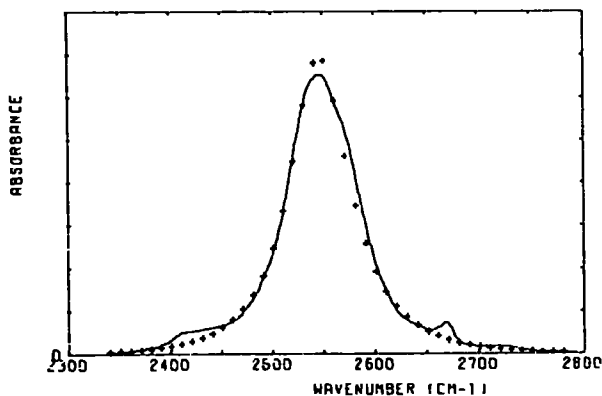


Fig. 8 Observed and fitted spectra of phenol(OD)-acetonitrile in CCl<sub>4</sub>. Background drawn, a value of  $\bar{\nu}_2 = 133$  cm<sup>-1</sup> has been assumed, variance ratio 17.8. The estimated data variances in the wings are too low, and there are obvious interferences.

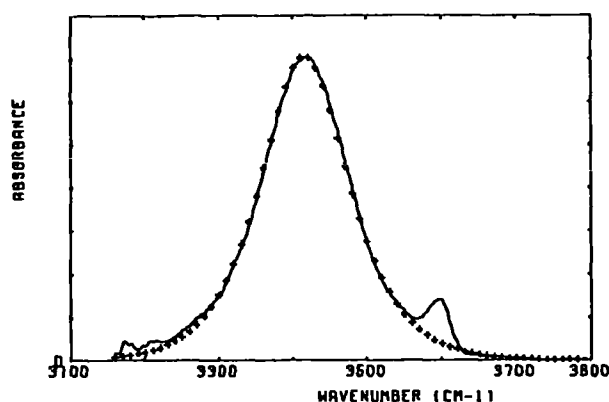


Fig 9 Observed and fitted spectra of phenol(OH)-acetonitrile in  $\text{CDCl}_3$ . Background real, variance ratio 5.5

$2590\text{ cm}^{-1}$ , and between  $2655$  and  $2685\text{ cm}^{-1}$ . A correction must also be applied to eliminate a large background slope. Attempts to determine  $\Delta$  and  $\bar{\nu}_2$  simultaneously have been unsuccessful, and the fitted curve of fig 8 has been obtained by assuming a value of  $133\text{ cm}^{-1}$  for  $\bar{\nu}_2$  and estimating the other parameters. The variance ratio is 17.8, again, this is likely to be too high as a result of underestimated data variances.

In fig 9 the spectrum of PhOH-acetonitrile in  $\text{CDCl}_3$  is shown, the data have been zero-weighted between  $3580$  and  $3620\text{ cm}^{-1}$ , and a correction has been applied to the slope of the real background. The variance ratio is 5.5, again, despite the apparently good fit, this provides evidence that the model is inadequate, or that the data are subject to systematic errors, or both.

### 5 The effect of isotopic substitution on vibrational relaxation

The effect of deuterium substitution on the parameters which characterise the  $\nu_o(\text{XH} \cdots \text{Y})$  or  $\nu_o(\text{XD} \cdots \text{Y})$  relaxation should be small, since the reduced mass  $m_2$  of I (2.3) changes but little. On the other hand the reduced mass  $m_1$  will be nearly doubled, and the  $\nu_s(\text{XH})$  frequency will be reduced by nearly  $2^{-1/2}$ . Owing to cross terms in the displacement coordinates occurring in the interatomic potential function these relations are only approximate; however, the product  $m_1 \omega_1^2$  should remain unaffected by deuterium substi-

tion provided that the potential energy function is a quadratic form. Subject to the same proviso, the product  $m_2 \omega_2^2$  should also be unaffected, and since deuterium substitution should have only a marginal effect on  $m_2$ , one would not expect a large change in  $\omega_2$  unless anharmonic effects are important.

The parameters  $\bar{\nu}_2$ ,  $\tau_c$ , and  $\gamma$  should thus be essentially unchanged by deuterium substitution. However, owing to the invariance of  $\langle r_2^2 \rangle^{1/2}$ ,  $K_{112}$ , and  $m_1 \omega_1^2$  under deuteration, the amplitude of modulation  $\Delta$ , given by

$$\Delta = K_{112} \langle r_2^2 \rangle^{1/2} / m_1 \omega_1, \quad (5.1)$$

(cf I (3.1) and I (2.17)), should obey the relation

$$\Delta(\text{H})/\Delta(\text{D}) = \omega_1(\text{H})/\omega_1(\text{D}) \quad (5.2)$$

The relaxation time  $\tau_r$  of the dipole transition moment, given by  $\tau_r = (\Delta^2 \tau_c)^{-1}$ , should obey the relation

$$\tau_r(\text{H})/\tau_r(\text{D}) = \Delta^2(\text{D})/\Delta^2(\text{H}) = [\omega_1(\text{D})/\omega_1(\text{H})]^2, \quad (5.3)$$

and the Kubo parameter  $\tau_c \Delta = (\tau_c/\tau_r)^{1/2}$  should vary as  $\Delta$  itself, i.e. in accordance with (5.2).

The effect of isotopic substitution on the vibrational relaxation of phenol-dioxan and phenol-acetonitrile in  $\text{CCl}_4$  is summarised in tables 2, 3 and 4. The  $\omega_1(\text{H})/\omega_1(\text{D})$  ratios given in table 2 are known to four significant figures, and can be regarded to all intents and purposes as exactly known quantities. In the case of phenol-acetonitrile neither the  $\Delta(\text{H})/\Delta(\text{D})$  nor the  $\tau_c \Delta^2(\text{H})/\tau_c \Delta^2(\text{D})$  ratio differs significantly (i.e. by more than two standard deviations) from its theoretical value. In the case of phenol-dioxan the  $\Delta(\text{H})/\Delta(\text{D})$  ratio differs from its theoretical value by a small but significant amount, and the  $\tau_c \Delta^2(\text{H})/\tau_c \Delta^2(\text{D})$  ratio is probably too low.

The difference between the estimates of  $\bar{\nu}_2$  for PhOH-dioxan and PhOD-dioxan is not significant at the 95% confidence level. However, systematic far-infrared studies of hydrogen-bonded systems in solution have established that small downward  $\nu_o(\text{XH} \cdots \text{Y})$  frequency shifts on deuteration are common, and that the effect can be ascribed to anharmonicity [14]. It is entirely possible that such an effect occurs in phenol-dioxan, despite the lack of significance of the present experimental results.

The derived parameters  $\tau_c$ ,  $\gamma$ ,  $\gamma/2\omega_2$ ,  $\tau_r$  and  $\tau_c \Delta$  are compared in table 3, the first three of these should be unaffected by deuteration (assuming  $\bar{\nu}_2$  to be un-

Table 2  
The effect of deuteration on the estimated parameters <sup>a)</sup>

Acid	Base	$\bar{\nu}_1$ (cm <sup>-1</sup> )	$\frac{\nu_1(\text{H})}{\nu_1(\text{D})}$	$\Delta$ (ps <sup>-1</sup> )	$\frac{\Delta(\text{H})}{\Delta(\text{D})}$	$\tau_c \Delta^2$ (ps <sup>-1</sup> )	$\left(\frac{\tau_c \Delta^2(\text{H})}{\tau_c \Delta^2(\text{D})}\right)^{1/2}$
PhOH	C <sub>4</sub> H <sub>8</sub> O <sub>2</sub>	3376.6 ± 0.2	1.3443	19.0 ± 0.1		10.2 ± 1.0	
PhOD	C <sub>4</sub> H <sub>8</sub> O <sub>2</sub>	2511.8 ± 0.2	± 0.0002	14.7 ± 0.1	1.29 ± 0.01	6.8 ± 0.4	1.23 ± 0.07
PhOH	CH <sub>3</sub> CN	3424.1 ± 0.3	1.3448	14.1 ± 0.1		11.3 ± 0.3	
PhOD	CH <sub>3</sub> CN	2546.1 ± 0.3	± 0.0002	10.4 ± 0.1	1.36 ± 0.01	6.6 ± 0.1	1.31 ± 0.02

<sup>a)</sup> Temperature 313 K. Solvent CCl<sub>4</sub>. Concentrations of acid and bases in table 1

Table 3  
The effect of deuteration on the derived parameters

Acid	Base	$\tau_c$ (ps)	$\gamma$ (ps <sup>-1</sup> )	$\gamma/2\omega_2$	$\tau_1$ (ps)	$\tau_c \Delta$
PhOH	C <sub>4</sub> H <sub>8</sub> O <sub>2</sub>	0.028 ± 0.001	23.9 ± 0.4	0.41 ± 0.01	0.098 ± 0.001	0.54 ± 0.01
PhOD	C <sub>4</sub> H <sub>8</sub> O <sub>2</sub>	0.031 ± 0.001	24.2 ± 0.5	0.44 ± 0.01	0.147 ± 0.001	0.46 ± 0.01
PhOH	CH <sub>3</sub> CN	0.057 ± 0.002	35.7 ± 2.3	0.71 ± 0.04	0.089 ± 0.003	0.80 ± 0.03
PhOD	CH <sub>3</sub> CN	0.061 ± 0.002	38.4 ± 0.8	0.77 ± 0.02	0.151 ± 0.003	0.64 ± 0.02

changed) whereas the fourth and fifth should vary as  $\omega_1^{-2}$  and  $\omega_1$  respectively. In every case the changes in  $\tau_c$ ,  $\gamma$  and  $\gamma/2\omega_2$  are within experimental error. The table shows clearly, however, that the  $\nu_s(\text{XH})$  transition dipole moment relaxation time  $\tau_1$  is increased on deuteration, owing to the reduced coupling between the vibrational modes, while the Kubo parameter  $\tau_c \Delta$  is reduced. Evidently motional narrowing is somewhat more pronounced in the deuterated species, which is observed in each case to have a narrower spectral profile than the corresponding protium species. Both the reduction in the second central moment (i.e.  $\Delta^2$ ) and

the increase in kurtosis affect the appearance of the band.

This change in the shape of the spectrum on deuteration is illustrated in table 4, where the widths of the bands at half height are compared. The ratios of the half-widths of the protium and deuterium species are 1.61 ± 0.05 for phenol-dioxan and 1.55 ± 0.05 for phenol-acetonitrile, both values being considerably greater than the corresponding amplitude of modulation ratios, which are estimated to be 1.29 ± 0.01 and 1.36 ± 0.01 respectively (and which have theoretical values of 1.345 and 1.344). This is entirely consistent

Table 4  
The effect of deuteration on half widths  $\bar{\nu}_{1/2}$  and amplitudes of modulation  $\Delta$

Acid	Base	$\tau_c \Delta$	$\bar{\nu}_{1/2}$ (cm <sup>-1</sup> )	$\frac{\nu_{1/2}(\text{H})}{\nu_{1/2}(\text{D})}$	$(2\pi c)^{-1} \Delta$ (cm <sup>-1</sup> )	$\frac{\Delta(\text{H})}{\Delta(\text{D})}$	$\frac{\nu_1(\text{H})}{\nu_1(\text{D})}$	$\left(\frac{\nu_1(\text{H})}{\nu_1(\text{D})}\right)^2$
PhOH	C <sub>4</sub> H <sub>8</sub> O <sub>2</sub>	0.54	127		100.7 ± 0.4			
PhOD	C <sub>4</sub> H <sub>8</sub> O <sub>2</sub>	0.46	79	1.61	78.2 ± 0.4	1.29 ± 0.01	1.344	1.807
PhOH	CH <sub>3</sub> CN	0.80	116		74.6 ± 0.5			
PhOD	CH <sub>3</sub> CN	0.64	75	1.55	55.2 ± 0.4	1.36 ± 0.01	1.345	1.809

with the value of the Kubo parameter  $\tau_c \Delta$  being smaller for the deuterated species in each case, indicating a more pronounced deviation of the spectrum from a gaussian ( $\tau_c \Delta \gg 1$ ) profile

## 6 Solvent effects

The spectra of phenol-acetonitrile in solution in  $\text{CCl}_4$  and  $\text{CDCl}_3$  are shown in figs 7 and 9. The widths at half height are  $116 \text{ cm}^{-1}$  and  $148 \text{ cm}^{-1}$  respectively, a difference of 28%. The parameters derived by curve fitting are given in table 1.

The downward shift in  $\bar{\nu}_1$  from  $3424.1 \text{ cm}^{-1}$  to  $3415.2 \text{ cm}^{-1}$  on changing to a more polar solvent is highly significant statistically even though it represents a decrease of only 0.3%. Two main explanations may be adduced: (1) that there is a specific interaction between the solvent molecules and the complex, leading to a strengthening of the hydrogen bond in the more polar solvent [15], or (2) that the structure of the complex is largely unaffected by the solvent, but the increased dielectric constant of the medium increases the reaction field acting on the complex, depressing the self-energy of the  $\nu = 0$  and  $\nu = 1$  vibrational states by different amounts [16,17]. Associated with each of these possible level shift mechanisms is a possible broadening mechanism. A strengthening of the hydrogen bond may be expected to increase the anharmonic coupling constant  $K_{112}$  and to reduce the  $K_{11}$  force constant, both of which would tend to increase the amplitude of modulation parameter  $\Delta$ . On the other hand, in a more polar solvent the variance of the random force acting on the hydrogen bond stretching vibration would be greater, and hence the damping constant  $\gamma$  of 1 (2.5) would be increased. This would result in a broadening of the band even if  $\Delta$  remained constant (except in the extreme slow modulation regime).

In view of the spectacular increase observed in the half-width of the  $\nu_s(\text{XH})$  absorption band on changing to a more polar solvent it is of considerable interest to examine whether the analysis of vibrational relaxation provides any evidence for the structure of the complex being changed by solvent effects. Broadly speaking, the parameters  $\bar{\nu}_2$  and  $\Delta$  are characteristic of the complex itself, whereas  $\tau_c \Delta^2$ , involving the characteristic time of the  $\nu_o(\text{XH} \cdots \text{Y})$  oscillatory sto-

chastic process, measures the interaction of the complex with the surrounding medium.

The estimated values of  $\bar{\nu}_2$  given in table 1 are  $133 \pm 5 \text{ cm}^{-1}$  and  $127 \pm 9 \text{ cm}^{-1}$  for phenol-acetonitrile in  $\text{CCl}_4$  and  $\text{CDCl}_3$  respectively, the difference is not statistically significant and provides no evidence that the  $\nu_o(\text{XH} \cdots \text{Y})$  force constant is affected by the solvent. The standard deviations are rather large, however, and too much importance should not be attached to the lack of significance.

It is dangerous to conclude solely on the basis of table 1 that the difference in  $\Delta$  is significant, since the estimates of  $\Delta$  and  $\bar{\nu}_2$  are quite strongly correlated, having partial correlation coefficients of nearly 0.9 in each case. Strictly speaking one cannot define a confidence interval for  $\Delta$  on the basis of these results, but only a confidence region involving both  $\Delta$  and  $\bar{\nu}_2$  (the small partial correlation coefficients involving the other two parameters being regarded as negligible). Furthermore, different methods were used for obtaining the backgrounds, which may have introduced systematic errors. In order to test the null hypothesis that the structure of the complex is unaffected by the change of solvent we reanalyse the spectra of phenol-acetonitrile in  $\text{CCl}_4$  and  $\text{CDCl}_3$ , supposing that the value of  $\bar{\nu}_2$  is known to be the same for each. We assume this value to be  $\bar{\nu}_2 = 133 \text{ cm}^{-1}$ .

The results of the analysis are given in table 5: the three independent parameters estimated by curve fitting are  $\bar{\nu}_1$ ,  $\Delta$  and  $\tau_c \Delta^2$ , while the remaining parameters characterising the relaxation are derived from these and from  $\bar{\nu}_2$ . The difference between the estimates of  $\Delta$  is  $0.9 \times 10^{12} \text{ s}^{-1}$  and the standard deviation of the difference is  $0.1 \times 10^{12} \text{ s}^{-1}$ , the difference is highly significant, so that one cannot exclude the possibility of the structure of the complex being affected by the solvent<sup>†</sup>. However, the  $\nu_s(\text{XH})$  amplitude of modulation is estimated to be only 6% greater.

<sup>†</sup> The alternative is that systematic errors are present because the backgrounds were determined in different ways. Using real backgrounds in both cases we find values of  $\Delta$  which differ insignificantly and variance ratios of about five for both fittings. However, we have reason to believe that the real background version of phenol-acetonitrile in  $\text{CCl}_4$  is unreliable, since the estimate of  $\Delta^2$  is appreciably greater than the second central moment of the band as determined by direct numerical integration. In the circumstances we are unable to draw very precise conclusions.

Table 5  
Solvent effects on PhOH-CH<sub>3</sub>CN spectrum a)

Solvent	PhOH conc (M)	CH <sub>3</sub> CN conc (M)	Back-ground	$\bar{\nu}_{1/2}$ (cm <sup>-1</sup> )	$\bar{\nu}_1$ (cm <sup>-1</sup> )	$\Delta$ (ps <sup>-1</sup> )	$\tau_c \Delta^2$ (ps <sup>-1</sup> )	$\tau_c$ (ps)	$\gamma$ (ps <sup>-1</sup> )	$\tau_c \Delta$	Variance ratio
CDCl <sub>3</sub>	0.025	2.5	real	148	3415.3 ± 0.2	15.1 ± 0.1	16.3 ± 0.3	0.072 ± 0.001	45.0 ± 0.9	1.08 ± 0.02	5.4
CCl <sub>4</sub>	0.025	2.5	drawn	116	3423.9 ± 0.3	14.2 ± 0.1	11.1 ± 0.3	0.055 ± 0.001	34.7 ± 0.8	0.78 ± 0.02	18.0
CCl <sub>4</sub>	0.025	2.5	real	116	3425.0 ± 0.2	14.9 ± 0.1	10.1 ± 0.2	0.046 ± 0.001	28.6 ± 0.4	0.68 ± 0.01	5.0

a) Temperature 313 K. The value of  $\bar{\nu}_2$  is assumed to be 133 cm<sup>-1</sup>. The real background version of PhOH-CH<sub>3</sub>CN in CCl<sub>4</sub> is suspect

in CDCl<sub>3</sub> than in CCl<sub>4</sub>, whereas the half-width of the band is 28% greater, so that any possible increase in strength of the hydrogen bond in the polar solvent can only account for a relatively small part of the increased breadth. By far the greater part can be attributed to the increase in the characteristic time,  $\tau_c$ , of the  $\nu_o(\text{XH} \cdots \text{Y})$  vibration, which is 0.055 ps in CCl<sub>4</sub> and 0.072 ps in CDCl<sub>3</sub>, the corresponding figures for  $\tau_c \Delta$  are 0.78 and 1.08.

The mechanism responsible for the altered profile is easily understood. The mean-square value of the random force acting on the hydrogen bond is greater in the more polar solvent, so that the damping constant  $\gamma$  is greater. This results in the autocorrelation function  $\langle r_2(t) r_2(0) \rangle / \langle r_2^2 \rangle$  of 1 (2.22) decaying more rapidly, the more rapid the decay the less cancellation there is in the oscillatory integrand of 1 (3.2), and the characteristic time of the modulation increases. The Kubo parameter  $\tau_c \Delta$  is thus increased, and the absorption band becomes more nearly gaussian in shape. The band thus appears much broader (being broader at half peak height) even though its second central moment is little changed. The apparent increase in breadth is simply due to a decrease in kurtosis.

It should be noted, however, that the viscosity of CDCl<sub>3</sub> is appreciably less than that of CCl<sub>4</sub> (0.46 and 0.74 cp, respectively, at 40°C). This shows immediately that the macroscopic viscosity of the solvent bears no close relationship to the dissipative term in the Langevin equation for the  $\nu_o(\text{XH} \cdots \text{Y})$  vibration.

The comparison of phenol-acetonitrile in CCl<sub>4</sub> and CDCl<sub>3</sub> was undertaken with a phenol concentration of 0.025 M and an acetonitrile concentration of 2.5 M in each case. We have also studied the effect of varying the concentration of excess acetonitrile from 0.1 M to 3.5 M. As the acetonitrile concentration increases there is a progressive shift of  $\bar{\nu}_1$  towards lower frequencies and a broadening of the absorption band. The estimated values of  $\tau_c$  increase systematically, but there is no evidence of any systematic trend in  $\Delta$  or  $\bar{\nu}_2$ . Again, the changes in the breadth of the band must be interpreted in terms of changes in the speed of modulation: as  $\tau_c \Delta$  increases the kurtosis of the band is reduced and it appears broader, despite the constancy of the second central moment  $\Delta^2$ . We have not yet repeated these experiments a sufficient number of times to give acceptable statistics, and do not give detailed results here.



## 7 Summary and conclusions

The most decisive result of this paper is the analysis of the PhOD-dioxan spectrum. Both chi-squared and internal-external variance ratio tests show that the theoretical result established in I provides a complete account of the  $\nu_s(\text{XH})$  absorption band profile, and that the discrepancies between the experimental and the fitted spectra can be entirely attributed to errors of observation.

This provides the strongest possible evidence that the bandshape is determined by the phase relaxation of the  $\nu_s(\text{XH})$  vibration, that this relaxation takes place mainly through anharmonic coupling of  $\nu_s(\text{XH})$  and  $\nu_o(\text{XH-Y})$  modes, as suggested originally by Bratos [3], and that the  $\nu_o(\text{XH-Y})$  relaxation is well described by the Ornstein-Uhlenbeck stochastic process. The model of the  $\nu_s(\text{XH})$  phase relaxation invokes the adiabatic approximation, its success in reproducing experimental spectra accurately demonstrates that  $\nu_s(\text{XH})$  energy relaxation must be a considerably slower process. The distinction between phase and energy relaxation of vibrational modes in liquids has been stressed by Laubereau, von der Linde and Kaiser [18].

The rotational diffusion performed by the hydrogen bonded species in solution appears to have little effect on its  $\nu_s(\text{XH})$  spectral profile [3], in sharp contrast to the case of diatomic or simple polyatomic molecules, where both vibrational and rotational relaxation influence the spectrum [19]. This may seem a surprising finding, but a very convincing explanation has previously been advanced by Bratos: the vibrational relaxation time for a hydrogen-bonded molecule in solution is at least an order of magnitude smaller than the rotational relaxation time, so that the  $\nu_s(\text{XH})$  phase coherence is completely lost during the time taken for the complex to reorient appreciably [3]. The fact that a complete understanding of the spectral profile of this complex can be obtained without considering rotational motion at all confirms the correctness of Bratos' argument, our estimate of 0.15 ps for the vibrational relaxation time lends added support.

In all the other cases examined variance ratio tests indicate that the agreement between experiment and theory is not perfect, this may be due either to systematic errors in the data, particularly where drawn-in backgrounds are used, or to the inadequacy of the model, or to both. It is possible that in these cases

other relaxation mechanisms, including rotational diffusion, have a small effect on the bandshapes which cannot be accounted for by the model. Nevertheless, the fitted curves of figs 6 to 9 are all in reasonably satisfactory agreement with the experimental spectra, showing that vibrational relaxation must be the dominant broadening mechanism.

In every case except one (that of PhOD-acetonitrile, where extra absorptions, possibly due to Fermi resonance, interfere with the main band) it has been possible to obtain a reasonable estimate of the  $\nu_o(\text{XH-Y})$  stretching frequency by analysis of the  $\nu_s(\text{XH})$  bandshape. This provides strong evidence that the  $\nu_s(\text{XH})$  vibration relaxes indirectly, via its coupling to the  $\nu_o(\text{XH-Y})$  mode. (Considering that in every case the  $\nu_o(\text{XH-Y})$  vibration is close to being critically damped, it is remarkable that Fourier components of this frequency can so easily be discerned in the dipole moment autocorrelation function.) It also shows that the  $\nu_s(\text{XH})$  relaxation is sensitive to the dynamics of the stochastic process describing the  $\nu_o(\text{XH-Y})$  oscillation, and not simply to its marginal distribution, as in Bratos' theory [3]. This is confirmed by our estimates of the Kubo parameter  $\tau_c\Delta$ , which lie between 0.5 and 1.1, showing that neither the slow nor the rapid modulation limiting approximations are satisfactory. The absorption bands studied are all subject to partial motional narrowing, and cannot be satisfactorily represented by either a gaussian or a lorentzian function.

Although one cannot be completely confident about the estimates of the parameters characterising the vibrational relaxation in cases where statistical tests indicate a significant lack of fit, these estimates are nevertheless in satisfactory agreement with theoretical expectations. The effect of isotopic substitution, change of solvent and variation in concentration of the excess base have all been studied.

The amplitude of modulation  $\Delta$  and the vibrational relaxation time  $\tau_r$  should in theory be related to the  $\nu_s(\text{XH})$  angular frequency by

$$\Delta(\text{H})/\Delta(\text{D}) = [\tau_r(\text{H})/\tau_r(\text{D})]^{-1/2} = \omega_1(\text{H})/\omega_1(\text{D}), \quad (8.1)$$

this relationship is well satisfied by both the phenol-dioxan and the phenol-acetonitrile species. The small discrepancies can probably be attributed to extra relaxation mechanisms not accounted for by the model, and to the fact that the theoretical relation

ship is only strictly valid for a potential function which is a quadratic form in the displacement coordinates, whereas the hydrogen-bonding potential is known to be appreciably anharmonic.

The reduction in the Kubo parameter  $\tau_c \Delta$  on deuteration provides a natural explanation of the apparently anomalous decrease in band half-width on deuteration. Both the decrease in  $\Delta$  (cf. (8.1)) and the increase in kurtosis affect the band profiles. Motional narrowing is more pronounced in the deuterated species because the vibrational relaxation time  $\tau_r$  is longer, this is a consequence of the weakening of the anharmonic coupling between the  $\nu_s(\text{XH})$  and  $\nu_o(\text{XH} \cdot \text{Y})$  modes, an effect which is well understood in the theory of hydrogen-bonded species in the gas phase [20].

The  $\nu_s(\text{XH})$  absorption band of the phenol-acetonitrile complex is 28% broader at half peak height but has a smaller kurtosis in solution in  $\text{CDCl}_3$  than in solution in  $\text{CCl}_4$ . Although the amplitude of modulation  $\Delta$  is estimated to be slightly larger in  $\text{CDCl}_3$  than in  $\text{CCl}_4$ , indicating that the anharmonic coupling between the modes of the complex may be slightly greater in the more polar solvent (so that the complex appears to be "stronger"), there is no doubt that the principal cause of the difference in half-width is a dynamic effect. The Kubo parameter  $\tau_c \Delta$  is 38% greater for the complex in  $\text{CDCl}_3$  than in  $\text{CCl}_4$  owing to the much larger value of  $\tau_c$  in the former solvent. The characteristic time of the  $\nu_o(\text{XH} \cdot \text{Y})$  vibration is greater in the more strongly interacting solvent, because of the oscillatory nature of the stochastic process which represents the motion. On the other hand, the  $\nu_s(\text{XH})$  relaxation time  $\tau_r$  is smaller. Thus, although the second central moment of the band is little changed, motional narrowing is less pronounced and the band half-width is considerably greater for the complex in  $\text{CDCl}_3$  than in  $\text{CCl}_4$ . Increasing the concentration of excess acetonitrile in a solution of phenol-acetonitrile in  $\text{CCl}_4$  also increases the rate of  $\nu_s(\text{XH})$  relaxation, and the effect on the breadth and kurtosis of the absorption band is similar.

One of the most interesting features of this work is that it provides a means of estimating the damping parameter  $\gamma$  occurring in the Langevin equation for the  $\nu_o(\text{XH} \cdot \text{Y})$  motion. The estimates of  $\gamma$  depend on the particular species and on the solvent, but are little affected by deuteration.

It is not possible, however, to interpret the damping constant in terms of the Stokes-Einstein relation, in analogy with the classical theory of the brownian motion.  $\gamma$  does not appear to be directly related to the viscosity of the solvent. However, there are indications that  $\gamma$  increases systematically with increasing polarity of the solvent, which suggests that the hydrogen bond vibration may relax through dipolar coupling with local electric field fluctuations.

Three main difficulties have been encountered in this work. First, a number of the systems we have attempted to study (in particular, certain complexes with pyridine) have  $\nu_s(\text{XH})$  bands which exhibit a fine structure, due probably to Fermi resonance between an infrared active normal mode of the base and the  $\nu_s(\text{XH})$  mode of the complexed acid. Such systems cannot be analysed by the theory given in I. However, one of us (G. N. R.), in collaboration with Professor S. Bratos, has recently extended the theory of I so as to allow for accidental degeneracies, and it is hoped to analyse spectra of these more complicated species later. The new theory is able to explain the origin of narrow transmission windows in the  $\nu_s(\text{XH})$  band without involving the extreme slow modulation approximation, which was the principal shortcoming of Bratos' theory [3].

Secondly, in several cases we have had difficulty in determining the background absorption with sufficient accuracy. In these circumstances the covariance of the estimates of  $\Delta$  and  $\bar{\nu}_2$  is excessively high and the results are unreliable. Attempts to avoid this problem by using drawn-in backgrounds are only partially successful, since they lead to a systematic underestimation of the data variances in the wings of the spectrum and hence to bias in the estimates. In several cases parameters obtained by these two methods differ by statistically significant amounts, and it is sometimes difficult to decide which is more reliable.

In view of these difficulties, our previous claim [2] that analysis of the  $\nu_s(\text{XH})$  bandshape provides a trustworthy means of estimating the  $\nu_o(\text{XH} \cdot \text{Y})$  frequency must be regarded with caution. If in any particular application of the method a  $\chi^2$  test indicates that the fit is satisfactory, and if the parameter covariances are acceptably low, there is no reason to doubt the estimate of  $\bar{\nu}_2$  and its standard deviation. Our analysis of the phenol(OD)-dioxan absorption band is a case in point. However, it seems to be only

in particularly favourable circumstances that one can be completely confident about this method of estimating  $\bar{\nu}_2$ , and if one wishes to extract reliable information about  $\Delta$  and  $\tau_c$  from the bandshape analysis it is preferable to measure  $\bar{\nu}_2$  in an independent experiment and thus to reduce the number of unknown parameters which need to be fitted.

Thirdly, we have been unable to study the temperature dependence of the relaxation parameters, partly through limitations of our apparatus and partly because phenol complexes freeze out of solution below about 240 K. In theory the amplitude of modulation  $\Delta$  should vary as  $[\coth(\hbar\omega_2/kT)]^{1/2}$ , (or as  $T^{1/2}$  when  $kT \gg \hbar\omega_2$ ), in accordance with I (3.1), and it would be desirable to test this relation experimentally. However, it would be of even greater interest to study the temperature dependence of the damping constant  $\gamma$ , as this could be expected to provide information about the nature of the random forces responsible for the relaxation of the  $\nu_o(\text{XH} \cdots \text{Y})$  vibration in solution. Self-associated alcohols in solution in  $\text{CCl}_3\text{F}/\text{C}_2\text{Br}_2\text{F}_4$  mixtures, which have been examined systematically at low temperatures by Asselin and Sandorfy [7], would be particularly suitable for study.

Much work on these problems remains to be done. It would certainly be desirable to repeat many of our experiments using a somewhat more sensitive spectrometer, in the hope of determining the backgrounds more accurately. We intend shortly to do so using a rapid-scanning interferometric spectrometer. It is also important to compare values of  $\bar{\nu}_2$  obtained by analysis of  $\nu_s(\text{XH})$  bandshapes with those obtained by direct measurement. We have been unable so far to record satisfactory far infrared spectra of those species which are most amenable to analysis in the mid infrared region of the spectrum, owing to the strong absorption of the bases (particularly of acetonitrile) between 100 and  $200 \text{ cm}^{-1}$ . New attempts are currently being made to record the far infrared spectrum of phenol-dioxan in  $\text{CCl}_4$ .

Far infrared spectroscopy raises other possibilities. The idea that the  $\nu_o(\text{XH} \cdots \text{Y})$  motion can be represented by the Ornstein-Uhlenbeck stochastic process is basic to this work, and must be regarded as largely vindicated by the results. The spectral density of the Ornstein-Uhlenbeck stochastic process is a known function of its parameter, so that the contribution of vibrational relaxation to the broadening of the far-

infrared  $\nu_o(\text{XH} \cdots \text{Y})$  band can easily be calculated (cf I (5.2)). It would thus be very interesting to analyse  $\nu_o(\text{XH} \cdots \text{Y})$  bandshapes in order to see whether they can be represented in terms of the Ornstein-Uhlenbeck spectral density function, and whether it is possible to obtain estimates of  $\gamma$ , as well as of  $\omega_2$ , which are consistent with those derived from mid infrared spectral analysis.

Inelastic scattering of thermal neutrons may also hold promise for the investigation of proton dynamics in hydrogen-bonded liquids. It is easy to derive an expression for the intermediate scattering function of an Ornstein-Uhlenbeck oscillator and hence to obtain the scattering function  $S(Q, \omega)$ . Indeed, current theories of neutron scattering by liquid metals assume a superposition of Ornstein-Uhlenbeck oscillators with a Debye model frequency distribution [21], the dilute hydrogen-bonded liquid is much simpler to describe. It would be interesting to record  $S(Q, \omega)$  for a hydrogen-bonded species  $\text{XH} \cdots \text{Y}$  (where the base Y is fully deuterated) in an aprotic solvent using a triple axis spectrometer. Analysis of the structure of the spectrum in the 15–20 meV energy gain region, and of the dependence of this structure on momentum transfer, should be able to provide considerable information about the relaxation of the  $\nu_o(\text{XH} \cdots \text{Y})$  mode, which would complement that derived from infrared absorption studies. It is not expected that rotational or translational motions will affect the shape of this structure very much since the correlation time of the  $\nu_o(\text{XH} \cdots \text{Y})$  vibration is of the order of 0.1 ps.

In order to understand the origin of the random forces responsible for the relaxation of the  $\nu_o(\text{XH} \cdots \text{Y})$  vibration it will be necessary to study systematically the factors which influence the damping constant  $\gamma$ . In particular, it would be interesting to investigate the dependence of  $\gamma$  on the masses and electric multipole moments of the XH and Y molecules forming the complex, on the dielectric properties and viscosity of the solvent, on the concentration of the excess base, and on the temperature. Any or all of the techniques discussed above may be able to provide information, though a combination of mid and far infrared spectroscopy would seem to be the most promising.

It would also be interesting to study the  $\nu_s(\text{XH})$  frequency  $\bar{\nu}_1$  as a function of the dielectric properties of the solvent, to see whether any correlations can be discerned between the frequency shifts and the param-

eters which describe the vibrational relaxation. Although the solvent effects on the  $\nu_s(\text{XH})$  bandwidth are largely non-specific (they can be represented in terms of a single relaxation parameter, the damping constant  $\gamma$ ), and although there seems to be systematic tendency for  $\bar{\nu}_1$  to decrease and  $\gamma$  to increase as the concentration of the excess base is increased, it is dangerous to argue without further detailed investigation that the mechanism responsible for the solvent shifts is necessarily non-specific. Either reaction-field effects [16, 17] or specific dipolar interaction of solvent (or excess base) molecules with the complexed phenol oxygen lone pairs, leading to structural changes in the complex [15], could account for the frequency shifts, systematic studies of the interrelation between frequency shifts and broadening through vibrational relaxation may help to resolve this issue.

The temperature dependence of the  $\nu_s(\text{XH})$  frequency may be relatively easy to explain by retaining the quadratic term of I (2.16) in I (2.18) one can derive an expression for the  $\nu_s(\text{XH})$  shift. This turns out, in first approximation, to be proportional to the mean-square amplitude of the hydrogen bond vibration, and hence proportional to the temperature (provided that this is not too low). However, this is a second-order effect in the cubic coupling constant  $K_{112}$ , and quartic coupling terms in the vibrational hamiltonian which contribute in first order may in fact be more important. Experimental studies of the temperature shift and its relation to the temperature dependence of the relaxation parameters would be interesting.

Finally, it should be remarked that a major purpose of studying proton dynamics in hydrogen-bonded species in solution is to obtain fundamental information about water, and eventually about biological processes which occur in aqueous solution. NMR studies of proton spin-lattice and spin-spin relaxation in biological materials are becoming more common. We are currently studying the relaxation of the uncoupled  $\nu(\text{OD})$  vibration of HDO in solution in  $\text{H}_2\text{O}$ . An interesting possibility exists of examining how this relaxation is modified in the presence of biological material. Such studies, if they can be successfully performed, may provide information about relaxation processes occurring in biological material on a sub-picosecond time scale, which would complement information about slower processes derived from NMR measurements.

#### Acknowledgement

We wish to thank Professors S Bratos, C Sandorfy, N Sheppard, F R S and Dr J L Wood for helpful discussions and correspondence. Dr R N Jones and Mr S Marlow kindly made available computer programmes developed by N R C Ottawa and A E R E Harwell respectively. We acknowledge financial support from the Royal Society, the Science Research Council (U K) and the Council for Scientific and Industrial Research (South Africa).

#### References

- [1] G N Robertson and J Yarwood, *Chem Phys* 32 (1978) 267
- [2] J Yarwood and G N Robertson, *Nature* 257 (1975) 41
- [3] S Bratos, *J Chem Phys* 63 (1975) 3499
- [4] D W Marquardt, *J Soc Indust Appl Math* 11 (1963) 431
- [5] J Overend, in *Infrared spectroscopy and molecular structure*, ed M M Davies (Elsevier, Amsterdam, 1963)
- [6] W G Rothschild, *J Chem Phys* 51 (1969) 5187, J Yarwood, *Advan Molec Relaxation Processes* 5 (1973) 375
- [7] M Asselin and C Sandorfy, *Chem Phys Letters* 8 (1971) 601
- [8] J W Tukey and J W Cooley, *Math Comput* 19 (1965) 297
- [9] R Fletcher, A E R E Report No R6799 (H M S O, London, 1974)
- [10] M J Hopper, A E R E Report No R7477 (H M S O, London, 1973)
- [11] O Kempthorne, *The design and analysis of experiments* (Wiley, New York, 1952), A F Mood, *Introduction to the theory of statistics* (McGraw-Hill, New York, 1950)
- [12] R Kubo, in *Fluctuation, relaxation and resonance in magnetic systems*, ed D ter Haar (Oliver and Boyd, Edinburgh, 1962)
- [13] W E Deming, *Statistical adjustment of data* (Wiley, New York, 1943)
- [14] S G W Ginn and J L Wood, *Spectrochim Acta* 23A (1967) 611, D L Cummings and J L Wood, *J Mol Struct* 23 (1974) 103
- [15] J L Bellamy, K J Morgan and R J Pace, *Spectrochim Acta* 22 (1966) 535, 27A (1971) 705
- [16] A D Buckingham, *Proc Roy Soc London* A248 (1958) 169, *Trans Faraday Soc* 56 (1960) 753
- [17] M Horak, J Polakova, M Jakoubkova, J Moravek and J Pliva, *Collect Czech Chem Commun* 31 (1966) 622, 36 (1966) 2757

- [18] A Laubereau, D von der Linde and W Kaiser, *Phys Rev Letters* 26 (1971) 954, 28 (1972) 1162,  
A Laubereau and W Kaiser, *Ann Rev Phys Chem* 26 (1975) 83
- [19] S Bratos, J Rios and Y Guissani, *J Chem Phys* 52 (1970) 439,  
S Bratos, Y Guissani and J-C Leicknam *Molecular motions in liquids*, ed J Lascombe (Reidel, Dordrecht, 1974)
- [20] G N Robertson, *Phil Trans Roy Soc (London)* A286 (1977) 25
- [21] A Rahman, K S Singwi and A Sjolander, *Phys Rev* 126 (1962) 997

APPENDIX 2

The Board of Studies in Chemistry requires that each postgraduate research thesis contain an appendix listing

- (a) all research colloquia, research seminars and lectures (by external speakers) arranged by the Department of Chemistry since 1 October 1976; and
- (b) all research conferences attended and papers read out by the writer of the thesis, during the period when the research for the thesis was carried out.

2.1 Research Colloquia, Seminars and Lectures by External Speakers  
Arranged by the Department of Chemistry of the University of Durham between 1 October 1976 and 30 September 1978.

20 October 1976

Professor J.B. Hyne (University of Calgary), "New Research on an Old Element - Sulphur".

10 November 1976

Dr J.S. Ogden (Southampton University), "The Characterization of High Temperature Species by Matrix Isolation".

17 November 1976

Dr B.E.F. Fender (University of Oxford), "Familiar but Remarkable Inorganic Solids".

24 November 1976

Dr M.I. Page (Huddersfield Polytechnic), "Large and Small Rate Enhancements of Intramolecular Catalysed Reactions".

8 December 1976

Professor A.J. Leadbetter (University of Exeter), "Liquid Crystals".

26 January 1977

Dr A. Davis (E.R.D.R.), "The Weathering of Polymeric Materials".

2 February 1977

Dr M. Falk, (N.R.C. Canada), "Structural Deductions from the Vibrational Spectrum of Water in Condensed Phases".

9 February 1977

Professor R.O.C. Norman (University of York), "Radical Cations; Intermediates in Organic Reactions.

23 February 1977

Dr G. Harris (University of St Andrews), "Halogen Adducts of Phosphines and Arsines".

25 February 1977

Professor H.T. Dieck (Frankfurt University), "Diazadienes - New Powerful Low-Valent Metal Ligands".

2 March 1977

Dr F. Hibbert (Birkbeck College, London), "Fast Reaction Studies of Slow Proton Transfers Involving Nitrogen and Oxygen Acids".

4 March 1977

Dr G. Brink (Rhodes University, South Africa), "Dielectric Studies of Hydrogen Bonding in Alcohols".

9 March 1977

Dr I.O. Sutherland (Sheffield University), "The Stevens' Rearrangement: Orbital Symmetry and Radical Pairs".

18 March 1977

Professor H. Bock (Frankfurt University), "Photoelectron Spectra and Molecular Properties: A Vademecum for the Chemist".

30 March 1977

Dr J.R. MacCallum (University of St Andrews), "Photooxidation of Polymers".

20 April 1977

Dr D.M.J. Lilley (Research Division, G.D. Searle), "Tails of Chromatin Structure - Progress towards a Working Model".

27 April 1977

Dr M.P. Stevens (University of Hartford), "Photocycloaddition Polymerisation".

4 May 1977

Dr G.C. Tabisz (University of Manitoba), "Collision Induced Light Scattering by Compressed Molecular Gases".

11 May 1977

Dr R.E. Banks (U.M.I.S.T.), "The Reaction of Hexafluoropropene with Heterocyclic N-Oxides".

18 May 1977

Dr J. Atwood (University of Alabama), "Novel Solution Behaviour of Anionic Organoaluminium Compounds: the Formation of Liquid Clathrates".

25 May 1977

Professor M.M. Kreevov (University of Minnesota), "The Dynamics of Proton Transfer in Solution".

1 June 1977

Dr J. McCleverty (University of Sheffield), "Consequences of Deprivation and Overcrowding on the Chemistry of Molybdenum and Tungsten".

6 July 1977

Professor J. Passmore (University of Brunswick), "Adducts Between Group V Pentahalides and a Postscript on  $S_7I^+$ ".

27 September 1977

Dr T.J. Broxton (La Trobe University, Australia), "Interaction of Aryldiazonium Salts and Arylazoalkyl Ethers in Basic Alcoholic Solvents".

19 October 1977

Dr B. Heyn (University of Jena, D.D.R.), " $\sigma$ -Organo-Molybdenum Complexes as Alkene Polymerisation Catalysts".



27 October 1977

Professor R.A. Filler (Illinois Institute of Technology),  
"Reactions of Organic Compounds with Xenon Fluorides".

2 November 1977

Dr N. Boden (University of Leeds), "NMR Spin-Echo Experiments  
for Studying Structure and Dynamical Properties of Materials Containing  
Interacting Spin- $\frac{1}{2}$  Pairs".

9 November 1977

Dr A.R. Butler (University of St Andrews), "Why I lost Faith  
in Linear Free Energy Relationships".

7 December 1977

Dr P.A. Madden (University of Cambridge), "Raman Studies of  
Molecular Motions in Liquids".

14 December 1977

Dr R.O. Gould (University of Edinburgh), "Crystallography to  
the Rescue in Ruthenium Chemistry".

25 January 1978

Dr G. Richards (University of Oxford), "Quantum Pharmacology".

1 February 1978

Professor K.J. Ivin (Queens University, Belfast), "The olefin  
metathesis reaction: mechanism of ring-opening polymerisation of  
cycloalkenes".

3 February 1978

Dr A. Hartog (Free University, Amsterdam), "Surprising recent  
Studies in Organo-magnesium Chemistry".

22 February 1978

Professor J.D. Birchall (Mond Division, I.C.I.Ltd.), "Silicon  
in the Biosphere".

1 March 1978

Dr A. Williams (University of Kent), "Acyl Group Transfer Reactions".

3 March 1978

Dr G. van Koten (University of Amsterdam), "Structure and Reactivity of Arylcopper Cluster Compounds".

15 March 1978

Professor G. Scott (University of Aston), "Fashioning Plastics to match the Environment".

22 March 1978

Professor H. Vahrenkamp (University of Freiburg), "Metal-Metal Bonds in Organometallic Complexes".

19 April 1978

Dr M. Barber (U.M.I.S.T.), "Secondary Ion Mass Spectra of Surfaces and Adsorbed Species".

16 May 1978

Dr P. Ferguson (C.N.R.S., Grenoble), "Surface Plasma Waves and Adsorbed Species on Metals".

18 May 1978

Professor M. Gordon (University of Essex), "Three Critical Points in Polymer Science".

22 May 1978

Professor D. Tuck (University of Windsor, Ontario), "Electrochemical Synthesis of Inorganic and Organometallic Compounds".

24 and 25 May 1978

Professor P. von R. Schleyer (University of Erlangen, Nürnberg),

- I. "Planar Tetra-co-ordinate Methanes, Perpendicular Ethylenes, and Planar Allenes".
- II. "Aromaticity in Three Dimensions".
- III. "Non-classical Carbocations".

21 June 1978

Dr S.K. Tyrlik (Academy of Science, Warsaw), "Dimethylgloxime-cobalt Complexes - Catalytic Black Boxes".

23 June 1978

Professor W.B. Person (University of Florida), "Diode Laser Spectroscopy at 16  $\mu\text{m}$ ".

27 June 1978

Professor R.B. King (University of Georgia, Athens, Georgia, U.S.A.), "The Use of Carbonyl Anions in the synthesis of Organometallic Compounds".

30 June 1978

Professor G. Mateescu (Cape Western Reserve University), "A Concerted Spectroscopy Approach to the Characterisation of Ions and Ion Pairs: Facts, Plans and Dreams".

15 September 1978

Professor W. Siebert (University of Marburg, West Germany), "Boron heterocycles as ligands in transition metal chemistry".

22 September 1978

Professor T. Fehlner (Notre Dame, U.S.A.), "Ferraboranes: syntheses and photochemistry".

2.2 Research Conferences Attended by the Author during the period  
1 October 1975 and 30 September 1978.

(i) 13 and 14 December 1976

The Chemical Society, Faraday Division, Symposium No. 11, "Newer Aspects of Molecular Relaxation Processes". The Royal Institution, London

(ii) 13, 14 and 15 September 1977

The Chemical Society, Faraday Division, General Discussion No. 64, "Ion-Ion and Ion-Solvent Interactions". St Catherine's College, Oxford.

